Direct Design of Partially Prestressed Concrete Beams For Combined Bending and Torsion

By

RABAH SAADI

Ingenieur Genie Civil

Ecole Nationale Polytechnique D'Alger

A Thesis submitted for the Degree of

Master of Science

Department of Civil Engineering

University of Glasgow

August 1988.

A MES PARENTS A QUI JE DOIT

A LA MEMOIRE DE MA SOEUR DALILA

A MES DEUX FRERES SID'AHMED ET SOFIANE

A MA SOEUR IMANE

ACKNOWLEDGEMENTS

The work reported herein was carried out in the department of civil engineering at the University of Glasgow under the general guidance of Professor A. Coull, whose help and encouragement is gratefully acknowledged.

The author would like to express his appreciation to D.R. Green for the provision of facilities in the departement.

The author is greatly indebted to Dr P. Bhatt, my respected supervisor. His encouragement, guidance, and patience shall always be mindful to me.

The author is grateful to Dr P.D. Arthur for his valuable advice and useful discussions.

My grateful thanks are also due to

* Mr G.Irving for the assistance in computational matters.
* The staff of the structures laboratory and in particular Mr Alan Barnett, Mr Alan Gray, Mr I. Todd, Mr B. Thompson and Mr J. Love for help with the experimental work.
* My friends J. Moussa, M. Souici, M. Bouazza, F. Abidi, Z. Merouani, S. Murthi and A. To for their useful dicussions and comments.
* My friends R. Manaa, M.Benredouane, S. Djellab, R. Adman and M. Ouldamara for their encouragement.
* The C.N.E.R.I.B. and the British Council for the financial support during the period of research.
* The staff of the general direction of C.N.E.R.I.B. for their encouragement and trust.
* The Slaven familly for encouragement and support.

* Finally, my thanks are reserved for my parents for their boundless patience, continual encouragement and financial support . My brothers Sofiane and Sid'Ahmed for their encouragement and trust.

SUMMARY

The thesis reports experimental and theoretical results on partially prestressed beams subjected to combined torsion and bending. The models were designed using the classical limit state concept of Nielsen using elastic stress field at ultimate load.

The experimental study consisted of testing six partially prestressed hollow concrete beams of square cross– section (300X300)mm. The main variables studied in this investigation are the amount of effective prestress and the corresponding area of steel designed according to Nielsen for a combined action of bending and torsion. The experimental data obtained indicated that the adopted approach showed satisfactory behaviour in terms of predictions of the ultimate strength of the beams and behaviour at serviceability loads under combined bending and torsion. The theoretical study was done using non– linear plane stress finite element programme. The finite element model provided fairly satisfactory agreement with experimental results.

LIST OF NOTATIONS

A_o	Cross– sectional area enclosed by centre–line of stirrups or beam wall
A_1	Area bounded by the lines connecting the centres of the corner longitudinal bars
A_2	Area bounded by the centreline of the shear flow
A_c	Cross sectional area
A_s	Cross– sectional area of one stringer
A_{sl}	Total cross– sectional area of longitudinal steel
$A_{sl,t}$	Cross– sectional area of top longitudinal steel
$A_{sl,b}$	Cross– sectional area of bottom longitudinal steel
A_{sv}	Area of stirrup leg
A_x	Area of steel per unit length in x direction
A_p	Area of longitudinal prestress in x direction
A_y	Area of steel per unit length in y direction
b	Body force per unit volume
[B]	Strain matrix
$[B]^T$	Transpose of strain matrix
b_t	Width of the section at the centroid of the tension steel
C	Torsional second moment of inertia
c	Concrete cover
C_f	Specified tolerance
c_{min}	Minimum concrete cover to tension steel
[D]	Material elastic property matrix
$[D_t]$	Material tangent matrix

E_c	Modulus of elasticity of concrete
E_s	Elastic modulus of steel
$E_c.I_{cr}$	Flexural rigidity
E_p	Eccentricity due to the applied prestress
F	force
F(T)	Stringer force due to torsion
F(M)	Stringer force due to bending
f_{cu}	Compressive cube strength of concrete
f_{cv}	Average compressive stress in the flexural compressive zone
f_c'	Compressive cylinder strength of concrete
f_d	Equivalent biaxial compression strength
f_{pe}	Effective stress of prestressing wires
f_{pu}	Ultimate stress of steel in prestressing wires
f_{px}	Yield stress of prestressing steel
f_t	Tensile strength of concrete
f_s	Yield stress of steel in tension
f_s'	Yield stress of steel in compression
f_{yl}	Yield stress of longitudinal steel (stringers)
f_{yv}	Yield stress of stirrups
f_x, f_y	Yield stress of steel in x and y axis
f_r	Modulus of rupture for concrete
G	Shear modulus of concrete
GC	Pre– cracking torsional rigidity
$G_{cr}C_{cr}$	Post– cracking torsional rigidity
H	Force in longitudinal bars
[K]	Structural stiffness matrix

$[K^{-1}]$	Inverse of structural stiffness matrix
K_0	Pre–cracking torsional stiffness
K_{cr}	Post–cracking torsional stiffness
K_i	Stiffness matrix for layer i
L	Span of beam
l_a	Lever arm
m	Ratio of volume of long steel to volume of stirrups
[N]	Matrix termed as the shape function
N_x	Applied in– plane force per unit width in x direction
N_{xc}	Concrete force in x direction
N_{px}	Axial force due to prestress
N_{sx}	Steel force in x direction
N_y	Applied in– plane force per unit width in y direction
N_{yc}	Concrete force in y direction
N_{yc}	Concrete force in y direction
N_{sy}	Steel force in y direction
P	External load vector
P_b	Applied bending load
P_{cr}	Load at first cracking
P_{cre}	Experimental cracking load
P_{crt}	Theoretical cracking load
P_d	Design load
P_e	Total effective prestress
P_p	Load vector due to effective prestress
P_i	Load vector due to external load
P_t	Total load vector
P_u	Ultimate load

P_{ue}	Experimental ultimate load
P_{ui}	Residual forces
P_{ut}	Theoretical ultimate load
P_y	Load at yield of steel
ΔP_i	Incremental load vector
ΔP_{ui}	Residual force vector
q	Shear flow
q_s	Traction force
R_x	Resultante of compressive stresses in x
R_y	Resultante of compressive stresses in y
s_v	Spacing of stirrups
T	Applied torsion
T_b	Bending component of applied torsion
T_c	Torque resisted by concrete
T_e	Elastic failure torque
T_{ep}	Elastic failure torque with the action of prestress
T_p	Plastic failure torque
T_{np}	Skew-bending failure torque
T_s	Torque resisted by steel
T_t	Torsional component of applied torque
T_u	Ultimate torsion
t	Thickness of beam element
t_e	Empirical value of thickness
t_i	Tickness of element layer
u	Perimeter of the section
(U,V)	Displacement at node in (X,Y) plane
x	Width of rectangular beam section

x_1	Width of stirrup centreline for rectangular beam
X,Y,Z	Global coordinates
y	Depth of rectangular beam section
y_1	Depth of stirrup centreline for rectangular beam section
τ	Shear stress
τmax	Max shear stress
τ_{xy}	Shear stress in x-y axis
τoct	Octahedral shear stress
τ_{nt}, γ_{nt}	Shear stress and strain in the crack
γ	Shearing strain
γ_{xy}	Shearing strain in x-y direction
δ	Displacement vector
δ^e	Vector of nodal displacement
δ_i	Displacement vector at any stage of loading
$\Delta\delta_{ui}$	Displacement vector due to residual forces
σ	Normal stress
σ_c	Diagonal concrete stress
σ_p	Normal stress due to prestress
σ_x, σ_y	Normal in plane stresses in x-y axis.
σ_1, σ_2	Major and minor principal stress
σ_n, σ_t	Normal and parallel stress resultant to crack direction
σ_i	Stress vector at any stage of loading
$\{\epsilon\}$	Strain vector
ϵ_i	Strain vector at any stage of loading

ϵ_l	Longitudinal steel strain
ϵ_v	Stirrup strains
ϵ_n, ϵ_t	Normal and parallel strain to the crack direction
θ	Angle of cracks to beam axis
θ_{cr}	Crack angle
υ	Poisson's ratio
ψ	Angle of twist
$d\psi/dz$	Rate of twist
α	St Venant's coefficient
α_p	Plastic coefficient
α_t	Coefficient depending on (y_1/x_1)
β	Geometric parameter
β_s	Shear retention factor

CONTENTS

CHAPTER ONE

INTRODUCTION

1.1 GENERAL BACKGROUND

In the design of reinforced concrete and prestressed structural members subjected to combined loading, Because of the nonlinear behaviour of these members, it is necessary to consider the interaction between the various forces in determining the ultimate strength. However, at present this is inconvenient. Existing design codes of practice BS: 8110[18,39], ACI[19] and others conservately recommend to design beams under combined loading for each case of loading and then sum the " results ". In this thesis an approach called " Direct Design Method " is used. In this approach a section is designed to resist a given set of forces using elastic stress fields and yield criterion for prestressed concrete members subjected to " in- plane forces ". The bulk of this thesis is devoted to the experimental investigation of beams designed using this approach.

1.2 OBJECTIVES AND SCOPE

The objectives of this study were:

(1) To experimentally study the behaviour of partially prestressed concrete beams designed according to " the direct design method ".

a) To make available the experimental data obtained.

b) To critically asses the adopted approach.

c) To gain a better insight into the behaviour of partially prestressed concrete beams subjected to combined bending and torsion. If these beams are subjected to pure torsion , how the amount of prestress will influence their torsional response.

(2) To use a detailed non- linear finite element programme to check the

validity of the basic assumptions adopted in the design method. And to compare the experimental and theoretical results.

1.3 LAYOUT OF THESIS

Chapter two reviews the results of beams subjected to torsion and torsion combined with bending. Torsion theory, mainly lower bound space truss analogy and upper bound skew–bending theory are reviewed. The torsion design procedures in some of the major codes of practice are summarised. Recent investigations relevant to combined loading are presented.

Chapter three is concerned with the description of the adopted " Direct Design Approach "in designing a section under combined loading.

Chapter four describes in detail the test rig which was designed to allow for the independent application of torsion and bending moment. The instrumentation used for measurement is fully presented. The test programme and the test models are described with details of concrete and steel characteristics.

In chapter five the experimental results are presented and discussed.

Chapter six describes the finite element method used and the results obtained.

The main conclusions drawn from this study are compiled in chapter seven where general comments are made and guidelines for further work are suggested.

CHAPTER TWO

REVIEW OF PREVIOUS INVESTIGATIONS

2.1 INTRODUCTION

There are four basic types of forces that act on a structural members: axial and shear forces, bending and twisting moments. They may exist simultaneously in any combination as dictated by the applied loads and geometry. At one time torsion was usually considered to be of secondary importance, and structure were often designed to resist bending and shear only, assuming that torsional moments could be taken care by the large safety factors used. Nowadays, flexural and shear design techniques have been considerably refined. Moreover, new structural forms that introduce out– of plane loading, have been developed and are in extensive use especially in urban motorways. As a result, structures are required to function as three– dimensional frames. Examples of structural members that carry significant torsional moments are: sprandel beams, edge beams of shells, some grid systems and curved alignments which are supported on a minimum number of piers for elevated roadways. Torsional moments rarely act in isolation. Many studies have been made to understand the basic behaviour under this condition. Considerable amount of experimental and theoretical work has been done on beams subjected to torsion. A detailled review is given in references[1,2]. As a result of this work design recommendations were incorporated in various codes of practice.

The aim of this chapter is to give a brief summary of recent works of beams subjected to:

– 1) Torsion

– 2) Torsion combined with bending

2.2 TORSION

The problem of torsion in a homogenous elastic circular member was first studied by Coulomb in 1784. He found that torsional moment, T, is proportional to the twisting angle, θ. St.Venant, in 1855 solved the puzzle regarding the torsion problem of rectangular members. He introduced the so called St.Venant's torsional inertia, C. The following equations were derived for a rectangular section.

$$T = C.G.d\psi/dz \qquad (2.1)$$

$$C = \beta.x^3.y$$

$$T = \alpha.x^2.y.\tau_{max} \qquad (2.2)$$

Where T: is the applied torque

C: is termed the torsional inertia and α and β represent a geometric parameters dependent on cross sectional dimensions $y > x$

G: modulus of rigidity

$d\psi/dz$: rate of twist

2.2.1 Experimental Investigation

In plain concrete beams subjected to pure torsion, failure was generally assumed to occur when the maximum tensile stress due to shear reaches the tensile strength of concrete. The beam fails by the formation of helical cracks as shown in Figure (2.1a). The angle of inclination of cracks to beam axis is approximately 45^0. However Hsu[1] observed with the help of high speed photographs, that when cracks develop on three sides of the beam failed in skew bending with the neutral axis parallel to the longer side of the section and inclined at 45^0 to the axis of twist shown in Figure (2.1b). Research into the behaviour of reinforced concrete beams subjected to torsion has indicated that the torsional strength of concrete beams can

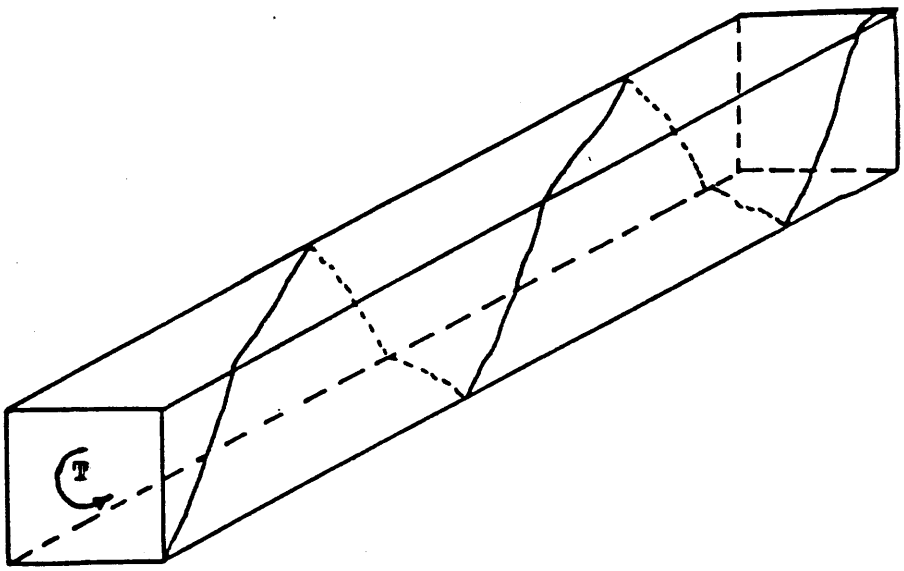

Figure (2.1.a) Helical Crack on plain Concrete Beam under pure Torsion .

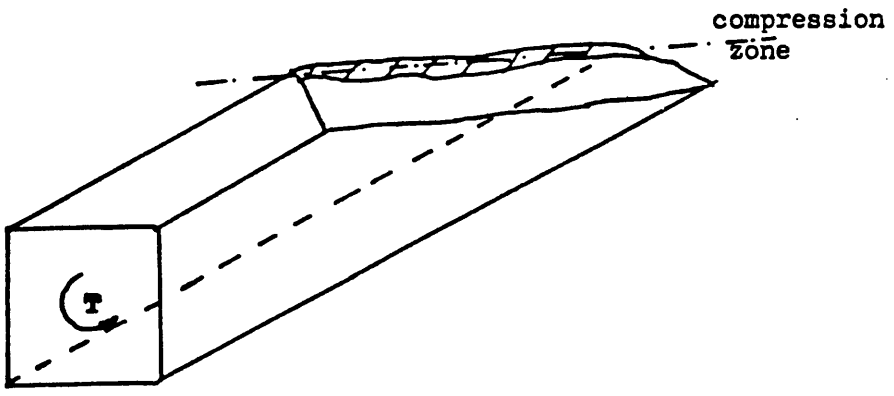

Figure (2.1.b) Skew Bending surface of rectangular section subjected to pure Torsion .

be increased by applying prestress without changing other geometric and material properties of the section. In this case, the inclination of the failure surface varies depending on the magnitude of prestress. Excessive prestress can result in brittle failure in compression.

2.2.2 Theoretical approach

2.2.2.1 Ultimate strength of plain concrete section subjected to pure torsion

Three theories have been developed to predict the torsional strength of plain concrete member: Elastic theory, plastic theory, and skew–bending theory. The elastic theory is based on St.Venant's theory. It is normally assumed that torsional failure of plain concrete member occurs when the maximum principale tensile stress σ_{max}, equals the tensile strength of concrete f_t. Since $\sigma_{max} = \tau_{max}$ in pure shear, the elastic failure torque, T_e, is given by:

$$T_e = \alpha.x^2.y.f_t \qquad (2.3)$$

Where α is termed St.Venant's coefficient depending on the ratio y/x. Comparison of test results with elastic theory indicate that due to the limited ductility of concrete, the elastic theory was found to considerably underestimate the failure strength of plain concrete beams by up to 50% in some cases[1,2].

Nadai proposed a plastic coefficient, α_p, to replace St.Venant's elastic coefficient. In other words, concrete may develop full plasticity and thus increase the ultimate strength. The plastic failure torque, T_p, can therefore be expressed by:

$$T_p = \alpha_p.x^2.y.f_t \qquad (2.4)$$

Where $\alpha_p = \{0.5 - (x/6y)\}$. The plastic coefficient is about 50% greater than the

elastic one, which can roughly account for the experimental observed extra strength. However the plastic theory has the following three weaknesses.

– 1) It is theoretically unsatisfactory as the principal tension is the prime cause of torsional beam failure and no significant plastic behaviour has been observed in tension of concrete.

– 2) Torsional failure of plain concrete members is quite brittle, there is no sign of plastic rotation.

– 3) Theory cannot account for the size effect. Tests have indicated that for " smaller " torsional specimens the calculated plastic torques are usually smaller than the test values, where as the opposite is true for " larger " specimens.

In view of the difficulties in using the classic elastic and plastic theories to accurately predict the ultimate strengths of plain concrete torsional members, Hsu[1] adopted the skew– bending theory, supported by photographic observations on the torsional failure mechanism of rectangular plain concrete beams. He indicated that, for such members under pure torsion, failure is caused by bending about an axis parallel to the wider face and inclined at an angle of 45^0 to the longitudinal axis of the beam. Hsu also suggested the following equation, based on the bending mechanism of torsional failure, for the torsional strength of plain concrete rectangular members. Figure (2.2) shows the applied torque resolved into two components, skew– bending T_b, and torsional T_t, on the failure surface. The bending component T_b is assumed to be responsible for the observed bending type failure. This can be expressed according to elastic bending theory as:

$$T_b = T.\cos\theta = x^2.y.\mathrm{cosec}\theta.f_r/6 \qquad (2.5)$$

Where f_r is the modulus of rupture of concrete and θ is the angle between tensile cracks on wider face and axis of beam. Assuming $\theta = 45^0$

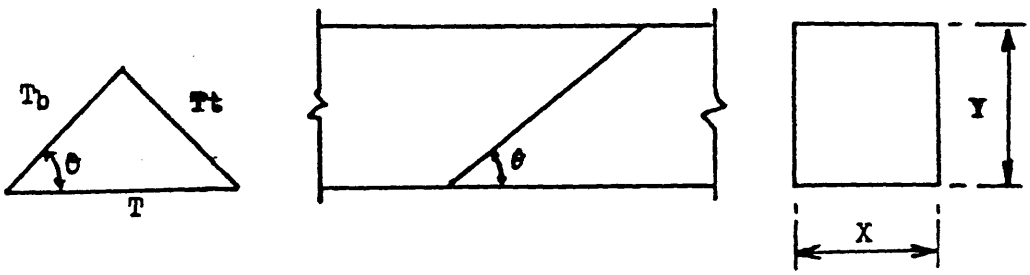

Figure(2.2 Components of applied Torque. (a) Tb - Bending component (b) Tt - Torsion component.

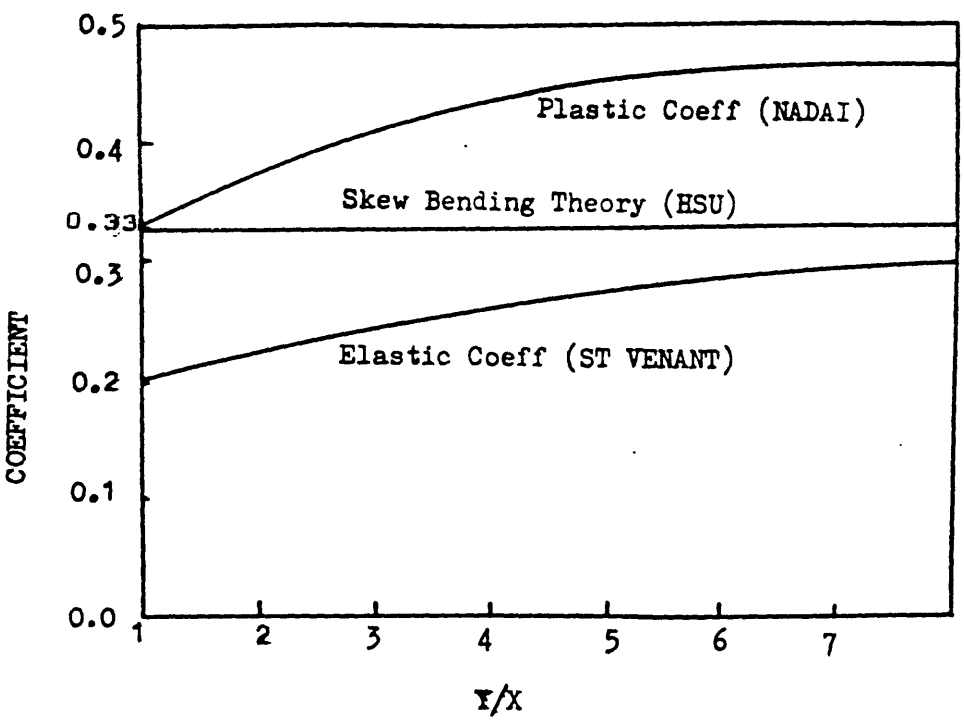

Figure(2.3 Comparison of Stress coefficient for Elastic, Plastic and Skew Bending Theories.

$$T = \{x^2.y/3\}[0.85.f_r] \qquad (2.6)$$

Where 0.85 is a reduction factor accounting for the effect of the perpendicular compression stress on the tensile strength of concrete. The skew– bending theory, therefore, provides a new failure criterion. Comparison of the elastic theory (Eq (2.3)); plastic theory (Eq (2.4)); and the skew bending theory (Eq (2.6)) reveals the following points:

(1) they all have the same geometric parameter x^2y, (2) the only differences are the nondimensional coefficient and the material constant. In both the elastic and plastic theories, the material constant is the direct tensile strength of concrete, f_t. In the skew– bending theory, it is the reduced modulus of rupture, $0.85f_r$. A comparison of the coefficients is shown in Figure (2.3); the skew– bending coefficient (a constant= 1/3) lies between the elastic and plastic coefficients, the later two being functions of y/x. Since Most of the torsional resistance of a member comes from the shear stress near the perimeter, It is useful to approximate the solid section as a thin– walled hollow tube. According to Bredt's thin tube theory, the maximum torque that can be resisted by the section can be expressed as:

$$T = 2.A_0.t.\tau \qquad (2.7)$$

Where A_0 is the area enclosed by " the centre line " of cross section of the tube. Figure (2.4) shows a tube with re– entrant corners but equation (2.7) ignores the considerable stress concentration which could take place at the corners.

2.2.2.2 *Ultimate strength of prestressed* concrete *section subjected to pure torsion*

The torsional strength of prestressed plain concrete member can also be developed with the three theories described previously. In the case of prestressed

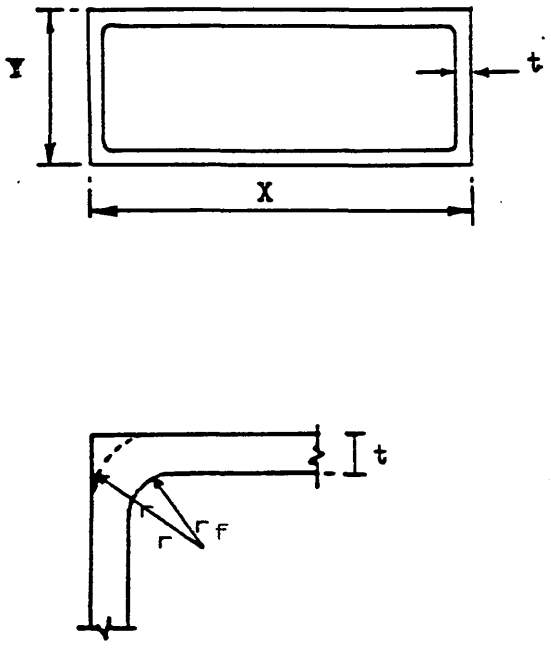

Figure 2.4 Rectangular Tube with re-entraint corners.

concrete beam subjected to pure torsion, the maximum principale tensile stress is given by.

$$\sigma = \frac{\sigma_p}{2} + \left[\left(\frac{\sigma_p}{2}\right)^2 + \tau^2 \right]^{\frac{1}{2}} \qquad (2.8)$$

Where,

σ_p : axial normal stress due to prestress

τ : maximum shear stress due to torsion

This equation may be re-arranged in the form of $\sigma = f_t$, then

$$\tau = f_t . \left[1 + \left(\frac{\sigma_p}{f_t}\right) \right]^{\frac{1}{2}} \qquad (2.9)$$

Hence the elastic failure torque can therefore be expressed as:

$$T_{ep} = \alpha . x^2 . y . \tau = \alpha . x^2 . y . f_t \left[1 + \sigma_p / f_t \right]^{\frac{1}{2}} \qquad (2.10)$$

Since $\alpha . x^2 . y . f_t$ in Eq (2.3) is the elastic torque without prestress we can write

$$T_{ep} = T_e \left[1 + \sigma_p / f_t \right]^{\frac{1}{2}} \qquad (2.11)$$

Similar conclusions hold for plastic and skew bending theories.

2.2.2.3 Ultimate strength of reinforced concrete beams subjected to pure torsion

Reinforced concrete beams subjected to torsion, generally, develop diagonal cracks when the maximum tensile stress is equal to the tensile strength of concrete. The reinforcement previously inactive now becomes stressed and the concrete sustain

diagonal compressive forces. Reports from some investigators[11,7] have suggested that the ultimate torsional strength of a beam T_u should be expressed as the sum of the torsion resistance of concrete T_c, and reinforcing steel T_s.

Hence,

$$T_u = T_c + T_s \qquad (2.12)$$

Where the value of T_c is commonly based on experimental results and is estimated as half the torque sustained at diagonal cracking. Contrary to that, other investigators [8,9,10] argued that the value of torque resisted by concrete decreases rapidly after cracking to become equal to zero as the applied load is increased. Before cracking, the percentage of steel has a negligeable effect on the torsional rigidity of the member (ie: all the members behave as plain concrete). Therefore, St· Venant's theory can be used. After cracking the behaviour can no longer be predicted by St Venant's theory. The ultimate strength and the post– cracking torsional rigidity (slope of the torque– twist curve after cracking) are greatly influenced by the percentage of steel.

The existing theories for calculating the torsional strength of members with longitudinal steel and stirrups can be roughly divided into two prominent categories.

– (1) The truss analogy type, and (2) skew– bending type. The result of these theories combined with experimental studies have been included in the design recommendations in various national codes. In the following a brief discussion of the two theories is presented

– A/ Space Truss Analogy

The first truss model to simulate the post– cracking action of a reinforced concrete member was proposed by Rausch in 1929.

A concrete member with an arbitrary cross section reinforced with longitudinal and hoop steel is assumed to act like a hollow section, so that the applied torsional

moment is resisted by the shear flow in the walls of the section. After cracking the concrete is seperated by 45^0 cracks into a series of helical members. These helical concrete members are assumed to interact with the longitudinal steel bars and the hoop steel bars to form a space truss. Each of the helical members is idealised into a series of 45^0 short straight struts connected at the joints as shown in detail (a) of Figure (2.5). The diagonal stress in the concrete struts is represented by a compression resultant force R_y or R_x on the depth or width of the beam which are given in terms of shear flow q as:

$$\begin{cases} R_x = \dfrac{q.x_1}{\sin\theta} \\ \\ R_y = \dfrac{q.y_1}{\sin\theta} \end{cases} \qquad (2.13)$$

Taking a section perpendicular to the struts, the corresponding diagonal stress σ_c is obtained as:

$$\sigma_c = \frac{R_y}{t.y_1.\cos\theta} = \frac{q.y_1}{t.y_1.\cos\theta\sin\theta} \qquad (2.14)$$

Therefore $$\sigma_c.t = \frac{q}{\sin\theta.\cos\theta} \qquad (2.15)$$

The force in each stringer H is obtained from the contribution of horizontal components of results R_y and R_x on the web and flange of the section.

$$H = \frac{1}{2}\left[R_y + R_x \right].\cos\theta$$

Therefore

$$H = \frac{1}{2} q \left[y_1 + x_1 \right] \frac{\cos\theta}{\sin\theta} = A_{s1}.f_{y1} \qquad (2.16)$$

Considering detail (b) of Figure (2.5), the lateral hoop bars are also idealised as chains of short straight bars connected to the concrete struts at the joints. The

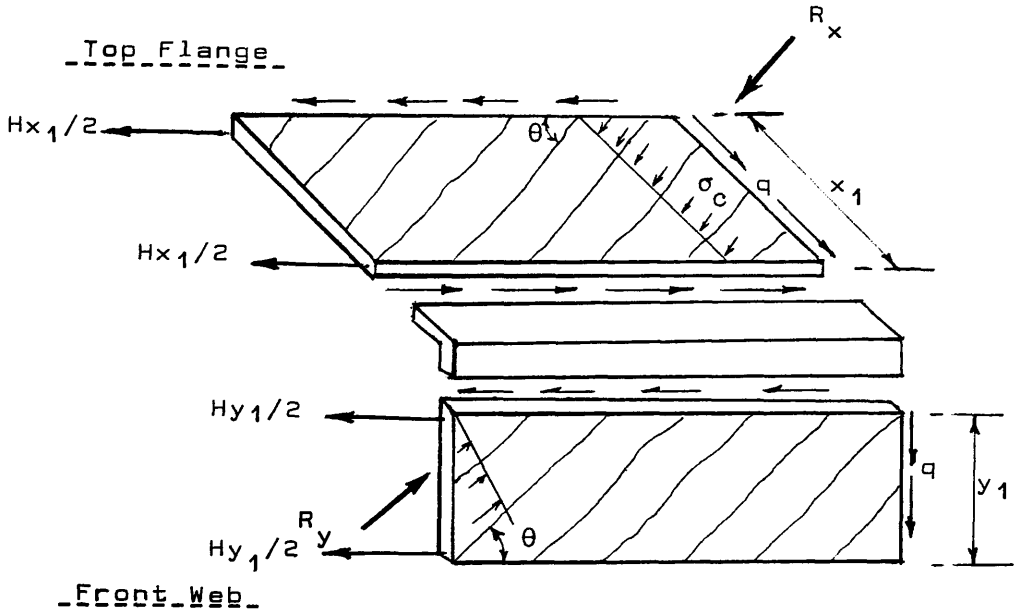

-(a) Forces in Beam Wall.

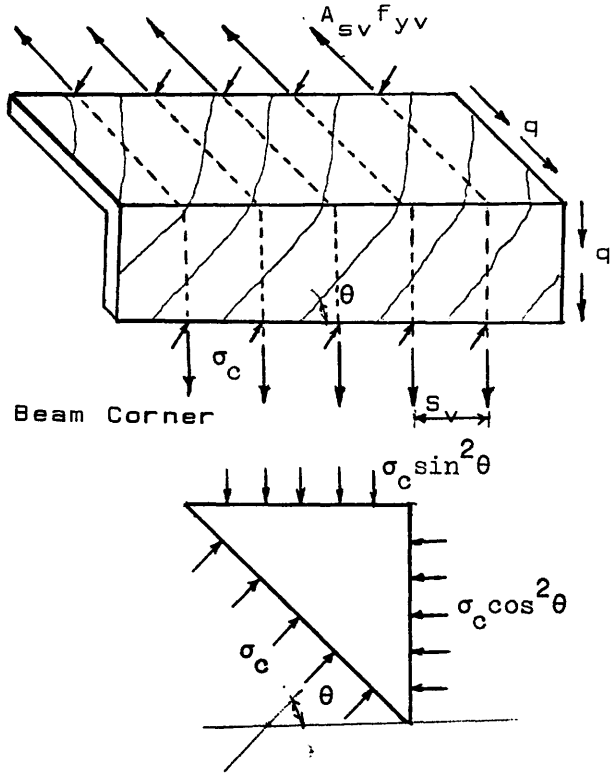

-(b) Forces in Beam Corner

Figure(2.5) Forces due to Torsion in Beam Walls.

equivalent force in each bar is expressed as:

$$\sigma_c.t.\sin^2\theta.s_v = A_{sv}.f_{yv}$$

Substituting for $\sigma_c.t$ from Eq (2.14) we get

$$A_{sv}.f_{yv} = q.s_v.\tan\theta \qquad (2.17)$$

The chains of hoop bars thus form a mechanism that will lengthen under an infinitisimal external torque. This tendency to lengthen is resisted by the longitudinal reinforcement. Figure (2.6) shows a generalised space truss model for hollow rectangular reinforced concrete beam under torsional loading. The space truss involves the following assumptions:

- (1) The space truss is made up of 45^0 diagonal concrete struts, longitudinal bars, and hoop bars connected at the joints by hinges.
- (2) A diagonal concrete member carries only axial compression, (ie: shear resistance is neglected).
- (3) Longitudinal and lateral bars carry only axial tension.
- (4) For a solid section, the concrete core does not contribute to the ultimate torsional resistance.

The shear flow $q = \tau.t$ is a function of the torsional moment T, and enclosed area of the centreline of stirrups A_0, and is expressed as:

$$q = T/2.A_o \qquad (2.18)$$

Where, t is the thickness of beam wall, τ torsional stress. By establishing the

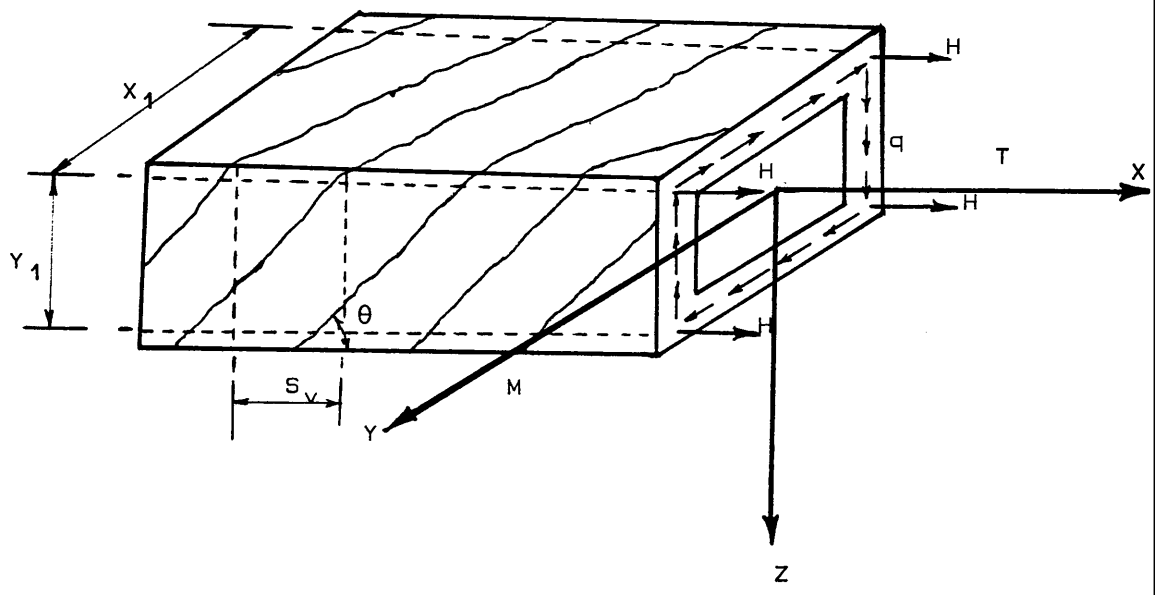

Figure(2.6) Space Truss Model for Pure Torsion.

equilibrium of internal and external forces Rausch arrived at general equation for the calculation of ultimate torque of reinforced concrete section, the ultimate torsional strength T_u is given by:

$$T_u = \frac{2.A_0.A_{sv}.\ f_{yv}}{s_v} = \frac{2.A_0.A_{sl}.f_{yl}}{u} \qquad (2.19)$$

Where T_u : Ultimate torsional resistance of reinforced concrete member.

A_0 : area bounded by the centre line of transverse hoop bar

A_{sv} : cross sectional area of a transverse hoop bar

f_{yv} : yield stress of a hoop bar

f_{yl} : yield stress of longitudinal bar

A_{sl} : total area of longitudinal bars

u : perimeter of the area bounded by the centre line of a complete hoop bar

s_v : spacing of stirrups

From equation (2.19), it follows that the total area of the longitudinal steel is related to that of the hoop bars through the equation:

$$\frac{A_{sl}.f_{yl}}{u} = \frac{A_{sv}.f_{yv}}{s_v} \qquad (2.20)$$

On the assumption that both longitudinal and hoop steel has the same yield strength Equation (2.20) becomes

$$A_{sl}.s_v = A_{sv}.u$$

The above equation states that the volume of all longitudinal steel within the spacing s_v should be equal to the volume of one complete hoop bar. This is the so—called equal volume principle employed by many codes of practice for the calculation of the longitudinal torsional reinforcement. For a reinforced rectangular section, for

example the ultimate torsional strength is given by:

$$T_u = 2x_1 . y_1 . A_{sv} . f_{yv}/s_v \qquad (2.21)$$

It is worth commenting that Rausch's concept of the space truss analogy is a brilliant combination of Bredt's thin tube theory for torsion and plane truss analogy for flexural shear in reinforced concrete, It gives a very clear idea of the main function of reinforcement and concrete in resisting torsion. From a theoretical point of view, the space truss analogy cannot take into account the effect of the shear resistance of the concrete struts, the dowel action of reinforcement and the contribution of concrete core observed in tests.

One aspect of detail at the corner as shown in Figure (2.6a) should be noted. The forces in the stirrups tend to spall the concrete which has to be resisted by a corner bar.

– B/ Skew– Bending Model

The basic characteristic of skew bending theory is the assumption of a skew bending failure surface. This failure surface is initiated by a helical crack on three faces of a rectangular beam, while the ends of this helical crack are connected by a compression zone near the fourth face as shown in Figure (2.7). The failure surface intersects both the longitudinal reinforcement bars and the closed stirrups. The forces in the reinforcement provide the internal forces and moments to resist the external applied loads. At failure, the two parts of the beam separated by the failure surface rotate against each other about a neutral axis on the edge of the compression zone. It is assumed that both the longitudinal steel and stirrups will yield at the collapse of the beam. By establishing the equilibrium of internal and external forces. The ultimate torsional strength expression is obtained as:

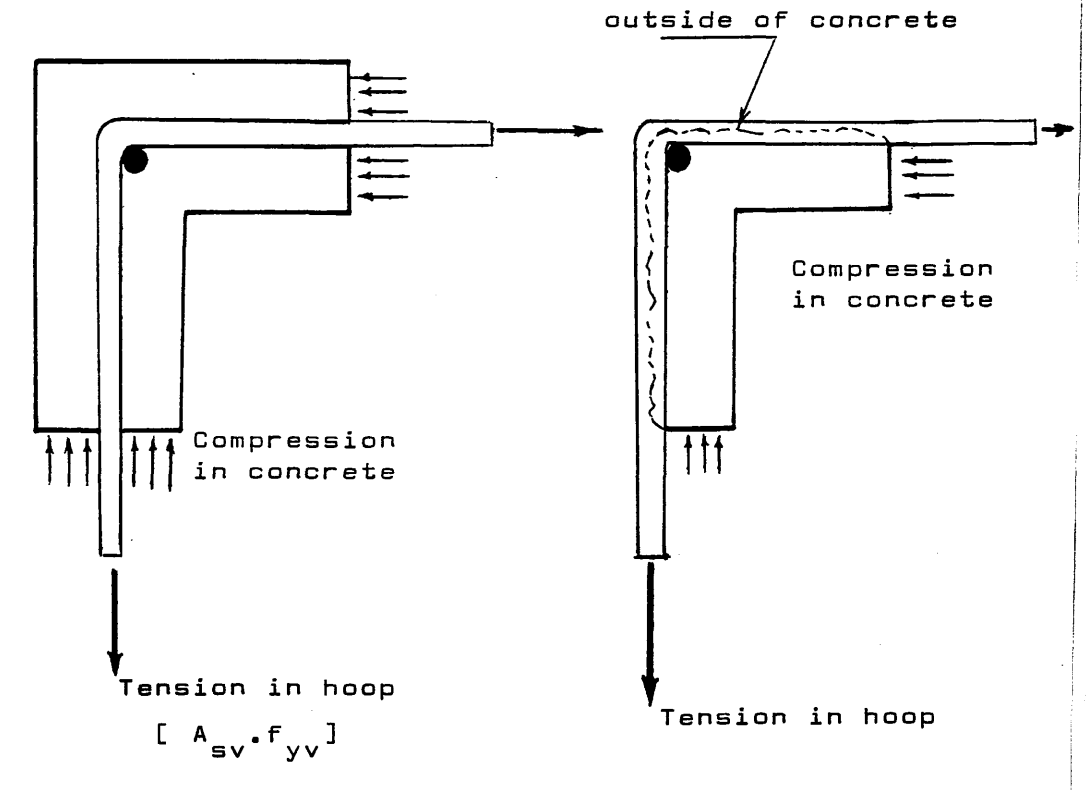

Figure(2.6a) Spalling of Concrete Cover.

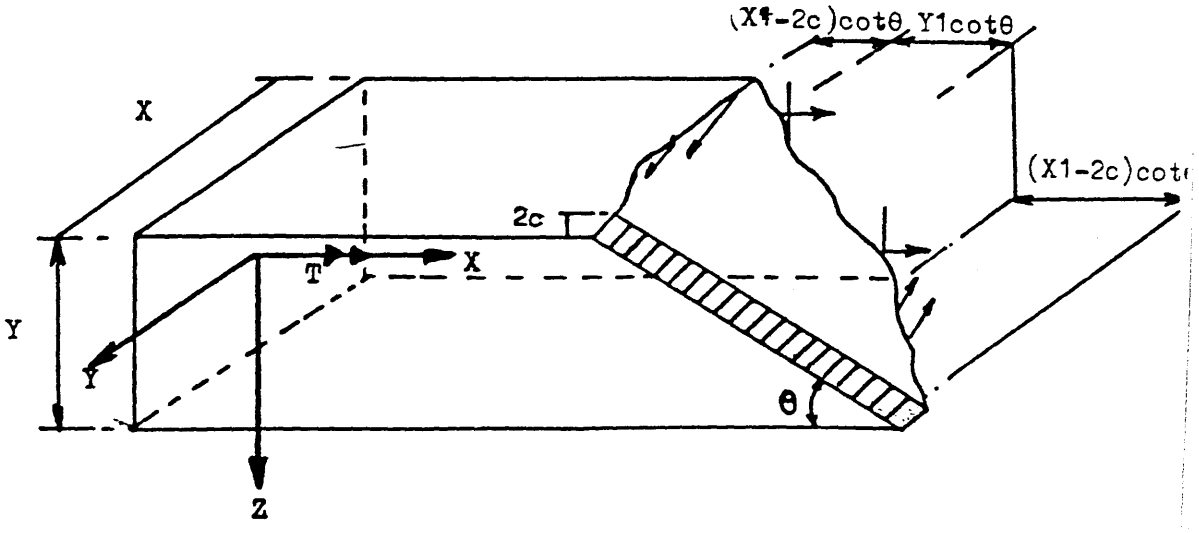

FAILURE SURFACE

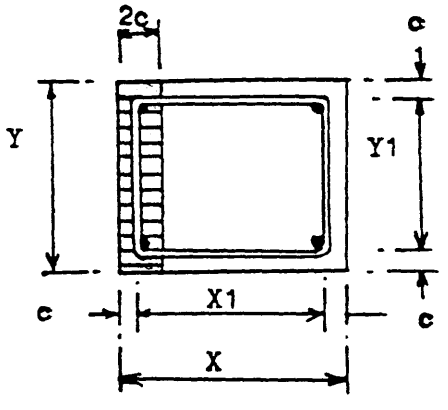

SECTION

Figure 2.7 Skew Bending idealisation for Beam under pure Torsion.

$$T_u = 2A_0 \frac{A_{sv} \cdot f_{yv}}{s_v} = 2A_0 \frac{A_{sl} \cdot f_{yl}}{u} \qquad (2.22)$$

This equation is identical to Eq (2.19) derived with the space truss model. By comparing the space truss model and skew bending model as expressed above it is observed that:

– (1) Concrete contribution plays no rule in the ultimate torque.

– (2) Both methods are centred on different idealised failure surface, but the final results prove that they lead to the same ultimate strength solution.

Hsu[1] re–examined the failure process and mechanism by studying a serie of solid and hollow rectangular sections under pure torsion. He suggested the following equation for the torsional strength of an undereinforced rectangular beam:

$$T_u = T_c + \left[0.66m \frac{f_{yl}}{f_{yv}} + 0.33 \frac{y}{x} \right] A_0 \frac{A_{sv} \cdot f_{yv}}{s_v} \qquad (2.23)$$

Where, x,y : section dimensions

T_c : torque carried by concrete

m : the volume of longitudinal steel to volume of stirrups

$(A_{sl}.s_v)/(A_{sv}.u)$

The area of longitudinal steel is required to be distributed around the perimeter is given as $A_{sl}/u = A_{sv}/s_v$. Hsu assumed that T_c is contributed by the shear resistance of the diagonal concrete struts.

2.2.2.4 Post–cracking stiffness under torsion

Few attempts have been made to evaluate the torsional stiffness after the cracking of concrete. Using Rausch's space truss model Hsu[15] derived an equation for the post–cracking torsional stiffness of reinforced concrete sections. Figure (2.8) shows a typical torque twist curve for a reinforced concrete member. The slope of the initial part of the torque–twist curve is the pre–cracking torsional stiffness

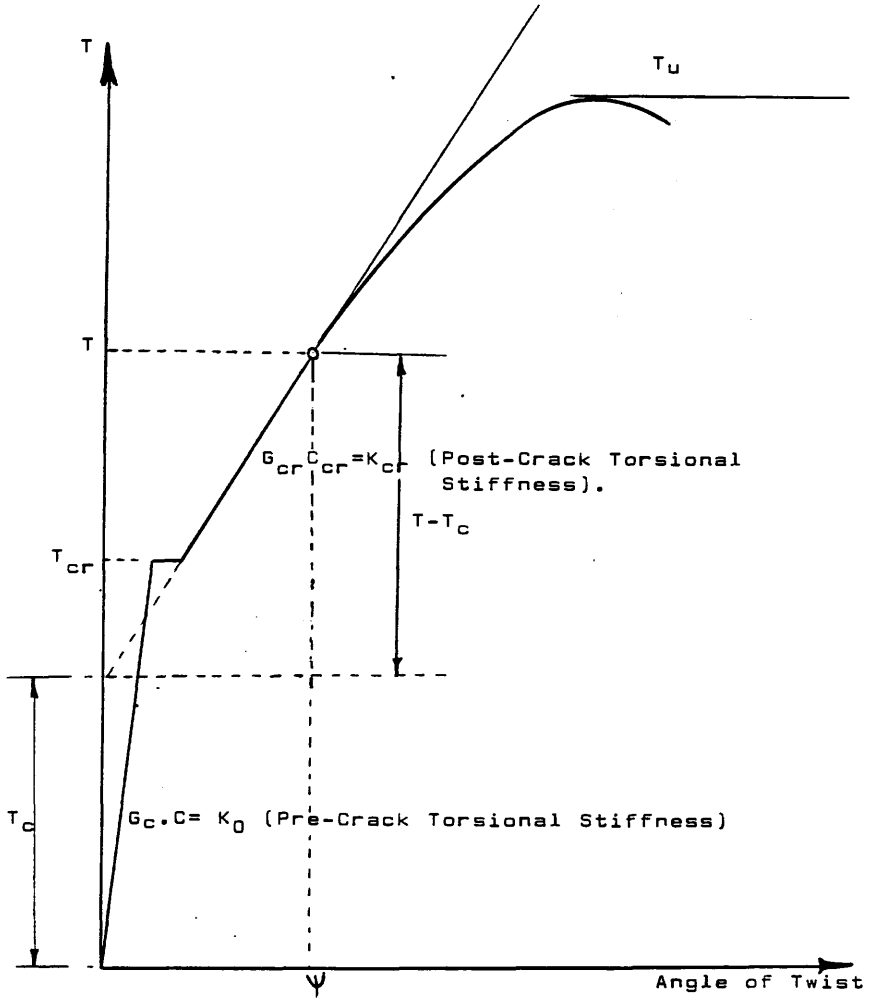

FIgure(2.8) Typical Torque-Twist Curve
of Reinforced Concrete Beam.

$K_0 = G_c.C$. After the cracking of concrete, the first part is approximated by a straight line and the slope is taken as the post–cracking torsional stiffness K_{cr}. The curve bends afterwards up to ultimate torque point. By assuming a tube of thickness t the post– cracking torsional stiffness of a hollow rectangular section is expressed as:

$$K_{cr} = G_{cr}.C_{cr} = \frac{4.E_s.A_0^2}{u\left\{\frac{4.E_s}{t.E_c} + \frac{u}{A_{sl}} + \frac{s_v}{A_{sv}}\right\}} \qquad (2.24)$$

Where, $G_{cr}.C_{cr}$: Post–cracking torsional stiffness

E_s : Young's modulus of elasticity of steel

A_0 : Area bounded by the centreline of reinforcement

A_c : Area of concrete

E_c : Concrete young's modulus

s_v : Stirrup spacing

u : Perimeter of area bounded by the center line of complete hoop bar

t : wall thickness assumed uniform

The slope of the straight portion as shown in Figure (2.8) represents the post– cracking torsional rigidity calculated by Eq (2.24). In the case of solid section the above section is issued using an effective wall thickness t_e given as:

$$t_e = 1.4\left[\frac{A_{sl}}{A_c} + \frac{A_{sv}.u}{A_c.s_v}\right].x \qquad (2.25)$$

This emperical quantity fitted test results but should not be construed as the actual wall thickness at ultimate strength.

From Figure (2.8), the extrapolation of the straight portion will intersect the vertical axis, giving a vertical intercept. This vertical intercept was found to be

$$T_c = 2.4\,[f_{cu}]^{\frac{1}{2}}\,[x^2.y/3]$$

By ignoring the very small pre-cracking rotations compared to those after cracking, the simplified equation for post-cracking stiffness becomes:

$$G_{cr}.C_{cr} = \frac{4.E_s.A_0^2}{u\left(\frac{u}{A_{sl}} + \frac{s_v}{A_{sv}}\right)} \qquad (2.26)$$

2.3 TORSION COMBINED WITH BENDING MOMENT

2.3.1 Introduction

The behaviour of reinforced concrete beams subjected to combined torsion and bending moment is difficult to predict because of the different failure patterns associated with pure bending and pure torsion. The mode of failure will therefore depend on the ratio of bending to torsional moment and other parameters like the volume and disposition of the reinforcement.

2.3.2 Experimental Investigation

Reinforced concrete beams provided with both longitudinal and transverse reinforcing steel generally behave similar to plain concrete beams before cracking. After cracking the beams continues to resist forces until failure. The angle of inclination of cracks to beam axis varies between the limits of pure torsion 45^0 and pure bending 90^0. The stress in steel remains negligeable until the section has cracked. After cracking, the steel strains increased by a large amount and continued to increase thereafter until failure.

2.3.3 Theoretical approach

2.3.3.1 Ultimate strength of beams under combined torsion and bending

Extensive work has been done to assess the ultimate strength of reinforced concrete beams subjected to combined torsion and bending. Summary of work was also reported in Lampert[12] where test results confirmed the use of the space truss as failure model throughout the whole range of torsion combined with bending. In the present chapter a failure model in the form of a space truss and skew–bending are presented and applied to the case of combined torsion and bending. Their validity have been confirmed by an extensive series of tests[30]. Using the postulated failure mechanism in section 2.2.2.3 for the case of pure torsion, ultimate strength equations are established from equilibrium consideration for combined loading. Figures (2.9) and (2.10a), (2.10b) show typical space truss and skew bending failure models. The basic assumption adopted in these models is that the internal compression forces are resisted along an inclined compression while the required tensile forces are supplied by transverse and longitudinal reinforcing steel at yield. The ultimate strength of a beam under pure torsion, assuming $\theta = 45^0$ is given by:

$$T_u = 2.A_0.A_{sv}.f_{yv}/s_v = 2.A_0.A_{sl}.f_{yl}/u \qquad (2.27)$$

Assuming that all stringers are equal in cross sectional area. The longitudinal steel will be equally distributed at the bottom and at the top of the beam. Hence top or bottom longitudinal steel will be equal to:

$$\frac{A_{sl}}{2} = (A_{sl,t})_{torsion} = \left\{\frac{T_u.u}{2A_0.f_{yl}}\right\}\frac{1}{2} \qquad (2.28)$$

$$\frac{A_{sl}}{2} = (A_{sl,b})_{torsion} = \left\{\frac{T_u.u}{2A_0.f_{yl}}\right\}\frac{1}{2} \qquad (2.29)$$

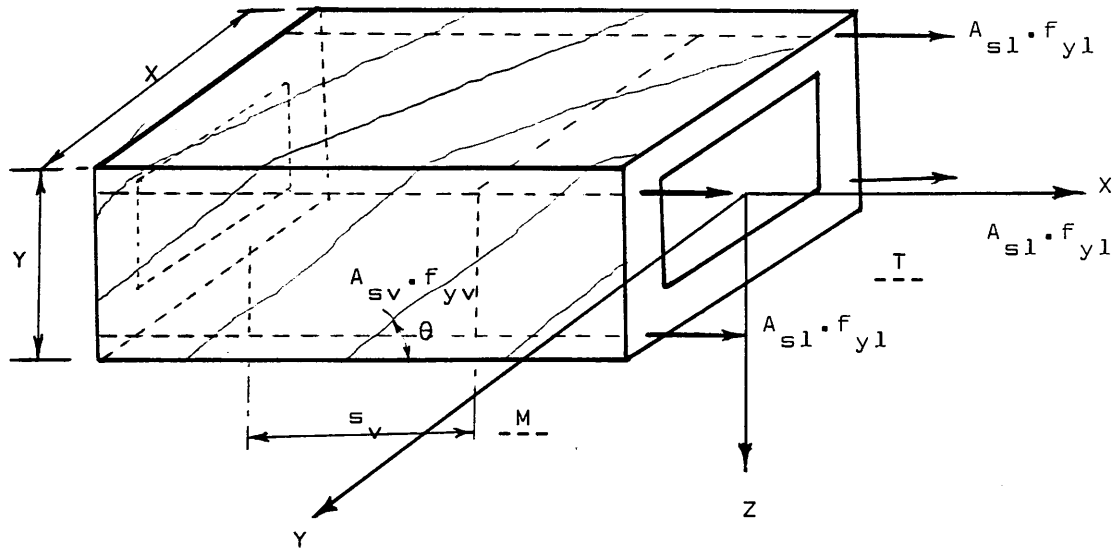

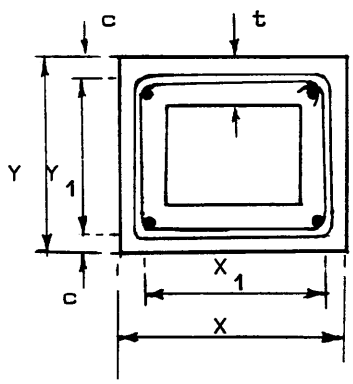

CROSS-SECTION OF BEAM

Figure(2.9) Space Truss Model for Beam under combined Bending and Torsion.

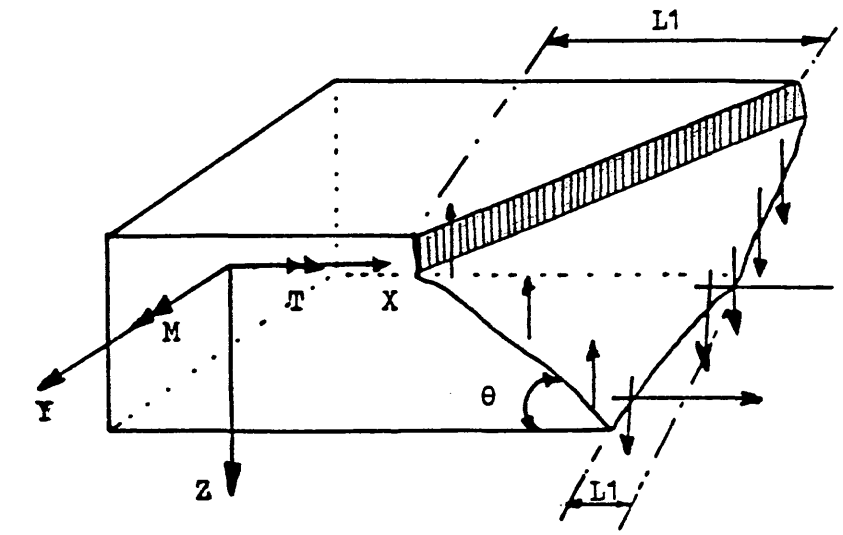

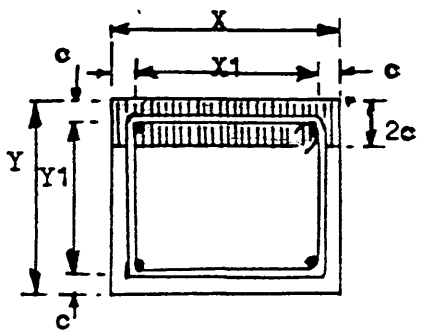

SECTION

Figure 2.10a Failure Surface for Combined Torsion and Bending in Skew bending model. (Bending dominated)

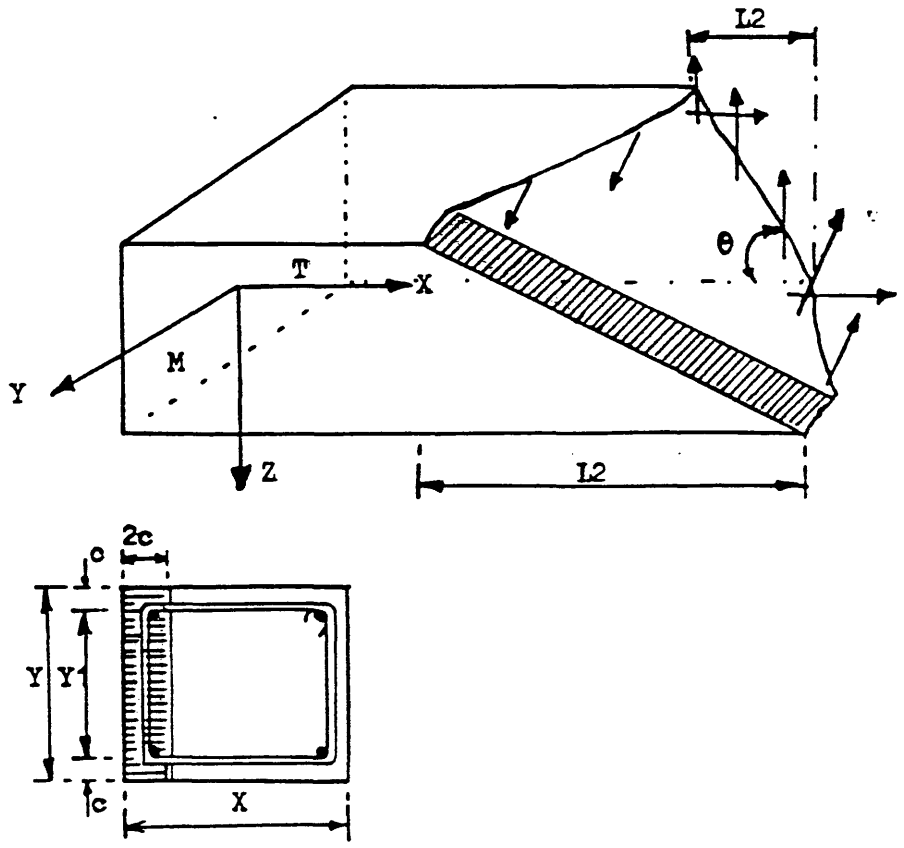

Figure 2.10b Failure Surface for Combined Torsion and Bending in Skew bending approach. (Torsion dominated)

Where $A_{sl,t}$ and $A_{sl,b}$ are the top and bottom longitudinal reinforcement. Assuming that longitudinal bars and stirrups yield first, the total area of longitudinal bars required to resist a bending moment M is given by:

$$(A_{sl,b})_{bending} = \frac{M}{f_{yl} \cdot y_1} \tag{2.30}$$

Figure (2.11) shows the supperposition of the stringer forces F(T) and F(M) due to torsion and bending if we first assume that yielding of the lower stringers and the stirrups will take place at failure. The area of longitudinal steel can therefore be expressed as:

$$(A_{sl})_b = (A_{sl,b})_{bending} + (A_{sl,b})_{torsion}$$

$$(A_{sl})_b = \frac{M}{f_{yl} \cdot y_1} + \left\{ \frac{T_u}{2A_0 \cdot f_{yl}} \right\} \frac{u}{2} \tag{2.31}$$

Letting $$M_u = (A_{sl})_b \cdot f_{yl} \cdot y_1 \tag{2.32}$$

Hence,

$$M_u = M + \frac{T_u}{2} \left\{ 1 + \frac{y_1}{x_1} \right\} \tag{2.33}$$

And the applied bending moment is given as:

$$M = M_u - \frac{T_u (1 + y_1/x_1)}{2} \tag{2.34}$$

The case of yielding of the upper stringers is now considered. The tensile force in the upper stringers due to torsion is counteracted by the compresssion due to bending. The total area of steel at the top is equal to:

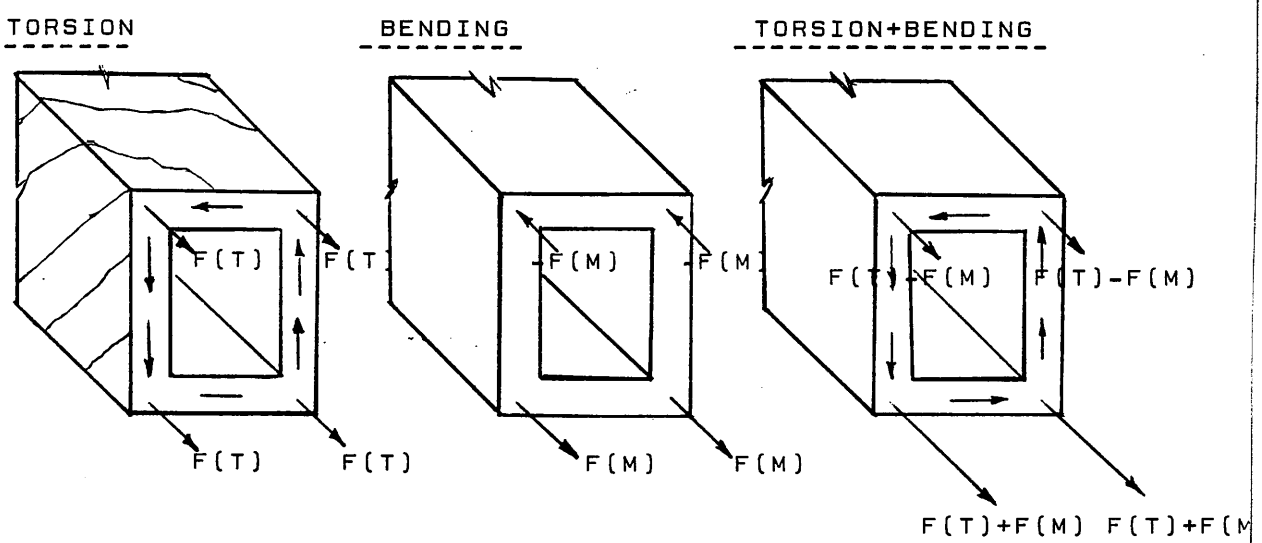

Figure(2.11) Superposition of Torsion and Bending
for reinforced concrete beam.

$$(A_{sl})_t = - \frac{M}{f_{yl} . y_1} + \{ \frac{T}{2A_0 . f_{yl}} \} \frac{u}{2} \qquad (2.35)$$

Hence equation (2.33) becomes

$$M = -M_u + \frac{T_u (1 + y_1/x_1)}{2} \qquad (2.36)$$

Based on the above derivation of the ultimate strength expression for reinforced concrete beams under torsion and bending, the following conclusions can be drawn.

1/ Space truss theory of reinforced concrete beam under torsion can be extended to cover combined loadings.

2/ The ultimate strength of beams in combined bending and torsion can be evaluated from the study of the equilibrium of external and internal forces in the failure surface.

3/ The total area of steel is made up of the summation of separate design equations (2.31) and (2.35). The concrete compresssion zone could be in the bottom or top flange depending on the direction of the applied moment. This lead to at least two types of failure modes. The first mode is dominated by bending while the other is dominated by torsion. However, in the bending compression zone, the longitudinal torsional steel may be reduced because of the tensile force due to torsion is counteracted by the compression due to bending. The transverse steel for pure torsion is unchanged by combined loading. The space truss theory allows yielding of transverse and longitudinal reinforcement producing a ductile behaviour before failure.

2.3.4 Prestressed Members

Prestressed concrete beams have been widely used in bridge construction, because they combine excellent torsional strength and rigidity with flexural strength. Yet only a few studies have been made on their strength and behaviour under

combined loadings. Ewida and Mc Mullen[6] extended the skew bending theory for predicting the behaviour of reinforced and prestressed concrete beams under combined loading. In another investigation, Collins and Mitchell[28] proposed design recommendations for prestressed and nonprestressed concrete beams using the truss model first suggested by Rausch. It is well known that prestress prevents the concrete beam from cracking and the beam will therefore behave as a homogeneous beam. However, once the concrete cracks the prestressed beam will behave as a reinforced concrete beam.

2.3.4.1 Post–cracking behaviour of prestressed concrete under combined bending and torsion

Based upon experimental results[5] it can be said that reasonable prestressing increases not only the crack resistance of torsion members but their torsional strength provided that longitudinal prestressed reinforcement does not yield. The strength of a prestressed concrete beam subjected to combined torsion and bending can be calculated fairly accurately by the space truss theory[10]. Prestressed concrete beams differ from reinforced concrete beams in having an axial stress and prestressing steel stressed to only the effective prestress. The prestress reduces principal tension and the prestressing steel provides reinforcement with an effective prestress equal to the difference between the true yield stress and the initial prestress. Prestressing steel affects only the expresssion for longitudinal steel given in Eq (2.31).

– Prestressing has a benefical effect as web cracking will be delayed and, hence the additional resistance of the concrete will remain active over a wider range.

2.3.5 Codes of practice

The strength of reinforced concrete beams subjected to combined bending and torsion moment according to the British[18,39], American[19] codes is based on the

algebric summation of the required steel contribution to resist bending and torsion moments.

2.3.5.1 A.C.I Procedure

The A.C.I design criteria for flexural strength follows very closely the design criteria of the british code. Accordingly, for rectangular sections with tension reinforcement only, the area of steel required for applied moment is expressed as:

$$(A_{sl})_b = \frac{M}{f_{yl} (y - a/2)} \qquad (2.37)$$

In which

$$a = \frac{(A_{sl,b}) . f_{yl}}{(0.708 . f_{cu} . x . y)}$$

Equation (2.23), based on the skew bending theory, is simplified for practical design by assuming equal volume steel and $f_{yv} = f_{yl}$. For rectangular sections the torsional strength is given by:

$$T = x^2 . y/3 \; (\; 2.4[f_{cu}]^{\frac{1}{2}} \;) + \alpha_t . x_1 . y_1 . A_{sv} . f_{yv}/s_v$$

Where $T_c = x^2 . y/3 \; (\; 2.4[f_{cu}]^{\frac{1}{2}} \;)$ is the torsional strength provided by concrete. Hence the area of transverse reinforcement needed to resist pure torsion is:

$$A_{sv} = \frac{1}{\alpha_t} \; \frac{(T - T_c) . s_v}{x_1 . y_1 . f_{yv}} \qquad (2.38)$$

Where $\alpha_t = (\; 0.66 + 0.33 y_1/x_1 \;) < 1.5$.

The corresponding area of longitudinal steel is given by:

$$A_{sl} = A_{sv} . u/s_v \qquad (2.39)$$

For combined torsion and bending, the total longitudinal steel area in the tension zone is

$$A_{sl,b} = \frac{M}{f_{yl}(y - a/2)} + \frac{A_{sv}}{s_v}(x_1 + y_1) \qquad (2.40)$$

The transverse reinforcement provided is unaffected by bending. Hence, is identical to the case of pure torsion.

2.3.5.2 BS 8110 (1985) procedure

The British code, CP110 (1972) has now become BS 8110 (1985). The same design procedure has been continued in the new code apart from a slight increase (about 6%) in the maximum permissible torsional shear stress. The code considers torsion, like shear and bond, in terms of the limit sate of collapse. Unlike the ACI code, BS 8110 considers the total torque, T, for the design, implying the neglect of concrete contribution. The space truss analogy is adopted and the stirrups area is calculated from:

$$\frac{A_{sv}}{s_v} = \frac{T}{[\ 0.8.x_1.y_1(0.87f_{yv})\ ]} \qquad (2.41)$$

And the total area of longitudinal reinforcement, A_{sl}, is given by

$$A_{sl} = \frac{A_{sv}}{s_v}\left[\frac{f_{yv}}{f_{yl}}\right] u \qquad (2.42)$$

According to BS: 8110 and adopting an equivalent rectangular stress distribution in the compression zone and assuming that reinforcement yields prior to crushing of concrete, the area of tension steel required for rectangular section is:

$$A_{sl,b} = \frac{M}{f_{yl}.l_a} \qquad (2.43)$$

Where l_a is the lever arm

Finally, under combined bending and torsion, the total longitudinal tension steel is:

$$A_{sl,b} = \frac{M}{f_{yl} \cdot l_a} + \frac{A_{sv}}{s_v} \left[\frac{f_{yv}}{f_{yl}} \right] \frac{u}{2} \qquad (2.44)$$

2.3.5.3 BS 5400 (1984)

According to the BS 5400, calculations for torsion are only required for the ultimate limit state and the torsional shear stresses should be calculated assuming a plastic shear distribution. Then calculations should be in accordance with the following equations.

$$\frac{A_{sv}}{s_v} \geq \frac{T_u}{0.8\, x_1 . y_1 (0.87 f_{yv})} \qquad (2.45)$$

$$\frac{A_{sl}}{u} \geq \frac{A_{sv}}{s_v} \left\{ \frac{f_{yv}}{f_{yl}} \right\} \qquad (2.46)$$

When prestressing steel is used as transverse steel, in accordance with Equation (2.45), or as longitudinal steel, in accordance with Equation (2.46), the stress assumed in design should not be lesser of 460 N/mm^2, or $(0.87 f_{pu} - f_{pe})$. Similar procedure as for the BS 8110 will be employed here in order to define the required area of steel reinforcement under the action of bending and torsion. BS 8110 give no information on prestressed beams subjected to bending and torsion. However, BS 5400 provides an information on cross section subjected to simultaneous flexural compressive stresses, where a lesser amount of longitudinal reinforcement is provided. The reduction in the amount of longitudinal reinforcement in the compressive zone may be taken as:

$$\frac{f_{cav.}(\text{Area of section subjected to flexural compression})}{0.87 . f_{yl}}$$

where,

f_{pe} : Effective prestress (ie: level of prestress after losses)

f_{cav}: Average compressive stress in the flexural compressive zone.

CHAPTER THREE

PROPOSED DESIGN PHILOSOPHY

3.1 INTRODUCTION

The aim of structural design is to make sure that the structures sustain safely the loads and deformations which may occur during construction and use and have adequate durability during the lifetime of the structure. A structure, or part of a structure, is rendered unfit for use when it reaches a limit state, defined as a particular state in which it ceases to fulfil the functions for which it was designed.

The current practice for the design of reinforced concrete structures according to the British code BS 8110[18], American code ACI 318[19] are based on the concept of limit state. The two basic categories of limit state are:

1) Ultimate Limit State: This limit state is associated with the maximum load carrying capacity of structure before collapse. Collapse may occur basically by the inability of the structure to carry any more load. This can happen because the structure has become unstable.

2) Serviceability Limit State: Serviceability limit state is reached if the structure suffers from excessive deflection, cracking, vibration etc., at working loads.

The usual practice is to design the structure for ultimate limit state and to check that the behaviour is satisfactory at working load.

The proposed direct design approach is based on the theory of plasticity and will be discussed in this chapter.

3.2 BRIEF REVIEW OF LIMIT STATE DESIGN BASED ON THE THEORY OF PLASTICITY

The plastic theory can be applied if the material properties exhibit perfectly

plastic response after yielding, e.g steel. The difficulty in applying plastic theory to reinforced concrete structure is that under different combination of stress, reinforced concrete members may not exhibit perfect plastic response. Therefore, it is possible that a collapse failure may occur in the concrete before yielding has redistributed the stresses. Practical considerations require the structure to have sufficient ductility so that redistribution of stress take place as cracking occurs. The plastic theory provides two different estimates of the ultimate load, an upper bound and a lower bound to the true ultimate load. The methods for determining these bounds are based on the following two theorems.

a) Lower Bound Theorem: If a stresses field can be found which in equilibrium with external forces and that the stresses do not exceed the limiting values for the members of the structure (ie, the yield stress of steel, and the compressive strength of concrete). Then the calculated load is less than or equal to the true collapse load.

b) Upper Bound Theorem: For an assumed system of "hinges", which transforms a structure into a mechanism, if the ultimate load is calculated on the basis of this mechanism using the principle virtual work, then the corresponding ultimate load is greater than or equal to the true collapse of the structure.

The upper bound value is on the unsafe side if the wrong mechanism is assumed, and the lower bound is on the safe side, but it may lead to an oversafe analysis or an uneconomic design.

Finally, the correct solution to the true ultimate load (which yield coincident upper and lower bound solution) should satisfy the conditions of classical plasticity, which are:

1) The Equilibriun Condition: The internal stresses must be in equilibrium with the externally applied loads.

2 The Mechanism Condition: Under the ultimate load, sufficient plastic hinges must exist to transform the structure into mechanism.

3) The yielding Criterion: The ultimate strength of the member must nowhere be exceeded.

3.3 DESIGN OF ORTHOGONAL REINFORCEMENT TO RESIST A GIVEN SET OF FORCES

The design of reinforcement for a given set of stresses has been studied extensively[20]. The design equations are established based on the following assumptions

− 1) The reinforcement is assumed to be symmetrically positioned with reference to the middle plane of the section in the two orthogonal directions as shown in Figure (3.5).

− 2) The reinforcement carries only uniaxial stress in its original direction.

− 3) The bar spacing is assumed to be small in comparison with the overall structure dimensions so that the reinforcement can be considered in terms of area per unit length rather than as individual bars.

− 4) The concrete is assumed to resist only compressive stress, and its tensile strength is neglected and exhibit the square yield criteria shown in Figure (3.3).

− 5) Steel is assumed to be perfectly plastic behaviour and to yield at stress of f_y in tension and f_y'.

3.3.1 Basic Theory

The present investigation is based on the classical theory of plasticity. The applied membrane forces N_x, N_y, N_{xy} acting on thin− walled concrete element of Figure (3.1) are equivalent to the sum of the stress resultants N_{xc}, N_{yc}, N_{xyc} of concrete and N_{sx}, N_{sy} of the reinforcement.

Hence,

$$\begin{cases} N_x = N_{xc} + N_{sx} \\ N_y = N_{yc} + N_{sy} \\ N_{xy} = N_{xyc} \end{cases} \quad (3.1)$$

a) Concrete

The principal concrete stresses are taken to be σ_1 and σ_2 with the major principal stress σ_1 at an angle θ to the x axis σ_1 is always greater than σ_2. All stresses are taken to be tension positive.

From Figure (3.6b) the concrete resistance is given by:

$$\begin{cases} N_{xc} = (\sigma_1 \cos^2\theta + \sigma_2 \sin^2\theta).t & (3.2a) \\ N_{yc} = (\sigma_1 \sin^2\theta + \sigma_2 \cos^2\theta).t & (3.2b) \\ N_{xyc} = [(\sigma_1 - \sigma_2).\cos\theta.\sin\theta].t & (3.2c) \end{cases}$$

b) Steel

From Figure (3.6c) the steel resistance in x and y direction is given as:

$$N_{sx} = A_x.f_x \quad (3.3a)$$

$$Nsy = A_y.f_y \quad (3.3b)$$

Where A_x and A_y represent the area of reinforcement per unit width in x and y, f_y and f_x their associated stresses, t is the thickness of the element.

Finally, by equating the applied stresses to combined resisting stresses, we have

$$\begin{cases} N_x = A_x f_x + \sigma_1.t.\cos^2\theta + \sigma_2.t.\sin^2\theta & (3.4a) \\ N_y = A_y f_y + \sigma_1.t.\sin^2\theta + \sigma_2.t.\cos^2\theta & (3.4b) \\ N_{xy} = (\sigma_1 - \sigma_2).t.\cos\theta.\sin\theta & (3.4c) \end{cases}$$

Let us consider the major principal stress σ_1 as tensile, since concrete cannot carry any tension. Therefore we set the value of $\sigma_1 = 0$.

Equations (3.4a) to (3.4c) give

$$\begin{cases} (N_x - N_{sx}) = \sigma_2 . t . \sin^2\theta & (3.5a) \\ (N_y - N_{sy}) = \sigma_2 . t . \cos^2\theta & (3.5b) \\ N_{xy} = -\sigma_2 . t . \cos\theta . \sin\theta & (3.5c) \end{cases}$$

Eliminating θ from (3.5a) to (3.5c)

$$(N_{sx} - N_x).(N_{sy} - N_{sy}) = N_{xy}^2 \qquad (3.6)$$

This equation represents the yield criterion for reinforced concrete element under in-plane loads. Nielsen based his design equations on the assumption that

$\sigma_2 < 0$ (ie: Compression)

$| \sigma_2 | < f_{cu}$, so that compression steel is never required. (ie: N_{sx} and N_{sy} are positive. From equations (3.5a) and (3.5b) the four different cases of reinforcement are established:

Case 1:

If $N_{sx} = 0$, $N_{sy} \neq 0$ Then $N_{sy} = (N_y - N^2_{xy}/N_x)$

$\sigma_2 . t . \sin^2\theta = N_x$, $-\sigma_2 . t . \sin\theta . \cos\theta = N_{xy}$, $\tan\theta = -N_x/N_{xy}$

$$\sigma_2 . t = -(N_x + N^2_{xy}/N_x) \qquad (3.7)$$

The concrete stress should not reach the compressive strength. If $\sigma_2 < -f_{cu}$, then the section should be redisigned with increased thickness t.

Case 2:

If $N_{sy} = 0$ and $N_{sx} \neq 0$ Then $N_{sx} = (N_x - N^2_{xy}/N_y)$

$\sigma_2.t.\cos^2\theta = N_y \qquad -\sigma_2.t\sin\theta.\cos\theta = N_{xy}, \quad \tan\theta = -N_{xy}/N_y$

$$\sigma_2.t = -\left(N_y + N^2_{xy}/N_y \right) \tag{3.8}$$

Case 3:

If N_{sx} and $N_{sy} \neq 0$. In this case we have to minimise the total quantity of steel $(N_{sx} + N_{sy})$. From the yield criterion given in equation (3.6)

$$N_{sy} = [\, N_y + N^2_{xy}/(N_{sx} - N_x)]$$

Therefore $N_{sx} + N_{sy} = N_{sx} + N^2_{xy}/(N_{sx} - N_x)$. Minimising the steel

$$\partial/\partial N_{sx} \left[N_{sx} + N_{sy} \right] = 0$$

$$\partial/\partial N_{sx} \left[N_{sx} + N_y + N^2_{xy}/(N_{sx} - N_x) \right] = 1 - \left[N^2_{xy}/(N_{sx} - N_x)^2 \right] = 0$$

Therefore

$$\{ N_{sx} - N_x \}^2 = \pm N_{xy}^2$$

so $N_{sx} - N_x = \pm |N_{xy}|$ as N_{sx} and $N_{sy} > 0$. Hence,

$$N_x - N_{sx} = -|N_{xy}| = \sigma_2.t.\sin^2\theta \tag{3.9}$$

$$N_y - N_{sy} = -|N_{xy}| = \sigma_2.t.\cos^2\theta \tag{3.10}$$

Finally

$$\sigma_2.t = -2|N_{xy}| \tag{3.11}$$

Case 4:

N_{sx} and N_{sy} are both equal to zero then $N_x.N_y = N^2_{xy}$

The principal stresses σ_1 and σ_2 are compressive. Thus no steel reinforcement is required

The principal stresses σ_1 and σ_2 are given by

$$\left.\begin{matrix}\sigma_1.t \\ \\ \sigma_2.t\end{matrix}\right\} = \frac{(N_x + N_y)}{2} \pm \left[\frac{(N_x - N_y)^2}{4} + N_{xy}^2 \right]^{\frac{1}{2}} \qquad (3.12)$$

According to Nielsen's design assumptions, compressive steel is not required. Nevertheless, in certain conditions, compression reinforcement is required in one or both directions. Thus, reinforcement can either be in tension, compression or no reinforcement required. Table (3.1) shows the possible combinations of reinforcement. For in-plane forces Nielsen[20] presented yield criteria for section having orthogonal reinforcement in tension only. This approach has been extended by Clark[21] to cover the possibility that compression reinforcement or skew reinforcement. Figure (3.1) summarises the four possible combinations from the 2-D situation, originally proposed by Nielsen. Finally having devided the relevant equations to each of the four cases considered in our study we define the minimum reinforcement required to each case.

3.4 PROPOSED ULTIMATE LIMIT STATE DIRECT DESIGN APPROACH

The equations derived in the previous section provide the optimum reinforcement to resist predetermined stress field for reinforced concrete structures.

One simply needs to calculate the predetermined stress field at the ultimate design load. This approach used in the present study called " Direct design method " is simple and straigth forward to apply and satisfies the three conditions of the theory of plasticity as follows.

3.4.1 The equilibrium condition

The equilibrium criterion specifies that the internal stresses must be in equilibrium with external loads. Elastic state of stress is defined under ultimate load. For complex structure, the elastic stress analysis is obtained by finite element method. Any other stress field in equilibrium can also be used but elastic stress field is the simplest to calculate.

3.4.2 The yield criterion

This condition defines the relationship between the " strength " and applied stress necessary to cause plastic flow at any point in the structure. Since the reinforcement for the given stresses is designed based on the yield criterion, the assumed stress does not violate the yield criterion.

3.4.3 Mechanism condition

The structure should develop sufficient plastic region to cause collapse at ultimate design load and is automatically satisfied because all parts of the structure will attain their ultimate strength under the design load since the reinforcement at each point has calculated so as to satisfy the yield criterion. Reinforced concrete has limited ductility. Therefore, a collapse in the concrete may occur before yielding has redistributed the stresses. This situation is overcomed by reducing the ductility demand. In order to achive a minimum redistribution such that most of the critical sections of the structure which yielded early are minimised.

3.5 APPLICATION OF THE DIRECT DESIGN METHOD TO PRESTRESSED MEMBERS

Our interest is to extend the above approach for reinforced concrete members to cover members partially prestressed along the axis. The object of this study is to investigate the applicability of the direct design procedure to partially prestressed beams subjected to combined action of bending and torsion. The optimum designs will be used as basis for designing the experimental models. In this investigation, we considered the combined action of bending and torsion, and effective prestress (ie: the amount of applied prestress after losses). The applied stresses are: N_x, N_y, N_{xy} and N_{px}, is the effective prestress along longitudinal axis parallel to x axis. where. The yield criteria is then given by:

$$[\ N_{sx} - (N_x+N_{px})\ ].(N_{sy}-N_y) - N_{xy}^2 = 0 \qquad (3.13)$$

The aim of this approach is to demonstrate how to use the unused part of prestressed steel as ordinary steel. In the case of combination of prestressing steel and ordinary steel it must be stipulated that both prestressing and ordinary steel should reach their yield stress at ultimate load. To ensure the simultaneous yielding prestressing steel tensioned to their normal effective stress f_{pe}. The prestressing steel is assumed to have an " effective " yield stress as:

$$f_{px} = (\ f_{pu} - f_{pe}\ ) \qquad (3.14)$$

Where f_{px} : Assumed yield stress of prestressing steel.

f_{pu} : Yield stress of prestressing steel

f_{pe} : Effective prestress

This is also illustrated in Figure (3.4a) and (3.4b) where the stress– strain curve of both steels are superposed to each other. The prestress is treated as an applied external force. The amount of prestressing present at each section can therefore be replaced by ordinary steel with an equivalent yield stress ($f_{pu} - f_{pe}$) and in accordance with Nielsen's design equations the required area of steel to resist the applied stresses is determined as:

$$\text{Total } A_x f_x = \underset{\text{of ordinary steel}}{\text{Quantity}} + \underset{\text{steel as ordinary steel.}}{\text{Equivalent area of Prestressing}} \qquad (3.15)$$

3.5.1 Computer program

The above design procedure is easily automated as follows in a simple program. For a given geometrical and mechanical properties of concrete, prestressing steel and prestress level and given volumes of moment and torsion.

– 1) Choose a number of section in beam as in Fig (3.8)

– 2) Evaluate at each section the flexural and shear stresses (σ_x, σ_y, τ_{xy})

– 3) Determine the effective prestress (σ_p)

– 4) Calculate the final state of stresses ($\sigma_x + \sigma_p$), σ_y, τ_{xy} at each section

– 5) Calculate the corresponding ($\sigma_x + \sigma_p$)/ $|\tau_{xy}|$ and $\sigma_y / |\tau_{xy}|$

– 6) Choose the right case for which the above expressions fulfill the approximate conditions, as shown in Figure (3.7)
Determine the steel areas in X and Y directions.

– 7) Determine the unused part of prestressing steel as ordinary reinforcing steel with the assumed yield stress f_{px}.

– 8) Calculate the principal concrete stresses.

– 9) Finally, Deduce the optimum amount of ordinary steel in each direction.

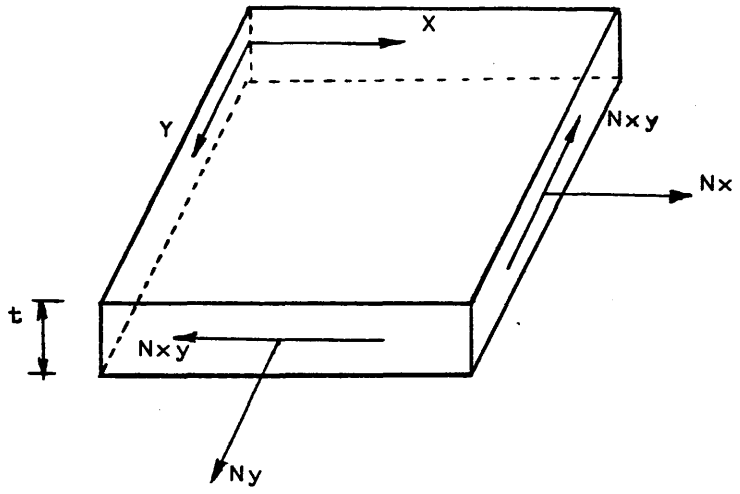

Figure(3.1) Element Under In-Plane Loading.

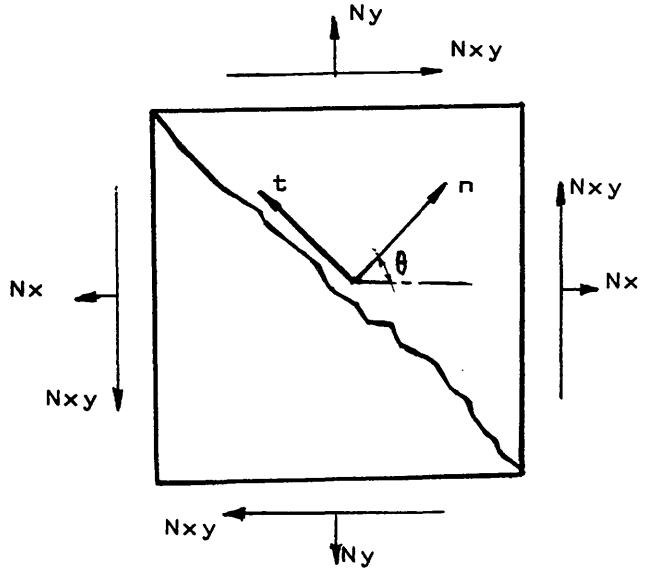

Figure(3.2) In-Plane Direct and Shear stress
On Element

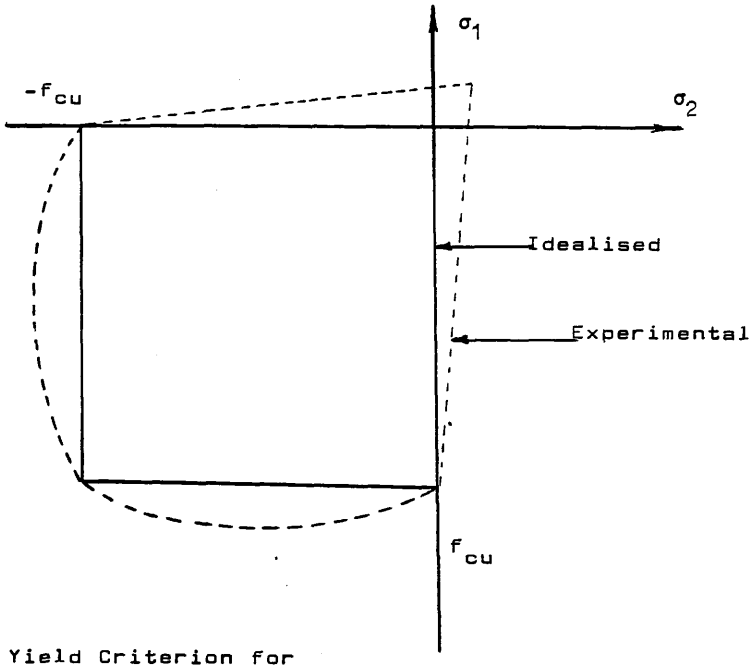

Figure(3.3) Yield Criterion for Concrete in Plane-Stress

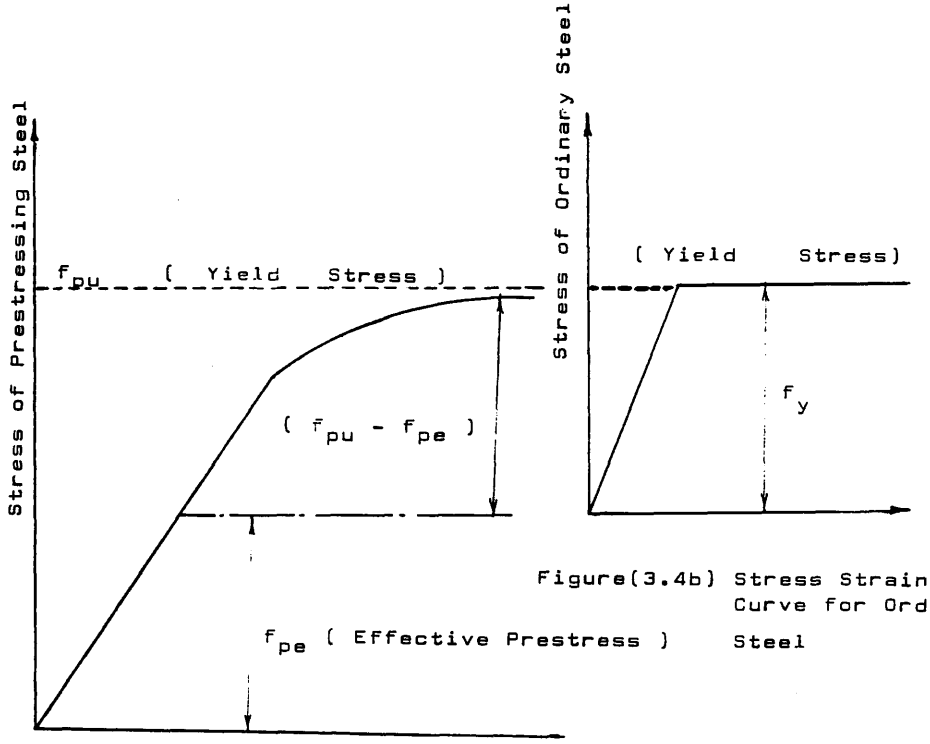

Figure(3.4b) Stress Strain Curve for Ord Steel

Figure(3.4a) Stress Strain Curve for Prestressing Steel.

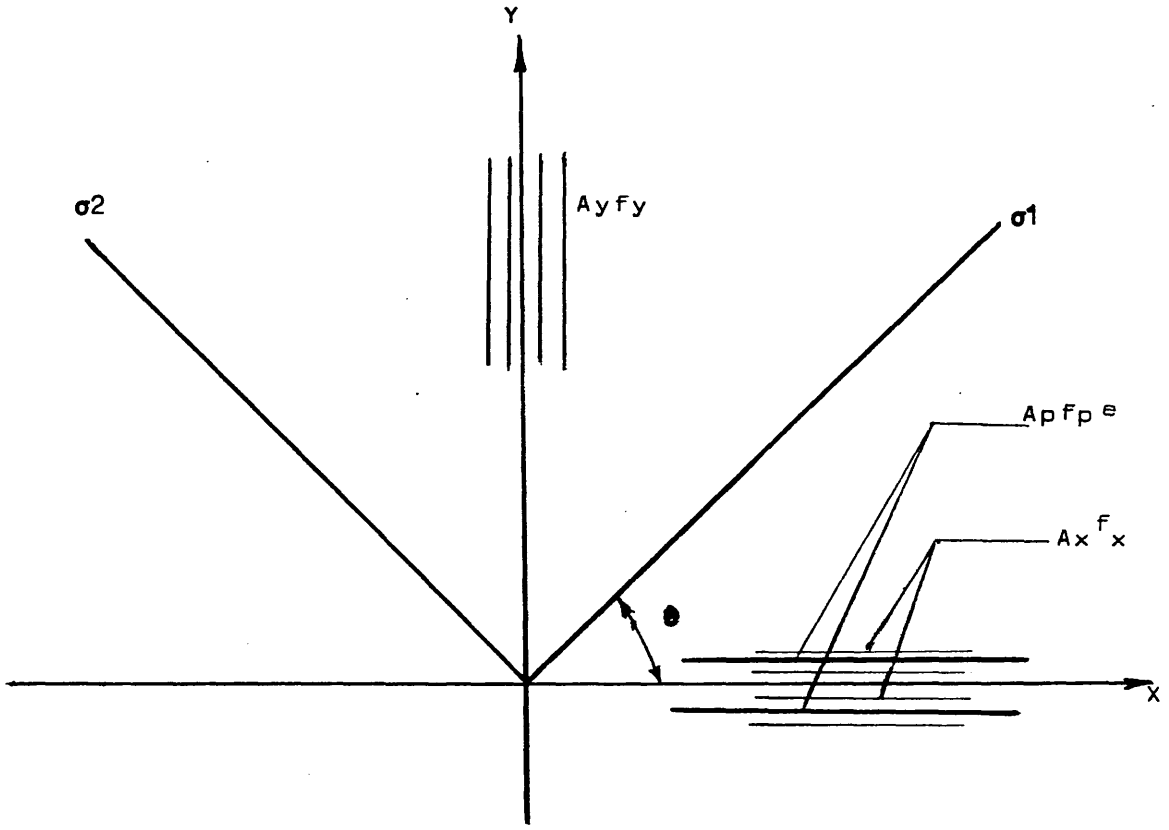

Figure(3.5) Direction of Reinforcing Steel and Principal Stress in Concrete.

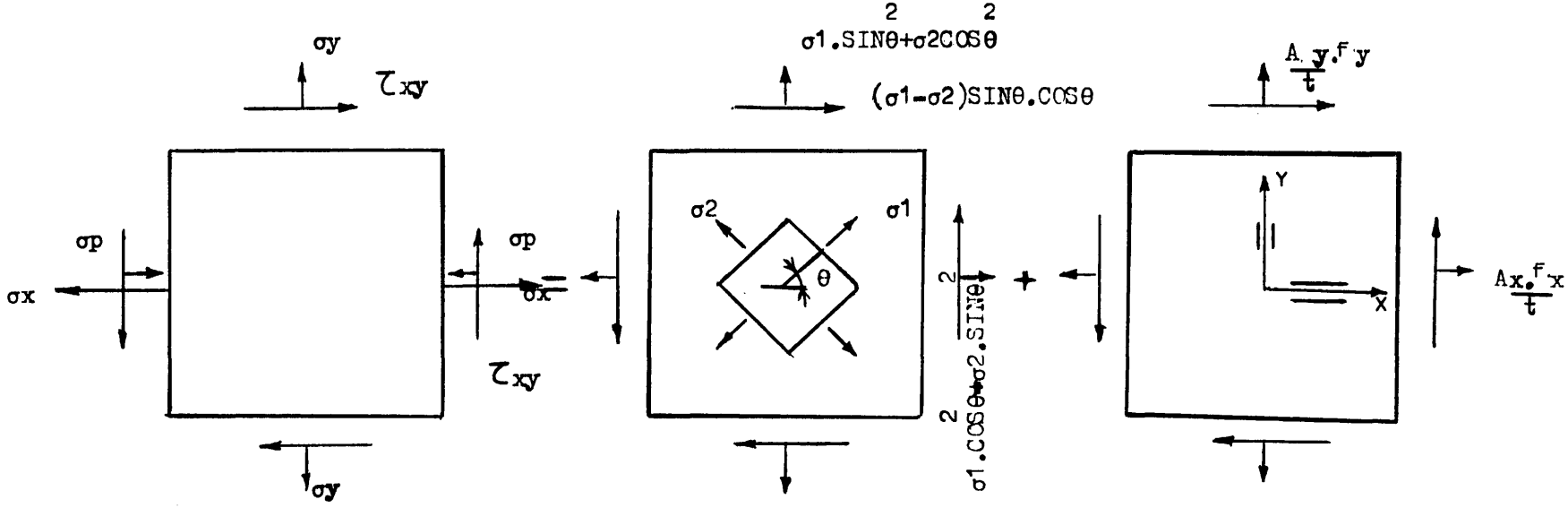

a) Applied Stress b) Concrete Resistance c) Steel Resistance

Figure(3.6) Equilibrum of Element under In-Plane Forces.

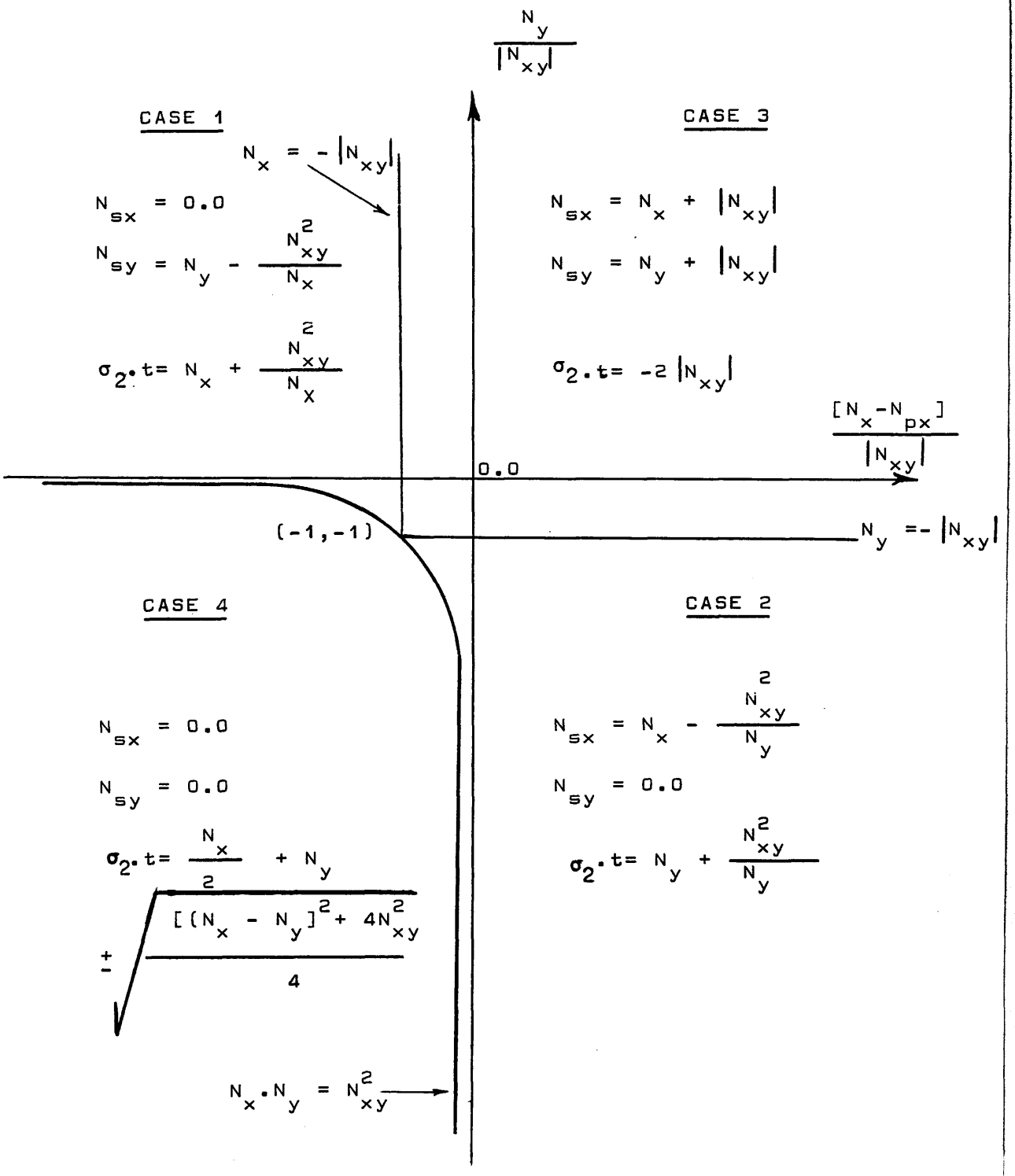

Figure(3.7) Graphical Representation of the four cases of Reinforcement.

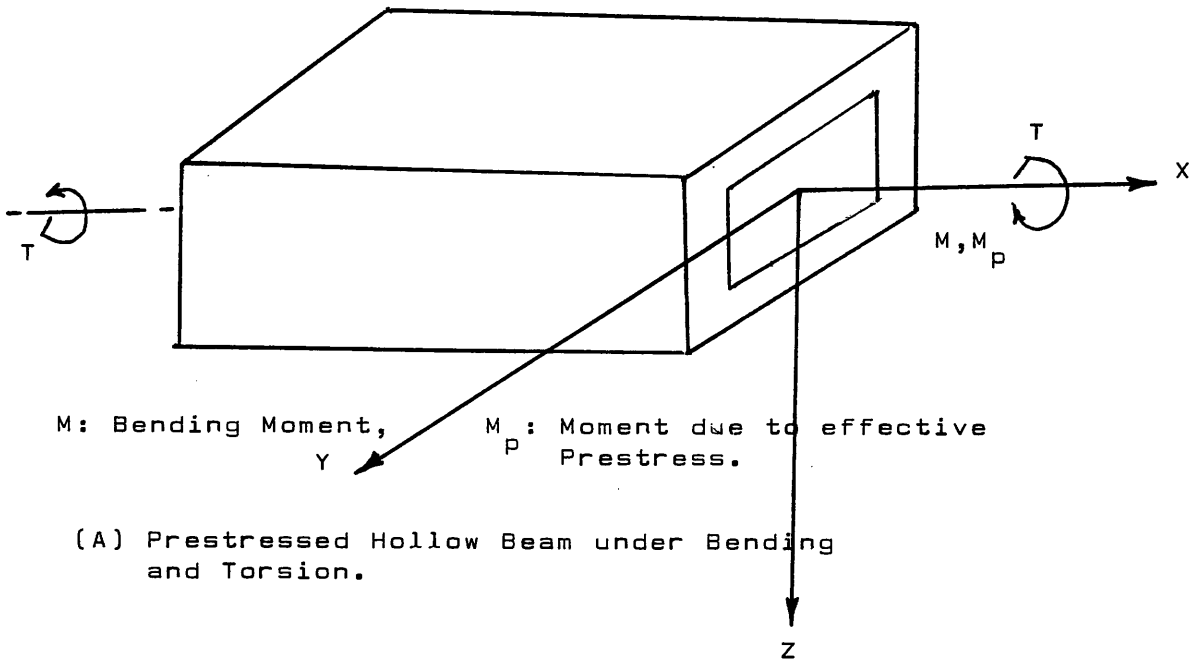

M: Bending Moment, M_p: Moment due to effective Prestress.

(A) Prestressed Hollow Beam under Bending and Torsion.

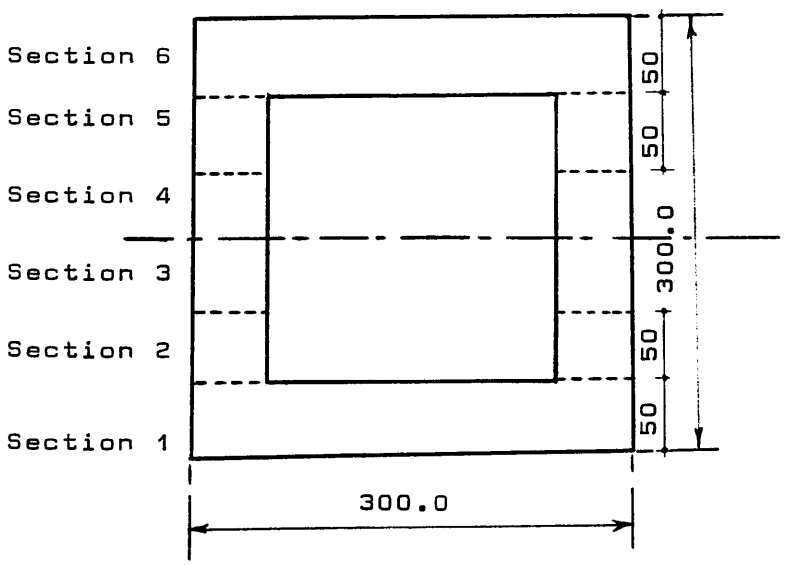

(B) Cross section divided into a series of sections

Figure(3.8) Representation of a series of section for the determination of the total steel area.

Table 3.1 – Summary of possible combination of reinforcement

case	Reinforcement	Known values	Method of solution
1	zero x,y tension	$f_y=f_s$; $f_x=0$ $\sigma_1 = 0$	Direct solution
2	zero y,x tension	$f_x=f_s$; $f_y=0$	Direct solution
3	x and y tension	$f_x=f_y=f_s$ $\sigma_1 = 0$	Minimisation of $(A_x + A_y)$
4	No reinforcement	$f_x=f_y=0$	Direct solution
5	zero x, y compression	$f_x=f_y'$; $f_x=0$; $\sigma_2 = f_{cu}$	Direct solution
6	zero y, x compression	$f_x=f_s'$; $f_y=0$; $\sigma_2 = f_{cu}$	Direct solution
7	x tension, y compression	$f_x=f_s$; $f_y=f_s'$ $\sigma_1=0$; $\sigma_2=f_{cu}$	Direct solution
8	y tension, x compression	$f_x=f_s'$; $f_y=f_s$ $\sigma_1=0$; $\sigma_2=f_{cu}$	Direct solution
9	No reinforcement	$f_x=f_y=f_s'$ $\sigma_2 = f_{cu}$	Minimisation of $(A_x + A_y)$

CHAPTER FOUR

EXPERIMENTAL INVESTIGATION

4.1 INTRODUCTION

This chapter describes in detail the experimental set up used to study the behaviour of partially prestressed hollow beams subjected to combined torsion and bending loadings.

The investigation of the beams was carried out to study the following aspects of:

- a) Load deflection relationship
- b) Torque– rate of twist relationship
- c) Crack pattern and crack propagation
- d) Ordinary and prestressing steel response
- e) Failure loads and failure characteristics

4.2 DESCRIPTION OF TESTING FRAME

4.2.1 General description

A three dimensional steel test– rig, shown in Figure (4.1) was designed to allow for the independant application of torsion and bending moment. Bending moment was applied by means of a hydraulic jack fixed to the main frame. Load was transfered to the model through a secondary steel beam mounted on the model by means of support bearings.

Details are shown in Figure (4.1). The rig can accommodate specimens of any cross section as long as their ends are rectangular in shape.

Torsion was applied independently through torsional arms fixed to each end of the model.

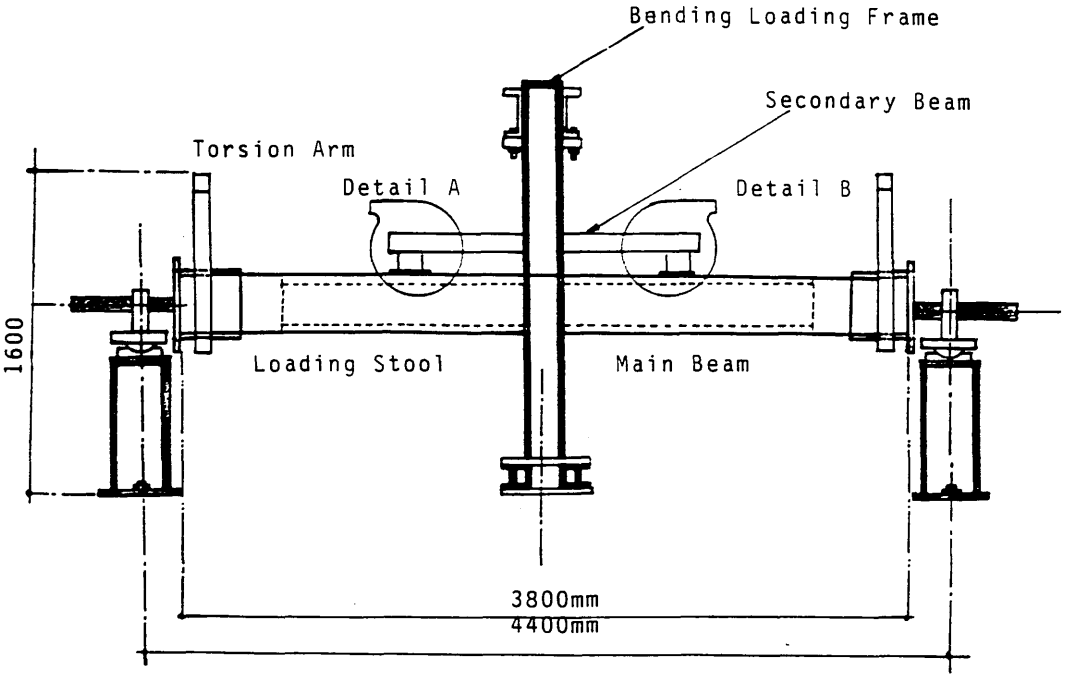

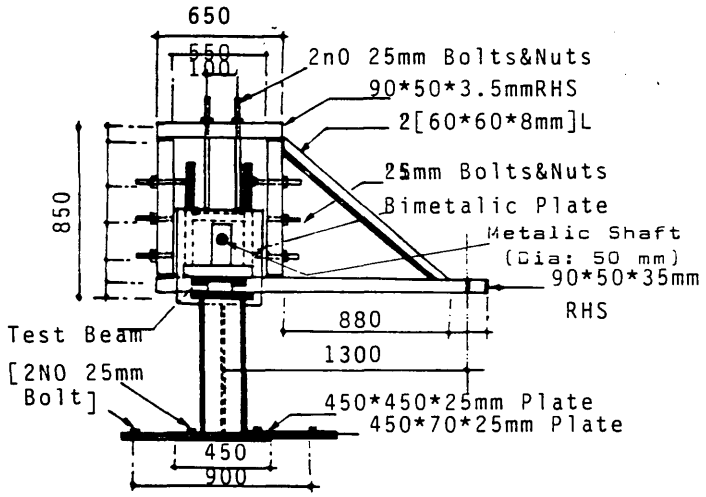

-Torsion Loading Arm--

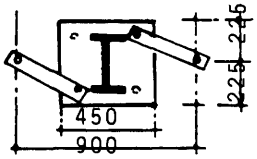

-Base Plan--

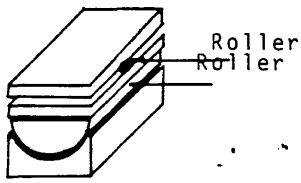

-Detail A-

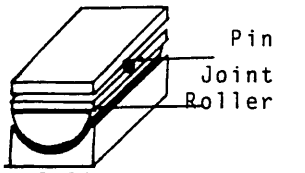

-Detail B-

Figure(4.1) Experimental Testing Frame And Details

4.2.2 Fixity of end boxes

The beam was fitted with a box at each end as shown in detail (c) of Figure (4.1) which consists of a supporting system composed of ((400,300)X500X25) mm steel plates fixed to the front plate to form a rectangular box. Top and side plates could be adjusted to fit the cross section of the specimen. No displacement or rotation of the plate is allowed. A 50 mm steel shaft is fixed to the front plate allowing for free rotation of the whole system about the longitudinal axis of the specimen.

This end box as shown in detail (c) can accommodate up to 500X400 rectangular sections. The cross sectional size of the tested beams was (300X300) mm.

Finally, the model once fitted with end boxes was mounted on two steel stanchion stools firmly fixed to the laboratory floor.

4.2.3 Installation of the specimen

The total length of a specimen was fixed at 3800 mm. The installation of the specimen involves the following steps:

(1) Placing the specimen horizontally in position

(2) Placing the torsional arm at each end of the specimen

(3) Fitting the specimen with an end box at each end
as shown in detail (c).

(4) Mounting the secondary beam on the set of bearing
allowing for axial movement and free rotation.

(5) Placing the hydraulic jacks

(6) Final checking of bolting all around the end boxes
to ensure transmission of the applied torque to the specimen

(7) Connecting the load cells, transducers and strain gauges
to the data− logger for continuous measurements.

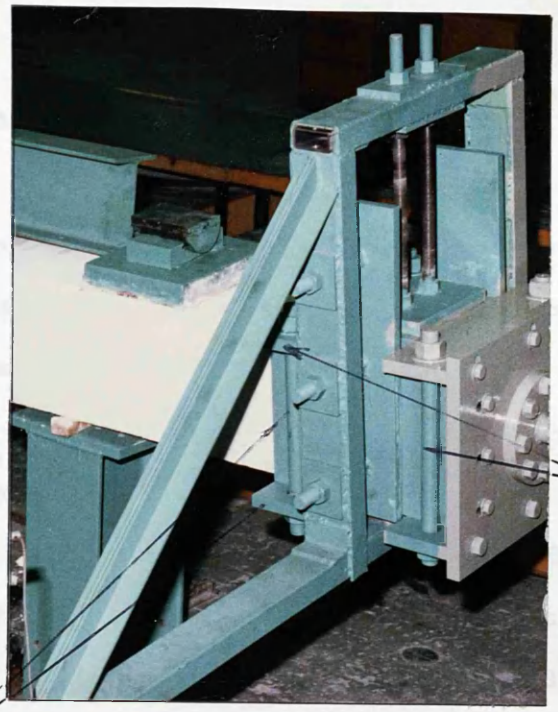

Detail C

View of a specimen fitted with an end box at its end.

50 mm Vertical Bolts to ensure a complete fixity of end box.

300x500x25 mm plate composing the end box.

Adjustable top and side plate of the end box

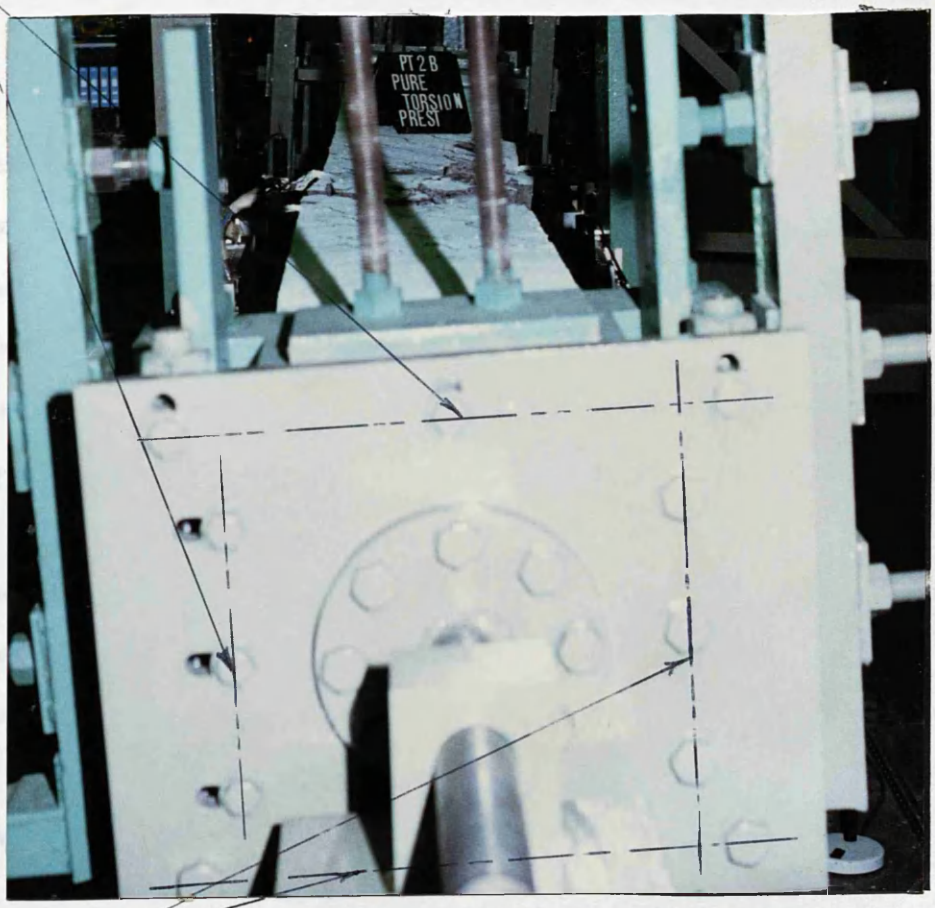

Fully fixed bottom and side plate to the front plate of the end box

4.3 INSTRUMENTATION

All specimens were instrumented to measure the applied loads (bending and torsion), lateral and longitudinal displacement, concrete, ordinary and prestressing steel strains and crack width.

4.3.1 Measurement of the applied loads

The loads were applied using a set of three 200 KN hydraulic jacks. Loads were measured by means of load cells of 100 KN capacity. The applied torque was equal to the reaction times the lever arm of length 1.30 m.

Experimentally, however, the two reactions were slightly different. The applied torque was taken as the average of the two load cells reading.

Figure (4.2) shows the loading arrangement for beams under combined torsion and bending.

4.3.2 Measurement of the angle of rotation

In order to obtain the angle of rotation, vertical displacement were measured at various point within the test span (1200) mm by means of linear voltage displacement transducer (LVDT).

Three transducers were located along the horizontal centreline of beam on both webs shown in Figure (4.3). Each pair of transducers was placed on the opposite side to

each other so that the angle of rotation is equal to the difference of vertical displacement divided by the respective horizontal distance between them.

It is assumed that the sides of the section remain undistorted as shown in Figure (4.4).

This allows the following relationships to be derived using similarity of triangles.

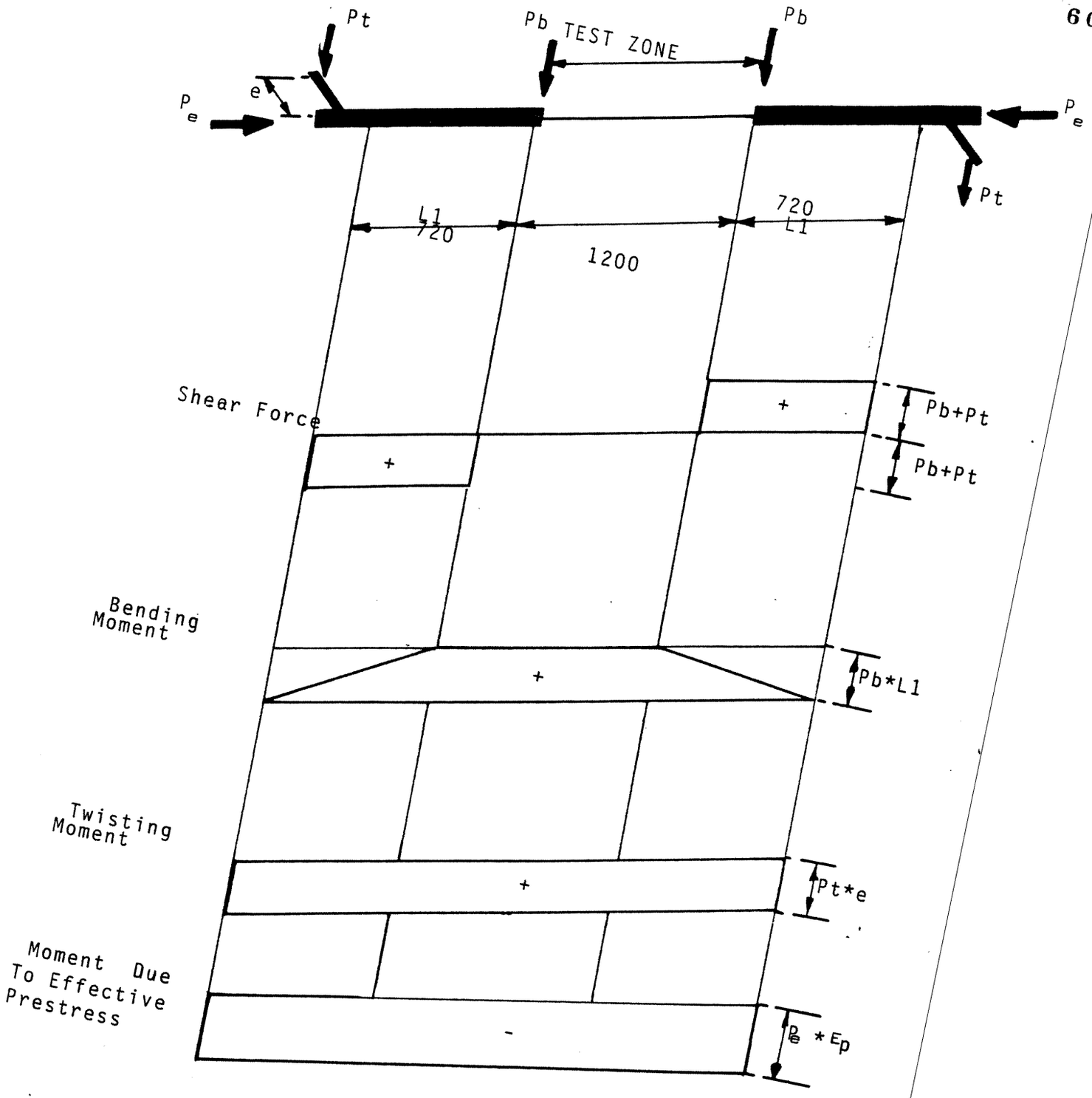

Figure(4.2) Loading Arrangement For Prestressed Beams Under Torsion And Bending.

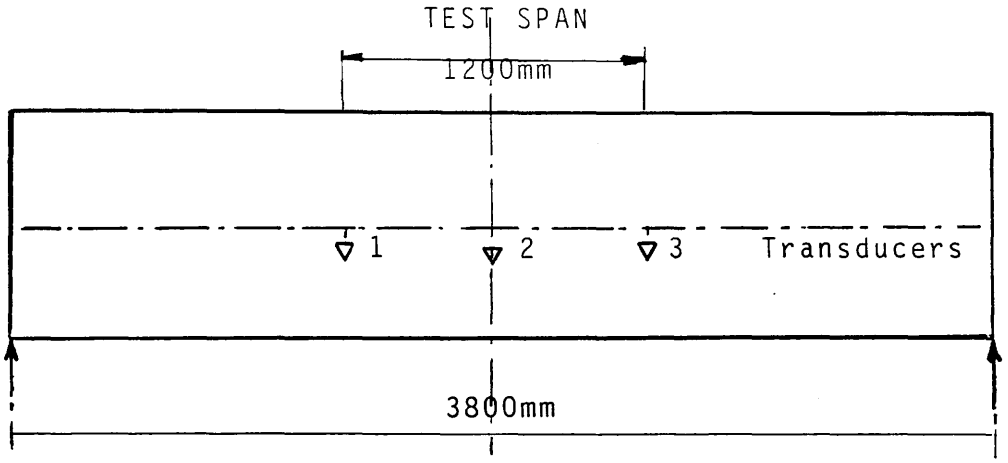

a)- Front Web

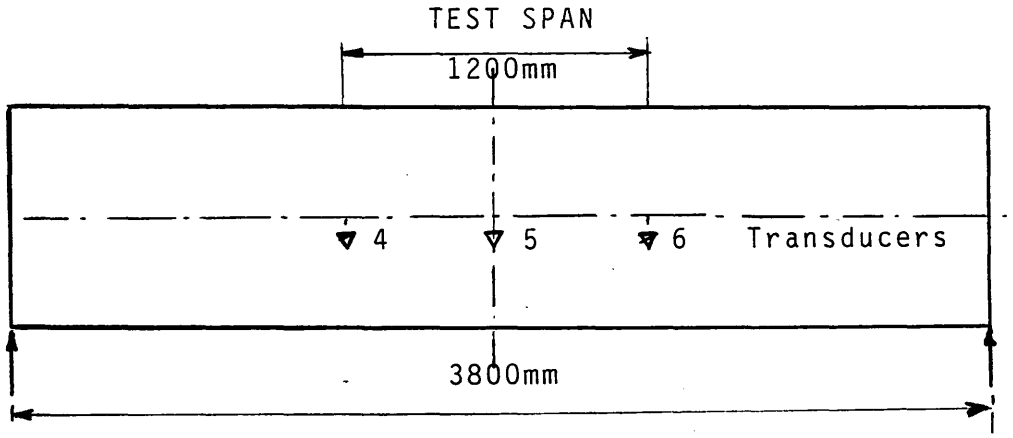

b)- Back Web

Figure(4.3) Transducers Locations On Webs Of Beams.

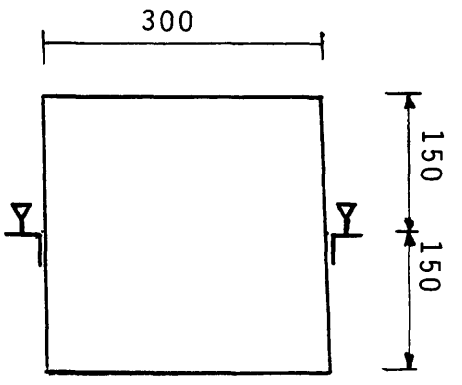

c)- Arrangement Of Transducers

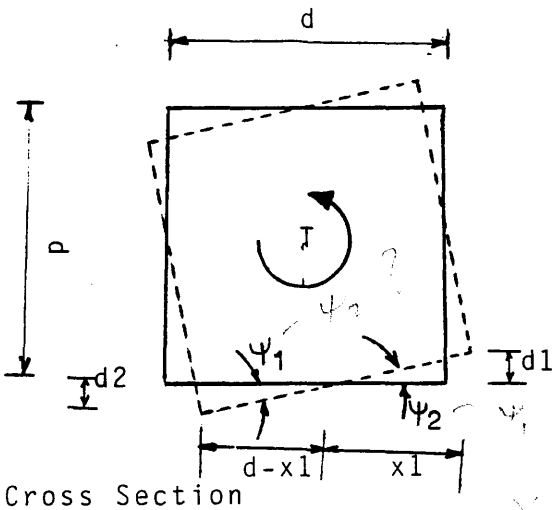

Figure(4.4) Assumed Rotation Of Cross Section
For Evaluation Of Angles Of Rotation

$\tan\psi_1 = d_1/x_1$ $\quad\quad$ $\tan\psi_2 = d_2/(d-x_1)$

$\tan\psi_1 = \tan\psi_2$ $\quad$ Hence $d_1/x_1 = d_2/(d-x_1)$

$$x_1 = d_1.d/[d_1 + d_2] \quad (4.1)$$

$$\tan\psi_1 = (d_1+d_2)/d \quad \psi_1 = \tan^{-1}[(d_1+d_2)/d] \quad (4.2)$$

4.3.3 Measurement of flexural displacement

To enable measurement of vertical displacements, transducers were fixed on a secondary frame located at midspan of beam and at 600 mm from the centreline of the beam as shown in figure (4.5). All measurement were taken at the bottom of the beam.

4.3.4 Measurement of ordinary and prestressing steel strains

Strain in steel was measured by means of 6 mm long electrical resistance strain gauge connected to a linear voltage processing data logger (type Orion A). The preparation of the strain gauge installation area required the surface to be filed and smoothened with sand paper. The contact surface was treated with M– prep conditioner. However the contact surface of the prestressing strand was covered with a stiff paste to obtain the appropriate surface in order to cement the strain gauges. Once dry the contact surface was treated with M– Prep conditionner and M– Prep neutraliser to remove dirt.

To measure strain in all bars, a pair of strain gauges was fixed on directly opposite faces of the bar. The strain on the bar at each stage was taken as the average reading of both gauges.

4.3.5 Measurement of concrete surface strains

Demec gauges were used for measuring concrete surface strains over a gauge

length of 100 mm. This gauge length was assumed to be sufficiently long to include several cracks. Figure (4.6) shows the section at which horizontal and vertical strain were measured on all faces of beam within the test span. The torsional cracking was expected to form at approximately 45^0 with the axis . Therefore, the pair of demec gauges oriented at 45^0 and parallel to the crack direction was intended to measure the compressive strain while the pair normal to the crack measured the " tensile strain". or crack opening displacement.

4.3.6 Measurement of crack width

Crack width was measured by means of a hand held crack width measuring microscope measuring to 0.02 mm. Cracks were selected covering all faces of the model, their widths were measured at each load increment. Angle of cracks on the faces of the specimens were recorded and the crack patterns were followed from the first stages up to failure and clearly marked.

4.4 MATERIALS USED

4.4.1 Concrete

The concrete mix consisted of rapid hardening portland cement (R.H.P.C), 10 mm Hyndford gravels and zone 2 Hyndford sand obtained from Lanarkshire. A mix proportion of 1:1.5:3 was designed for an average cube strength of 50 N/mm^2 at seven days. A minimum slump of 100 mm was specified for the mix. Six cubes of size 100 mm and at least four cylinders of size (150mm X 300mm) were cast with each specimen. The cubes were used to determine the cubes strength, two cylinders were used for the determination of split tensile strength and the other two for the determination of Young's modulus according to the British standard BS 18, part 1. Figure (4.7) shows a typical concrete stress– strain curve.

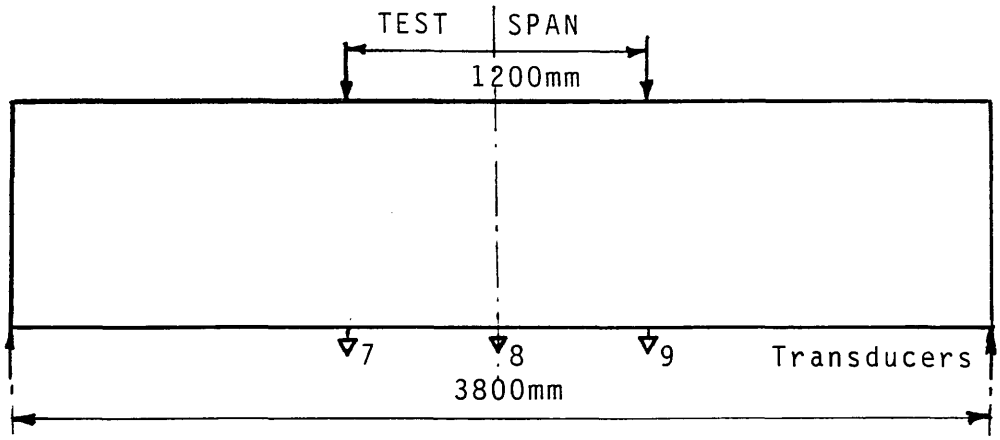

a)-Bottom Flange

Figure(4.5) Transducers Locations On Bottom Flange For Evaluation Of Vertical Displacements

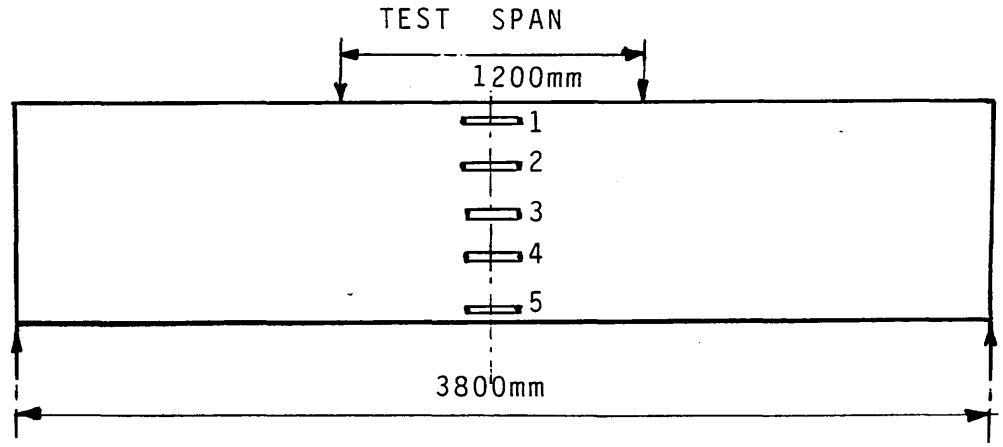

b)-Top Flange

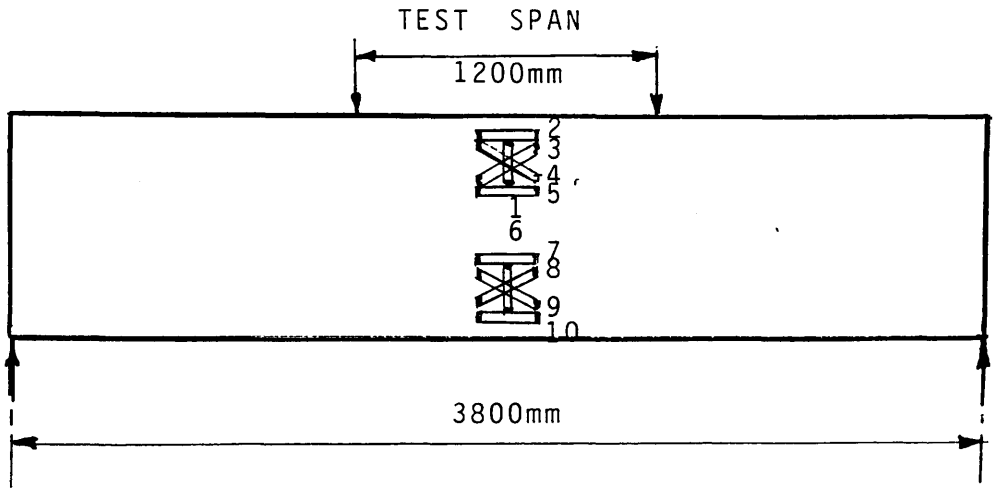

c) Front And Back Web

Figure(4.6) Location Of Demec Gauges On The Concrete Surface Of Flange And Webs Of Beams

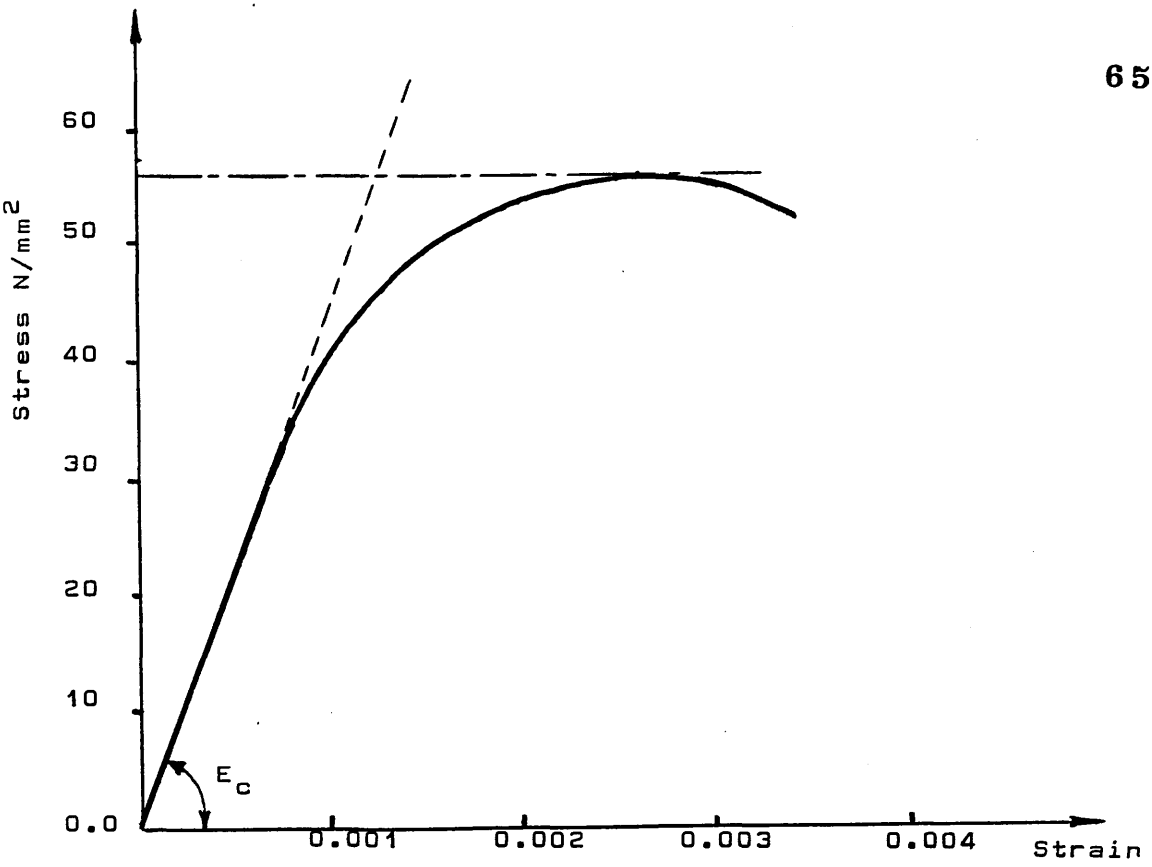

Figure(4.7) Typical Concrete Stress Strain Curve.

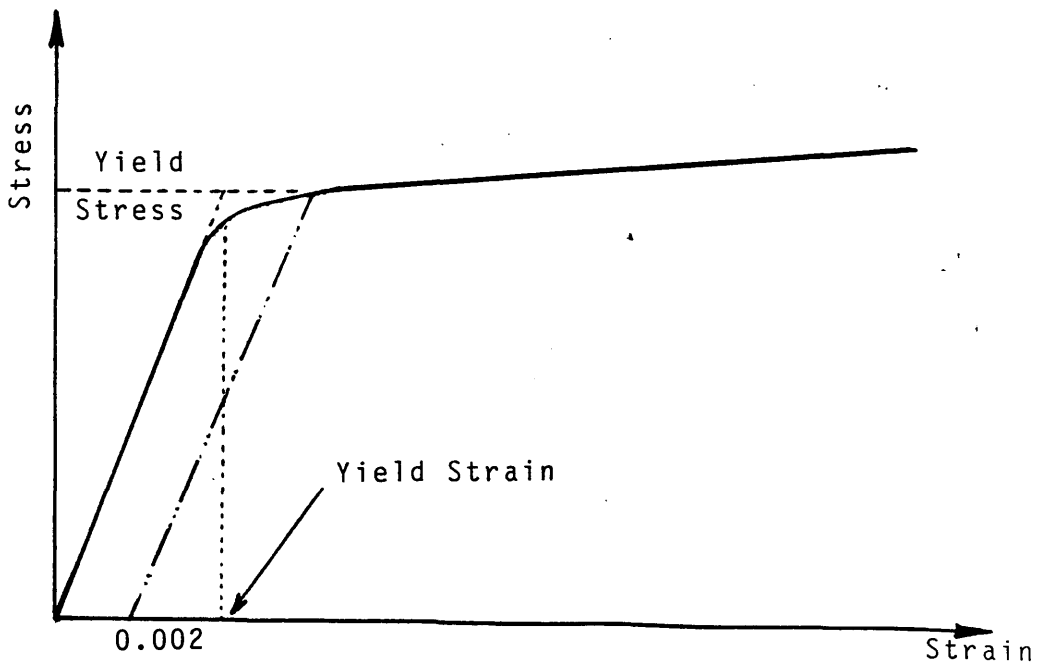

Figure(4.8) Definitions Of Yield Stress And Strain Of Steel Reinforcement.

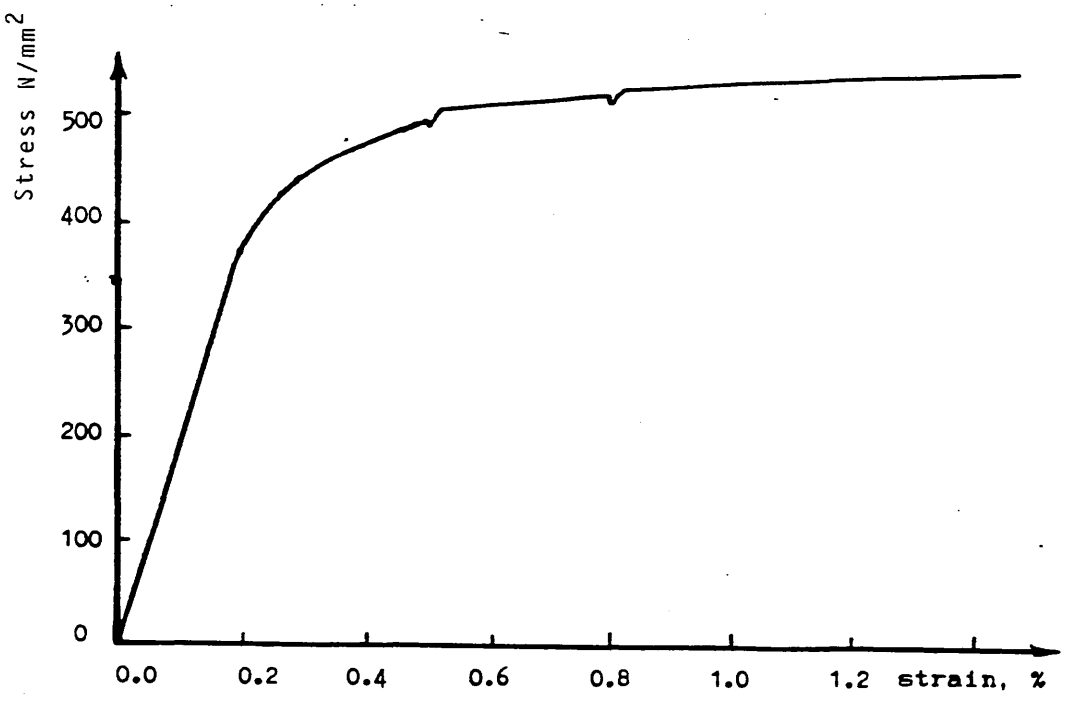

Figure(4.9) Typical Stress-Strain Curve For a Bar Of 08mm Diameter.

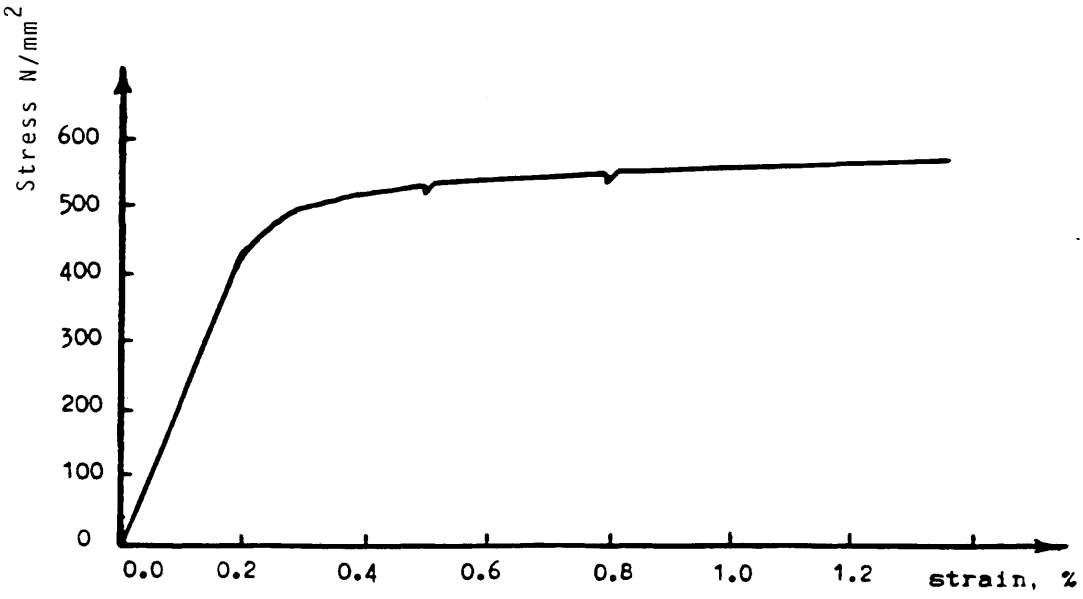

Figure(4.10) Typical Stress-Strain Curve For a Bar Of 10mm Diameter

4.4.2 Ordinary reinforcing steel

High yield steel deformed bars of diameter 8 and 10 mm were used as reinforcement. Typical stress– strain curves for each diameter obtained from the testing machine are presented in Figures (4.9) and (4.10). The yield point for all the bars was not well defined (see details in Figure (4.8)). The yield stress was taken as the stress corresponding to 0.2% proof strain. Table (4.1a) shows the properties for all the bars used.

4.4.3 Prestressing steel

The prestressing steel was 5 mm diameter high tensile steel wires. At a latter stage 8 mm strands were used to allow for high amount of prestress.
Figures (4.11a) and (4.11b) show the stress– strain behaviour while Table (4.1b) give the properties of a typical batch of each type.

4.5 PROPERTIES OF THE SPECIMENS

4.5.1 Strain gauging

Figure (4.12a) shows various measurement devices In order to record the strains in steel. Two stirrups nearest to midspan were strain gauged as shown in Figure (4.12b). For the longitudinal bars, strain gauges were positioned also at midspan. Once the selection of positions established. The strain gauges are fixed at these chosen positions.

4.5.2 Reinforcing cage and formwork

The formwork was made up of two parts, an open external box and a polystyrene block of dimension (200X200X2640mm). The open external box was made up of 20 mm thick plywood strengthened by 50X50 mm horizontal and vertical battens. The overall length of all models was 3800 mm. Figure (4.13) shows the

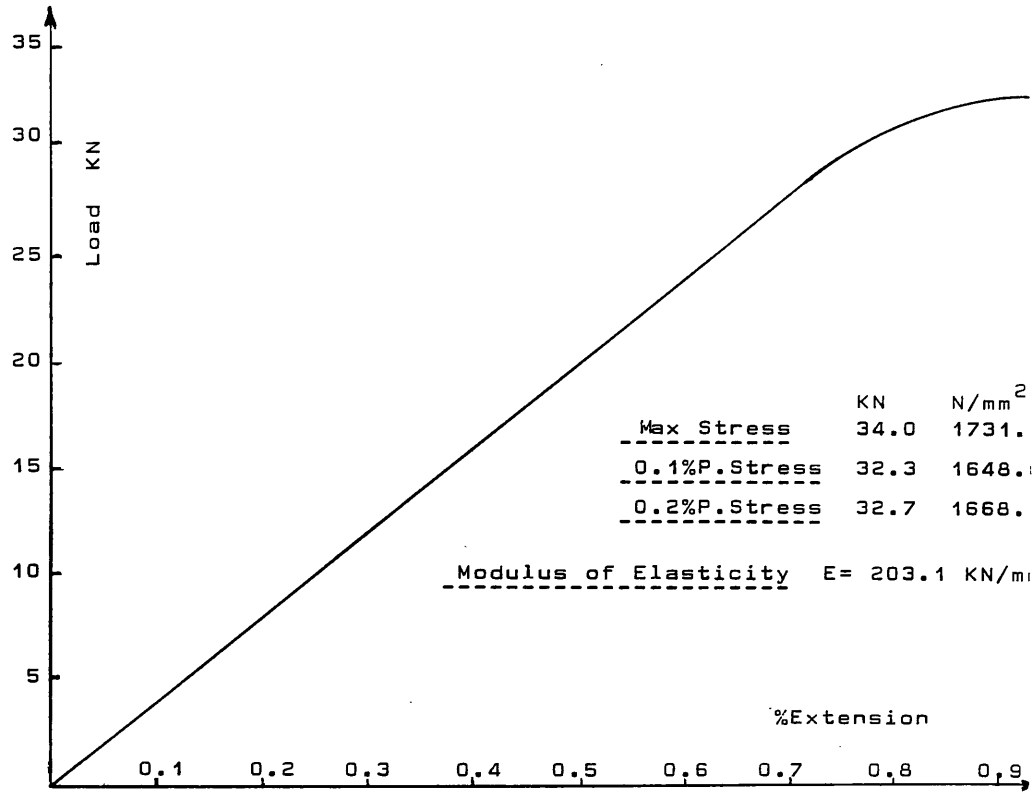

Figure(4.11a) Typical Stress-Strain Curve for a 5 mm Prestressing Wire.

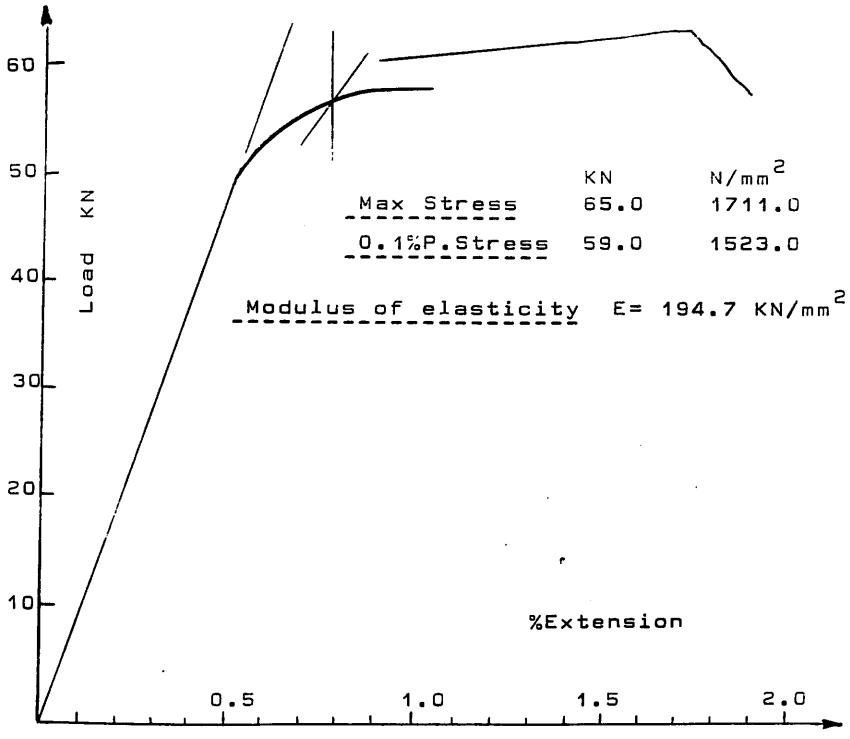

Figure(4.11b) Typical Stress-Strain Curve for 8 mm Strand.

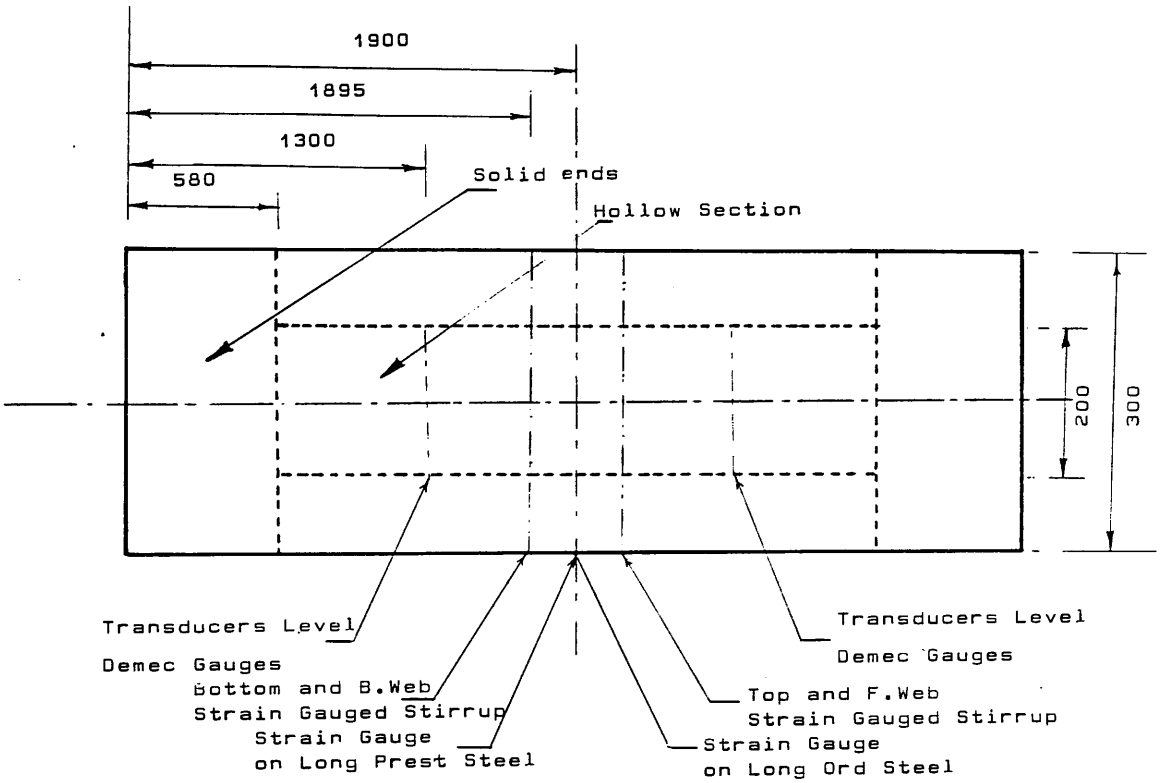

Figure(4.12a) Specimen Showing Various Measurement Devices.

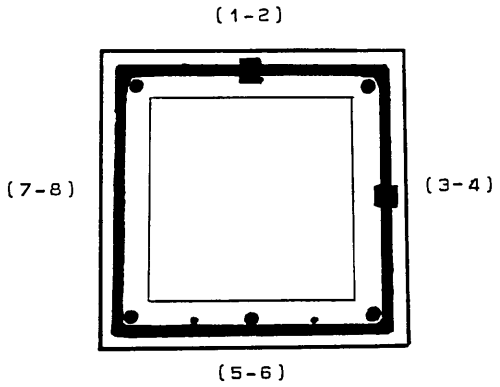

Figure(4.12b) Location of Stirrup Strain Gauges at Midspan.

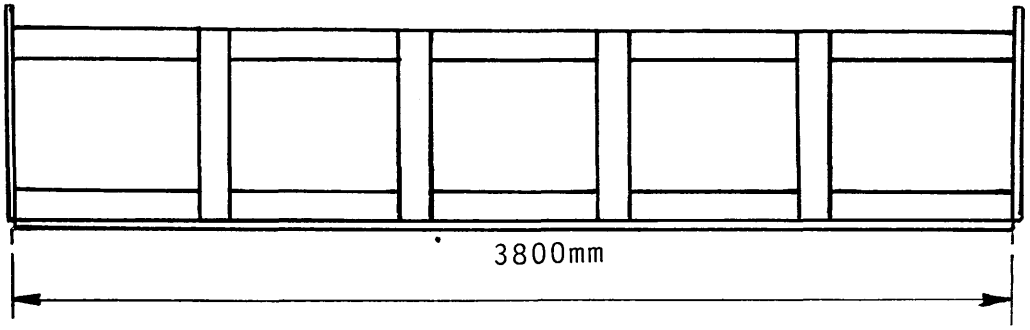

a)- Elevation Of Formwork

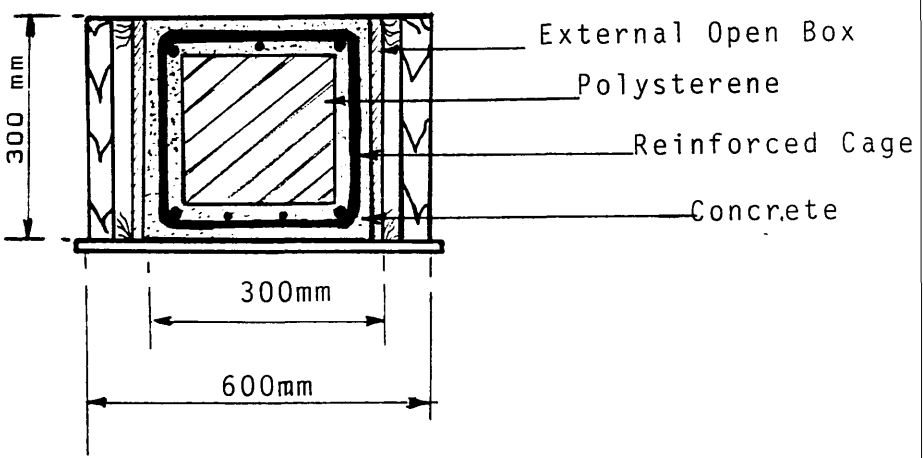

b)-Cross-Section Of Formwork

Figure(4.13) Typical Formwork For Models

details of the formwork. The preparation of the formwork consists of placing the polysterene block inside the reinforcing cage and to insert them into the open external box already coated with demoulding grease. Care was taken to maintain space in position. Once the end pieces of the open box were screwed the formwork was ready for casting. In order to avoid local failure the ends of beam (580 mm in distance) were heavily reinforced and filled solid with concrete.

4.5.3 Tensioning apparatus

Two alternative tensioning devices were employed, one for the wires and the other for the strands. For the wires a hand controlled P.S.C monowire jack operated by hydraulic pump with a delivery pressure of 70 N/mm^2 was used. A CCL 100 KN jack was used to stress the 8 mm strand. Figures (4.14a) and (4.14b) show the two tensioning devices. The prestressing wires were passed through the bearing plates of the prestressing frame and the end plates of the forms, the former provided the reaction for the tensioning force. The anchorage was provided by the use of split– wedge and barrel– type anchor grips. Before tensioning, the wires were cleaned to be free from loose rust and dirt.

4.5.4 Tensioning process

The distance between the outer faces of the bearing plates was approximately 7.3 m. All the tendons were straight and stressed individually. The stress in each tendon was increased at a gradual and steady rate. The tendons were overstressed by about 5% for two minutes to reduce stress– loss due to relaxation of the prestressing steel. Then the stress was reduced to the required level and the tendon was anchored. After the anchorage of the tendon, the force exerted by the tensioning apparatus was decreased gradually to avoid any shock to the tendon or anchorage. The prestressing force applied was checked by strain measurement on the wires and also by means of 203 Demec gauge readings on collars attached to the wires. the

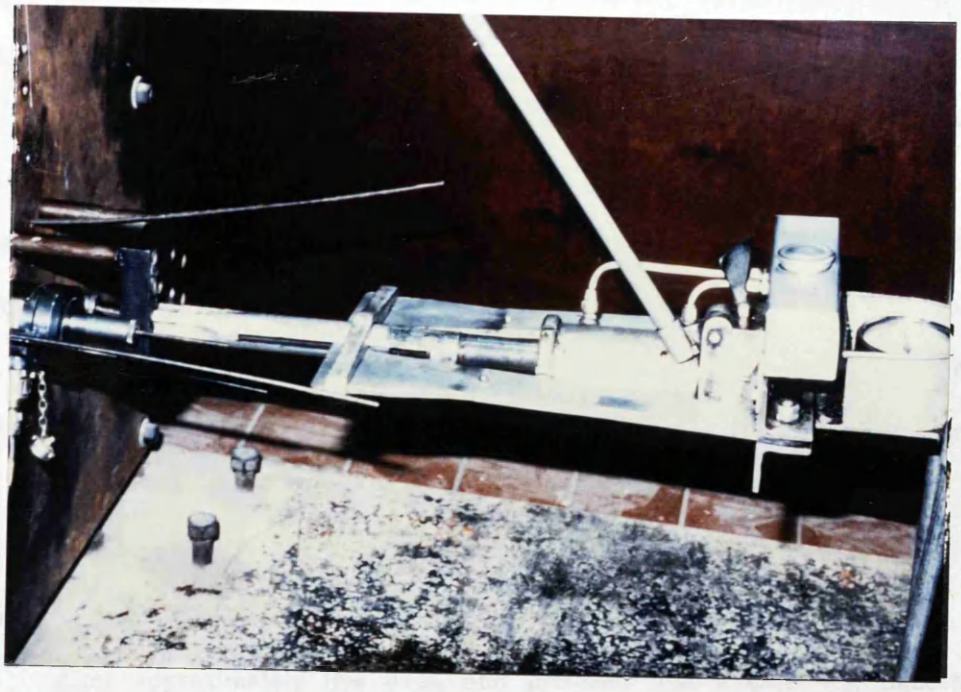

Figure(4.14) Tensioning Apparatus For Prestressing Wires of 5 To 7mm Diameter.

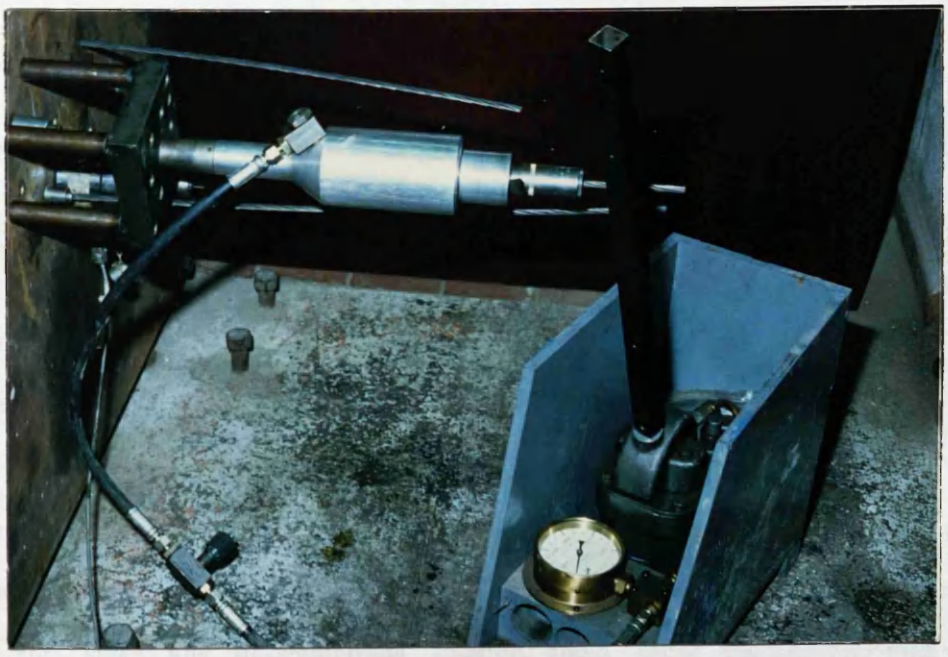

Figure(4.15) Tensioning Apparatus For Prestressing Strands of 8 to 12 mm Diameter

two agreed with in acceptable accuracy.

4.5.5 Mixing and casting

The concrete was cast after the stressing of the tendons. It was mixed in pan– type mixer. The aggregates, cement and sand were mixed dry for one minute approximately, then the water was added. During the casting of the model, the mould was vibrated by means of tremix vibrator bolted to the center of the mould base. A poker vibrator was also used in the early stages to improve compaction in the test zone. After 24 hours, the side shutters were removed. The control specimen were then removed from the moulds.

4.5.6 Transfer of the applied prestress

After approximately five days, and provided that a cube test indicated that the required strength had been reached[39] the wires were released all together and uniformly by an inward movement of one of the bearing plates.

Before and after the transfer, reading were taken on strain gauges which had been fixed on prestressing steel for estimating the prestressing losses.

4.6 TEST PROCEDURE

The loading system provides a uniform torque along the beam length and uniform bending moment in the test span. In the loading sequence, 15 to 20 increments were applied each increment representing approximately 6% of the design load.

Every effort was made to have the entire beam set up symmetrical with respect to the beam centroidal axis and to keep the loading symmetrical during each load increment, since any unsymmetrical rotation could cause the center load to be applied eccentrically thus creating a lateral thrust and additional bending and

torsional moments in the beam. For the application of combined loadings, the loads applied were such that the ratio of torsion to bending was constant for each load increment.

The loading process was continued until failure is noted by either a continuous drop of applied load or a sudden fall of that value.

Crack propagation was marked at each load increment on the concrete surface at the tip of each crack.

4.7 TEST PROGRAMME

4.7.1 Description of test specimen

The test specimens forms two series as follows:

– a/ Series 1

The series consists of four hollow beams designed according to the classical limit capacity concept to assess the accuracy of the proposed direct design method for combined bending and torsion. The beams were square in section (300x300)mm with wall thickness of 50 mm. The main variables studied in this series were the amount of prestress and the corresponding area of ordinary steel for a constant ratio of torsion to bending equal to 1.0. Figures (4.16) and (4.17) show details of beam cross– sectional reinforcement for series 1. Tables (4.3) to (4.6) give the design calculations for tested beams, where the section numbers illustrated in Figure (4.19). As shown in those tables the design equations required no longitudinal steel in the top section in all cases (TB1B to TB4B). However 2 No 10 mm diameter top longitudinal bars were provided for stirrup anchorage.

– b/ Series 2

This series consists of two hollow beams subjected to pure torsion of which one was designed according to the classic limit capacity and the other was to investigate the effect of varying the amount of prestress on the strength of the beam. Test PT1B

was designed for pure torque of 32 KNm. The main difference between these beams was the amount of prestress as given in Table (4.7) and (4.8). Figure (4.18) shows details of beam cross– sectional reinforcement for series 2.

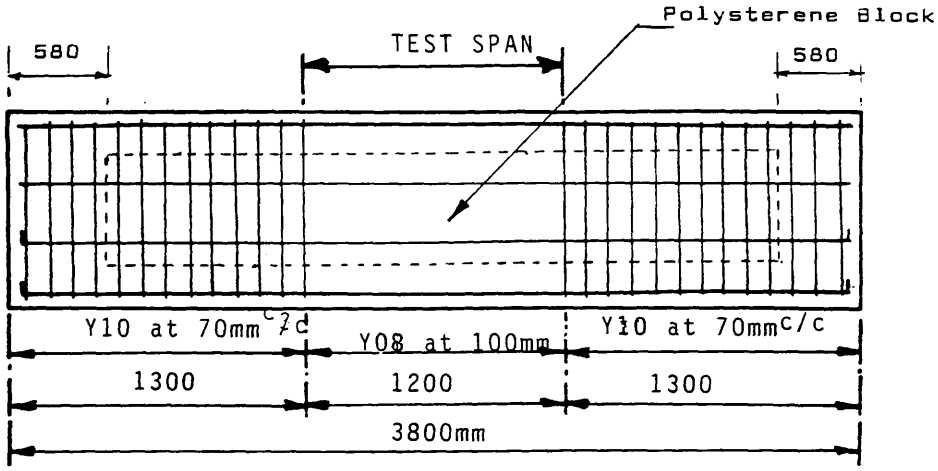

a)- General Elevation Of Test Model TB1B In Series 1

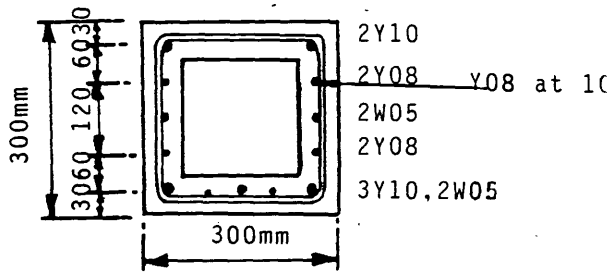

a)- TB1B (T/B=1)
Hollow Section

4 (5mm Diameter) Wires.

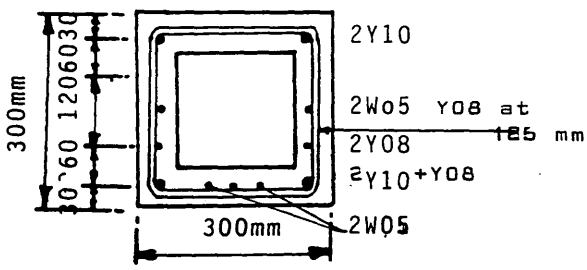

b)- TB2B (T/B=0.8)
Hollow Section

4 (5mm Diameter) Wires.

Figure(4.16) Reinforcement Details At Test Span In Series1

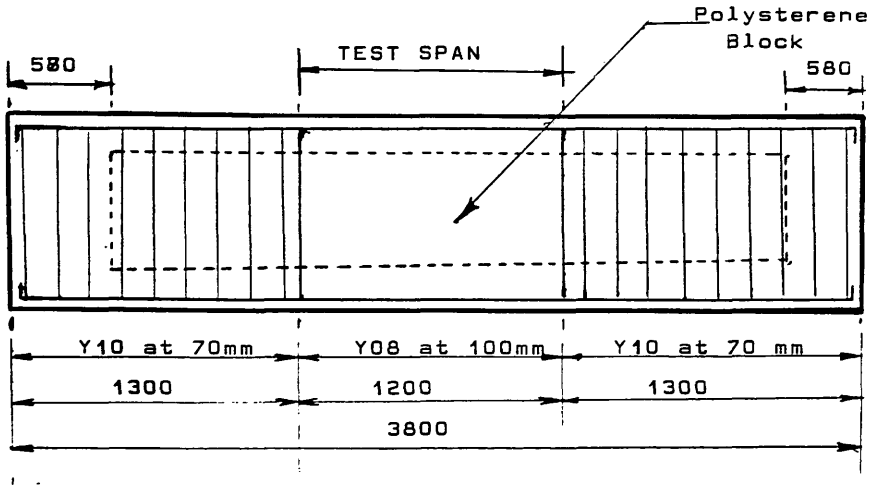

Figure(4.17) Reinforcement Details at Test Span in Series 1

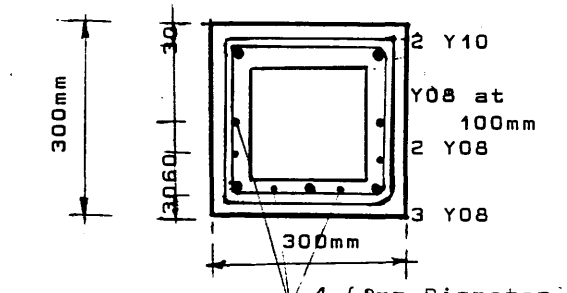

-a) TB3B (T/B=1)
Hollow Section

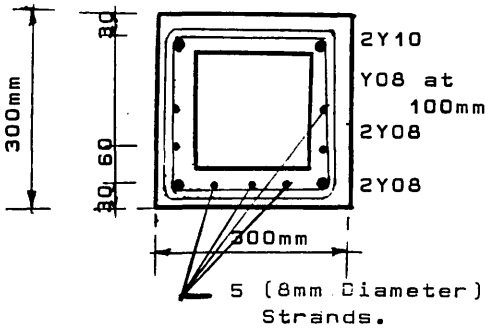

-b) TB4B (T/B=1)
Hollow Section

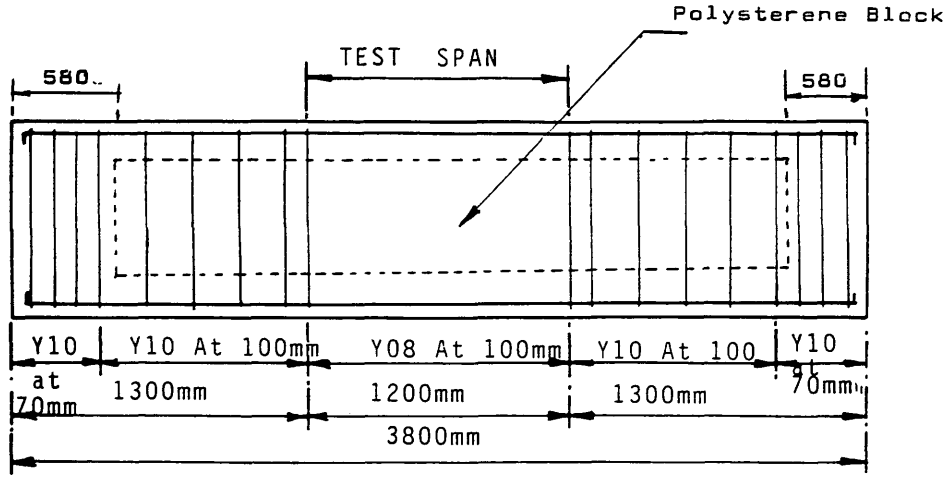

a)-General Elevation Of Test Model PT1B In Series 2

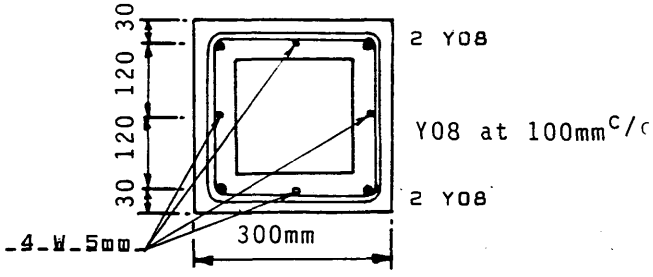

a)-PT1B(Pure Torsion)

Hollow Section

4 (5mm Diameter Wires.

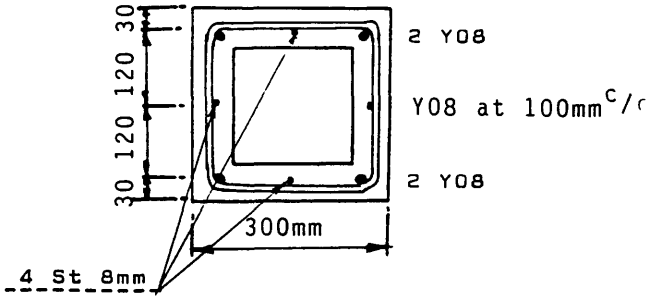

4 (8mm Diameter) Strands.

b)-PT2B(Pure Torsion)

Hollow Section

Figure(4.18) Reinforcement Details At Test Span In Series2

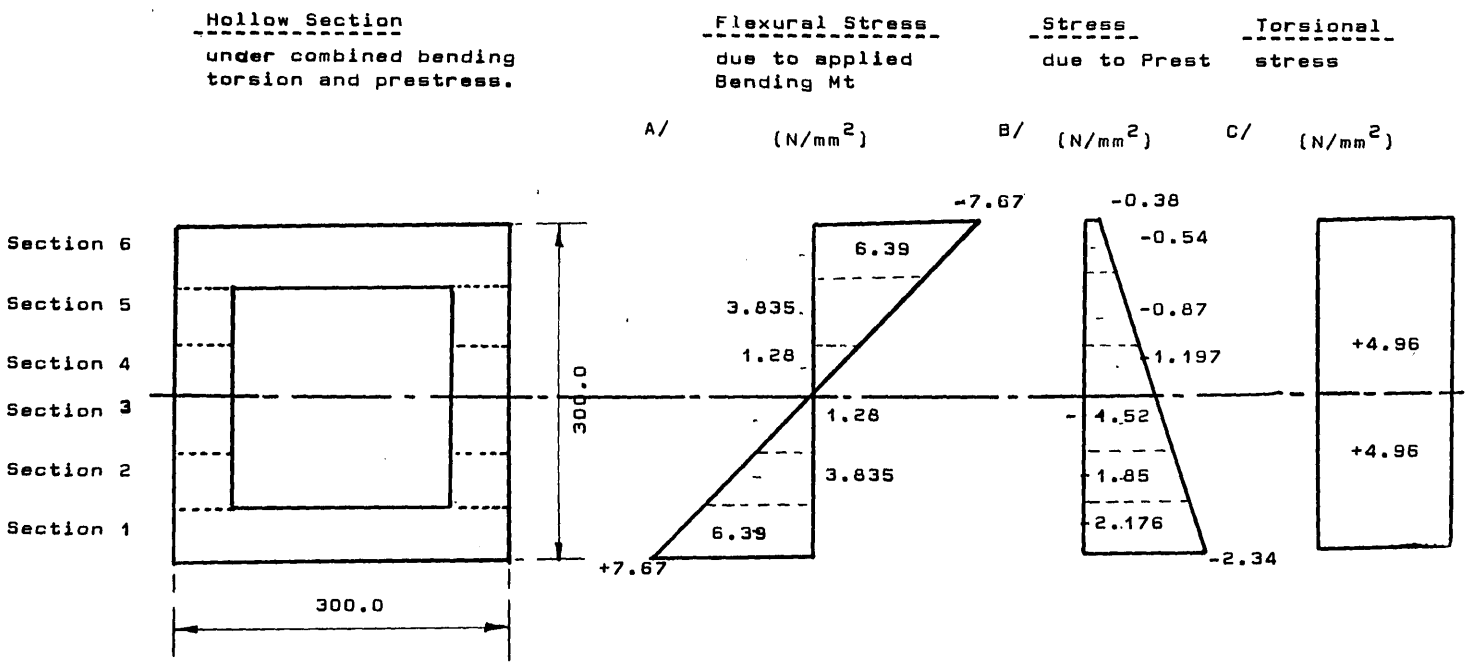

Figure(4.19) Combination of Stresses in Different Sections.

Table(4.1a) Properties of the ordinary steel.

Bar Size (mm)	Area (mm^2)	Yield Stress (N/mm^2)	Yield Strain	Young's Modulus (KN/mm^2)
8	50.0	477.0	0.00243	203.0
10	79.0	523.0	0.00254	211.0

Table(4.1b) Properties of the prestressing steel.

Tendon Size (mm)	Area (mm^2)	Max Stress (N/mm^2)	0.1%Proof Stress (N/mm^2)	Young's Modulus (KN/mm^2)
5	20.0	1731.0	1650.0	203.10
8	50.24	1711.0	1523.0	194.70

Table(4.2) Properties of Concrete for The Tested Beams.

Beam Mark	Eff.Prestress When Tested P_e (KN)	Compressive Stren of Cubes f_{cu} (N/mm^2)	Comp-Strength of Cylinders Test f'_c (N/mm^2)	Split Cylinder Tensile Strength f_t (N/mm^2)	Modulus of Elast - E_c (KN/mm^2)
TB1B	68.0	50.30	39.6	2.9	21.5
TB2B	68.0	51.5	45.6	3.7	26.0
TB3B	132.8	52.7	40.0	3.0	24.1
TB4B	160.0	55.0	37.0	3.5	25.6
PT1B	68.0	44.7	35.0	2.8	23.0
PT2B	99.30	48.0	39.9	3.20	23.4

Table(4.3) Reinforcement Details of Beam TB1B determined by the adopted Approach " DDA "

Sections	Flexural Stress σ_x (N/mm^2)	Stress due to Prestress σ_p (N/mm^2)	Torsional Stress τ_{xy} (N/mm^2)	Additional Steel in x-dir $\frac{A_x f_x}{t}$ (mm^2)	Equivalent Prest Steel in X-dir $\frac{A_p(0.87f_{pu}-f_{pe})}{t}$ (N/mm^2)	Tot- Steel in Y-dir $\frac{A_y f_y}{t}$ (mm^2)	Adopted Area in-x A_x (mm^2)	Adopted Area in-y A_y (mm^2)
Section 1	6.39	-2.176	4.96	7.49 224.7	1.68	4.96 496.0	(3 Y10) 236.0	
Section 2	3.835	-1,85	4.96	5.52 55.2	1.43	4.96 496.0	(2 Y08) 101.0	
Section 3	1.28	-1.52	4.96	3.52 35.2	1.20	4.96 496.0		
Section 4	-1.28	-1.197	4.96	2.48 15.5	0.93			Y08 at 100 mm (503.0)
Section 5	-3.835	-0.87	4.96	0.93 9.30	0.67			
Section 6	-6.39	-0.54	4.96	0.0	0.42	3.55 355	(2 Y10) 157.0	

NB: - Estimated effective prestress $P_e = 0.85P_i$
- Actual measured effective prestress $P_e = 0.8@P_i$

- P_i: Initial prestress.
- See Figure(4.19) for position of sections.

Table(4.4) Reinforcement Details of Beam TB2B determined by the adopted Approach "DDA "

Sections	Flexural Stress	Stress due to Prest.	Torsional Stress	Additional Steel in X-dir	Equivalent Prest Steel in X-dir	Tot-Steel in Y-dir	Adopted area in-x	Adopted area in-y
	σ_x (N/mm^2)	σ_p (N/mm^2)	τ_{xy} (N/mm^2)	$\frac{A_x f_x}{t}$ (mm^2)	$\frac{A_p(0.87f_{pu}-f_{pe})}{t}$ (N/mm^2)	$\frac{A_y f_y}{t}$ (mm^2)	A_x (mm^2)	A_Y (mm^2)
Section 1	6.39	-2.176	3.96	6.49 194.7	1.68	3.96 396.0	207.5 (2 Y10 +Y08)	
Section 2	3.835	-1.85	3.96	4.52 45.2	1.43	3.96 396.0	(2 Y08) 101.0	Y08 at 125 mm
Section 3	1.28	-1.52	3.96	2.54 25.4	1.18	3.96 396.0		
Section 4	-1.28	-1.197	3.96	0.55 5.50	0.93	3.96 396.0		(402.0)
Section 5	-3.835	-0.87	3.96	-0.75	0.66	3.96 396.0		
Section 6	-6.39	-0.54	3.96	0.0 -	0.42	3.96 396.0	(2 Y10) 157.0	

NB: -Estimated effective prestress $P_e = 0.85P_i$

-Actual measured prestress $P_e = 0.823P_i$

Table(4.5) Reinforcement Details of Beam TB38 determined by the adopted Approach " DDA "

Sections	Flexural Stress	Stress due to Prest.	Torsional Stress	Additional Steel	Equivalent Prest Steel in X-dir	Tot-Steel in Y-dir	Adopted area in-x	Adopted area in-y
	σ_x (N/mm^2)	σ_p (N/mm^2)	τ_{xy} (N/mm^2)	$\frac{A_x f_x}{t}$ (mm^2)	$\frac{A_p(0.87f_{pu}-f_{pe})}{t}$ (N/mm^2)	$\frac{A_y f_y}{t}$ (mm^2)	A_x (mm^2)	A_Y (mm^2)
Section 1	6.39	-4.25	4.96	4.11 123.3	2.99	4.96 496.0	(3 Y08) 151.0	
Section 2	3.835	-3.61	4.96	2.65 26.5	2.54	4.96 496.0	(2 Y08) 101.0	Y08 at 100 mm (503.0)
Section 3	1.28	-2.99	4.96	1.216 12.16	2.07	4.96 496.0		
Section 4	-1.28	-2.33	4.96	-0.287 -	1.64	4.96 496.0		
Section 5	-3.835	-1.7	4.96	-1.78 -	1.20	4.96 496.0		
Section 6	-6.39	-1.063	4.96	0.0	0.75	3.30 330.0	(2 Y10) 157.0	

NB: -Estimated effective prestress $P_e = 0.83P_i$

-Actual measured prestress $P_e = 0.8P_i$

Table(4.6) Reinforcement Details of Beam TB4B determined by the Adopted Approach "DDA"

Sections	Flexural Stress	Stress due to Prest.	Torsional Stress	Additional Steel	Equivalent Prest Steel in X-dir	TH Steel in Y-dir	Adopted area in-x	Adopted area in-y
	σ_x (N/mm^2)	σ_p (N/mm^2)	τ_{xy} (N/mm^2)	$\frac{A_x f_x}{t}$ (mm^2)	$\frac{A_p(0.87f_{pu}-f_{pe})}{t}$ (N/mm^2)	$\frac{A_y f_y}{t}$ (mm^2)	A_x (mm^2)	A_Y (mm^2)
Section 1	6.39	-5.54	4.96	1.92 57.6	3.89	4.96 496.0	(2 Y08) 101.0	Y08 at 100 mm (503.0)
Section 2	3.835	-4.61	4.96	0.95 9.5	3.24	4.96 496.0		
Section 3	1.28	-3.88	4.96	-0.0273 -	2.59	4.96 496.0		
Section 4	-1.28	-2.71	4.96	-1.01 -	1.93	4.96 496.0		
Section 5	-3.835	-1.83	4.96	0.0 -	1.29	4.32 432.0		
Section 6	-6.39	-0.90	4.96	0.0 -	0.63	3.37 337.0	(2 Y10) 157.0	

NB: -Estimated effective prestress $P_e = 0.8P_i$

-Actual measured effective prestress $P_e = 0.776P_i$

Table(4.7) Reinforcement Details of Beam PT1B determined by the Adopted Approach " DDA "

Sections	Flexural Stress	Stress due to Prest.	Torsional Stress	Additional Steel $_x$ in	Equivalent Prest Steel in X-dir	Tot Steel in Y-dir	Adopted area in-x	Adopted area in-y
	σ_x (N/mm^2)	σ_p (N/mm^2)	τ_{xy} (N/mm^2)	$\frac{A_x f_x}{t}$ (mm^2)	$\frac{A_p(0.87f_{pu}-f_{pe})}{t}$ (N/mm^2)	$\frac{A_y f_y}{t}$ (mm^2)	A_x (mm^2)	A_Y (mm^2)
Section 1	0.0	-1.36	4.96	2.55 76.5	1.05	4.96 496.0	(4 Y08) 202.0	Y08 at 100 mm (503.0)
Section 2	0.0	-1.36	4.96	2.55 25.5	1.05			
Section 3	0.0	-1.36	4.96	2.55 25.5	1.05			
Section 4	0.0	-1.36	4.96	2.55 25.5	1.05			
Section 5	0.0	-1.36	4.96	2.55 25.5	1.05			
Section 6	0.0	-1.36	4.96	2.55 76.5	1.05	4.96 496.0		

NB: -Estimated effective prestress $P_e = 0.85P_i$

-Actual measured effective prestress $P_e = 0.81P_i$

Table(4.8) Reinforcement Details of Beam PT2B determined by the adopted Approach " DDA "

Sections	Flexural Stress	Stress due to Prest.	Torsional Stress	Add- Stee in X-dir	Equivalent Prest Steel in X-dir	Tot Steel in Y-dir	Adopted area in-x	Adopted area in-y
	σ_x (N/mm^2)	σ_p (N/mm^2)	τ_{xy} (N/mm^2)	$\frac{A_x f_x}{t}$ (mm^2)	$\frac{A_p(0.87f_{pu}-f_{pe})}{t}$ (N/mm^2)	$\frac{A_y f_y}{t}$ (mm^2)	A_x (mm^2)	A_Y (mm^2)
Section 1	0.0	-1.99	4.96	1.57 47.10	1.4	4.96 496.0	(4 Y08) 202.0	Y08 at 100 mm (503.0)
Section 2	0.0	-1,99	4.96	1.57 15.7	1.4			
Section 3	0.0	-1.99	4.96	1.57 15.7	1.4			
Section 4	0.0	-1.99	4.96	1.57 15.7	1.4			
Section 5	0.0	-1.99	4.96	1.57 15.7	1.4			
Section 6	0.0	-1.99	4.96	1.57 47.10	1.4	4.96 496.0		

NB: -Estimated effective prestress $P_e = 0.83P_i$

-Actual measured effective prestress $P_e = 0.8P_i$

CHAPTER FIVE

EXPERIMENTAL RESULTS AND DISCUSSION

5.1 INTRODUCTION

In this chapter the experimental results are presented and discussed. The experiments were conducted to :

1) Assess the validity of the proposed direct design approach based on classical limit capacity concept for partially prestressed beams with respect to service and ultimate load behaviour

2) Gain a better insight into the behaviour of partially prestressed beams designed according to the direct design method

3) Use the experimental results to check the reliability of the nonlinear plane stress finite element model for the analysis of these types of cross section under the combined action of bending, torsion and prestress.

5.2 EXPERIMENTAL RESULTS

The principal test results are presented in Table (5.4). As described in chapter four all the specimens were designed and detailed according to the direct design approach except PT2B. The design calculations representing the total areas of reinforcing steel are summarised in Table (5.1). The design torque T_d and the design bending moment B_d were both 32 KNm, except for specimen TB2B for which T_d was 25.6 KNm. The beams were designed assuming the steel yield stress of 500 N/mm^2 and concrete cube stregth of 50 N/mm^2. The assumed yield stress of prestressing steel were (f_{pu} = 1731 N/mm^2 for 5mm diameter wire and 1711 N/mm^2 for 8mm diameter strand). The average steel yield stresses for 8 mm diameter bar used for stirrup was f_{yv}= 477 N/mm^2 and for 10mm longitudinal bars

used f_{yl}= 523 N/mm^2. The average concrete cube strength was near 50 N/mm^2 except for TB4B for which it was 55 N/mm^2. Full details of material properties are given in Tables (4.1a), (4.1b) and (4.2).

5.2.1 Series 1

The object of this series was to test the validity of the direct design method using Nielsen's design equations for partially prestressed beams under the combined action of bending and. The primary variable within this series were the amount of prestress and the amount of ordinary reinforcing steel provided. The series consisted of four beams. The first set of beams named TB1B and TB2B were tested in a test rig which allowed rigid body rotation of the specimen about an axis below the beam bottom. This led to unsatisfactory results. Afterwards, the test rig was altered to ensure that the axis of rotation was coincident with the axis of the beam.
Details of the original and modified test set up are shown in Figure (5.1a) and (5.1b). Beams TB3B and TB4B were tested with the new test– rig.

5.2.1.1 Specimen TB1B

The beam was pretensionned by 5mm diameter stress relieved, indented wires. Four wires were used, each of which was initially tensioned to 20 KN. The total effective prestressing force at the time of test was 68 KN. The release of prestress caused minor secondary cracks to appear before the test at the ends.
During test, the loads were applied in small increments of about 2 KNm for torsional and bending moment making a total of 16 increments up to the failure.
The first cracks to form were of flexural nature. The diagonal cracks appeared afterwards and were more prominent than the first cracks, usually extending in an inclined direction from a small flexural crack near the bottom. However, only a few inclined cracks were observed on the top flange. Between 0.49 and 0.85 design load, more inclined cracks were observed on both webs and flanges. Once these diagonal cracks began to form, they opened up within the test zone . With further increase

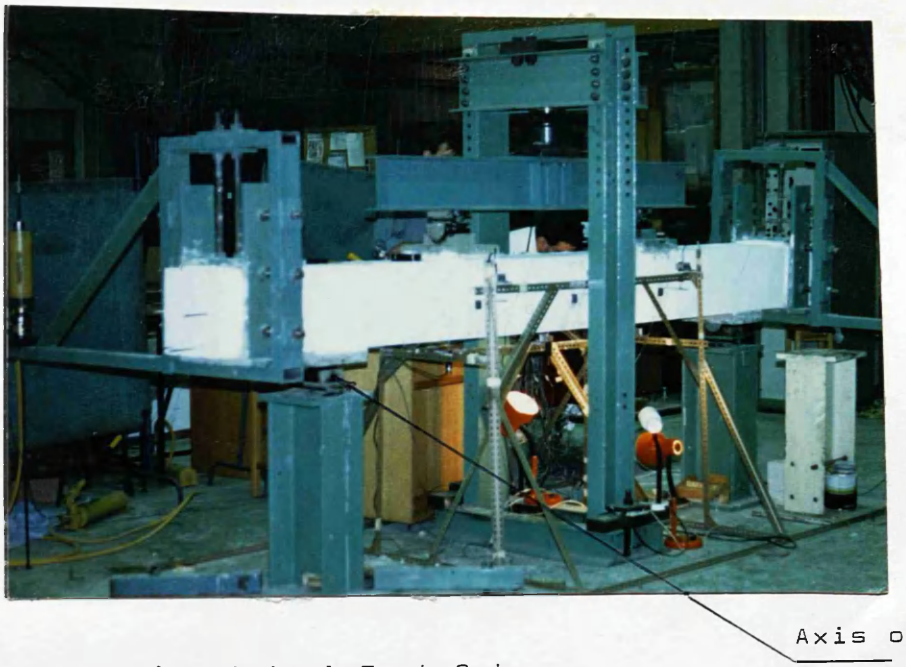

Figure(5.1a) Original Test Setup.

Note: The axis of rotation is below the tested beam.

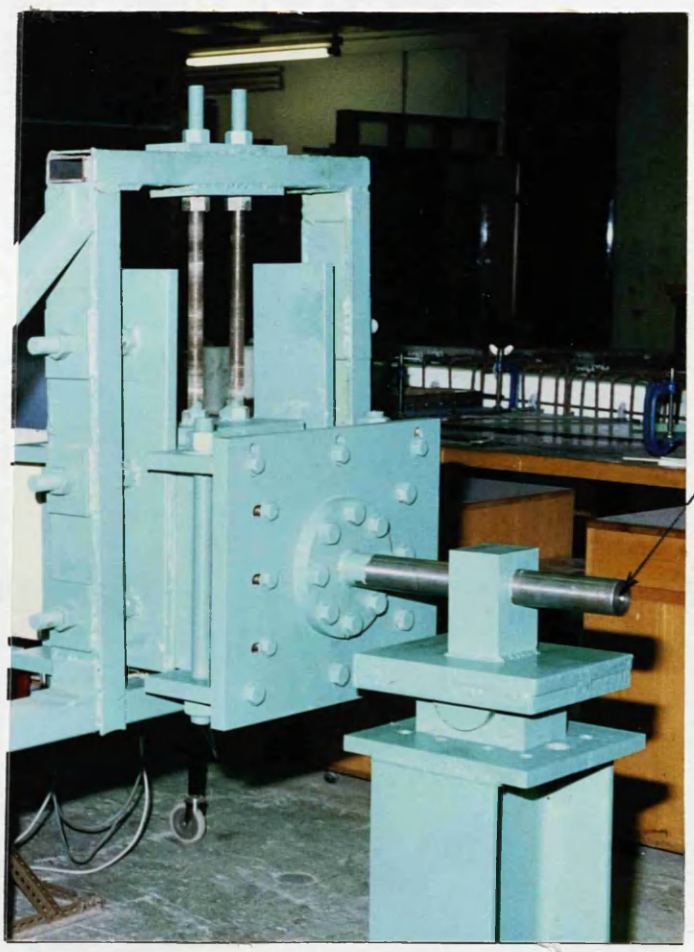

Figure(5.1b) Improved test setup.

Note: The axis of rotation coincide with the central axis of the beam.

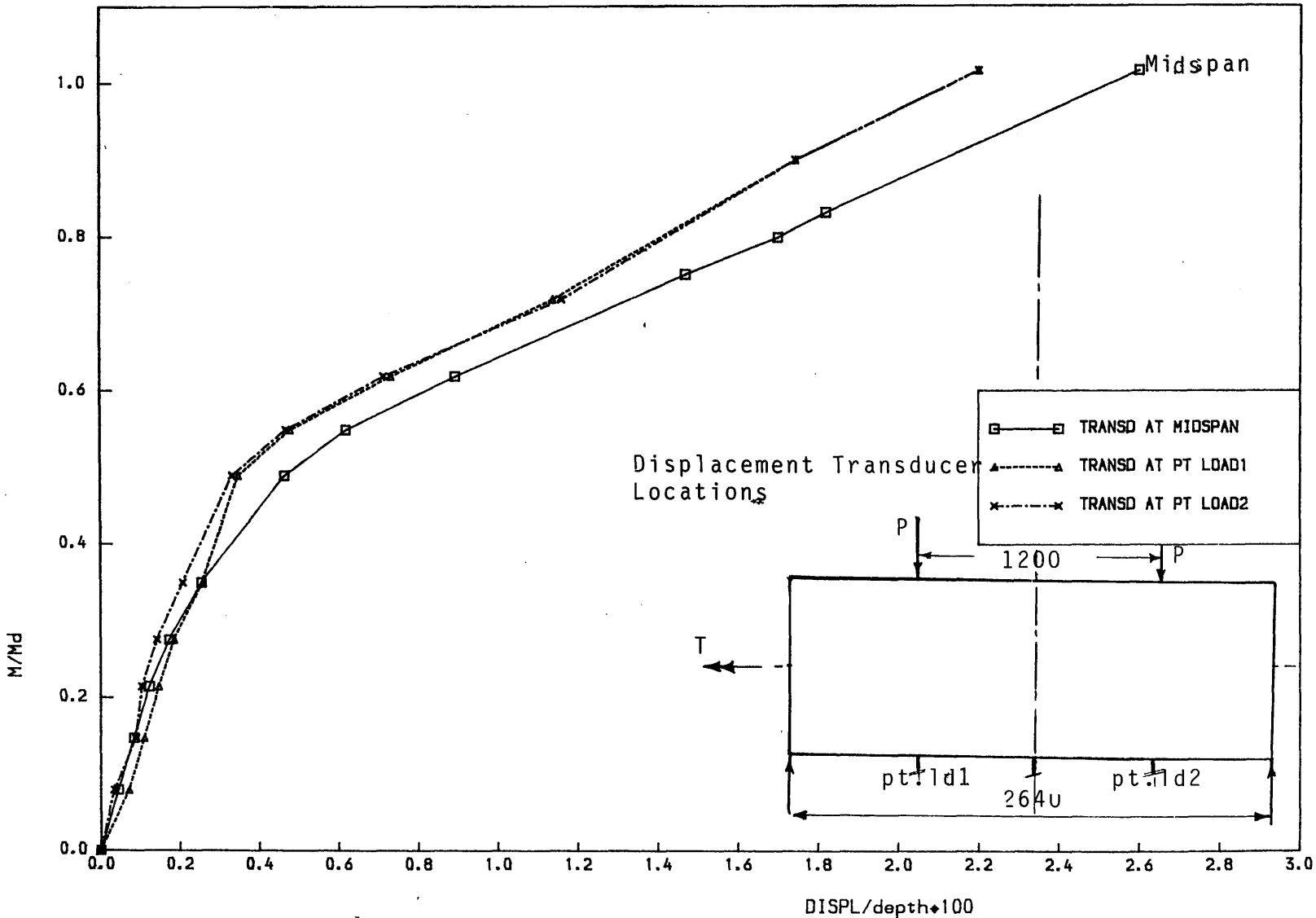

Figure (5.2) Applied Load Vs Vertical Displacement On Central Transducers For Model TB1B Pe=68 KN , Ep=-60 mm

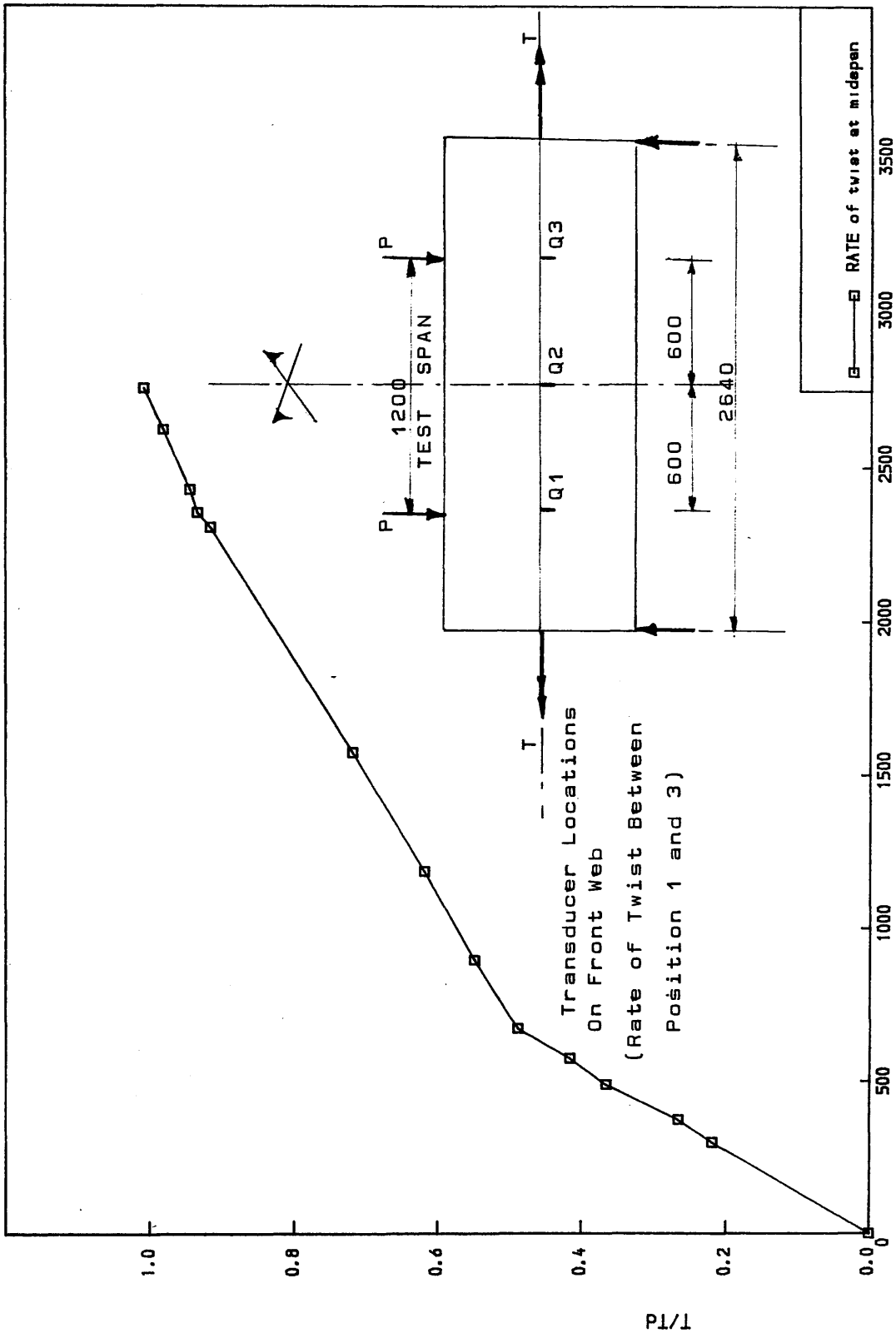

Figure (5.3) Torque Vs Rate of Twist at Midspan
For Model TB1B Pe=68 KN , Ep=-60mm

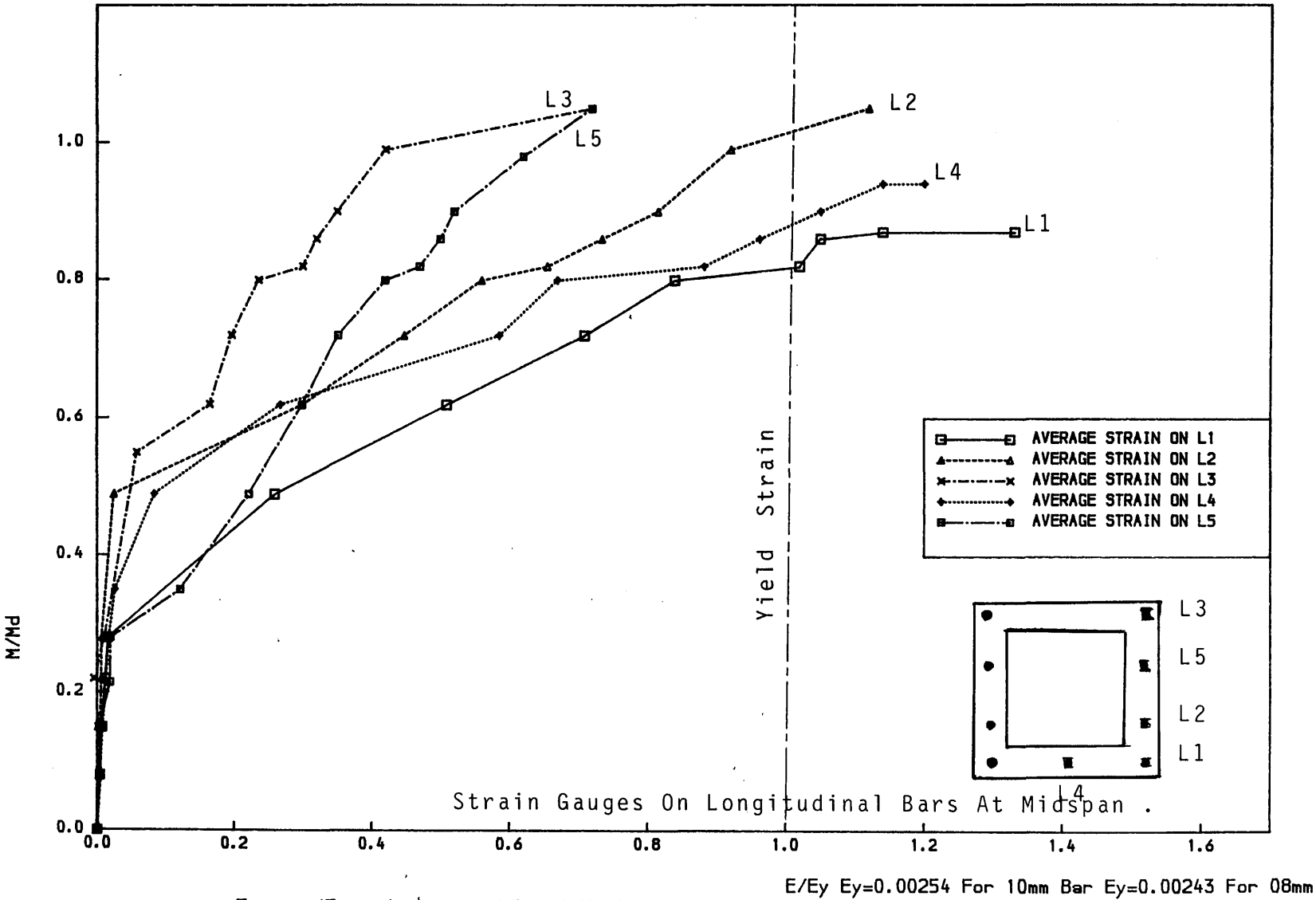

Figure (5 . 4) Applied Load Vs Longitudinal steel strains At Midspan
For Model TB1B Pe=68 KN , Ep=-60mmm

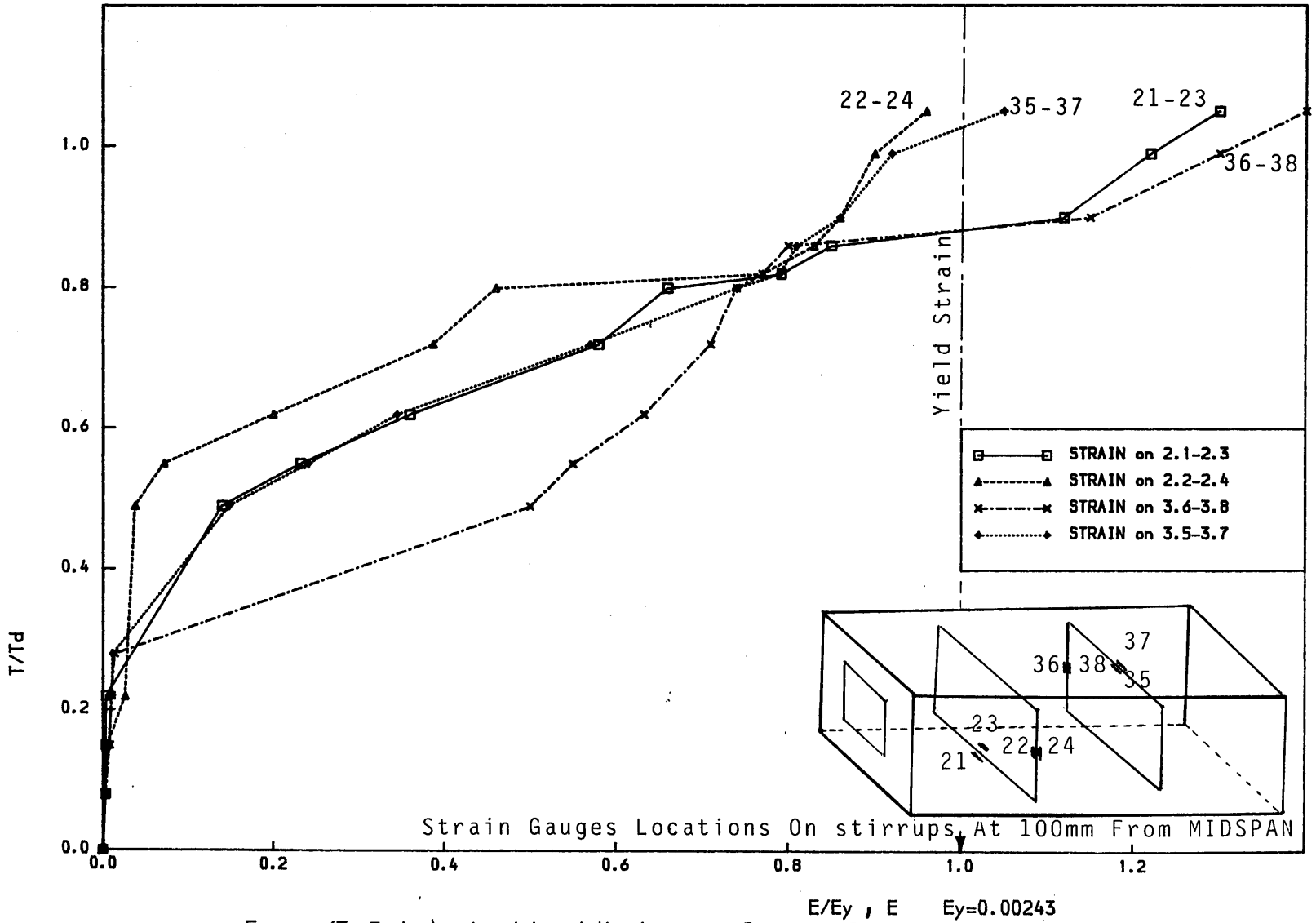

Figure (5.5) Applied Load Vs Average Stirrup Strains at 100 mm From Midspan For Model TB1B Pe=68 KN , Ep=-60mm

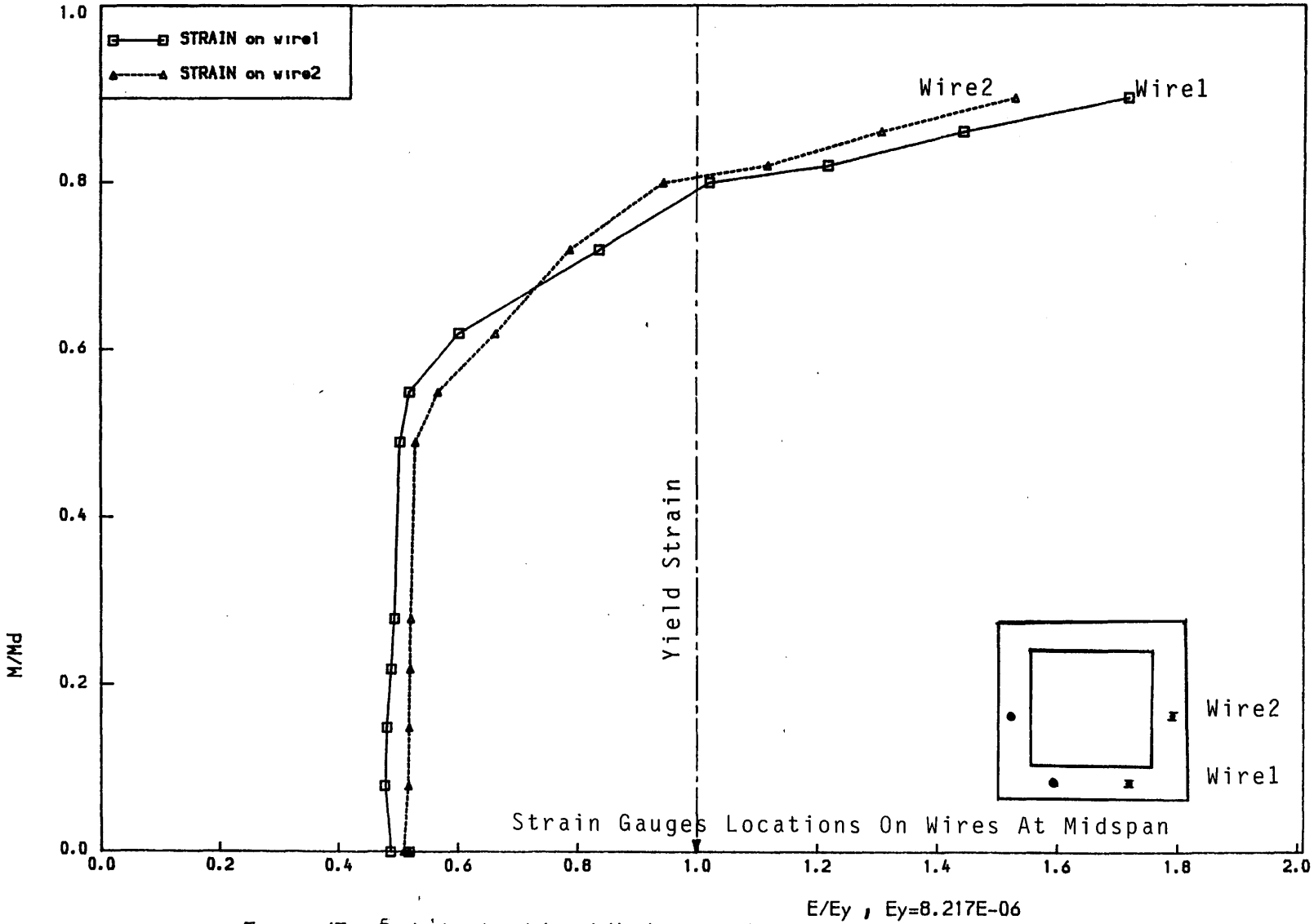

Figure (5. 6) Applied Load Vs Longitudinal Prestressing Steel Strains For Model TB1B Pe= 68 KN , Ep=-60mm

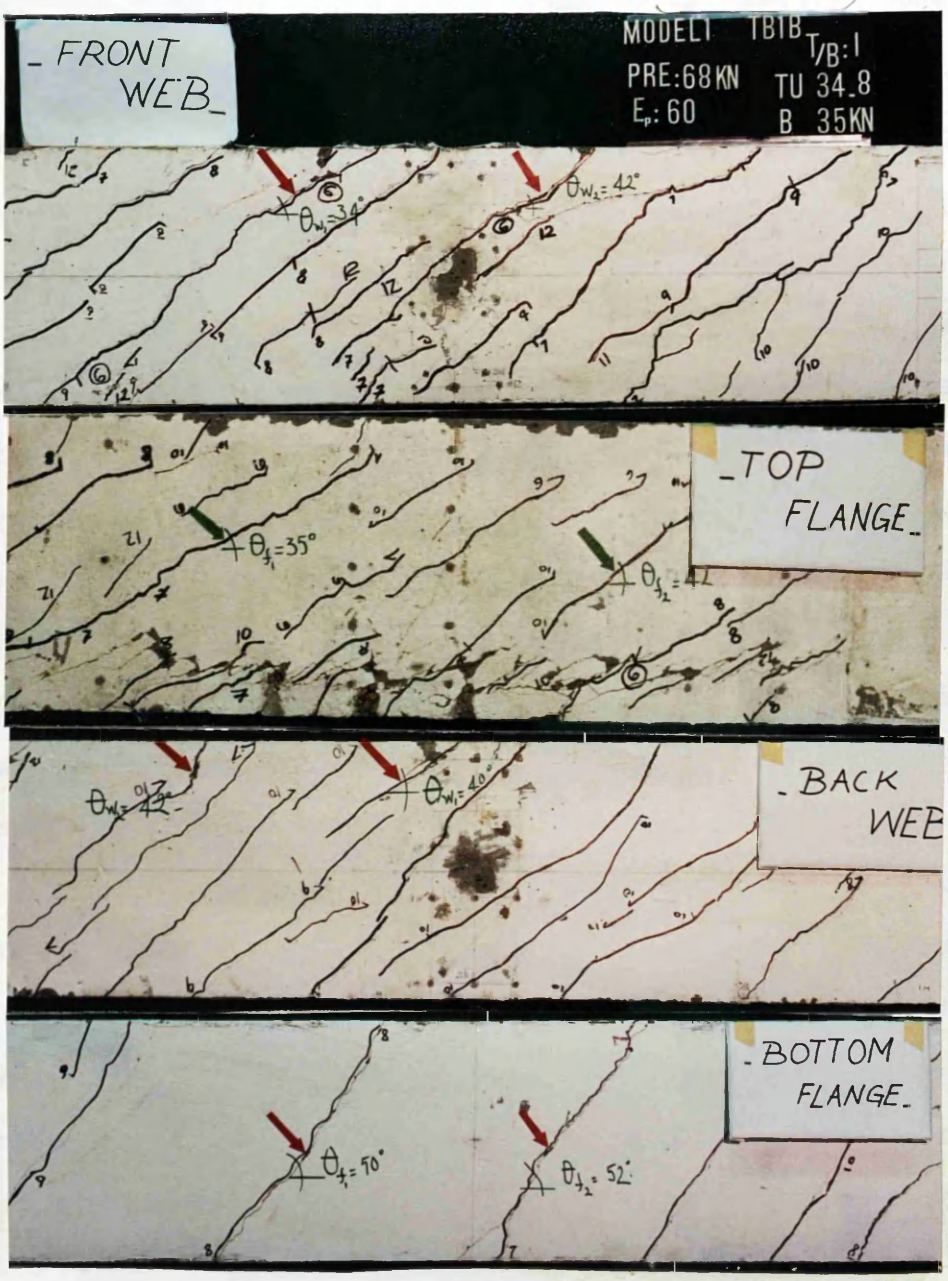

Figure(5.7) Crack Development at load stage (Beam TB1B- Torsion/Bending=1.0, P_e =68KN E_p= -60mm).

in loads, either the flexural cracks extended upward as diagonal cracks, or the diagonal cracks, which formed near the center of the front web, extended up and down to join or to form cracks in the top and bottom flanges.

Top flange cracks were usually the last to form. Between 0.90 and 1.10 of design load, horizontal cracks appeared at the section of prestressing wires. At ultimate load, the beam showed violent failure due to the combined action of prestress and the twisting moment. The addition of bending caused considerable desintegration of the beam at failure. The test zone had suffered severe cracking by this stage.

Figure (5.3) shows the torque twist curve. The behaviour is linear up to the cracking. Due to microcking and inelasticity of concrete at higher stresses, the torque– twist relationship became slightly non– linear above 0.50 of design load. This is also reflected in the steel strains. Strains in reinforcement are shown in Figure (5.4) for longitudinal bars, (5.5) for stirrups, (5.6) for prestressing steel. All the bars carried insignificant strains before cracking, indicating the negligeable contribution of steel towards the overall stiffness in the pre– cracking stage. Similar behaviour is also noted for the concrete surface strains which unfortunately were not properly recorded for this specimen but will be shown later for the all remaining specimens. Figure (5.7) shows the final crack pattern on all faces of specimen TB1B. The first yield of steel occured at the bottom longitudinal steel (0.8Xdesign load for the bottom prestressing wires and 0.82Xdesign load for longitudinal corner steel bar) The inclination of the cracks to the longitudinal axis varied between 34^0 to 52^0 as can be seen from the figure.

5.2.1.2 Specimen TB2B

The beam had the same amount of effective prestress as TB1B but it was designed for ultimate torsion moment T_d = 25.6 KNm and bending moment B_d= 32 KNm. The total amount of ordinary steel is shown in Table (5.1). The first diagonal crack started to develop at a load of 0.43 design load. These cracks travelled upwards on both sides of the beam with the same inclination till they

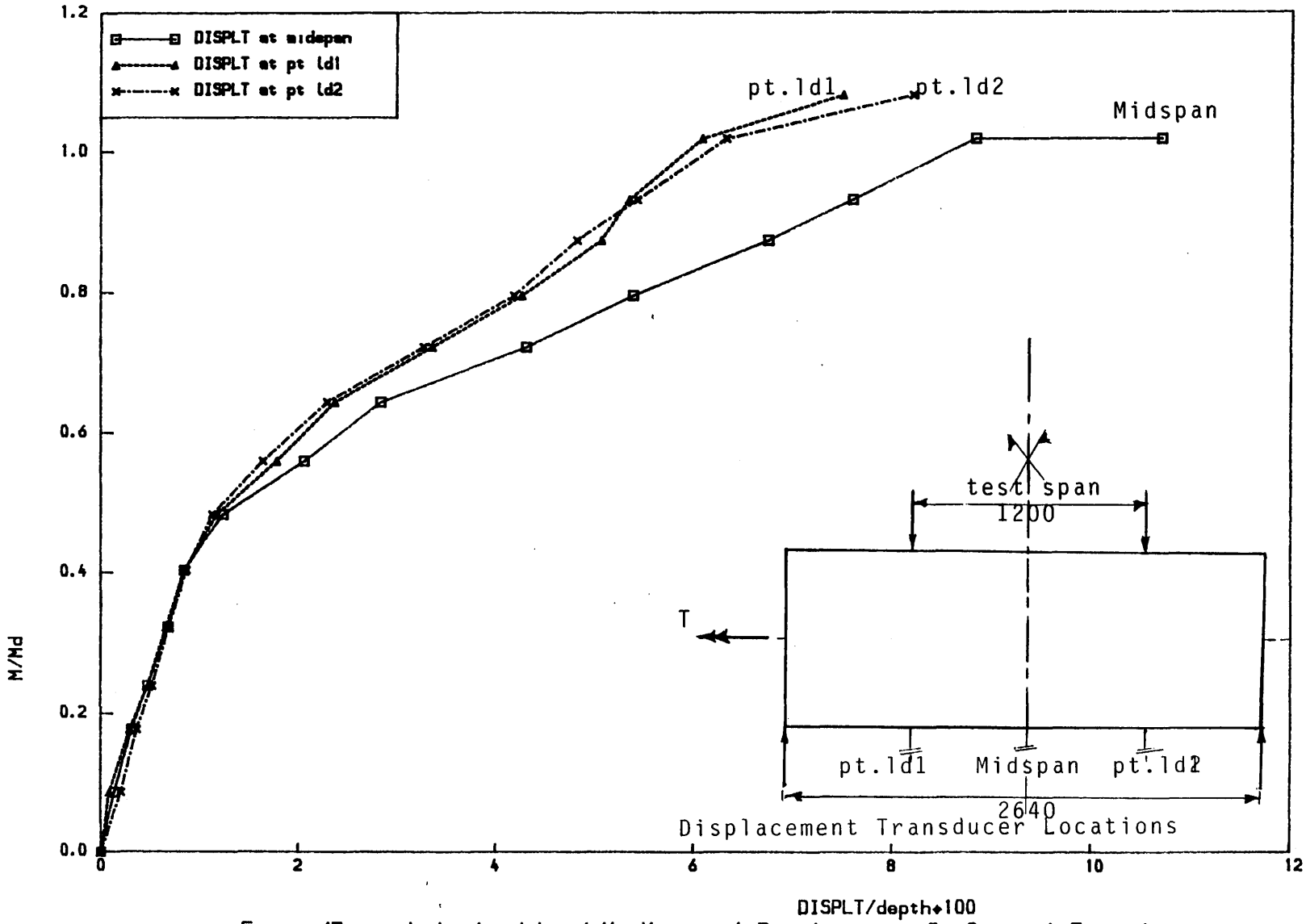

Figure (5. 8) Applied Load Vs Vertical Displacement On Central Transducers For Model TB2B Pe=68 KN , Ep=-60 mm

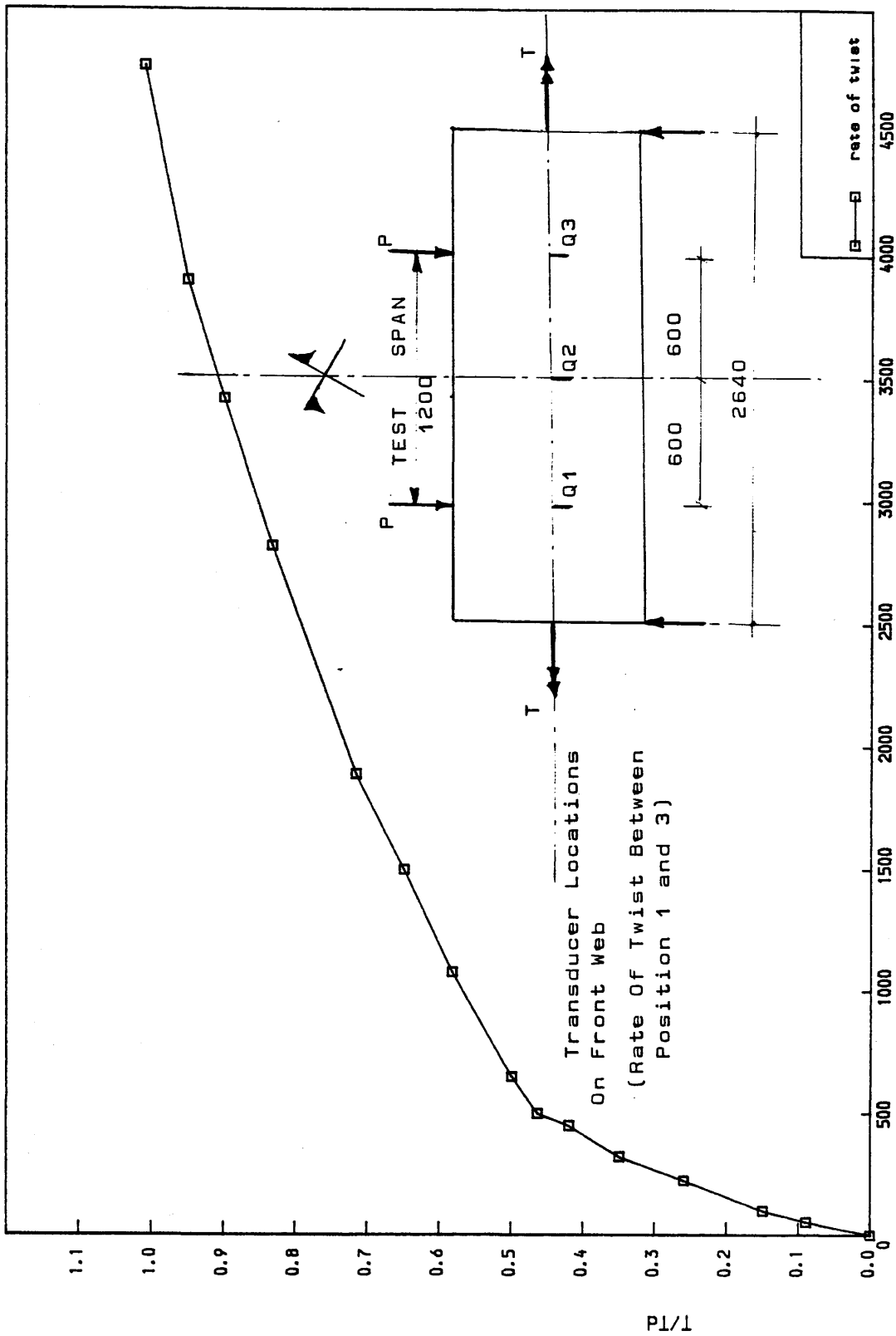

Figure (5.9) Torque Vs Rate of Twist For Model TB2B
Pe= 68 KN , Ep=-60 mm

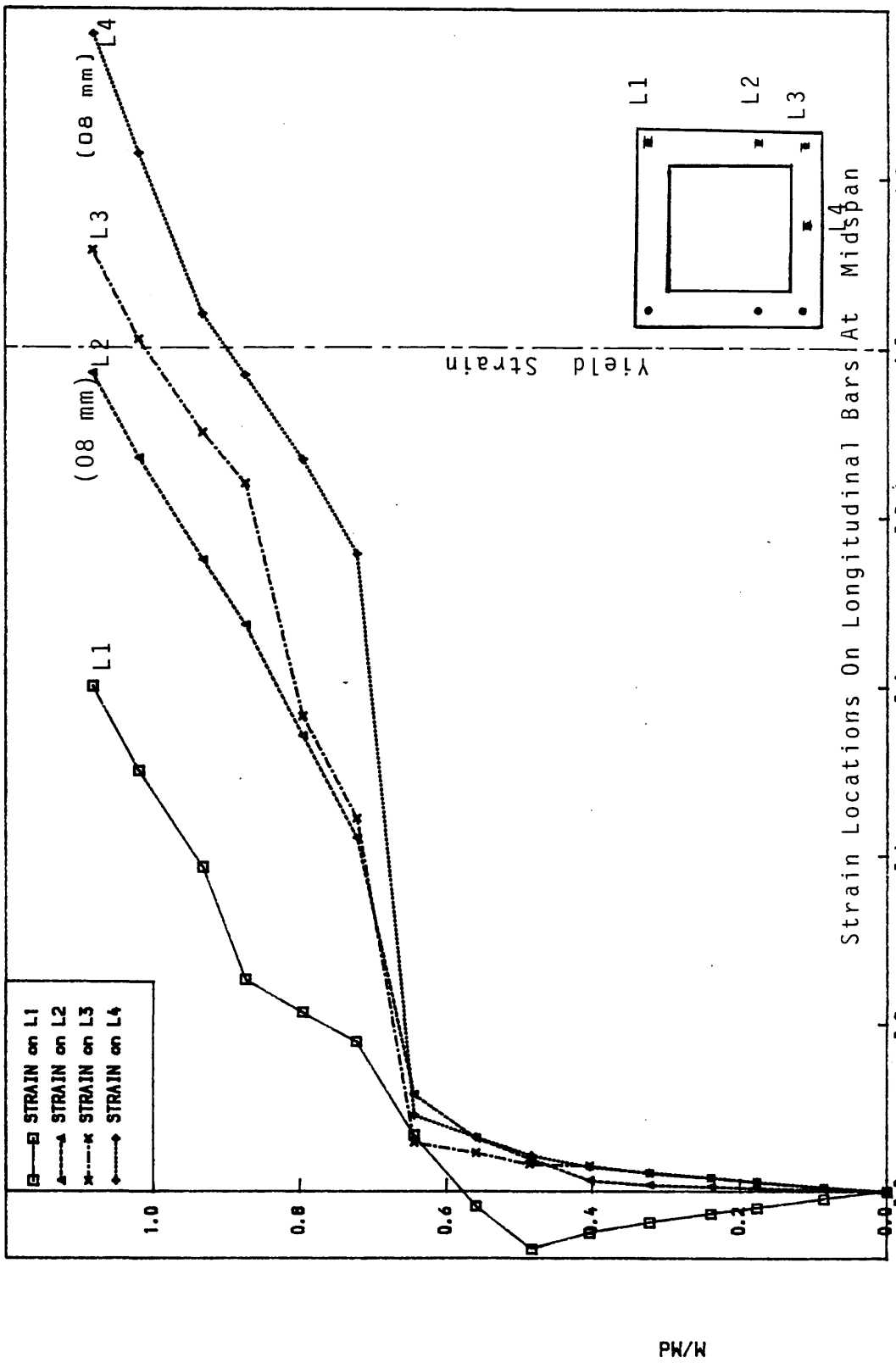

Figure (5. 10) Applied Load Vs Longitudinal Steel Strains At Midspan For Model TB2B Pe=68 KN , Ep=-60 mm

E/Ey Ey=0.00254 For 10mm Bar Ey=0.00243 For 08mm

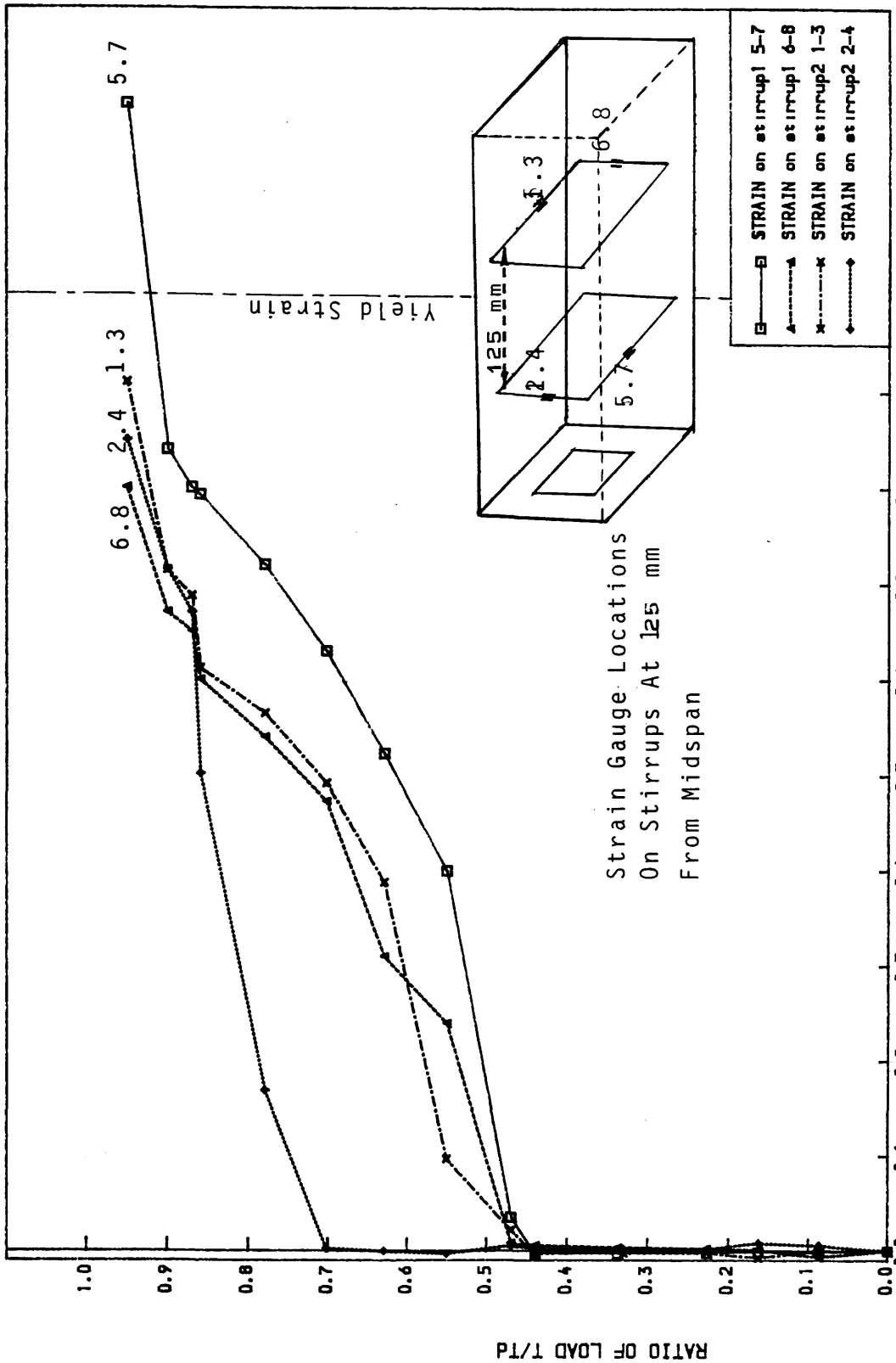

Figure 15. 11) Applied Load Vs Average Stirrup Strains At Midspan For Model TB2B Pe=68 KN , Ep=-60 mm

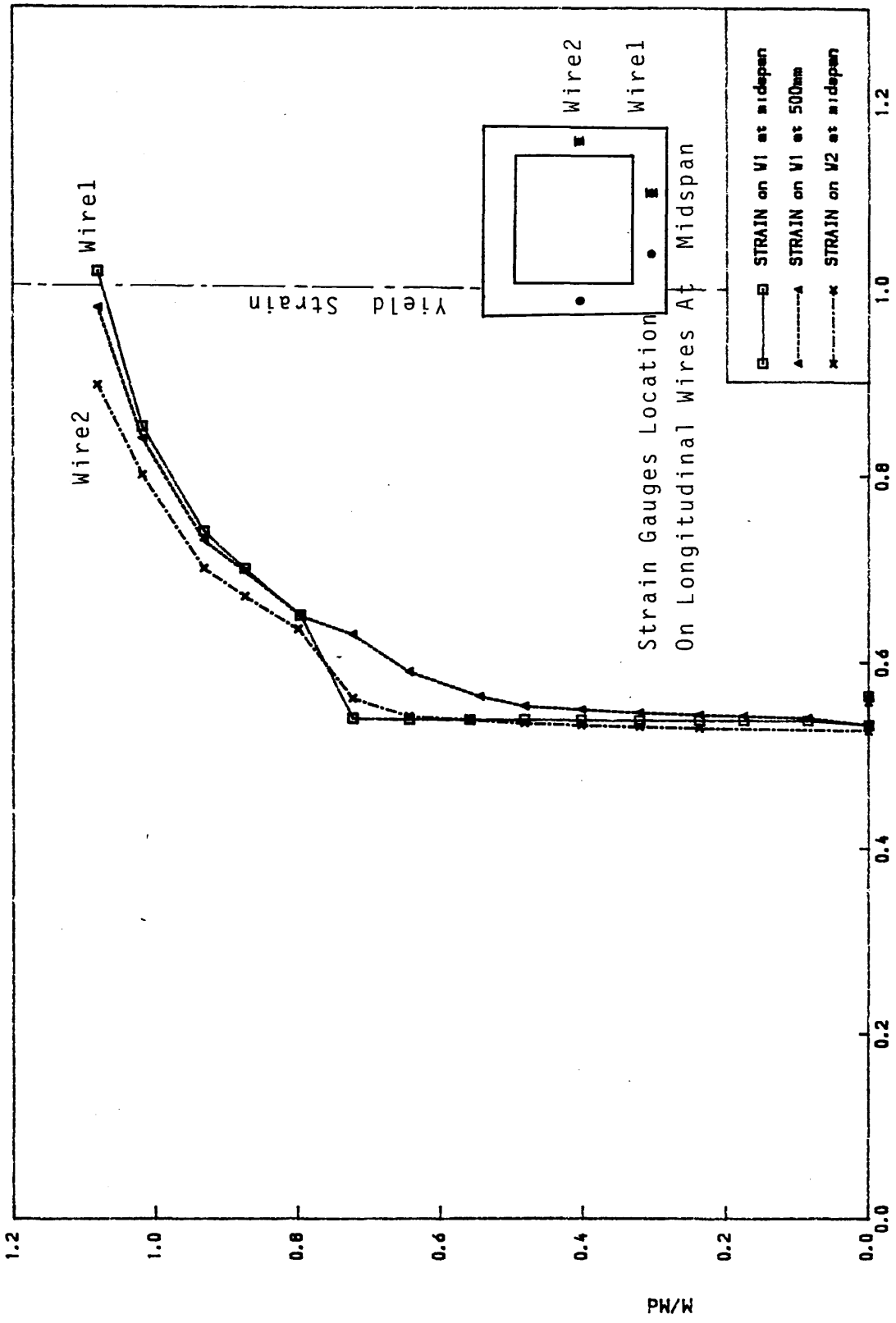

Figure (5.12) Applied Load Vs Longitudinal Prestressing Steel Strains For Model TB2B Pe= 68 KN , Ep=-60mm

Figure(5.13) Crack Development at each load stage
(Beam TB2B- Torsion/Bending =1.0, P_e =68KN
and E_p =-60mm).

Note: Crushing on top flange.

reached a point near the top flange of the beam.

Between loads of 0.50 and 1.0 design load, the diagonal cracks which formed near the center of the front web, extended up and down to join the flexural cracks already developed in the bottom flange.

The inclination of cracks on all sides of the beam showed in Figure (5.13) varied from 34^0 to 60^0. The first yield of steel occured at the bottom longitudinal steel (at 0.92 design load for longitudinal steel and 1.07 design load for prestressing steel).

The relationship of twisting moment to angle of twist is shown in Figure (5.9), indicate linear relations under low loads and non linear variation under higher loads.

The observations during the experiment were fairly similar to specimen TB1B.

Figure (5.10) to (5.12) present the steel strain. There is an initial straight part followed by a sudden change in slope after cracking and continuous increase with loading up until failure. Figure (5.13) shows the development of cracks on the four faces. The beam failed after a load of 1.08Xdesign load .

5.2.1.3 Specimen TB3B

The beam was prestressed by means of four strands of 8 mm diameter, each of which was initially tensioned to 40 KN. The total effective prestress at the time of test was 132.8 KN. The design torque T_d and the design bending moment were both 32 KNm. The amount of transverse and longitudinal reinforcement was varied in similar way as for the first set of beams, depending on the amount of prestress provided. The observations during the experiment were fairly similar as for TB1B and TB2B. The strains in reinforcement are shown in figures (5.16) to (5.18). Insignificant strains were recorded before cracking followed by a large increase after cracking. The ultimate load, however was higher than the previous as shown in table (5.5). Similar behaviour to TB1B regarding torque– twist variation shown in Figure (5.15) and load vertical displacement shown in figure (5.14) was observed. Both ordinary and prestressing steel reached yield strain as the beam approached its ultimate capacity. Figure (5.20) shows the crack pattern and their propagation with

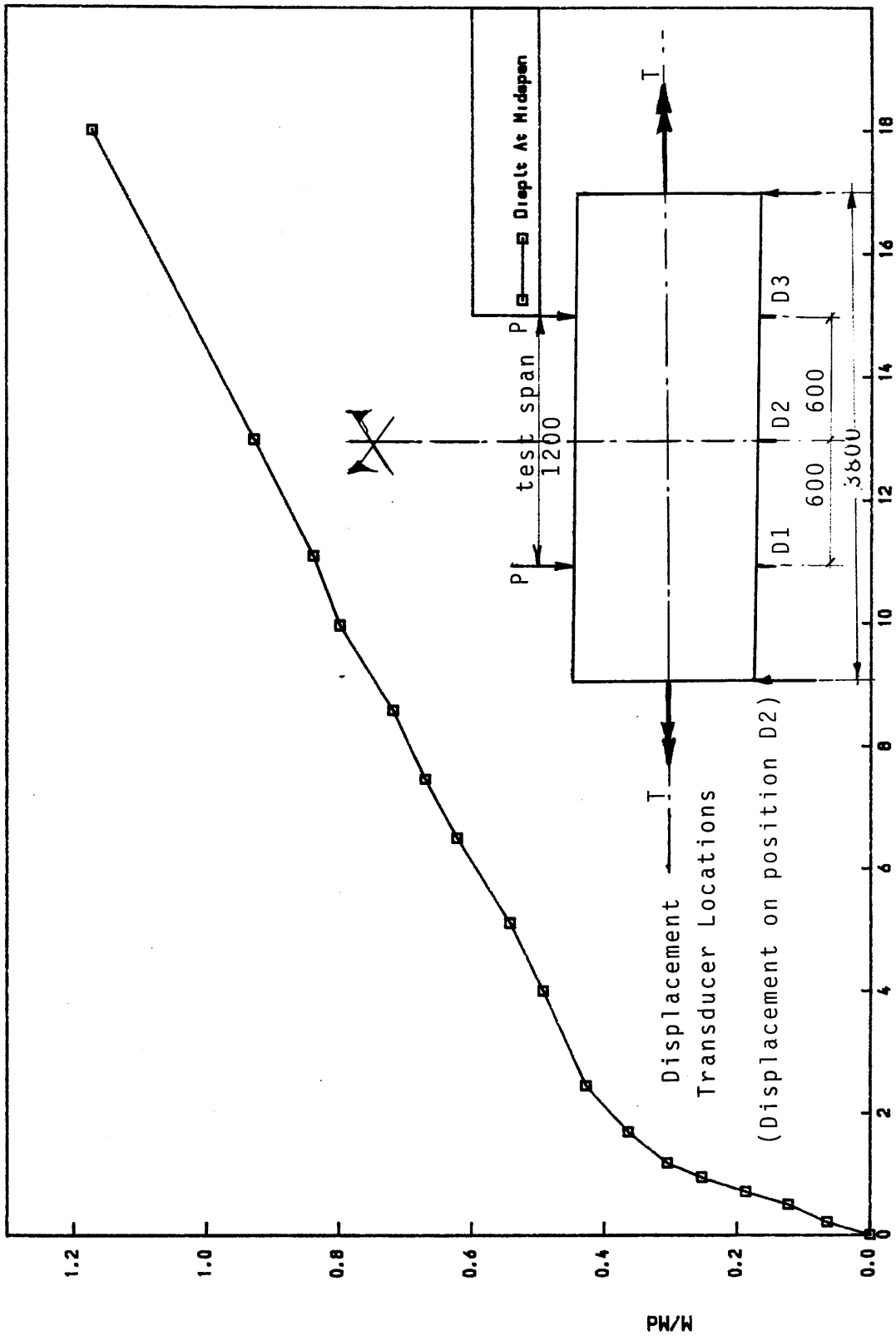

Figure (5.14 Applied Load Vs Vertical Displacement On Central Transducers For Model TB3B Pe= 132.8 KN , Ep= -60 mm

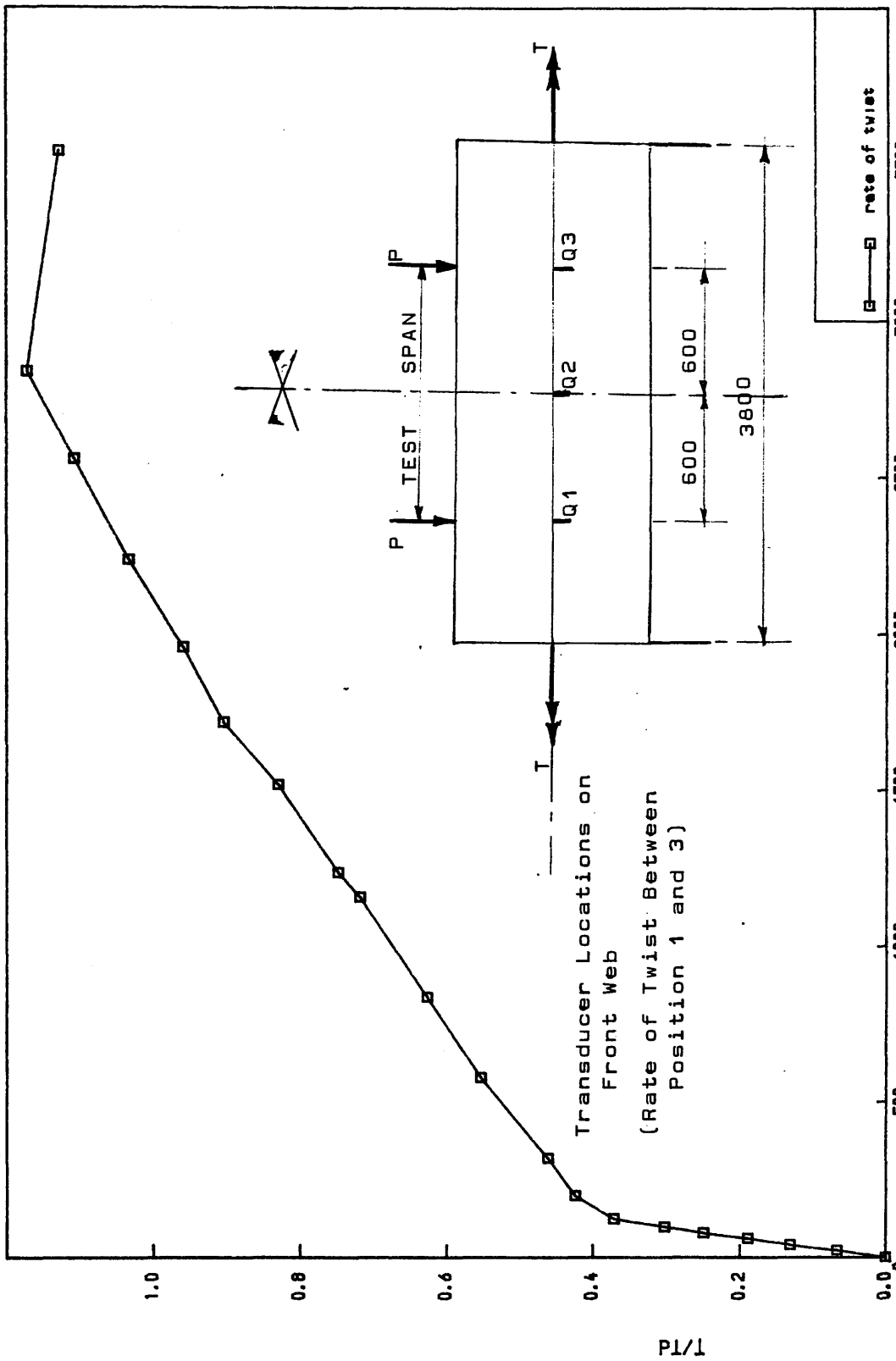

Figure (5.15) Torque Vs Rate of Twist at Midspan
For Model TB3B Pe= 132.8 KN , Ep= -60 mm

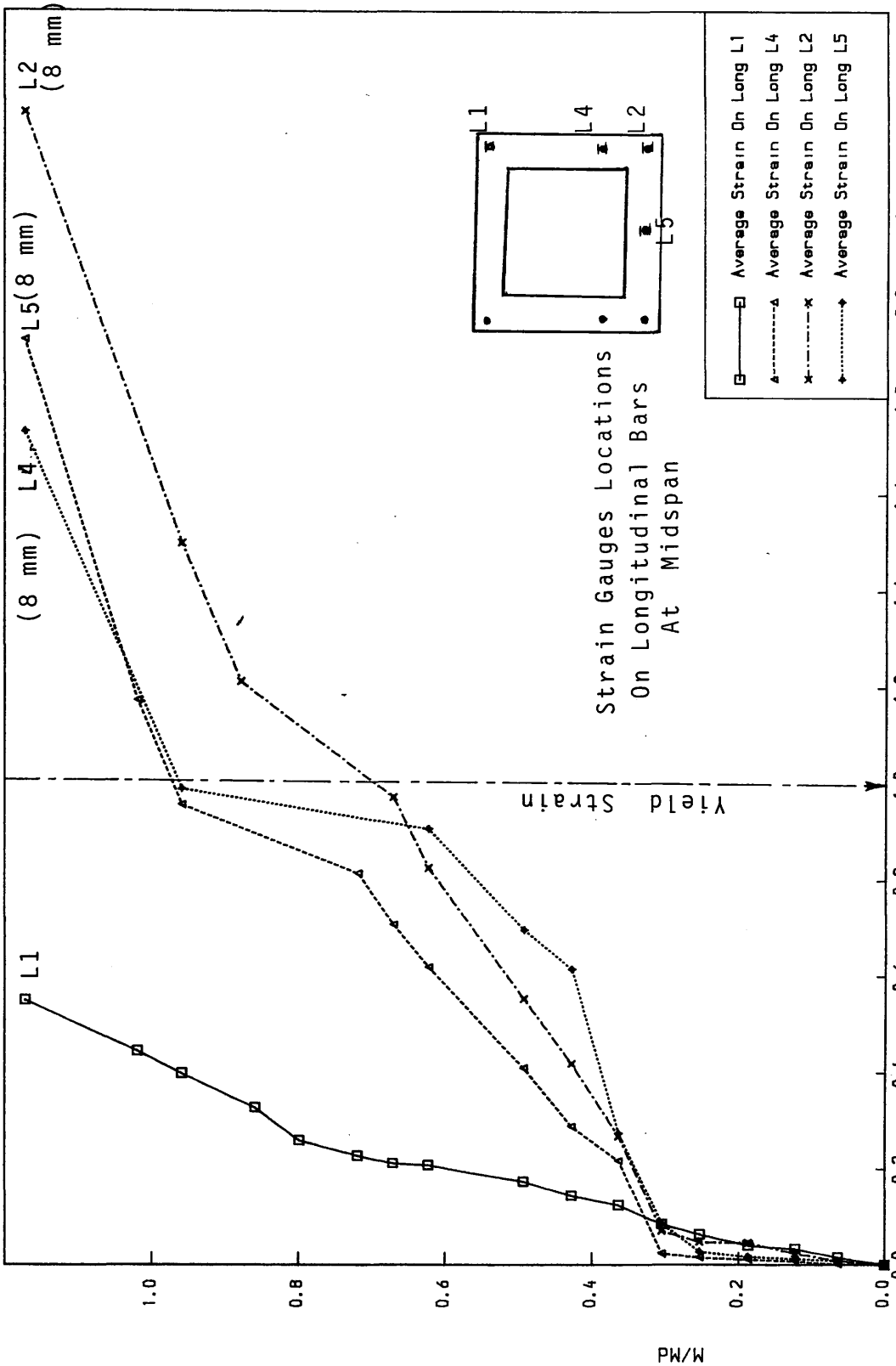

Figure (5. 16) Applied Load Vs Longitudinal Steel Strains At Midspan For Model TB3B Pe=132.8 KN , Ep=-60 mm

E/Ey Ey=0.00254 For 10mm Bar Ey=0.00243 For 08mm

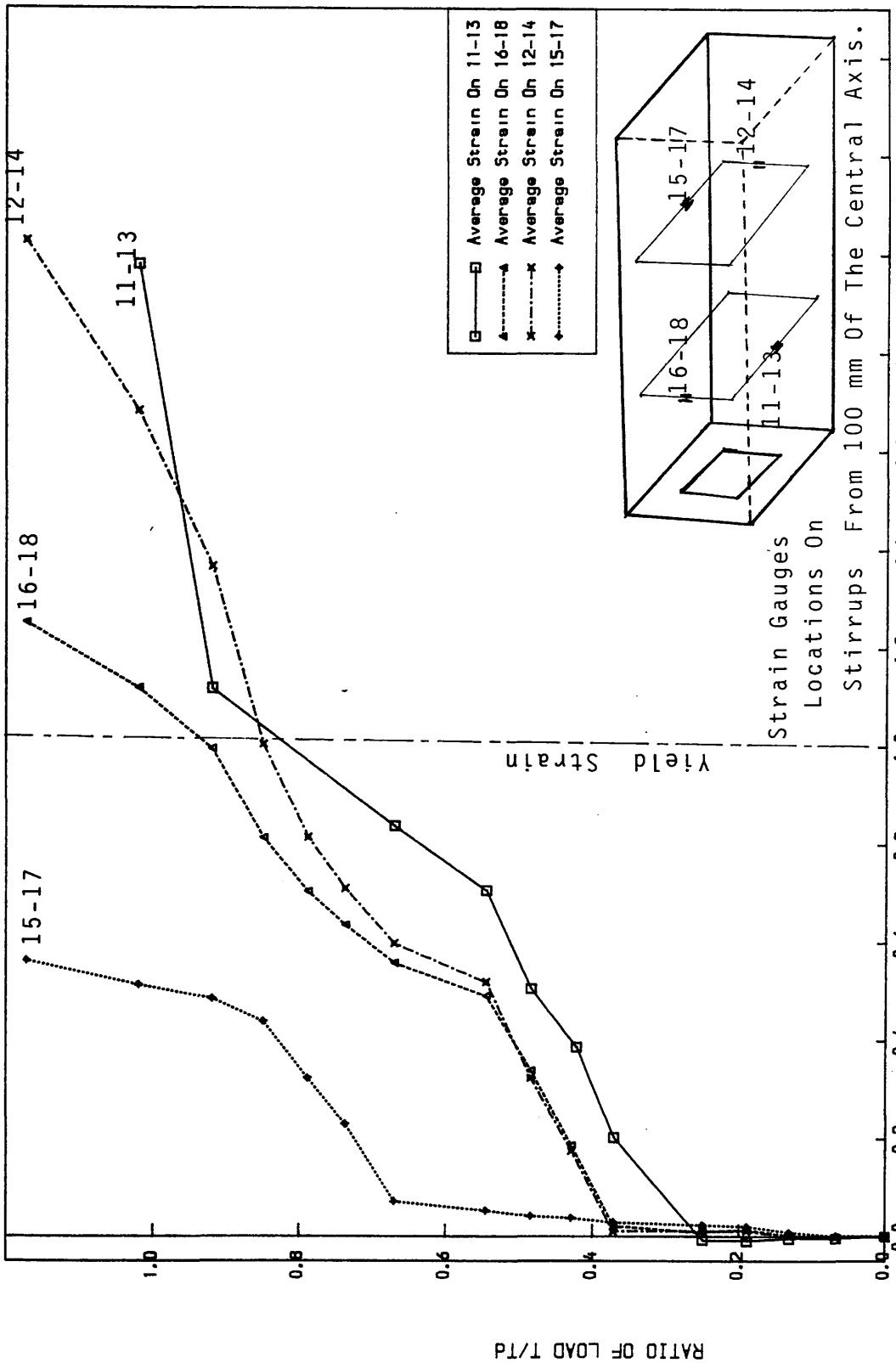

E/Ey Ey=0.00254 For 10mm Bar Ey=0.00243 For 08mm

Figure (5. 17) Applied Load Vs Average Stirrup Strains At Midspan For Model TB3B Pe=132.8 KN , Ep= -60 mm

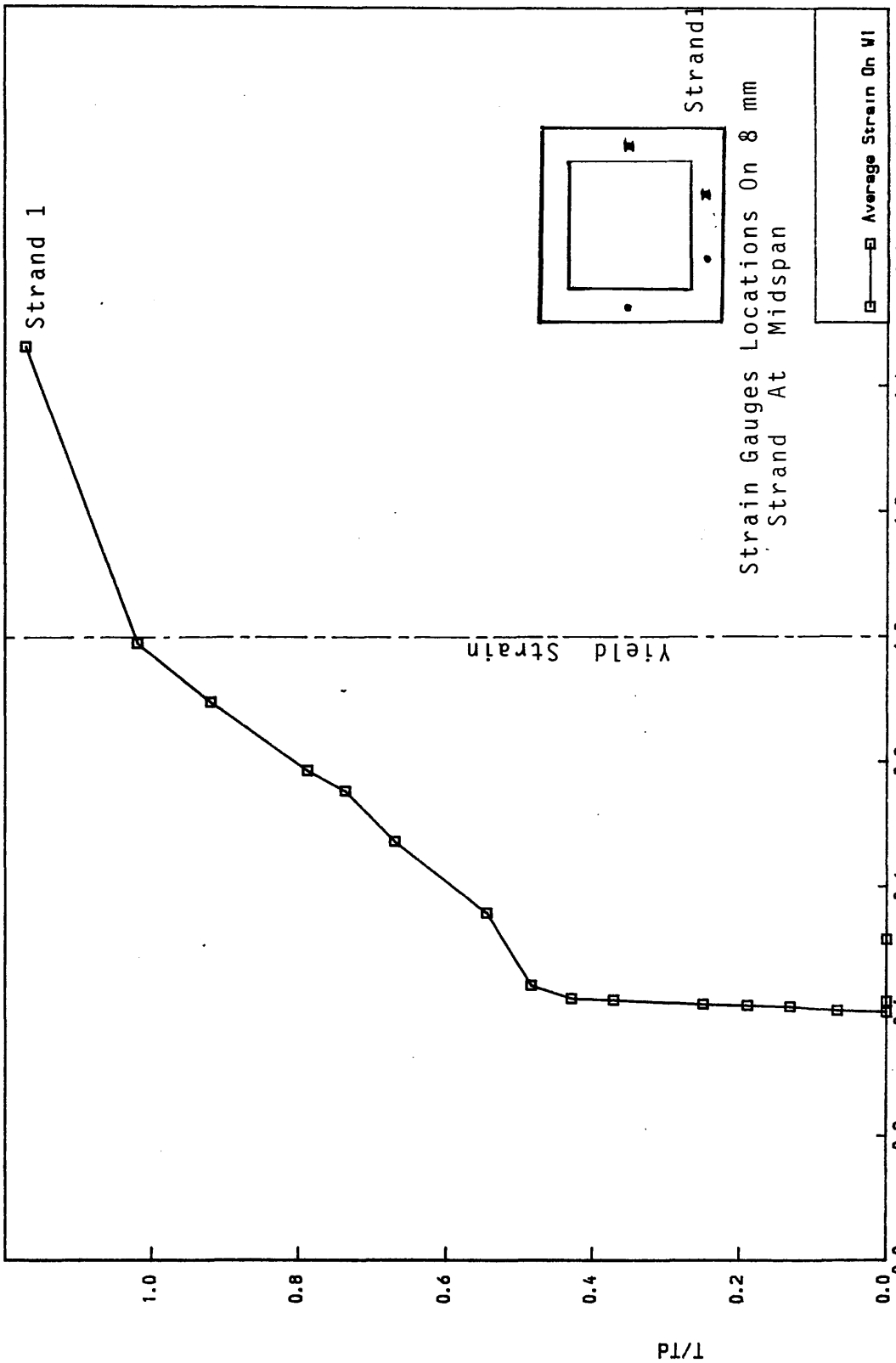

Figure (5. 18) Applied Load Vs Longitudinal Prestressing Steel Strains
For Model TB3B Pe= 132.8 KN , Ep= -60 mm

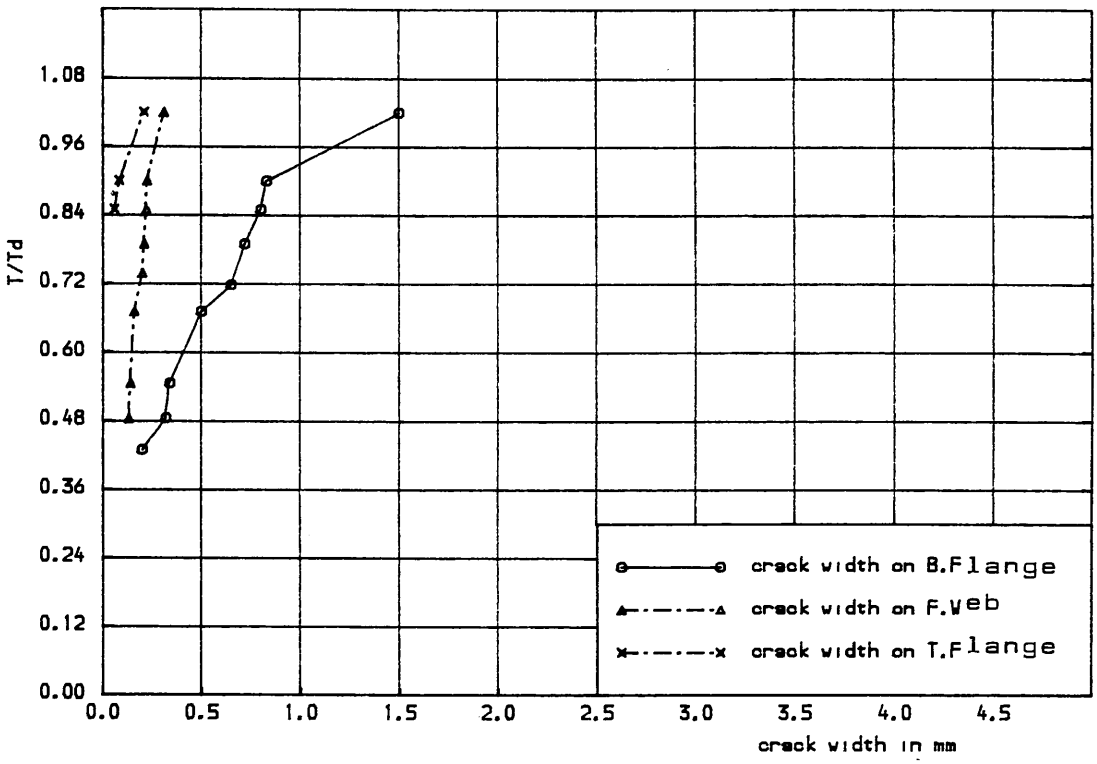

Figure(5.19)applied load vs crack width of concrete

.(a) FOR MODEL TB3B T/B=1

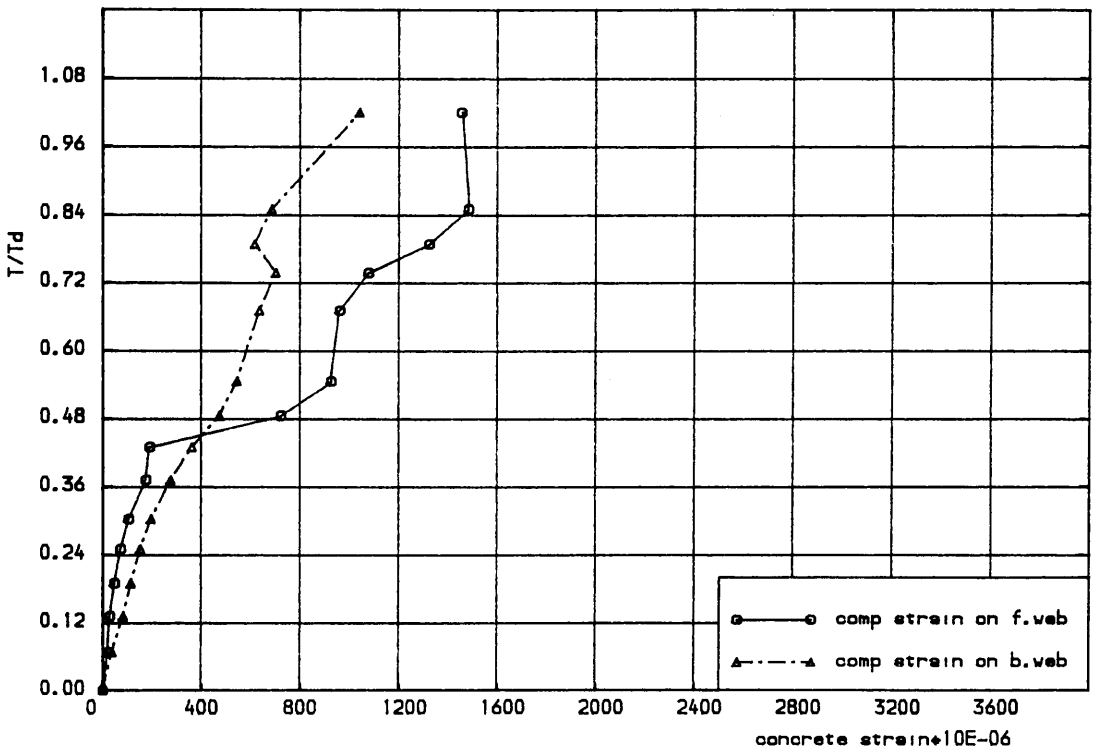

Figure(5.19) APPLIED LOAD COMBINATION VS CONCRETE SURFACE COMP STRAINS

.(b) FOR MODEL TB3B T/B=1

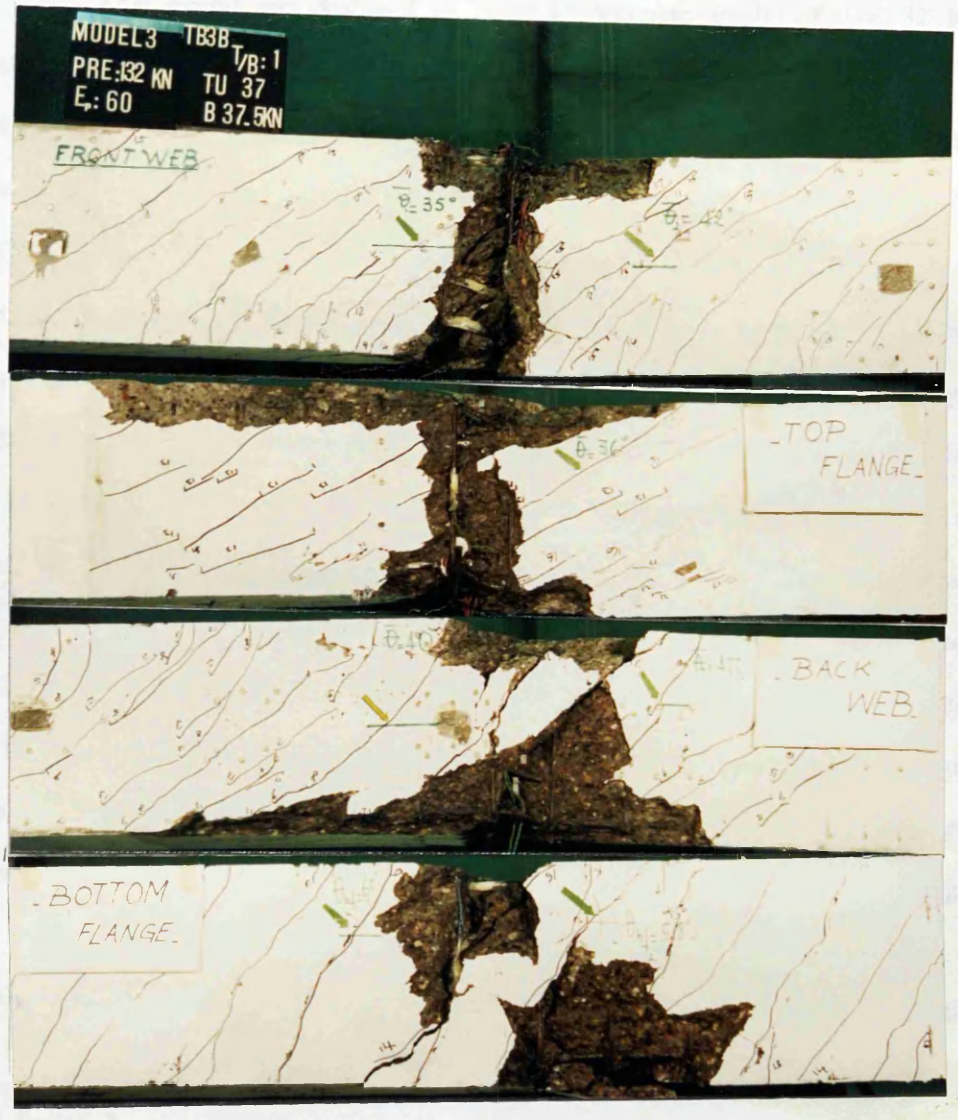

Figure(5.20) Crack Development at each load stage
(Beam TB3B- Torsion/Bending= 1.0
P_e =132KN, E_p= -60mm).

Note: Large tensile crack on back web and
Desintegration of beam

the increase of loading. The angle of cracks varied from 40^0 to 60^0.

5.2.1.4 Specimen TB4B

This model was designed to resist an ultimate torsion T_d = 32 KNm and bending moment M_d = 32 KN. It was prestressed by means of five 8 mm diameter strand, each of which had 32 KN as effective prestressing force. The behaviour pattern of specimens TB3B and TB4B which were tested in the same test rig were similar. Figure (5.22) was not produced due to transducers fault. At a load 0.38Xdesign load inclined cracks started appearing on the webs and bottom flange. Some of them extended through the depth of the webs and bottom flange. Very small deformation was observed at this stage. Between loads 0.38Xdesign load and full design load, more spiral cracks developed in the webs and flanges. The angle of inclination of the cracks to beam axis as shown in Figure (5.26) varied between 42^0 and 52^0 on all faces onf the beam. Steady increase in deformation was noted from 0.4Xdesign load as shown in Figure (5.21). The first yield of steel was observed on the stirrups at 0.76Xdesign load, existing cracks widened considerably leading to a rapid increase in deformation. The strain on longitudinal steel and stirrups were almost at yield or had exceeded the yield strain as shown for bottom longitudinal steel bars in Figure (5.23) and bottom prestressing strand in Figure (5.25). Figure (5.26) shows the crack pattern and their propagation with the increase of loading.

5.2.2 Series 2

This series consisted of two beams designated PT1B and PT2B. The specimens had the same cross–sectional as the first series. The object of this series was to study the behaviour of partially prestressed beams under pure torsion where PT1B was designed according to the direct design approach. While PT2B was tested to analyse the behaviour of partially prestressed beams and the effect of prestress on the crack resistance and strength.

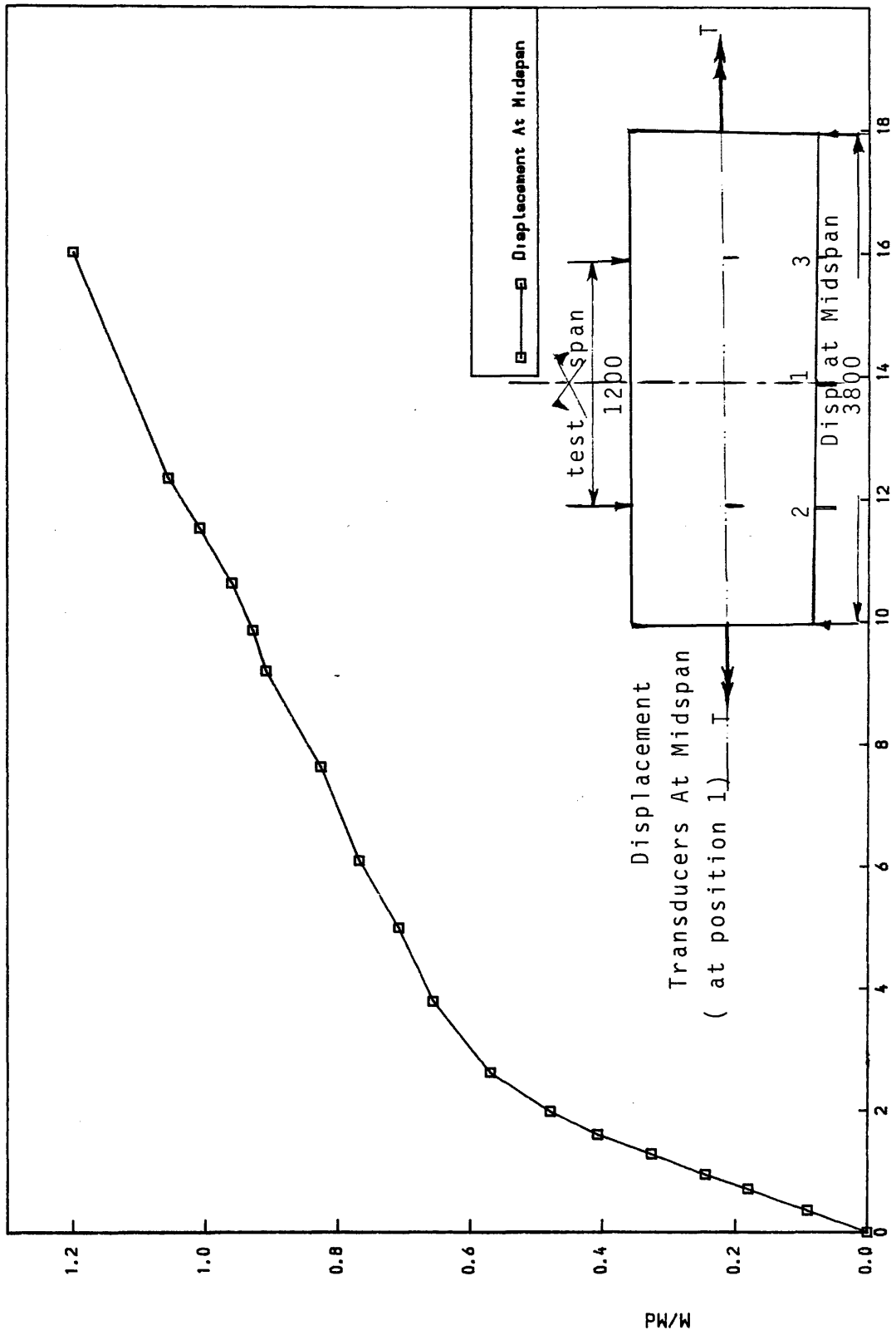

Figure (5. 21) Applied Load Vs Vertical Displacement On Central Transducers For Model TB4B Pe= 160 KN , Ep= -72 mm

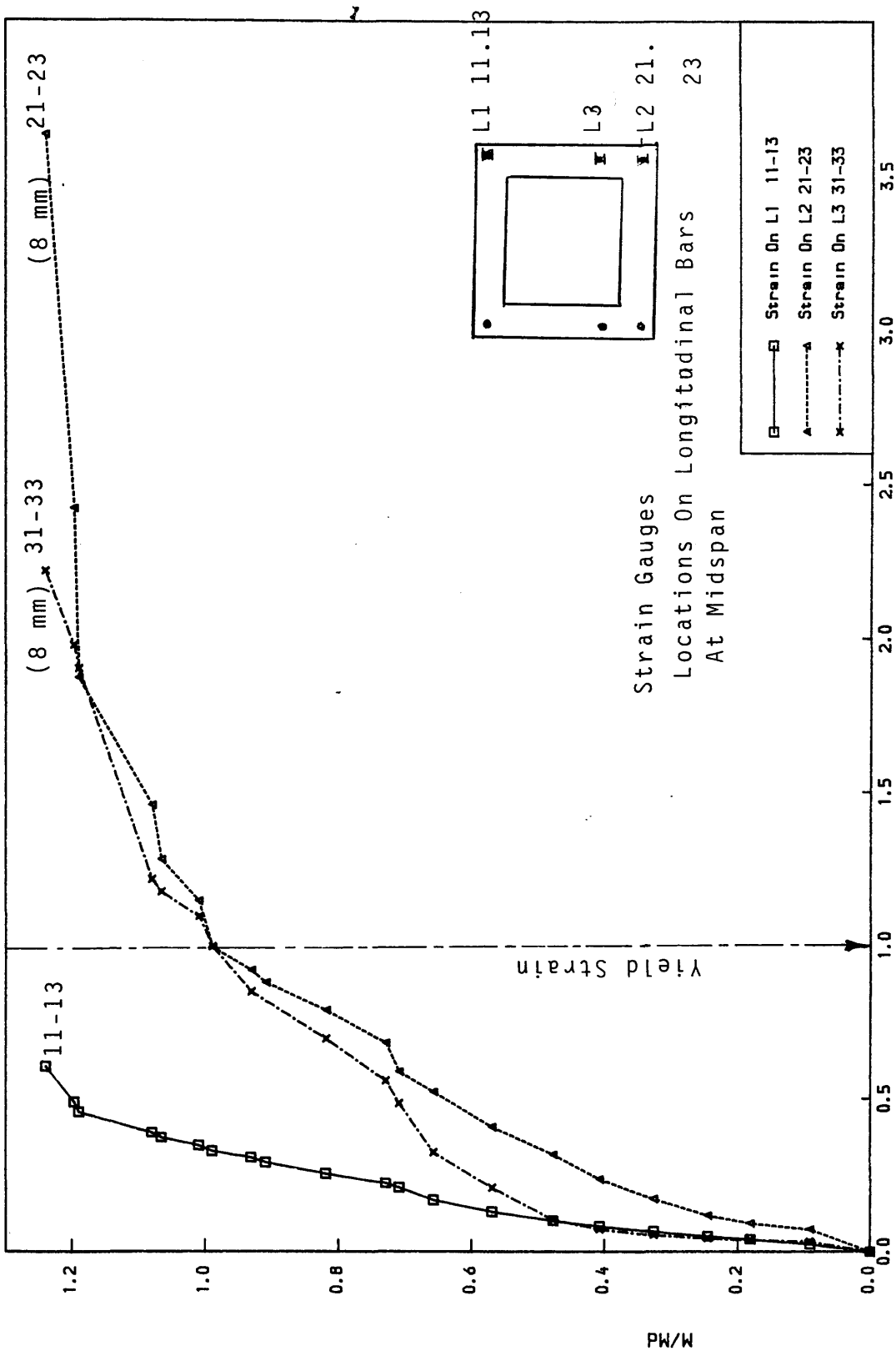

Figure (5. 23) Applied Load Vs Longitudinal Steel Strains At Midspan
For Model TB4B Pe= 160 KN , Ep= -72.0 mm

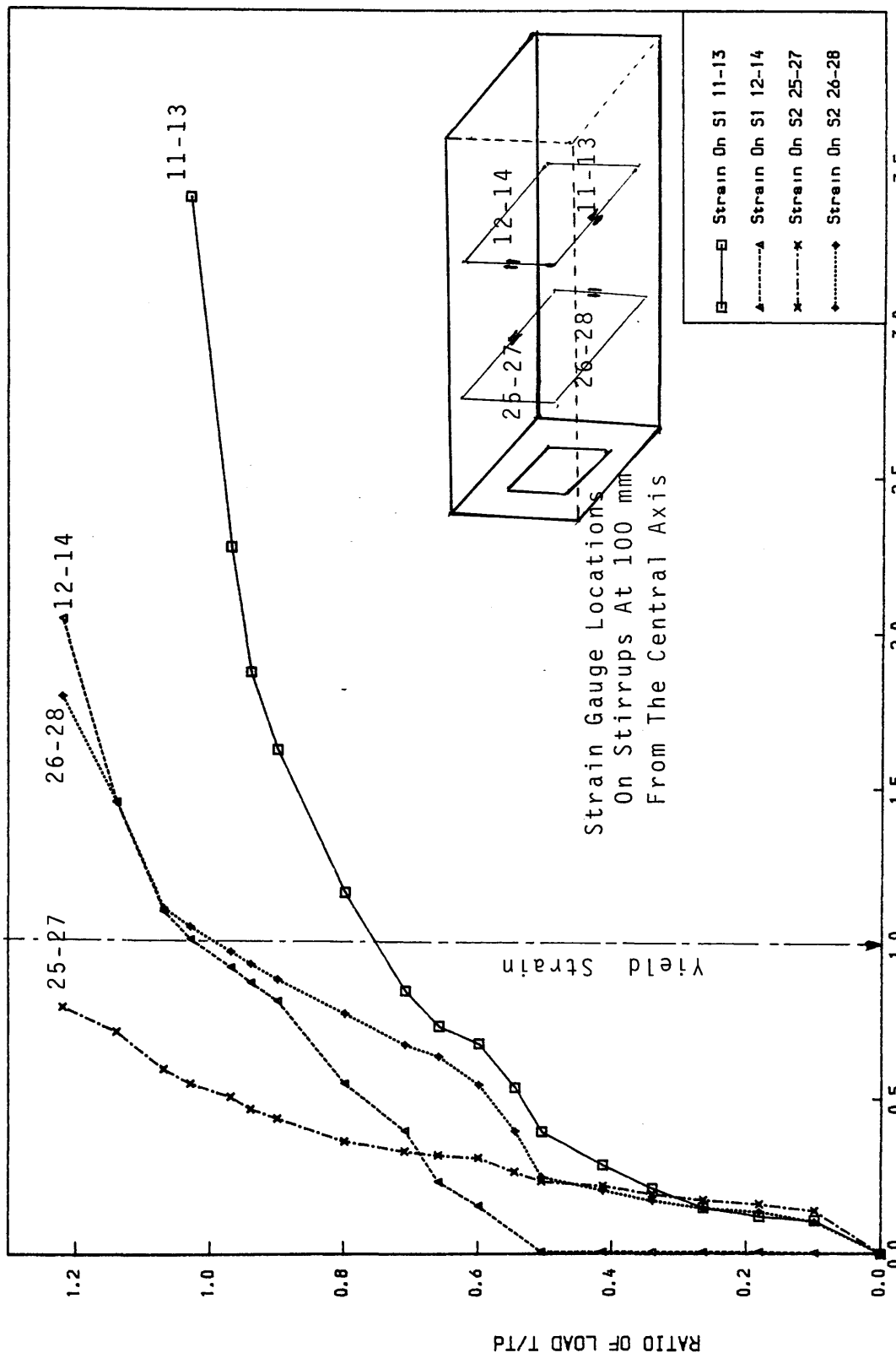

Figure 15. 24) Applied Load Vs Average Stirrup Strains At Midspan For Model TB4B Pe=160 KN , Ep= -72 mm

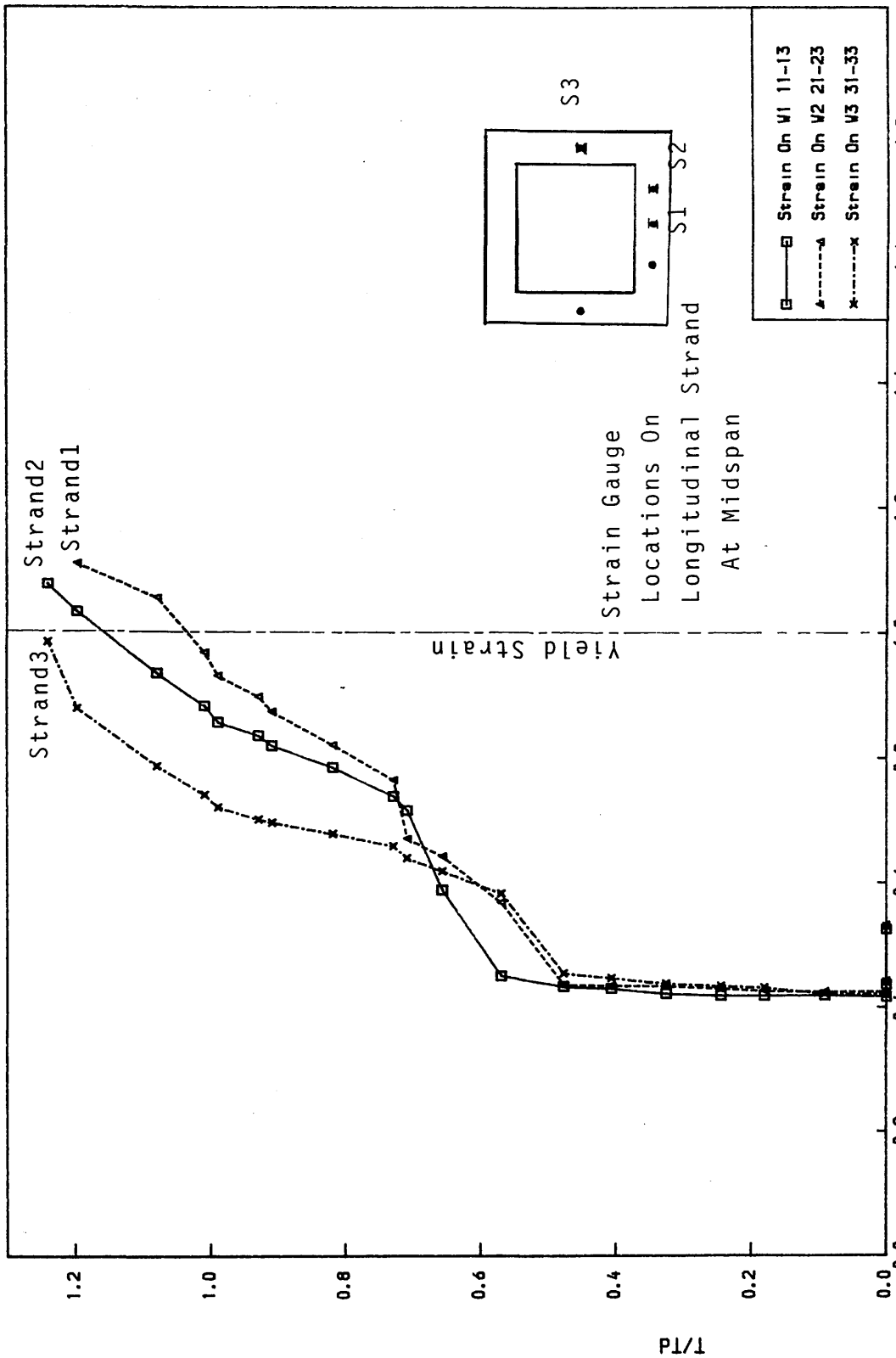

Figure (5. 25) Applied Load Vs Longitudinal Prestressing Steel Strains For Model TB4B Pe= 160 KN , Ep= -72 mm

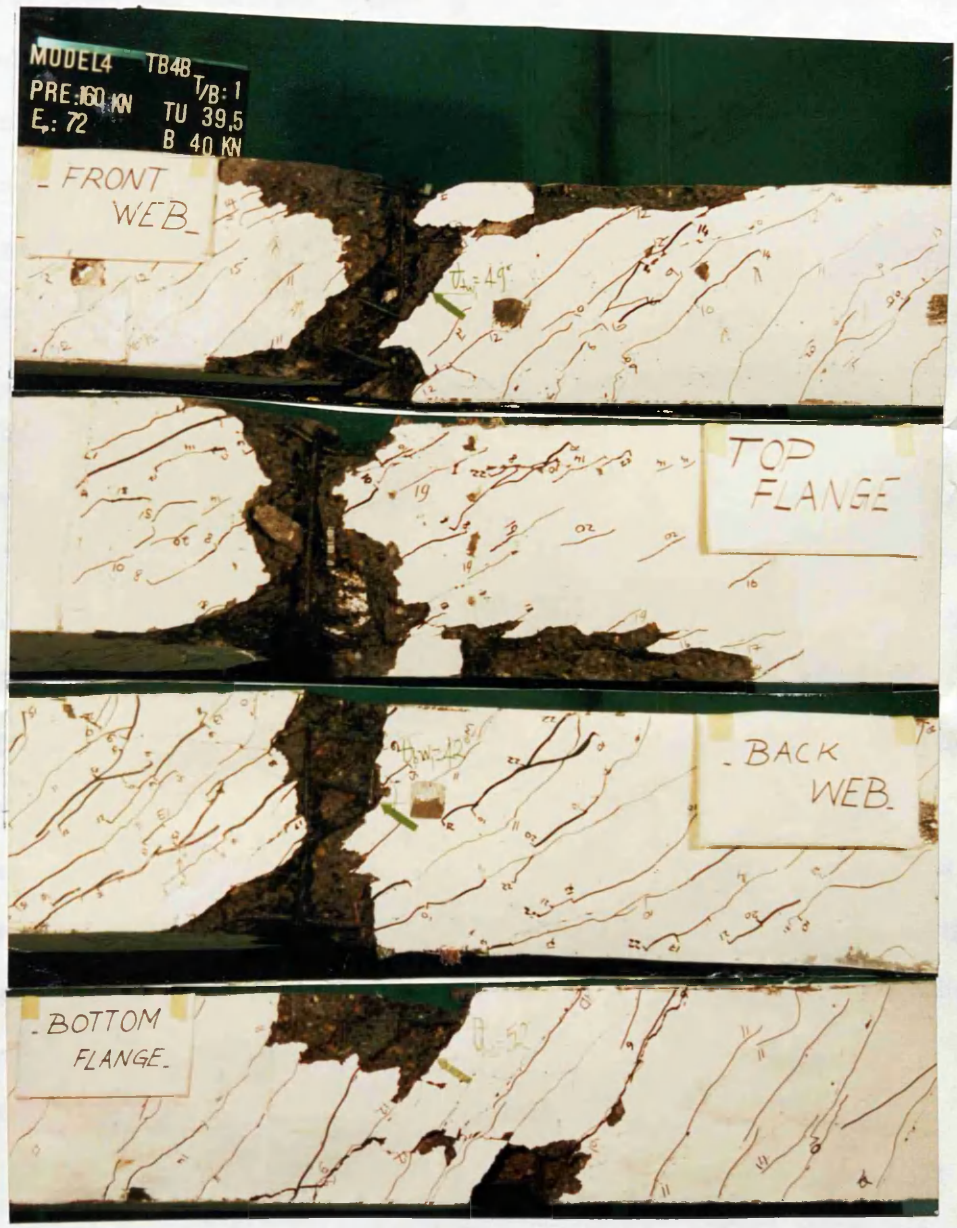

Figure(5.27) Crack Development at each load stage

(Beam TB4B- Torsion/Bending=1.0, Pe=160 KN,

Ep=-72mm.

Note Torsion Cracks and Complete Desintegration

Of Beam

5.2.2.1 Specimen PT1B

Model PT1B was designed according to the direct design approach for ultimate torsion of T_d= 32 KNm.

The beam was uniformly stressed by means of four 5 mm diameter wires each of which had 20 KN as initial prestressing force. The measured effective prestressing force in each wire at the time of test was 17 KN. The load was applied in small increment of 0.06Xdesign load. Cracking started at approximately 45^0 to the longitudinal axis. Upon further loading the cracks spread almost simultaneously on all faces maintaining the same angle of inclination. As loading increased, the spiral nature of torsional cracking became apparent as the cracks extended on all four faces. Figure (5.27) shows the torque twist curve for specimen PT1B. The behaviour is essentially linear up to the cracking torque. The steel response is given in Figures (5.28) to (5.30). Prestressing steel developed yield strain as beam approached its ultimate capacity (the first yield observed was at 0.956 design load). Nearly equal tensile strains were observed in the top and bottom longitudinal bars.

The concrete surface principal compressive strains are shown in Figure (5.31). These behaved linearly, and were small in value up to the cracking torque . A sudden increase was noticed after cracking. Figure (5.32) shows the process of crack propagation on the four faces. The rapid propagation of torsional cracking is clearly seen as loading progressed. The inclination of the cracks to the longitudinal axis varied between 40^0 to 53^0.

5.2.2.2 Specimen PT2B

This investigation was undertaken to analyse the behaviour of prestressed concrete beam under pure torque. The amount of prestress provided for this beam was (1.5) times the amount provided for PT1B. However, the same amount of ordinary steel as PT1B was provided. PT2B was initially prestressed by four 8 mm diameter strands, each of which had 30 KN as prestress force. During the test the measured effective prestressing force on each strand was 24.8 KN as compared to

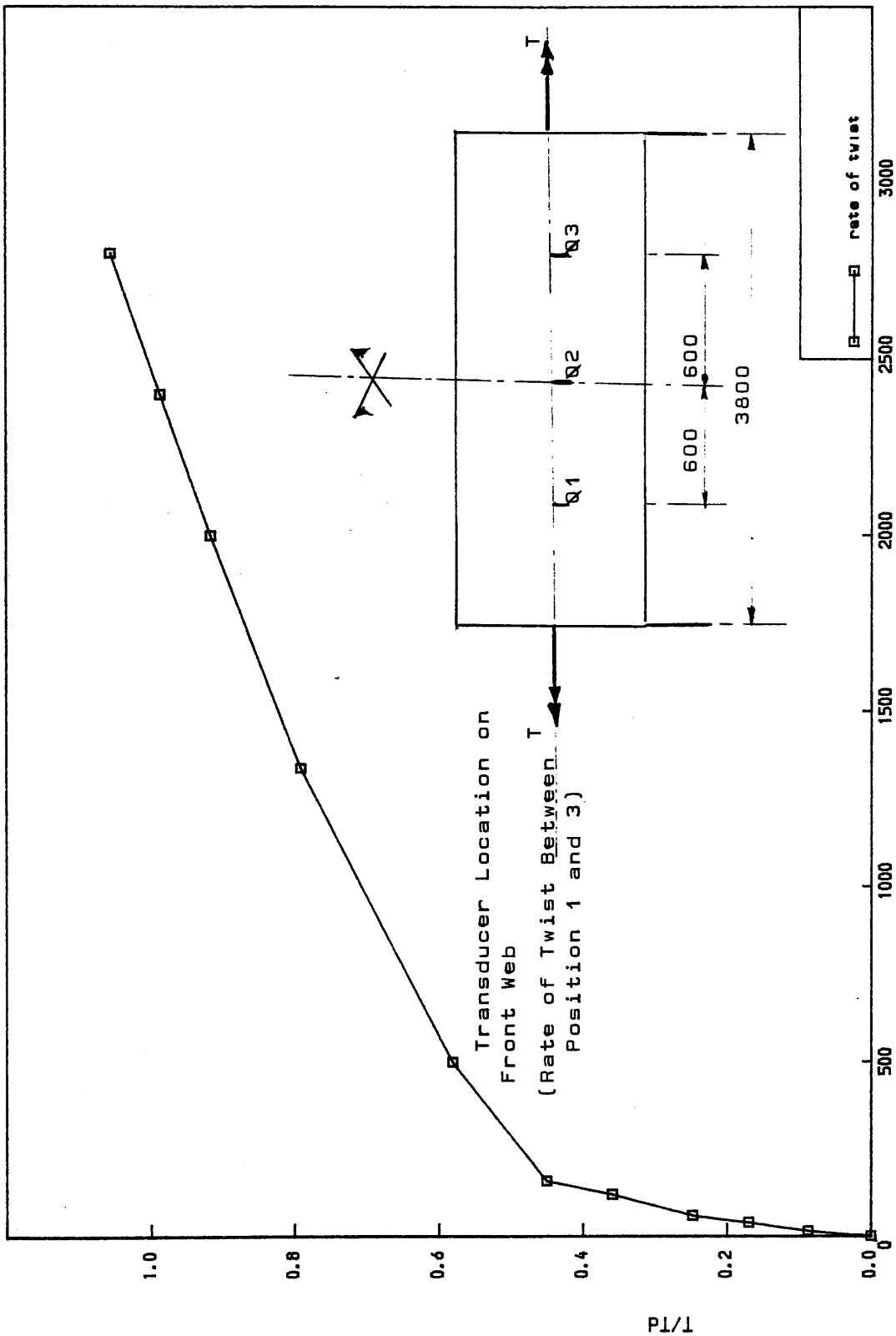

Figure (5.27) Torque Vs Rate of Twist at Midspan
For Model PT1B " Pure Torsion " Pe= 68 KN , Ep= 0.0

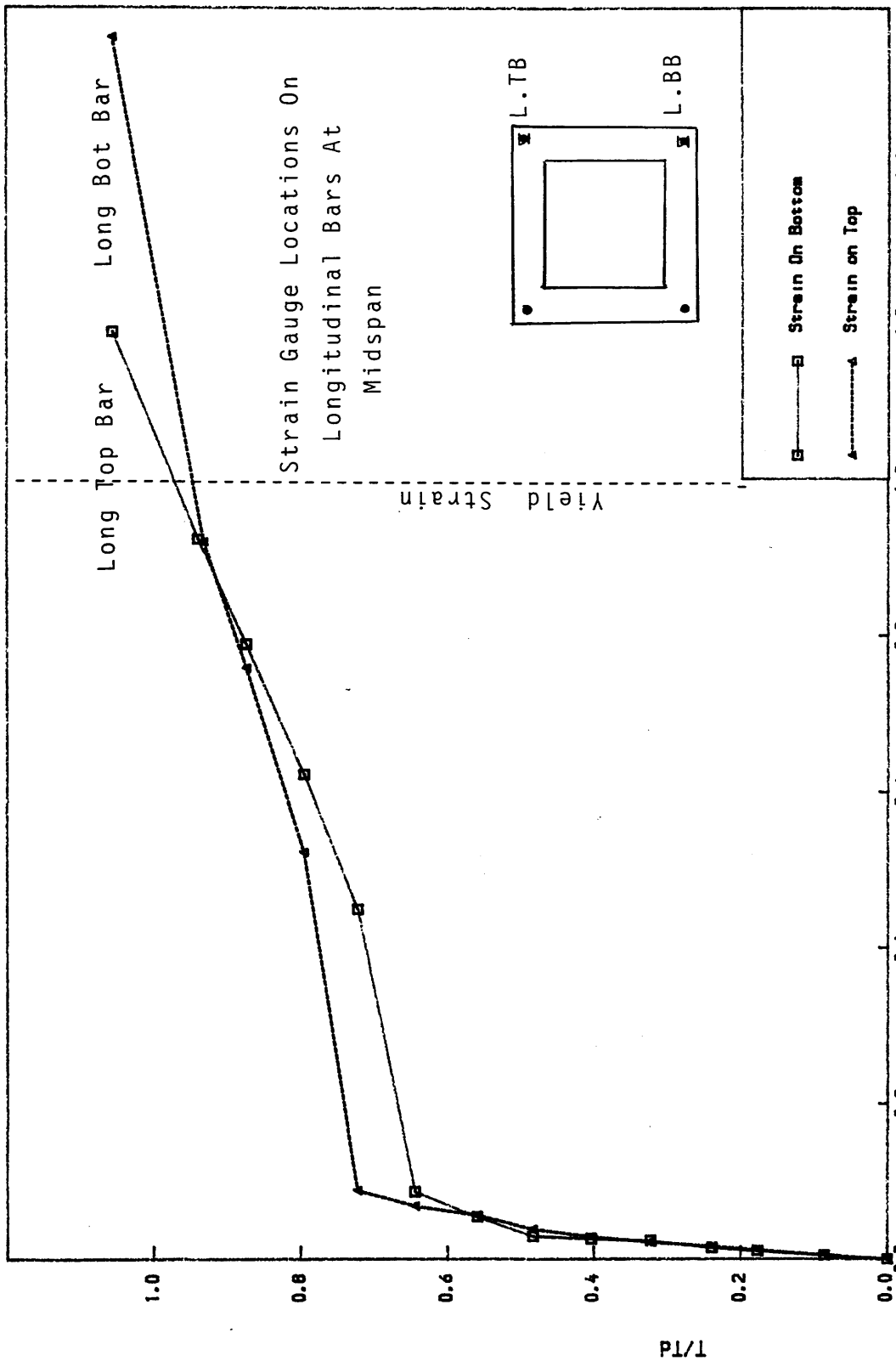

Figure (5. 28) Torque Vs Longitudinal Steel Strains For Model PT1B "Pure Torsion" Pe= 68 kn , Ep= 0.0

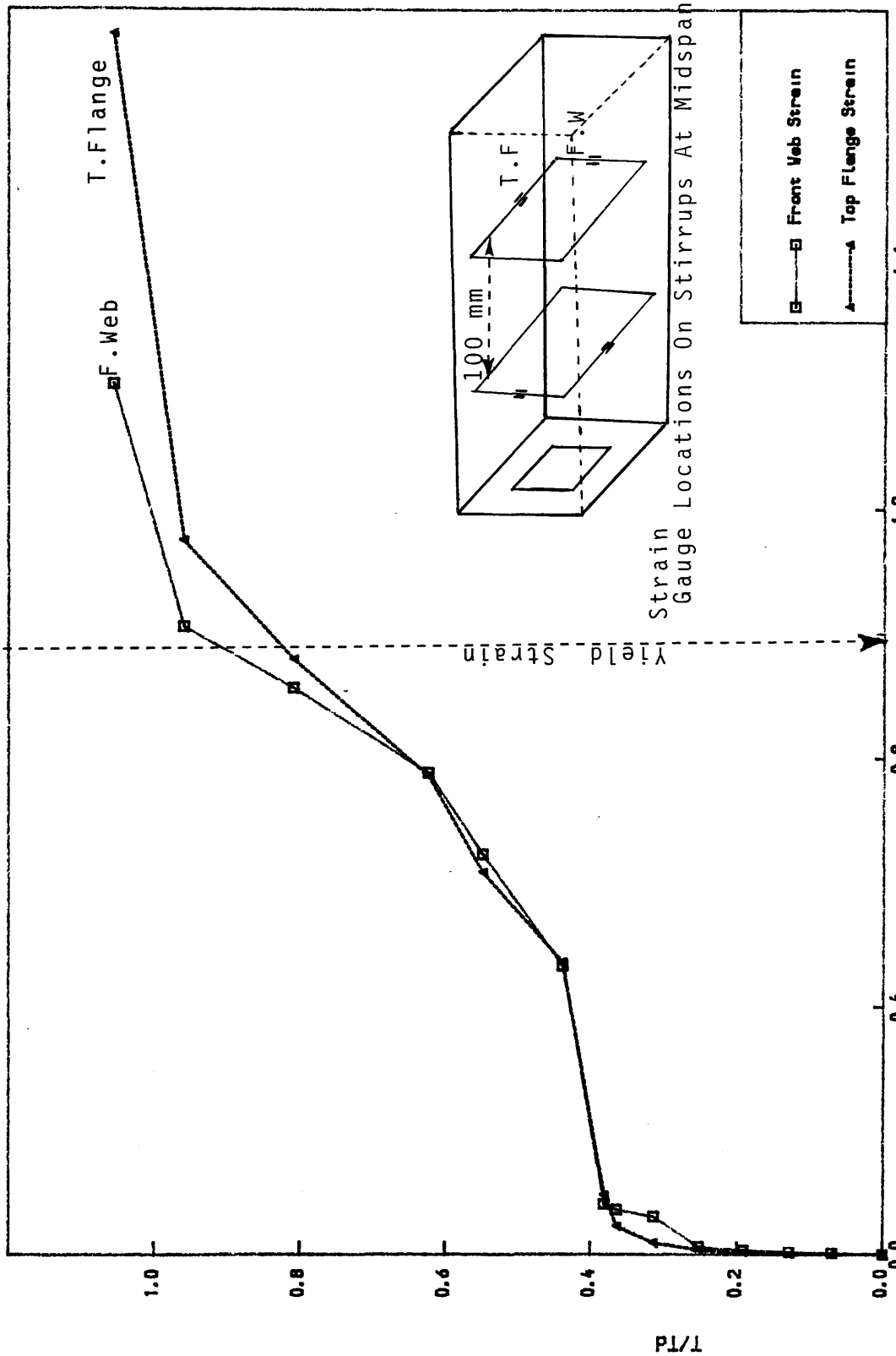

Figure 15.29) Torque Vs Stirrup Steel Strains For Model PT1B
"Pure Torque" Pe= 68 KN , Ep= 0.0
Ey=0.00243 For 08 mm Bar

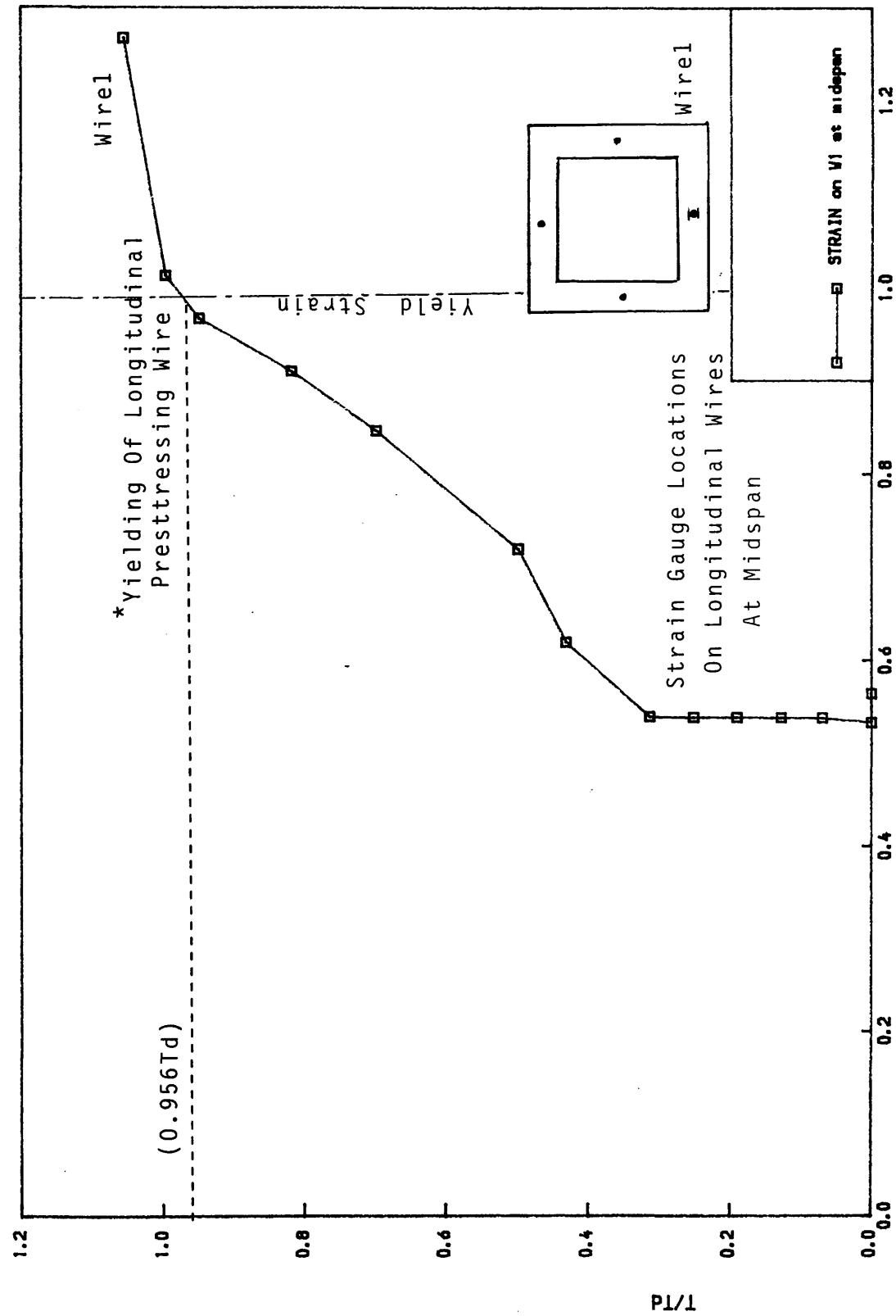

Figure (5. 30) Applied Load Vs Longitudinal Prestressing Steel Strains For Model PT1B "Pure Torsion" Pe= 68 KN , Ep= 0.0

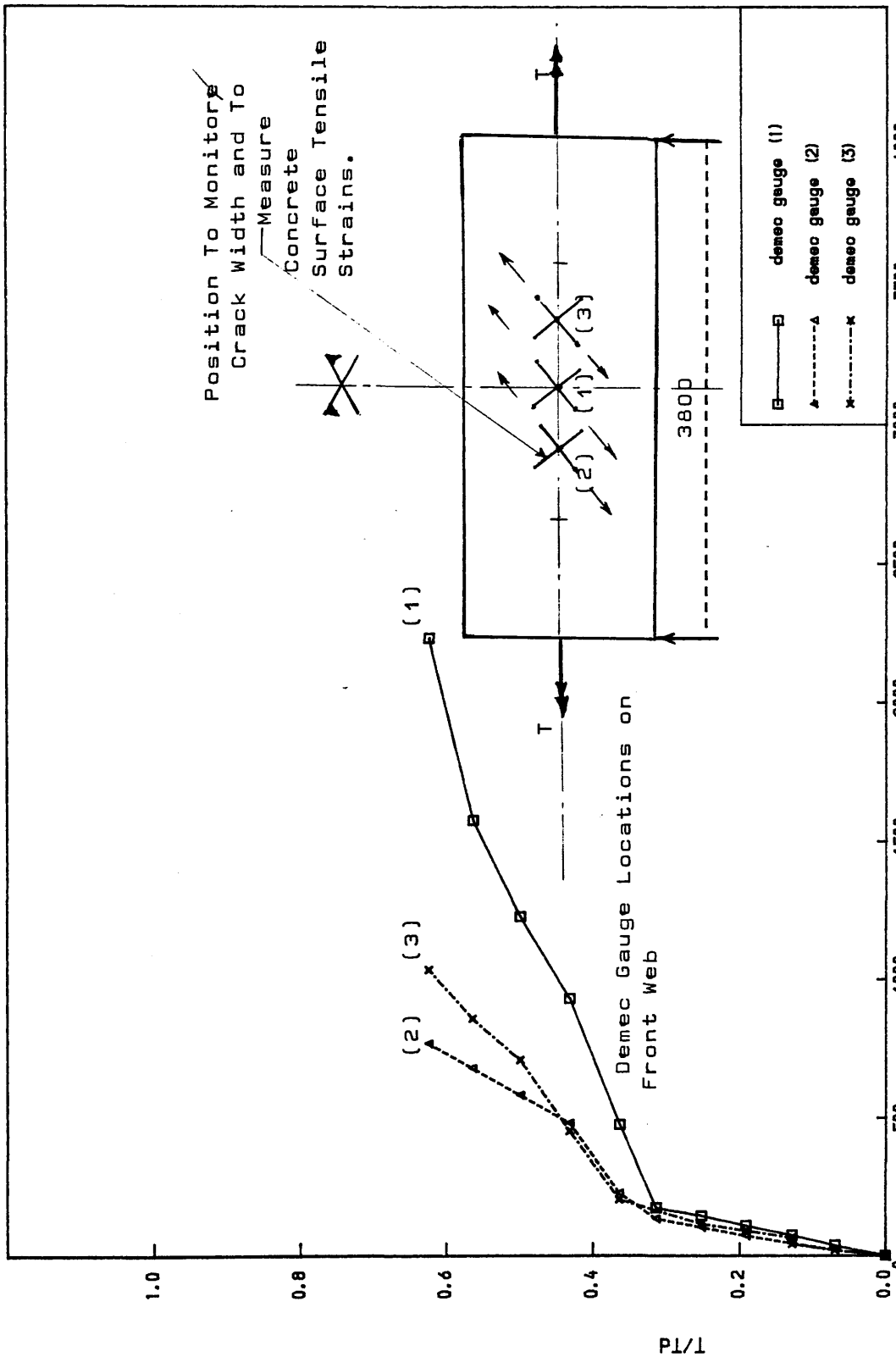

Figure (5.31) Torque Vs Principal Compressive Surface Strains
For Model PT1B "Pure Torsion" Pe= 68 KN , Ep= 0.0

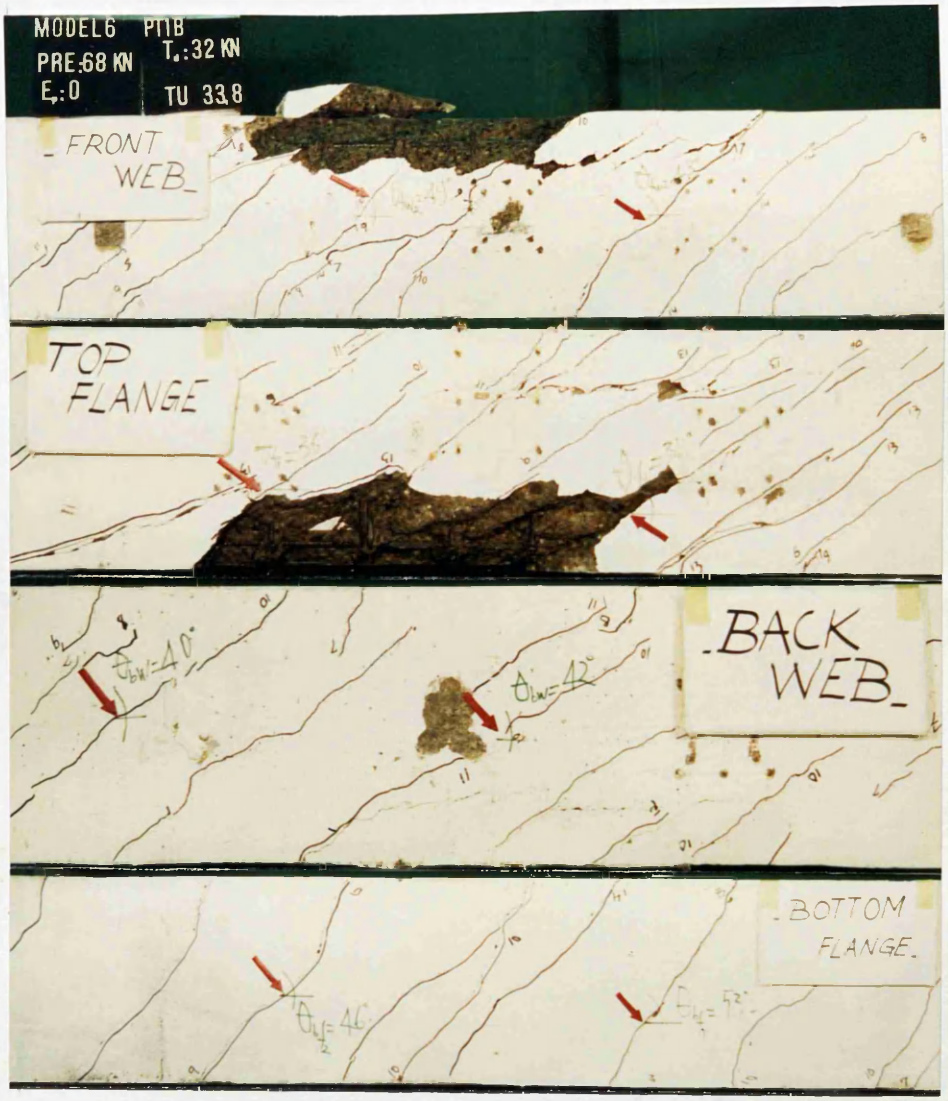

Figure(5.32) Crack Development at each stage load
(Beam PT1B- Pure Torsion, P_e= 68KN, E_p=0.0)

Note: Crushing on the top flange.

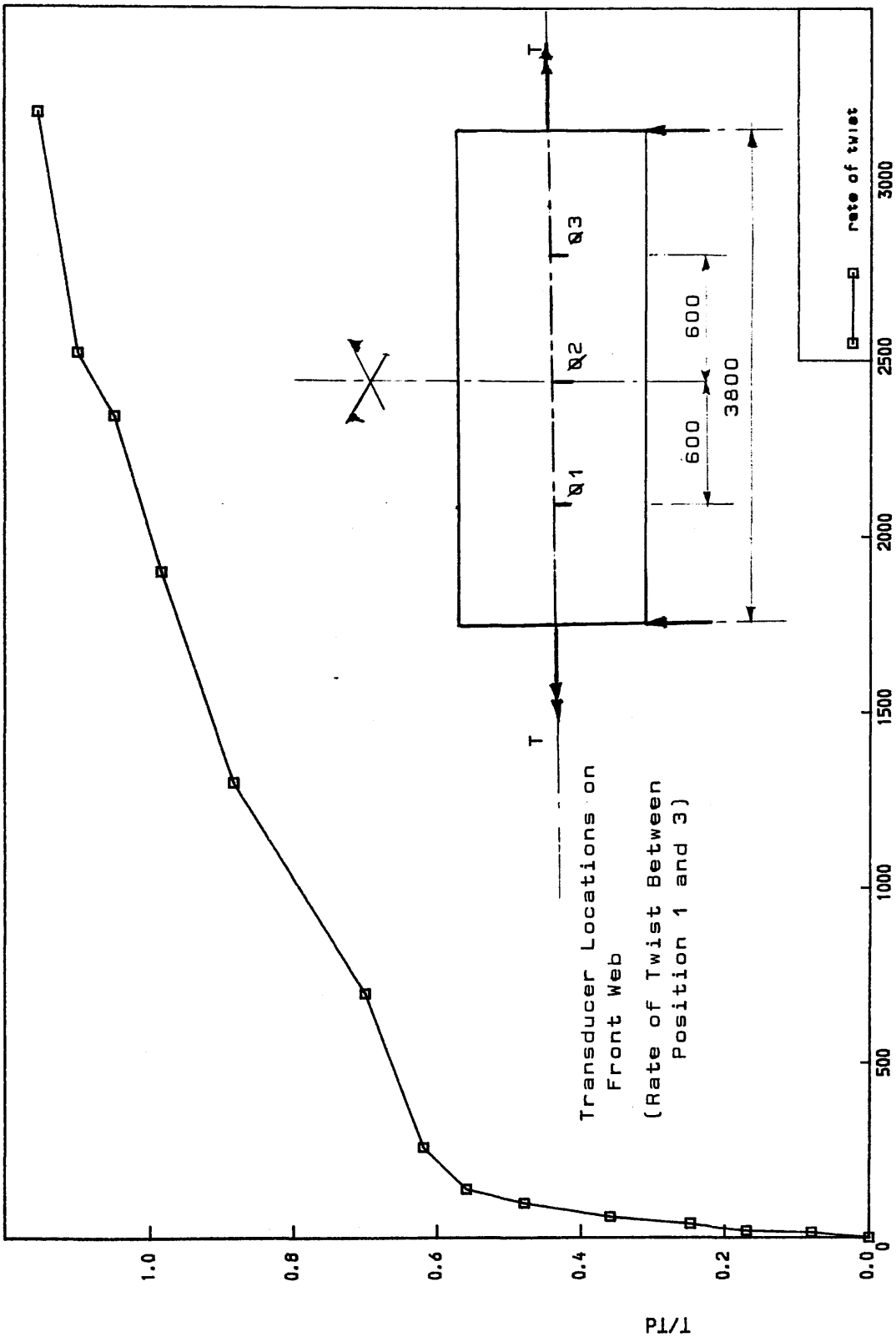

Figure (5.33) Torque Vs Rate of Twist at Midspan
For Model PT2B " Pure Torsion " Pe= 99.3 KN , Ep= 0.0

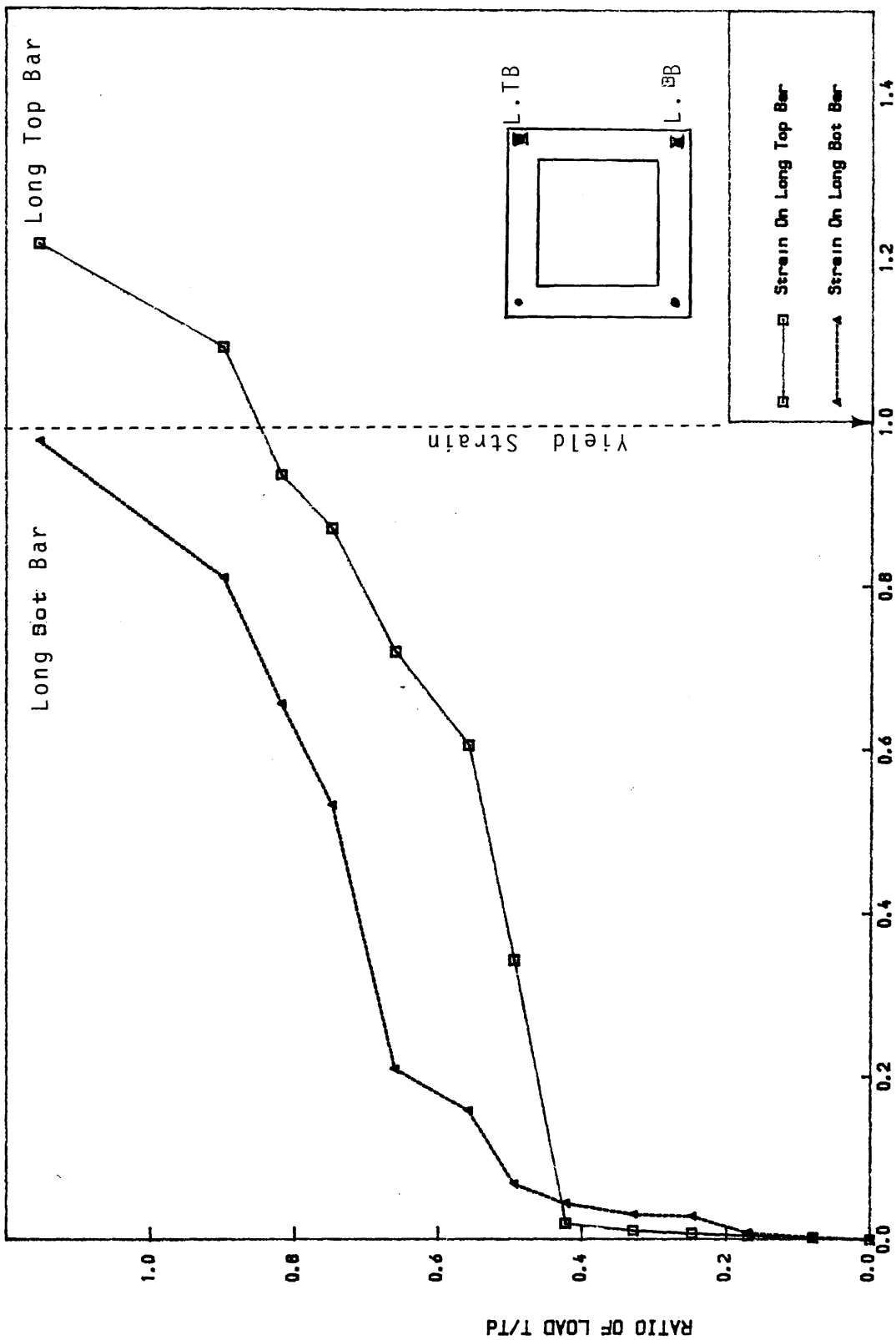

Figure (5. 34) Applied Load Vs Average Longitudinal Steel Strains For Model PT2B Pe=99.30 KN , Ep= 0.0 mm

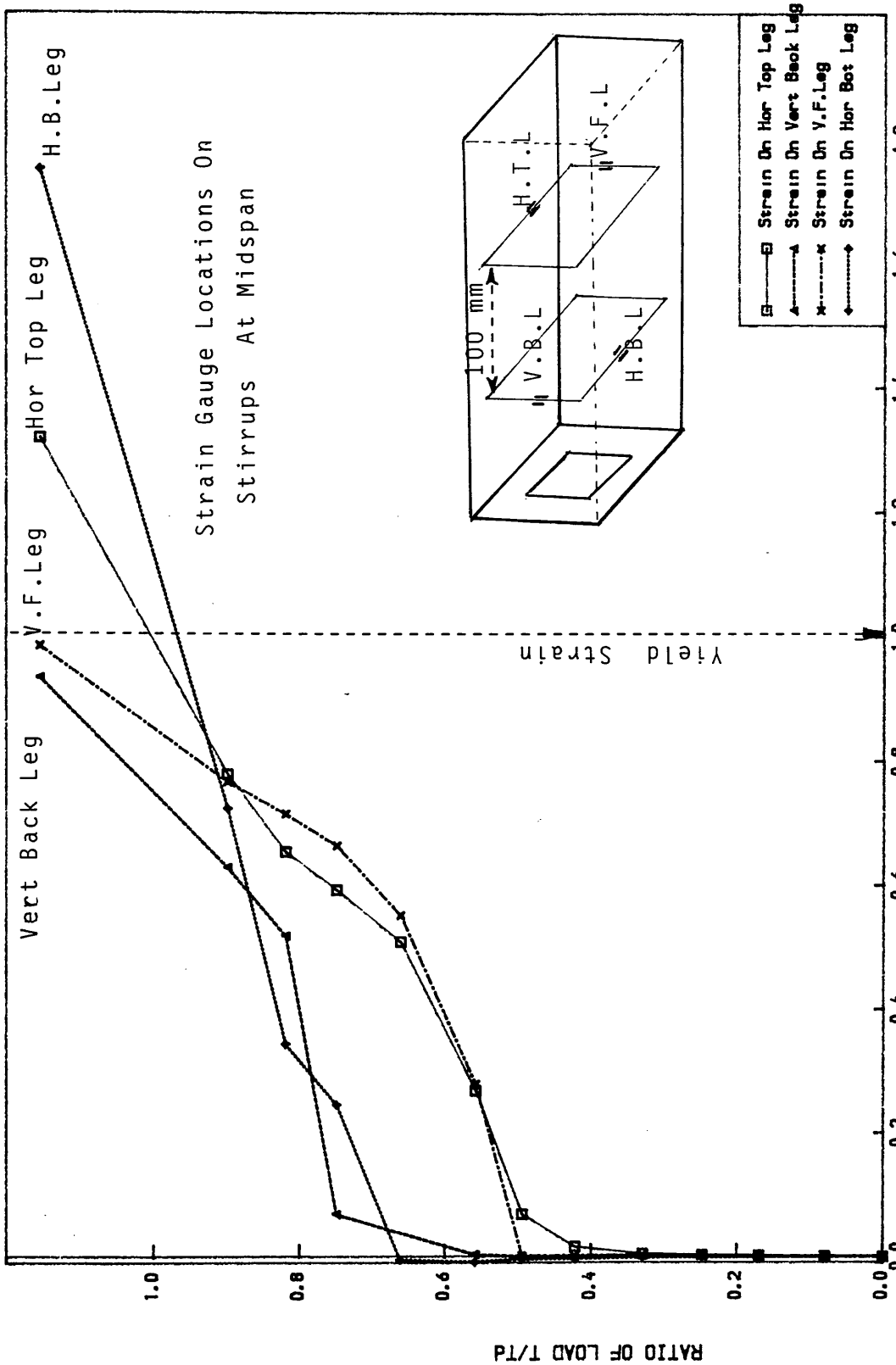

Figure (5. 35) Applied Load Vs Average Stirrup Strains At Midspan For Model PT2B Pe=99.30 KN , Ep= 0.0 mm

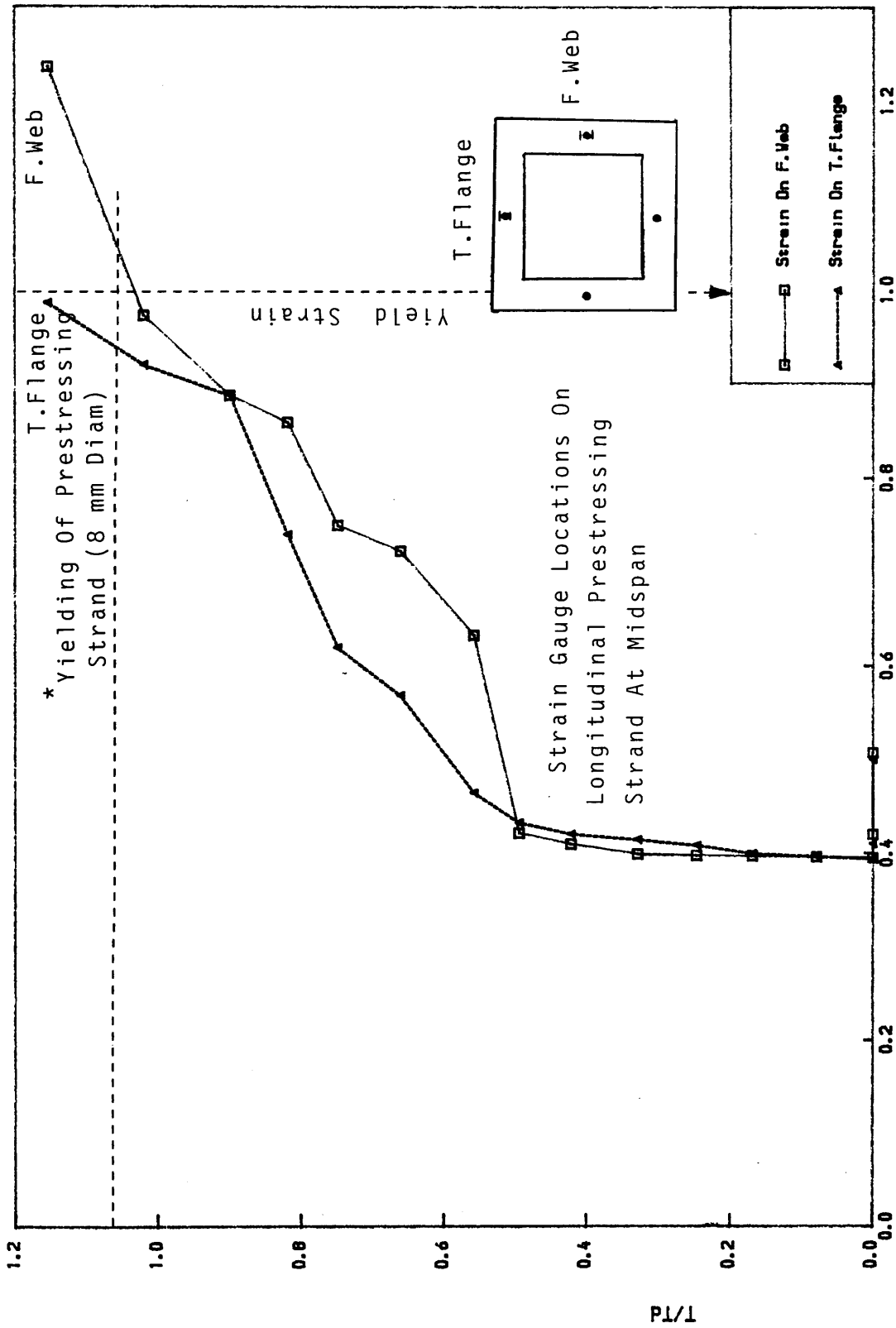

Figure 15.36) Applied Load Vs Longitudinal Prestressing Steel Strains For Model PT2B "Pure Torsion" Pe= 99.30 KN , Ep= 0.0

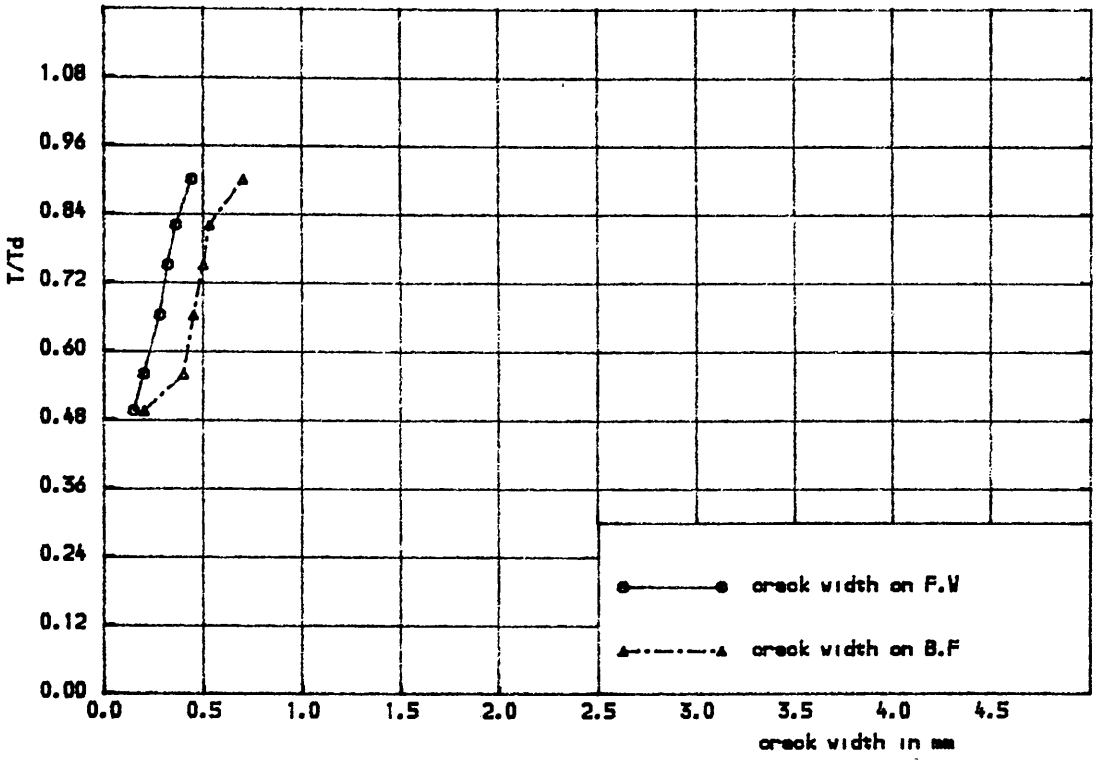

Figure (5.37) applied load vs crack width of concrete

. (a) FOR MODEL PT2B Design Torque Td= 32 KN

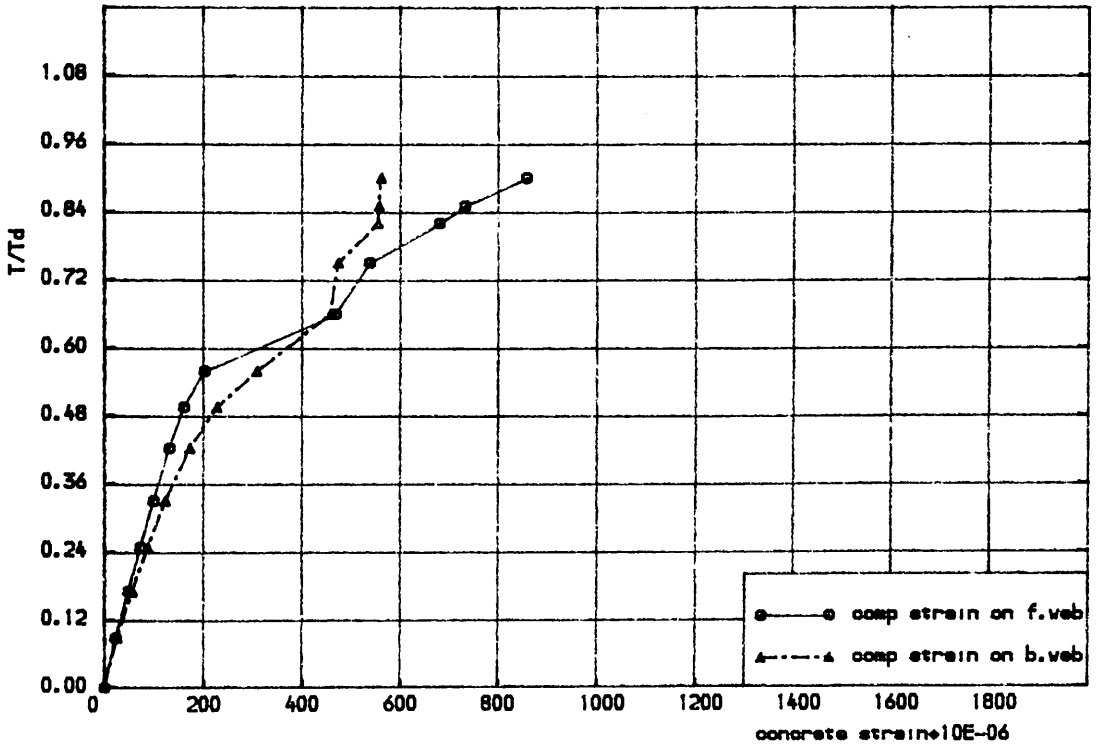

Figure (5. 37b) APPLIED TORQUE VS CONCRETE SURFACE COMP STRAINS FOR MODEL PT2B Td=32 KN

Figure(5.38) Crack Development at each load stage
(Beam PT2B- Pure Torsion, P_e= 99.3 KN, E_p= 0.0)
Typical Torsion Failure.

Note: Spalling of Concrete at the Corners and Crushing on the Top Face.

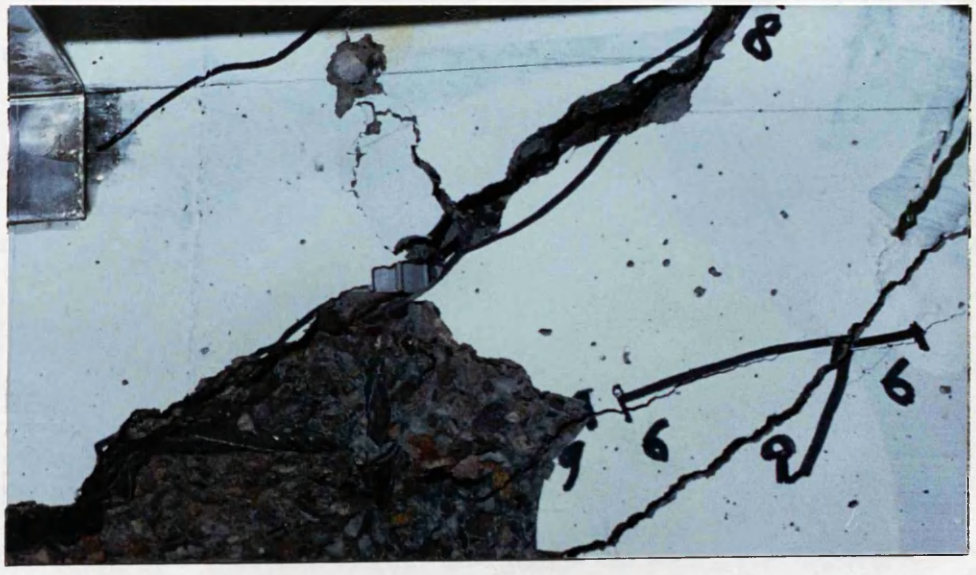

Note: Wide Diagonal Tensile Cracks Leading to Violent and Destructive Failure.

the 17 KN effective prestress provided for PT1B).

Generally, similar behaviour to PT1B regarding crack initiation and propagation was observed. The cracking torque, as should be expected, was higher at 18 KN. The pattern of torsional cracks were well developed at each increment of load during the experiment. Cracks appeared at larger spacings. The torsional stiffness before cracking is increased by prestressing. Figures (5.34) to (5.36) show the steel response of all types of steel used for specimen PT2B. They were again of similar behaviour, as the previous specimen. Nearly equal tensile strain were developed on the prestressing strands. The first yielding was observed at 1.14 of design load.

Figure (5.37a) shows torque vs crack width. The crack width was smaller than for specimen PT1B. Figure (5.37b) shows the measured concrete surface compressive strains versus the applied torque. The figure indicates clearly that their values were small before the cracking load and increased suddenly upon cracking.

Figure (5.38) shows the crack pattern of specimen PT2B. The cracks were generally about 45^0 to the axis of the beam. The actual failure of the specimen was violent accompanied by a loud bang

5.3 OBSERVATION AND COMMENTS TO ALL BEAMS

The aim of this section is to summarise the behaviour of all models already described in Section 5.2 under the following headings

- 1) Deflection
- 2) Twist
- 3) Crack pattern
- 4) Concrete surface strains
- 5) Steel response
- 6) Failure loads and failure models

5.3.1 Deflection

The load– deflection relationship can be classified into three stages.

a) Behaviour before cracking

b) Behaviour after cracking

c) Behaviour after yield of steel

Prior to the first crack, very small deflection was observed for the first set of beams in comparison to the other models. After cracking however, the flexural stiffness of the section deteriorates progressively. At this particular stage, the load deflection curve is non– linear accompanied by the yielding of steel and development of several closely spaced flexural torsion– cracks and leading to a rapid increase in deflection until final collapse of the beam. Table (5.2) compares the post cracking flexural stiffness expressed as a percentage of the pre– cracking value for all specimens. The table reveals that the ratio of the post to pre– cracking torsional stiffness ranges between 12 to 22%. Comparison of the flexural stiffness between TB3B and TB4B under identical combined loading but different amount of prestress shows that TB4B is slightly stiffer than TB3B.

5.3.2 Twist

Similar to the load deflection curves, the torque– twist curves can be classified into three stages:

a) Behaviour before cracking

b) Behaviour after cracking

c) Behaviour after yielding of steel

As can be seen in all experimental torque– twist curves the behaviour is essentially linear before cracking. The effect of varying the amount of prestress produce a slight increase in the pre– cracking torsional stiffness. Indeed, the cracking torque is mainly a function of prestress. Table (5.3) lists cracking torque for all specimens.

Torsional stiffness is greatly reduced after cracking occurs especially for specimen under pure torsion. It drops to about 5 to 20% of the uncracked value. Table (5.3) also reveals that the post– cracking stiffness increased with the increase of prestress.

5.3.3 Crack pattern

Torsional cracks are distinguished by the " helical " nature and also by their rapid propagation compared to flexural cracking. Cracks observed on the top flange extended through the depth when approaching the ultimate load. This behaviour is attributed to the induced compressives stresses in the top flange of the beam which resist the tendency for cracks to develop.

5.3.4 Steel strains

Longitudinal prestressing steel, ordinary steel and closed stirrup did not carry any measurable strains before cracking. After cracking, gradual increase in strain was observed in steel as shown in Figures (5.23), (5.24), (5.25) for model TB4B. The steel strains, after cracking, were found to continuously increase with loading on all type of reinforcement. The load vs steel strains curves show that at failure of all specimens yielding had occured in at least one of the longitudinal or transverse reinforcement. The strains of the longitudinal bars provided in the top flange for the stirrup anchorage were less than yield strain.

5.3.5 Concrete surface strains

Two set of demec gauges oriented at 45^{0} to the longitudinal axis were used, in order to measure the compressive strains parallel to the cracks and the tensile strains normal to the cracks. The compressive strains were similar to steel strains. Once cracks passed between the demec gauges, it was dificult to measure the tensile strain accross the crack.

5.3.6 Failure Modes

The failure modes can be studied through the crack propagation and patterns together with the yielding of steel. The present experimental work clearly showed the flexural torsional cracks and the simultaneous yielding of steel at ultimate loads. All the tested models failed in a ductile fashion at a load beyond the design load.

5.4 ANALYSIS OF TEST RESULTS

5.4.1 Serviceability limit state

The service load behaviour according to BS 8110[18] is based on one of the following criterion.

- a) Deflection limit
- b) Maximum crackwidth limit

From the experimental data it has been observed that the tested beams reached the limiting service deflection at high load level. The usual practice in the design of reinforced concrete structures is to design for the ultimate limit state and then check for serviceability limit state. The service load in our case will be a fraction of the design load by considering that the loads on the tested beams are mainly live loads. Thus, assuming an ultimate limit state load factor of 1.6, the service load according to BS 8110[18] is obtained as $0.625 \times P_d$. The corresponding service deflection from the test results are smaller than the service limit deflection of (span/250). It was also observed from Figure (5.19a) that the service crack width load of model TB3B was slightly of identical to the service load ($0.625 \times P_d$).

The steel remained elastic under all serviceability conditions. From the above observations the general service behaviour of the tested beams was concluded to be satisfactory.

5.4.2 Ultimate limit state

Tables (5.4) and (5.5) give the summary of the ultimate behaviour on the beams tested in this investigation. The failure load of all models exceeded the design load. The results of all models show clearly that flexural– torsional failure occured with the simultaneous yielding of prestressing and ordinary steel.

– a/ First yield of steel

The load at first yield of steel occured beyond the serviceability limit load in all tested models. The average load at first yield of steel for series 1 is 0.893xdesign load (for ordinary steel) and 0.985xdesign load (for prestressing steel). These values are much higher than the service load of 0.625xdesign load. These results show that the classical limit capacity concept ensure practically the simultaneous yielding of both prestressing and ordinary steel with good agreements.

– b/ Ultimate loads

The failure or ultimate loads are defined as the maximum loads which can be resisted by the member.

Table (5.4) shows the ratio of experimental ultimate load to design load where most of the beams tested in this investigation failed in excess of the design load. The average ultimate failure loads for specimen tested under combined loading is $(1.15).P_d$ and that by not including the contribution of self weigth and sundries to the ultimate moment defined in Appendix B which in fact represent 9.75% of the design moment. This results shows that the adopted approach gives very satisfactory failure loads under combined loadings.

5.5 CONCLUSIONS

The following conclusions are drawn from the present study on partially prestressed concrete sections subjected to combined bending and torsion.

1) The behaviour of all tested beams was found to be essentially linear until cracking of concrete. After cracking the steel strains stresses and the concrete surface strains greatly increased and continued to increase thereafter until failure.

2) Partially prestressed beams showed violent failure at ultimate load.

3) The average ultimate failure loads for all the beams tested in this study was $(1.15).P_d$ for T/B= 1.0 and $(1.06).P_d$ for pure torsion.

4) Very large rotations were necessary for the beams to develop their ultimate failure loads.

5) The behaviour of partially prestressed beams under combined loading is similar to that of reinforced concrete regarding crack patterns and failure modes.

6) Large reduction of torsional stiffness occured after cracking of concrete, especially for specimen PT1B and PT2B. The average of post to pre-cracking stiffness ranged between 5 to 20%.

7) Prestressing can raise the strength of beam under combined bending and torsion and increase the linear elastic stage

8) Finally, the experimental tests offered consistent data for assessing the adopted design method. All the beams designed according to the direct design approach behaved satisfactorily. Both deflections and crack widths in the working load range were within acceptable limits, as defined by BS 8110[18]. All the beams recorded failure loads close to their design loads.

Table(5.1) Properties and Experimental Results of the tested beams.

Beam Mark	T/B	Design Moments		Effective Prest		Total Reinforcing Steel (mm^2)				Ultimate Mts.	
		Torsion T_d (KNm)	Bending M_d (KNm)	P_e (KN)	E_p (mm)	Long Steel		Stirrup		T_u (KNm)	M_u (KNm)
						By-DDA-	Adopted	By-DDA-	Adopted		
TB1B	1.0	32.0	32.0	68	-60	330.6	438.0	496.0	503.0	34.8	35.0
TB2B	0.8	25.6	32.0	68	-60	270.8	308.5	396.0	402.0	27.6	34.6
TB3B	1.0	32.0	32.0	132.8	-60	162.0	252.0	496.0	503.0	37.0	37.5
TB4B	1.0	32.0	32.0	160.0	-72	68.0	101.0	496.0	503.0	39.5	40.0
PT1B	1/0	32.0	0.0	68	0.0	82.0	101.0	496.0	503.0	33.8	-
PT2B	1/0	-	0.0	99.3	0.0	-	101.0	496.0	503.0	36.9	-

Note: The adopted area is the total longitudinal steel area on the cross section.
(Sum of the provided area on each section.See Details in Table(4.3) to (4.8)).

Table(5.2) Post-Cracking Slope of Load-Deflection Curves.

Beam Mark	T/B	Design Moments		Eff.Prestress		Post-Cracking Slope of Load Deflection Curves.	Ratio of Post-Crack to Pre-Cracking Stiffness %
		Torsion Td (KNm)	Bending Md (KNm)	P_e (kn)	Ep(mm)		
TB1B	1.0	32.0	32.0	68.0	-60.0	5.0	13.0
TB2B	0.80	25.6	32.0	68.0	-60.0	5.50	12.22
TB3B	1.0	32.0	32.0	132.8	-60.0	4.87	20.29
TB4B	1.0	32.0	32.0	160.0	-72.0	5.20	20.80
PT1B	1/0	32.0	0.0	68.0	0.0	-	-
PT2B	1/0	-	0.0	99.30	0.0	-	-

Table(5.3) Post-Cracking Slope of Torque-Rate of Twist Curves.

Beam Mark	T/B	Design Moments		Eff.Prestress		Cracking-Load (KNm)	Post-Cracking Slope of Torque-Rate of Twist	Ratio of Post-Crack-Precracking
		Torsion Td (KNm)	Bending Md (KNm)	P_e (KN)	Ep(mm)			
TB1B	1.0	32.0	32.0	68.0	-60.0	13.0	9.0	11.0
TB2B	0.8	25.6	32.0	68.0	-60.0	10.20	11.5	12.5
TB3B	1.0	32.0	32.0	132.80	-60.0	14.76	10.0	11.60
TB4B	1.0	32.0	32.0	160.0	-72.0	16.0		
PT1B	1/0	32.0	0.0	68.0	0.0	14.47	3.90	5.16
PT2B	1/0	-	0.0	99.30	0.0	18.0	10.20	10.60

Table(5.4) Summary of the experimental results.

Beam Mark	T/B	Design Moments		Ultimate Moments		Ratio of Crack Load to Design Load	Ratio of Ult Load to Design Load
		Torsion T_d (KNm)	Bending M_d (KNm)	Torsion T_u (KNm)	Bending M_u (KNm)	P_{cr}/P_d	P_u/P_d
TB1B	1.0	32.0	32.0	34.8	35.0	0.41	1.094
TB2B	0.8	25.6	32.0	27.6	34.6	0.41	1.08
TB3B	1.0	32.0	32.0	37.0	37.5	0.46	1.17
TB4B	1.0	32.0	32.0	39.5	40.0	0.50	1.23
PT1B	1/0	32.0	0.0	33.8	-	0.45	1.056
PT2B	1/0	-	0.0	36.9	-	-	-

NB: The bending moment due to the sundries and self weight haven't been included into calculation of ultimate moments ($M_0 = 0.0975M_d$).
(See Details in Appendix A)

Table(5.5) Summary of Results.

Beam Mark	T/B	Design Moments		Cracking Load	(Load at Yield of Steel).P_d		Ultimate Load / P_d
		Torsion	Bending	P_{cr}	Ordinary Steel	Prestressing Steel	P_u / P_d
TB1B	1.0	32.0	32.0	13.0	0.82	0.80	1.09
TB2B	0.8	25.6	32.0	10.2	0.90	1.08	1.08
TB3B	1.0	32.0	32.0	14.76	0.87	1.026	1.17
TB4B	1.0	32.0	32.0	16.0	0.98	1.10	1.23
PT1B	1/0	32.0	0.0	14.47	1.03	0.956	1.06
PT2B	1/0	-	0.0	18.0	-	-	-

Note: Beam PT2B had not been designed according to the Direct Design Approach.

CHAPTER SIX

NONLINEAR ANALYSIS

6.1 INTRODUCTION

Nowadays, the finite element method is recognised as a very powerful method of analysis in the field of structural mechanics and many other fields. Its basic concept and methodology are very well established and have been published widely. The finite element method being a powerful analytical tool for predicting the behaviour of concrete structures, it can be used to model properly non– linear material properties such as cracking of concrete and tensile yielding of steel reinforcement and other effects which previously have been treated in a very approximate manner. Despite the maturity of non– linear finite element modelling of structural concrete, various difficulties still need to be resolved, and basic research continues on improving both material modelling as well as solutions techniques.

6.2 FINITE ELEMENT FORMULATION

6.2.1 Introduction

The standard procedure of finite element analysis is well known, and is therefore not described in detail here. The method of representing structural concrete in finite element analysis has been described in numerous publications [32,33,36]. Only a brief description is given here. In the finite element method any continum system is divided into a series of elements of geometric shape which are connected at a finite number of points known as nodal points, at which the displacement is assumed to have unknown values. The variation of displacement δ within any element is described in terms of the nodal values by means of interpolation functions given by:

$$\delta = N.\delta^e \tag{6.1}$$

Once the displacement is specified inside an element, the strains are given by:

$$\epsilon = B.\delta^e \tag{6.2}$$

Where B is the strain matrix generally composed of derivatives of shape functions and δ^e is the vector of nodal displacements of the element. The stresses are given by :

$$\sigma = D.\epsilon \tag{6.3}$$

Where D is the material stress strain matrix.

From this the external nodal force is related to the nodal displacement through the structural stiffness matrix in the form:

$$P = K.\delta \tag{6.4}$$

where the stiffness matrix,

$$K = \int_V .[B]^T.D.B.dv \tag{6.5}$$

The equivalent nodal forces, vector

$$P = \int_V .[N]^T.b.dv + \int_S .[N]^T.q_S.ds \tag{6.6}$$

Where b is the body force per unit volume, q_S the applied surface traction.

6.2.2 Formulation of the element stiffness

In the present study, an isoparametric eight node layered element shown in Figure (6.1) was used in which the thickness of the element is divided into finite number of layers. Each layer consists of a homogeneous material which is assumed to resist in–plane stresses. The element stiffness matrix defined above in Eq (6.5) is expressed in this case for the ith layer as:

$$K_i = \{ \int\int [B]^T . D . B . dx . dy \} \qquad (6.7)$$

Therefore the element stiffness matrix can be written as .

$$K = \sum_{i=1}^{n} K_i \text{ layer} \qquad (6.7a)$$

Gauss Legendre integration rules have been chosen in order to evaluate numerically the element stiffness matrix.

6.3 MATERIAL MODELING

6.3.1 Introduction

The analysis of reinforced concrete structures, requires a full understanding of the mechanical properties of materials under various states of stress. Many constitutive models have been proposed to describe concrete behaviour under multiaxial stresses. The behaviour of concrete in uniaxial and biaxial state of stress is not introduced in this chapter. However, the representation of cracking and the failure criteria for concrete are discussed.

6.3.2 Failure criterion for concrete

In general, there are two major types of failures of concrete viz. Denoting

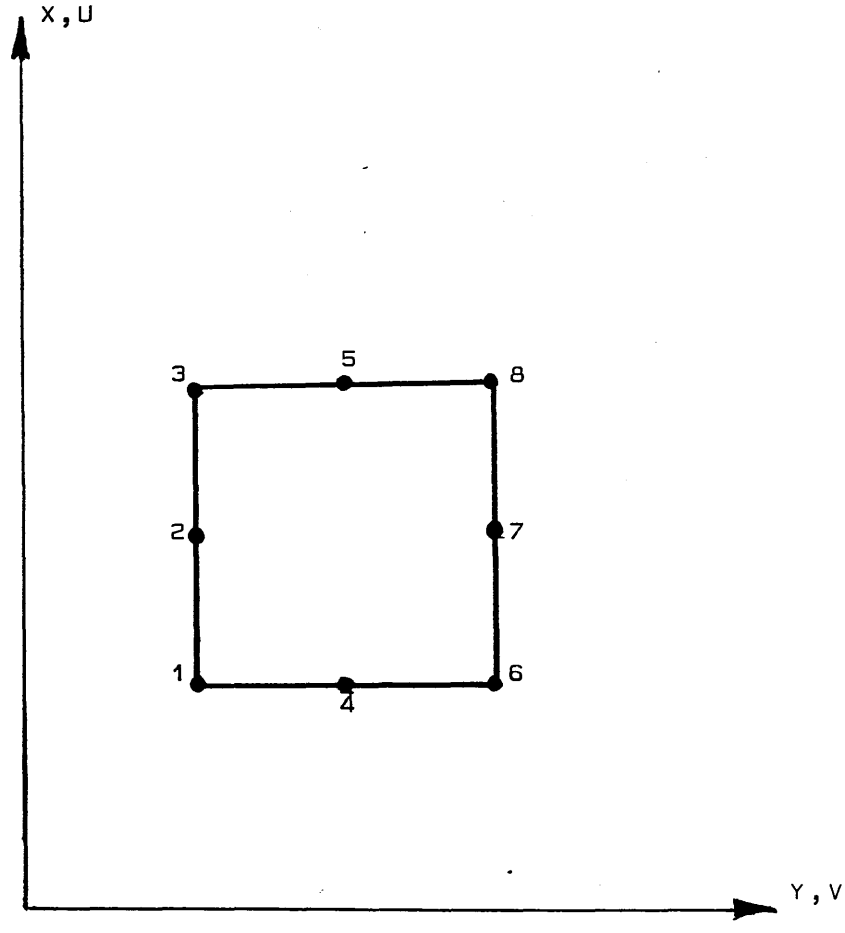

Figure(6.1) Finite element used in the present study.

these tensile and compressive types. The tensile type of failure is defined as " cracking " where a major crack rapidily appears in the direction normal to the principal tensile stress. The compressive type of failure is defined as " crushing ". There are many failure criteria proposed for concrete. Among those the strength of concrete under combined shear and direct stress may be predicted closely by the octahedral shear stress failure criterion. The yield surface for biaxial stress in concrete shown in Figure (6.2) can be approximated to the form

$$\tau - a - b.\sigma_{oct} = 0 \qquad (6.8)$$

where,

$$\tau_{oct} = \frac{[2]^{\frac{1}{2}}}{3} [\ (\sigma_x^2 + \sigma_y^2 - \sigma_x.\sigma_y + 3\tau_{xy}^2\ )\ ]^{\frac{1}{2}} \qquad (6.9)$$

and

$$\sigma_{oct} = \frac{(\sigma_x + \sigma_y)}{3} \qquad (6.10)$$

Eq (6.8) represents two expressions; one is valid for biaxial compression, while the other is valid for the biaxial tension and tension– compression regions.

a and b are constant to be determined from test data for uniaxial tension " f_t " and uniaxial compression " f_c " and equivalent biaxial compression strength " f_d ". By introducing these values into Equation (6.8), we obtain the failure suface parameters as follows.

1) Compression yielding

– i) For uniaxial compression of $\sigma_x = -f_c$, $\sigma_y = 0$, $\tau_{xy} = 0$, then

$\tau_{oct} = \{\ [2]^{\frac{1}{2}}/3\ \}.f_c$ and $\sigma_{oct} = -f_c/3$. Then by

$$a - (f_c/3)b = \{\ [2]^{\frac{1}{2}}/3\}.f_c \qquad (6.11)$$

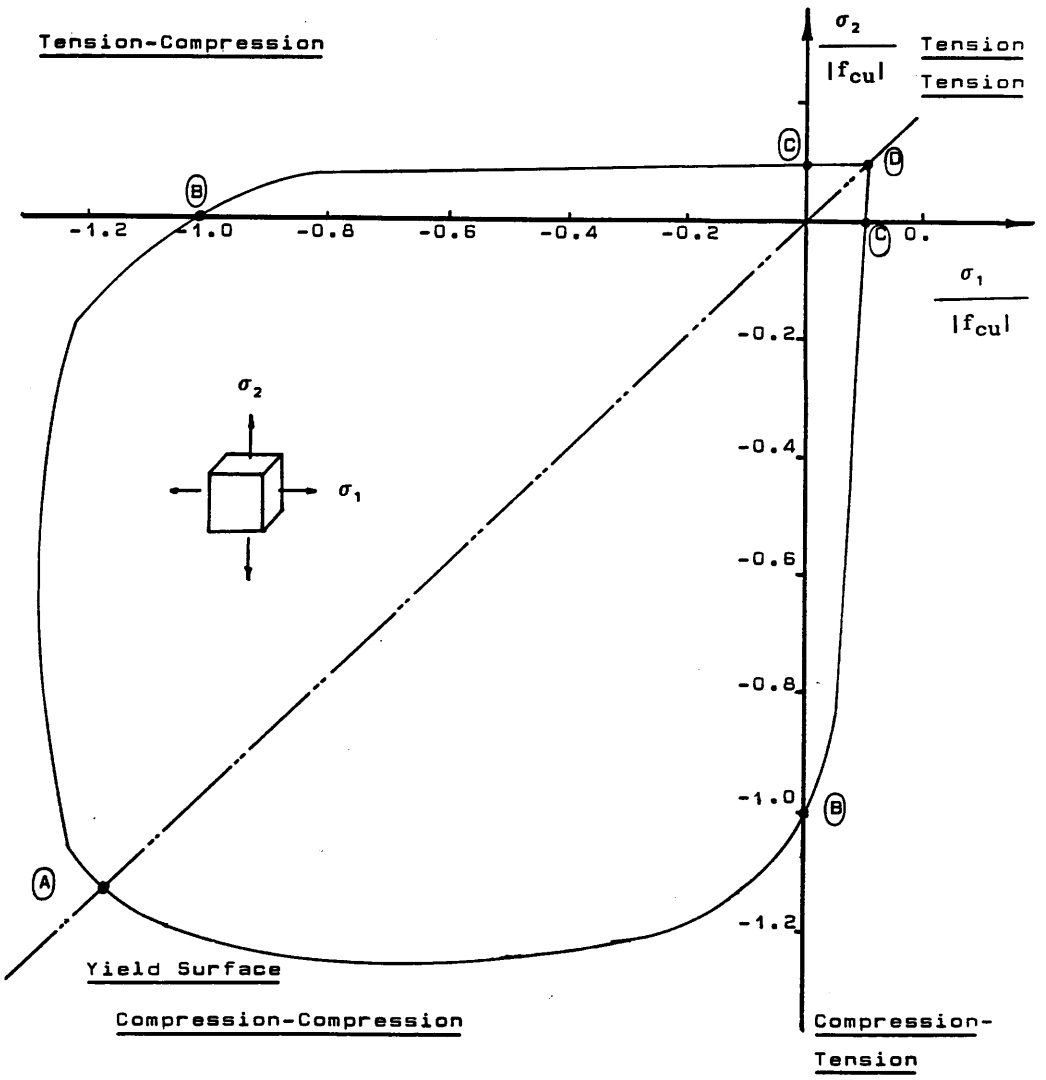

Figure(6.2) Biaxial Strength Envelope for Concrete.

– ii) For biaxial compression of $\sigma_x = \sigma_y = -f_d$ then

$$\tau_{oct} = \{ [2]^{\frac{1}{2}}/3\}.f_d \text{ and } \sigma_{oct} = -2f_d/3$$

$$a - (2f_d/3)b = \{[2]^{\frac{1}{2}}/3 \}.f_d \qquad (6.12)$$

Solving equations (6.11) and (6.12) the yield criterion is given by

$$\tau_{oct} + [2]^{\frac{1}{2}} \frac{n_1-1}{2n_1-1} \sigma_{oct} - \frac{[2]^{\frac{1}{2}}}{3} \frac{n_1}{2n_1-1} f_c \qquad (6.13)$$

Where $n_1 = f_d/f_c$.

Taking $n_1 = 1.16$ from Figure (6.2) then

$$\frac{\tau_{oct}}{f_c} + 0.1714 \frac{\sigma_{oct}}{f_c} - 0.4143 = 0 \qquad (6.14)$$

2) Compression tension yielding

By adopting the same procedure

$$\begin{cases} \sigma_x = -f_c, \ \sigma_y = 0, \ \tau_{xy} = 0 \\ \sigma_x = f_t, \ \sigma_y = 0, \ \tau_{xy} = 0 \end{cases}$$

We obtain

$$\begin{cases} a - (f_c/3)b = \{ [2]^{\frac{1}{2}}/3 \}.f_c \\ a - (f_t/3)b = \{ [2]^{\frac{1}{2}}/3 \}.f_t \end{cases} \qquad (6.15)$$

Solving these equations the yield criteria is given by:

$$\tau_{oct} + [2]^{\frac{1}{2}} \frac{1-n_2}{1+n_2} \sigma_{oct} - \frac{2[2]^{\frac{1}{2}}}{3} \frac{n_2}{1+n_2} f_c \qquad (6.16)$$

Where $n_2 = f_t/f_c$.

Equation (6.16) is used to indicate the boundary condition between cracked and uncracked concrete in tension– compression and biaxial tension– regions.

Taking $n_2 = 0.10$ Equation (6.16) becomes:

$$\frac{\tau_{oct}}{f_c} + 1.157 \frac{\sigma_{oct}}{f_c} - 0.0857 = 0 \qquad (6.17)$$

3) Biaxial tension yielding

Since there is no increase in ultimate strength due to biaxial tensile loading, the simple condition given in Eq (6.18) is sufficient to represent the yield criteria in tension– tension zone.

$$[\ \sigma_1/f_t\ ]^2 + [\ \sigma_2/f_t\ ]^2 - 1.0 = 0 \qquad (6.18)$$

Where σ_1 and σ_2 are the principal tensile stresses.

6.3.3 Failure types for concrete

Figure (6.2) illustrates a typical biaxial strength envelope for concrete subjected to proportional biaxial loading. This figure can be divided into three regions symmetrical about $\sigma_1 = \sigma_2$ axis.

1/ Biaxial compresion A– B

2/ Failure under biaxial tension C– D

3/ Failure under tension compression stresses B– C

For biaxial compression, the failure model is the crushing type, but for biaxial tension, the failure mode is a cracking type. For tension– compression, two failure

modes are observed. Cracking failure will take place under stress conditions where the tensile stress is relatively large ($\sigma_1/f_t > 0.3$ and $\sigma_2/f_c < 0.85$) and crushing failure will take place under high compression– low tension stress state ($\sigma_2/f_c > 0.9$ and $\sigma_1/f_t < 0.25$).

6.4 DETAIL OF MATERIAL MODEL ADOPTED

In the present layered finite element model, each layer is of one material only and is assumed to be in state of plane stress. For plane stress assumptions in the elastic stage, the stresses of an isotropic concrete layer is related to the corresponding strains by:

$$\begin{Bmatrix} \sigma_x \\ \sigma_y \\ \tau_{xy} \end{Bmatrix} = \frac{E}{1-\nu^2} \begin{bmatrix} 1 & \nu & 0 \\ \nu & 1 & 0 \\ 0 & 0 & (1-\nu)/2 \end{bmatrix} \begin{Bmatrix} \epsilon_x \\ \epsilon_y \\ \epsilon_{xy} \end{Bmatrix} \qquad (6.19)$$

In which E_c is the modulus of elasticity and ν Poisson's ratio of concrete.

6.4.1 Cracking model

The most commonly models used in representing concrete in finite element analysis are:

– a) Discrete cracking model

– b) Smeared cracking

The smeared crack system shown in Figure (6.3a) was adopted in this study. Smeared crack model assumes that cracks are distributed over the entire element or integration point, where cracks are usually assumed to occur perpendicular to the maximum principal stress when the appropriate cracking criterion has been exceeded. Cracking is modelled by altering the value of the coefficients in the material

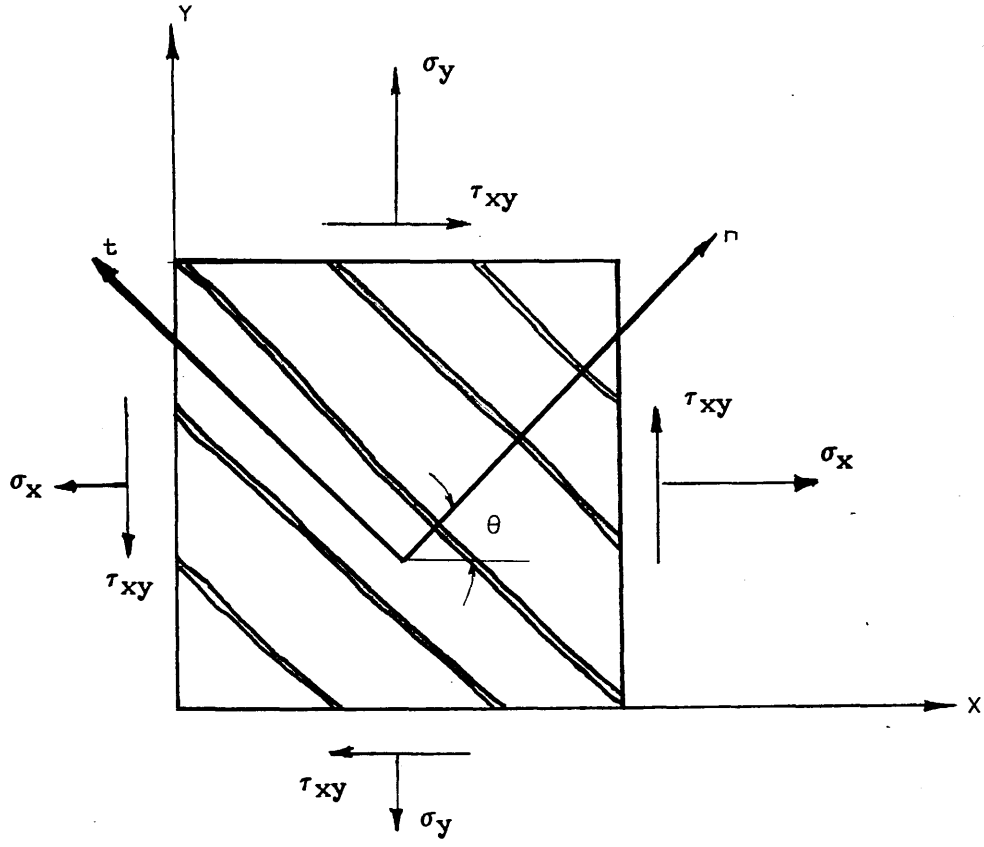

Figure(6.3.a) Smeared Crack idealisation.

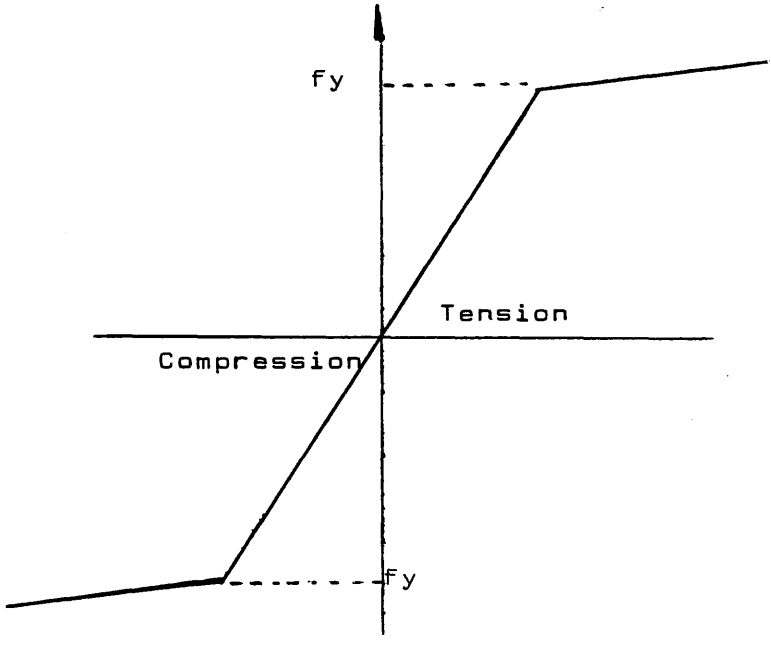

Figure(6.3.b) Idealisation stress-strain curve for steel.

property matrix associated with a direction normal to the crack. This approach is easier to apply because the initial crack direction are not constrained by the mesh. The stress–strain relationship for plane stress in the crack direction will be expressed as:

$$\begin{Bmatrix} \sigma_n \\ \sigma_t \\ \tau_{nt} \end{Bmatrix} = D_t \begin{Bmatrix} \epsilon_n \\ \epsilon_t \\ \gamma_{nt} \end{Bmatrix} \qquad (6.20)$$

Where,

σ_n, σ_t : normal stresses normal and tangential to the crack direction

ϵ_n, ϵ_t : normal strains normal and tangential to the crack direction

τ_{nt}, γ_{nt}: shear stress and strain in the cracked concrete

After cracking has occured, the cracked concrete becomes an orthotropic material with the modulus of elasticity associated with the coordinate system aligned to the cracked direction being zero. Therefore for singly cracked concrete

$$[\ D_t\ ] = \begin{bmatrix} 0 & 0 & 0 \\ 0 & E_c & 0 \\ 0 & 0 & \beta_s G \end{bmatrix} \qquad (6.21)$$

In which E_c is the Young's modulus and β_s is the shear retention factor whose value varies between 0 and 1.0. As can be seen the modulus of elasticity of concrete is reduced to zero in the direction normal to the crack and a reduced shear modulus $\beta_s G$ is assumed on the cracked plane to account for the aggregate interlocking or shear friction that are present at the crack surface.

In this model once the cracks form, their direction is assumed to be fixed as long as it remains open. Secondary cracking are allowed to form orthogonal to the

primary crack. After two cracks take place, the material matrix D_t becomes

$$[\ D_t\ ] = \begin{bmatrix} 0 & 0 & 0 \\ 0 & 0 & 0 \\ 0 & 0 & \beta_s G \end{bmatrix} \qquad (6.22)$$

6.4.2 Modelling of steel behaviour

Steel reinforcement is assumed to carry only uniaxial stress. Its modelling is straightforward because its stress–strain relations are well defined when bending and dowel resistance are ignored. In the present study the individual bars are smeared into equivalent steel layer with uniaxial properties.

The idealisation of stress strain for steel shown in Figure (6.3b) is characterised by an elastic plastic behaviour.

6.5 MODELLING OF THIN WALLED BEAM

In this investigation, the finite element method was adopted to obtain the elastic stress field through linear analysis for design purposes and to carry out nonlinear analysis of the designed structure. The aim was to investigate the reliability of the basic assumption of " the direct design procedure ".

Attention is focussed on the analysis of thin walled beams under the action of bending moment and torsion. Our interest is to analyse this type of structural member with simplified two dimensional finite element models in order to reduce greatly the cost and time of computation associated with three dimensional analysis.

The compatibility in the two dimensional idealisation of box girders is ensured by the technique of " node freedom array " as follows. As shown in Figure (6.4),

(a) To ensure shear transfer between adjoining plates of the beam, compatibility of displacement along the line of intersection at the common edge of adjoining plates is

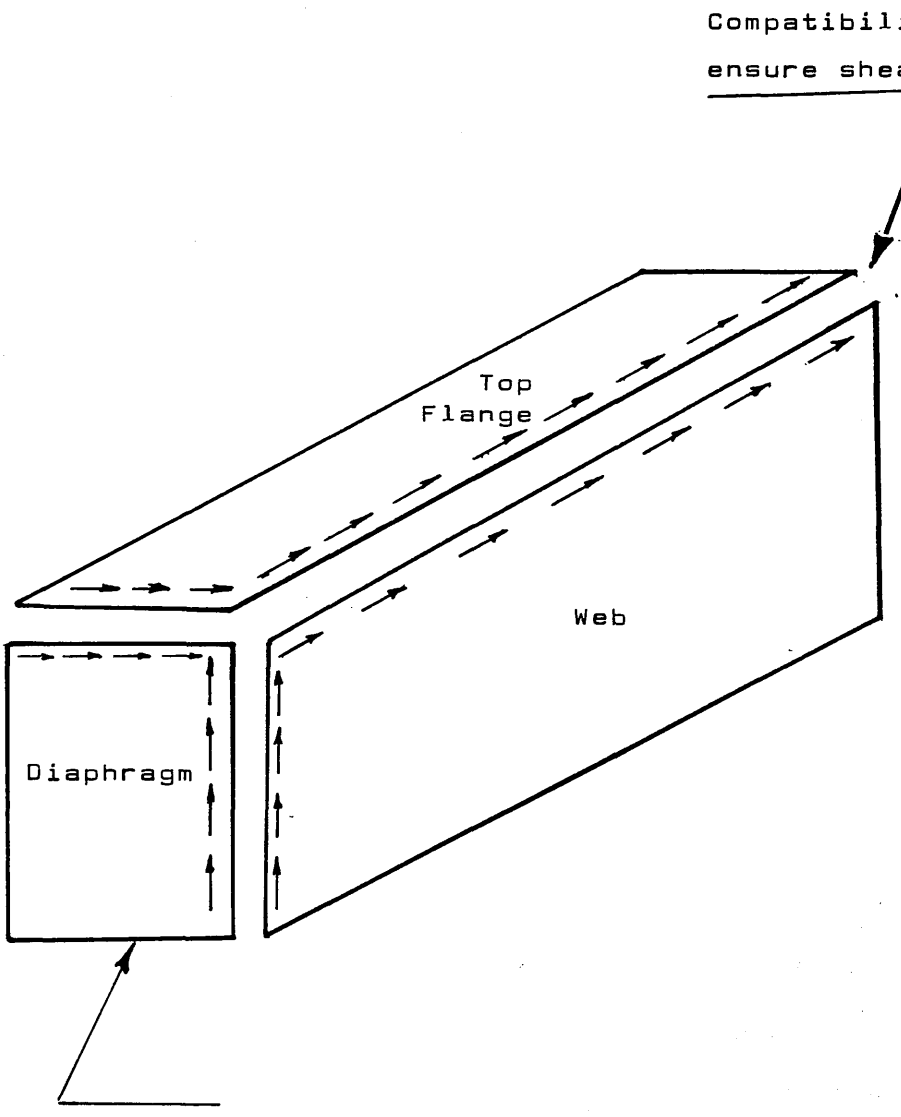

Figure(6.4) Idealisation of hollow beam in plane stress analysis.

maintained by introducing geometrical constraints.

(b) To reduce cross–sectional distortion, end diaphragms are introduced in the analysis.

To illustrate this technique, consider the case of an L–beam under loading as shown in Figure (6.5a). By neglecting the out of plane bending of the plates, the web and flange composing the L beam are considered as thin plates in a state of plane stress. The axial displacement along the junction of the two adjoining plates are assumed to be equal for both plates. However the displacement normal to the junction in both plates are considered independant of each other. Figure (6.5b) shows the idealisation of L–beam using the proposed technique. Each independant displacement is given a freedom number. If the two plates meet at common edge, then there are three possible independant displacements. This means that for displacement along the junction between the plates, the freedom number for nodes at the junction will be as shown in Table (6.1). This technique as illustrated above is now considered for the analysis of box beams. Figure (6.6) shows a rectangular box beam and its plane stress idealisation, where x–displacement along the common edge between the flange and webs are made equal. The z–displacement corresponding to the common edge between the flanges and diaphragm are also made equal and the y–displacement along the junction between the webs and diaphragm are made equal. However, along the common edge the y–displacement of the webs and z–displacement of the flanges are independant. This information is used to assemble the structural stiffness matrix.

6.6 PROCEDURE IN NONLINEAR ANALYSIS

The program uses a modified Newton–Raphson incremental–iterative approach. The method involves fewer stiffness calculations than the full Newton–Raphson approach and thus economies in cost and time of computation are gained. The

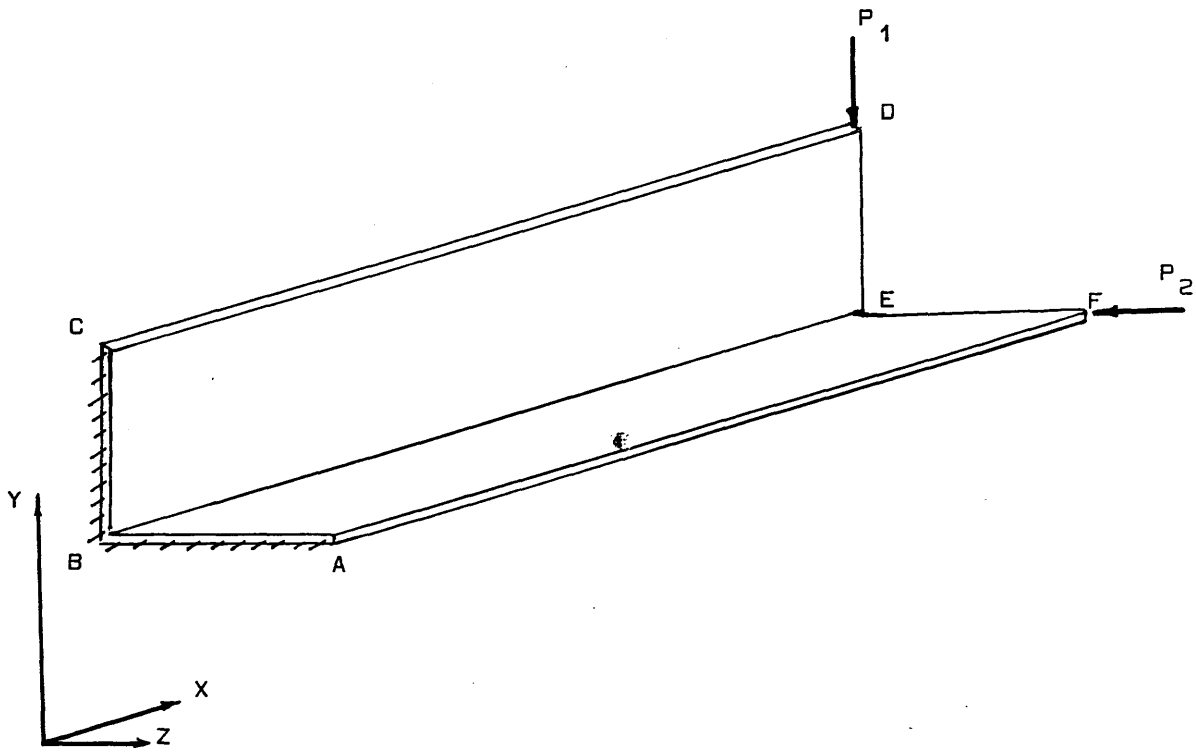

Figure(6.5a) L-Beam under Loadings.

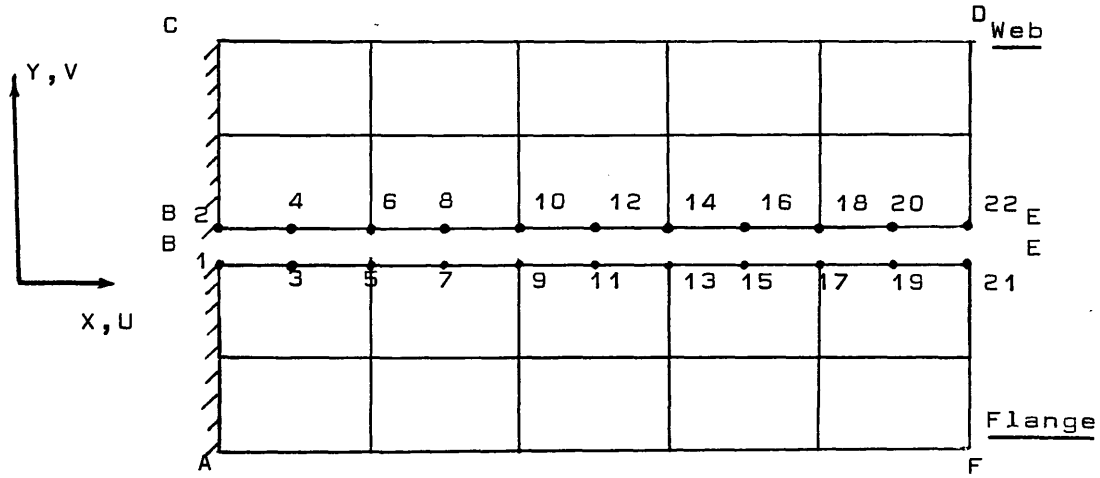

Figure(6.5b) Two dimensional finite element idealisation of an L-beam.

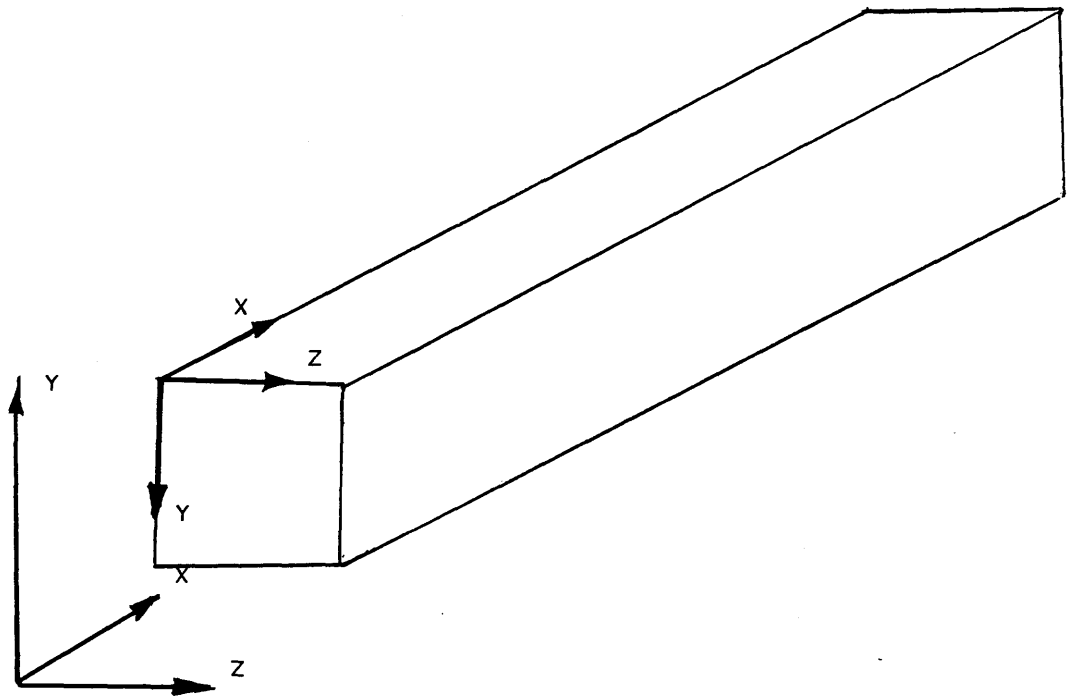

(a) General view of rectangular box beam

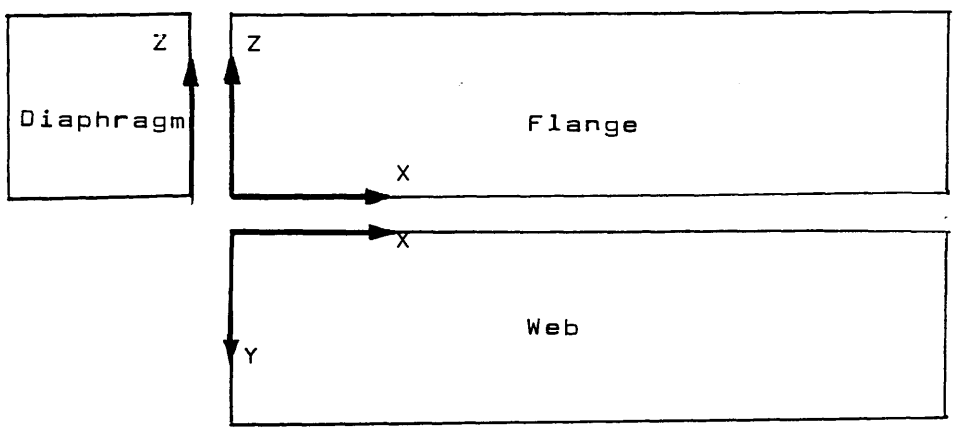

(b) Layout of plates composing the beam box to be anlysed under plane stress.

Figure(6.6) Two dimensional idealisation of a beam box.

procedure consists of applying a load system to a structure in small increments. If the total stress level is in equilibrium with the applied loading system then,

$$P_t = \int_V [B]^T . \sigma . dv \qquad (6.23)$$

Where P_t is the total load vector

$$P_t = \{ (P_i) + (P_p) \} \qquad (6.23a)$$

P_i : Applied load vector

P_p : Load vector due to effective prestress

σ : Total stress vector

For the calculation of the unbalanced nodal forces, the method of residual forces is used. The basic technique is that, at any stage a load system equivalent to the total stress level is evaluated and checked against the applied loading system. The difference between the two will result in a set of residuals that are a measure of lack of equilibrium. these residuals as defined in Eq (6.23b) are then applied to the structure to restore equilibrium.

$$P_{ui} = \int_V [B]^T . \sigma . dv - P_t \qquad (6.23b)$$

The process is then repeatedly continued to dissipate the residuals P_{ui} to some specific value so equilibrium can be achived.

6.6.1 Convergence criterion

The convergence criterion used to monitor the progress of a solution and detect failure of the structure are usually based on some norm of either the residual forces, displacements or energy. In the present work, convergence is based on residual force norm which is the only realistic measure to satisfy equilibrium. A force convergence criterion is used in this analysis and convergence is achived if

$$\frac{\left[\{P_{ui}\}^T . P_{ui} \right]^{\frac{1}{2}}}{\left[\{P_t\}^T . P_t \right]^{\frac{1}{2}}} \leqslant C_f \qquad (6.24)$$

Where C_f is specified tolerance.

6.6.2 Basic steps in the method used

1/ Apply to the idealised model a combination of loadings composed of an increment of the applied load ΔP_i and the total load P_p representing the amount of effective prestress. The equivalent displacement will therefore be expressed as:

$$\{\Delta\delta_i\} = [K]^{-1} \{ (\Delta P_i) + (P_p) \} \qquad (6.25)$$

Where K is the stiffness matrix based on the material condition at the start of the increment.

2/ Calculate the strain and stress at this stage

$$\Delta\epsilon_i = [B].\Delta\{\delta_i\} \qquad (6.26)$$

$$\Delta\sigma_i = [D].\{\epsilon_i\} \qquad (6.27)$$

3/ Estimate total displacement, strains and stresses by adding the incremental values to the previous ones.

$$\begin{cases} \delta_i = \delta_{i-1} + \Delta\delta_i \\ \epsilon_i = \epsilon_{i-1} + \Delta\delta_i \\ \sigma_i = \sigma_{i-1} + \Delta\sigma_i \end{cases} \qquad (6.28)$$

4/ Check the stress state against the yield criteria.

5/ Define the equivalent nodal forces due to σ_i and calculate the out of balance force.

$$\{ P_{ui} \} = \int [B]^T . \sigma_i . dv - \{ (P_i) + (P_p) \} \qquad (6.29)$$

$\{ (P_i) + (P_p) \}$ total external applied load vector

6/ Check to see if the force norm satisfy convergence criterion, if satisfied apply new load increment and repeat steps from (1) to (6). If not apply the residual force (P_{ui}) and determine the corresponding displacement $\Delta\delta_{ui}$

$$\Delta\delta_{ui} = [K]^{-1} . \{ P_{ui} \} \qquad (6.30)$$

7/ Go back to step 2 and repeat process until convergence is achieved. Further details of this program are given in reference[25].

6.7 NUMERICAL APPLICATION

The aim of this section is to check the reliability of the modified nonlinear plane stress program in order to analyse box girders. The beam tested by J.Ebiriri[23] was chosen for trial analysis. The box beam was analysed in plane stress as illustrated in Figure (6.7), this idealisation uses an assemblage of flat plates composing the beam. The beam was designed for combined ultimate torque and bending of 32 KNm. The torsional and bending moment are applied as shear flow and two points loads at the boundaries of the test span.

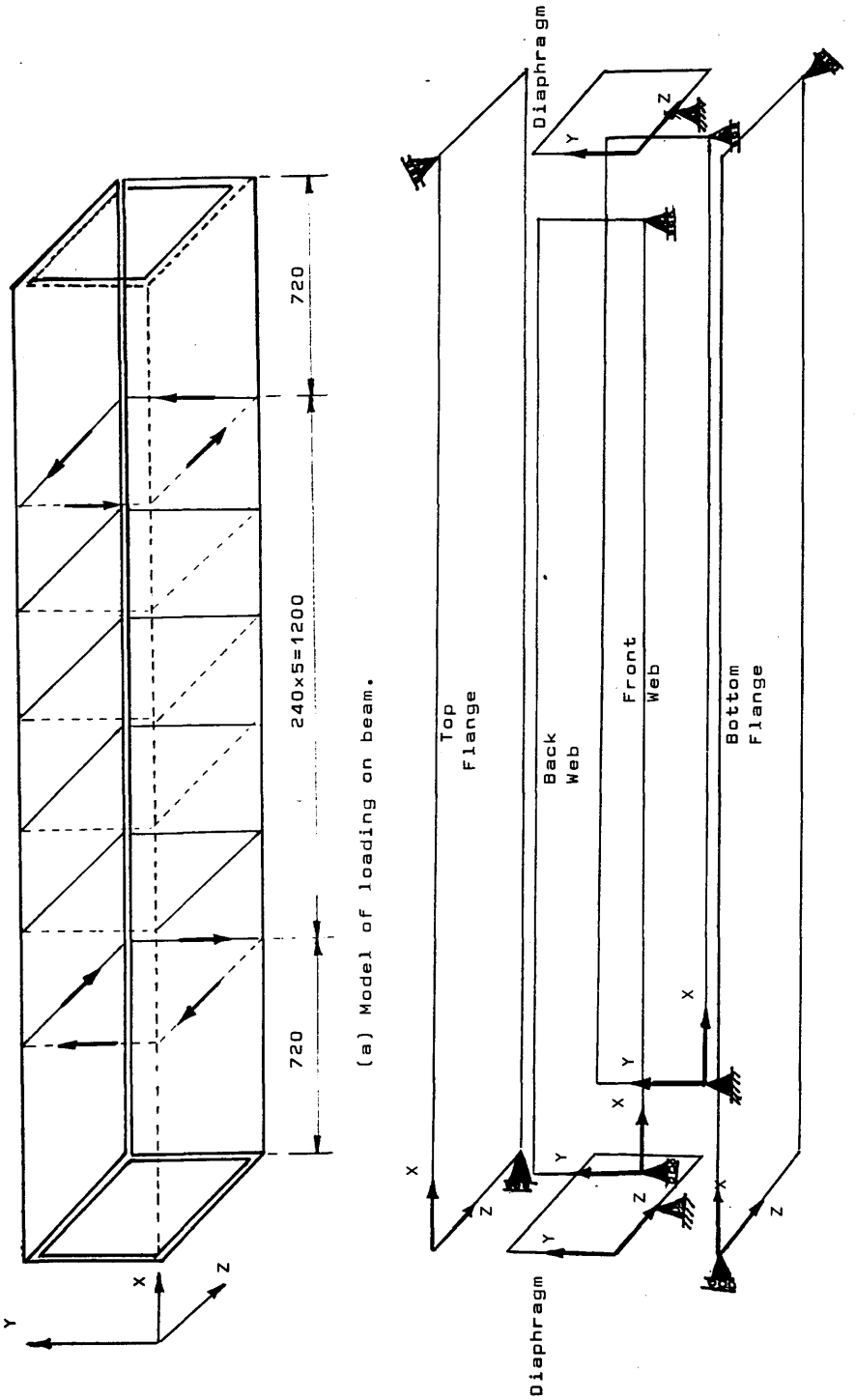

(a) Model of loading on beam.

Figure(6.7) Plane stress idealisation of box beam
(Boundary condition of beam)

6.7.1 Beam description

The beam was of square hollow section (300x300)mm and had a thickness of 50 mm. The beam's dimensions and reinforcement details are summarised in Reference[23]. The beam was simply supported on an effective span 2640 mm. A trial finite element mesh as shown in Figure (6.8) was used, where boundary conditions are also shown.

6.7.2 Nonlinear analysis

The parameters likely to affect the rate of convergence can be classified into two groups: Viz, solution parameters and quasi– material parameters.

i/ Solution parameters

a/ Convergence tolerances

b/ Number of iterations

c/ Mesh size

d/ Method of updating the stiffness.

ii/ Quasi– materials parameters

a/ Shear retention parameters

b/ Tension stiffning parameters

In the present work the effect of altering the material parameters haven't been investigated. The finite element mesh illustrated in Figure (6.8) was adequate under elastic conditions and it was assumed that it would be sufficient for nonlinear analysis. This idealisation was used also for the tested beams. The material properties used for the trial analysis are

-Compressive strength of concrete = 60 N/mm^2

-Tensile strength of concrete $=0.05\ f_c$ = 3.0 N/mm^2

-Young modulus of concrete = 39.5 kN/mm^2

-Poisson ratio of concrete = 0.15

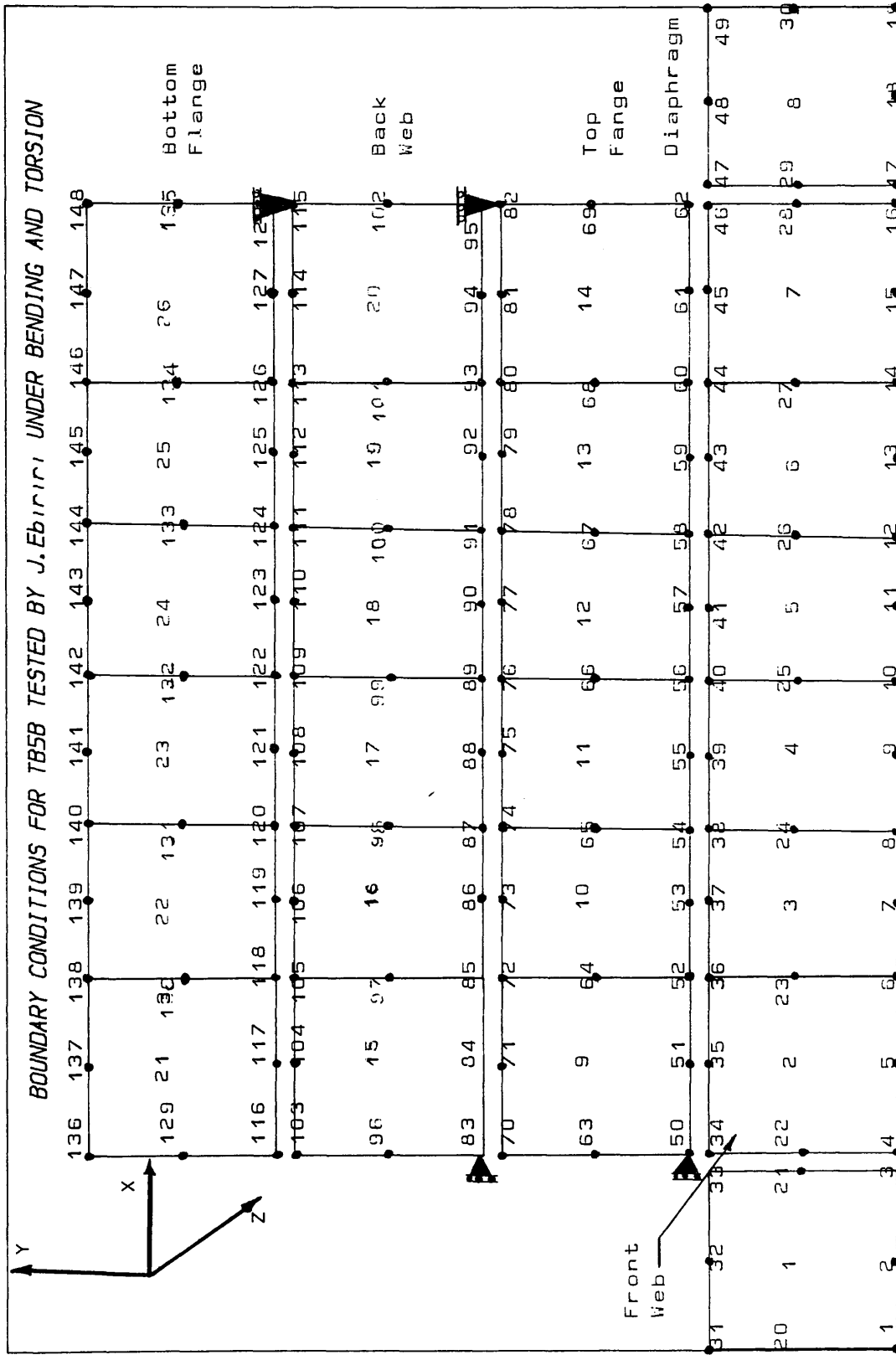

Figure(6.8) Mesh Idealisation For TB5B Beam Tested by (23)

-Yield stress of steel = 500.0 N/mm^2

-Young modulus of steel = 210 kN/mm^2

In this investigation the first load increment was equal to the estimated cracking load. However, the subsequent load increment have been calculated as a percentage of the cracking load (P_{cr}).

The convergence force tolerance was set at 10% which reasonably maintains equilibrium. The shear retention parameter was set at $\beta_s = 0.4$. Figure (6.9) shows a comparison between the reported experimental curve and the predicted one, for beam designated TB5B [23]. However, it can be clearly seen that the ultimate load prediction was slightly higher. The ratio of theoretical to experimental ultimate load was found equal at 1.04. The beam analysed herein failed by yielding of the bottom steel at the bottom flange and formation of compression hinge at the top flange. From this trial analysis, we conclude that both theoretical and experimental results agree satisfactorily at ultimate load level.

6.8 COMPARISON OF THEORETICAL AND EXPERIMENTAL RESULTS

In the present analysis the prediction of the overall behaviour, ie: load deflection curve, ultimate loads will be assessed first. Local behaviour such as steel strain will be considered second. The properties of concrete and steel used for the analysis are given in chapter four. In all the analysis, a (3x3) gauss integration rule is used. A maximum number of iteration of 30 was specified and the convergence tolerance was set at 10%.

6.8.1 Analysis of results

The finite element mesh consisting of 26 elements as illustrated in Figure (6.8) was adopted for all tested beams, while Figure (6.10) shows the modelling of

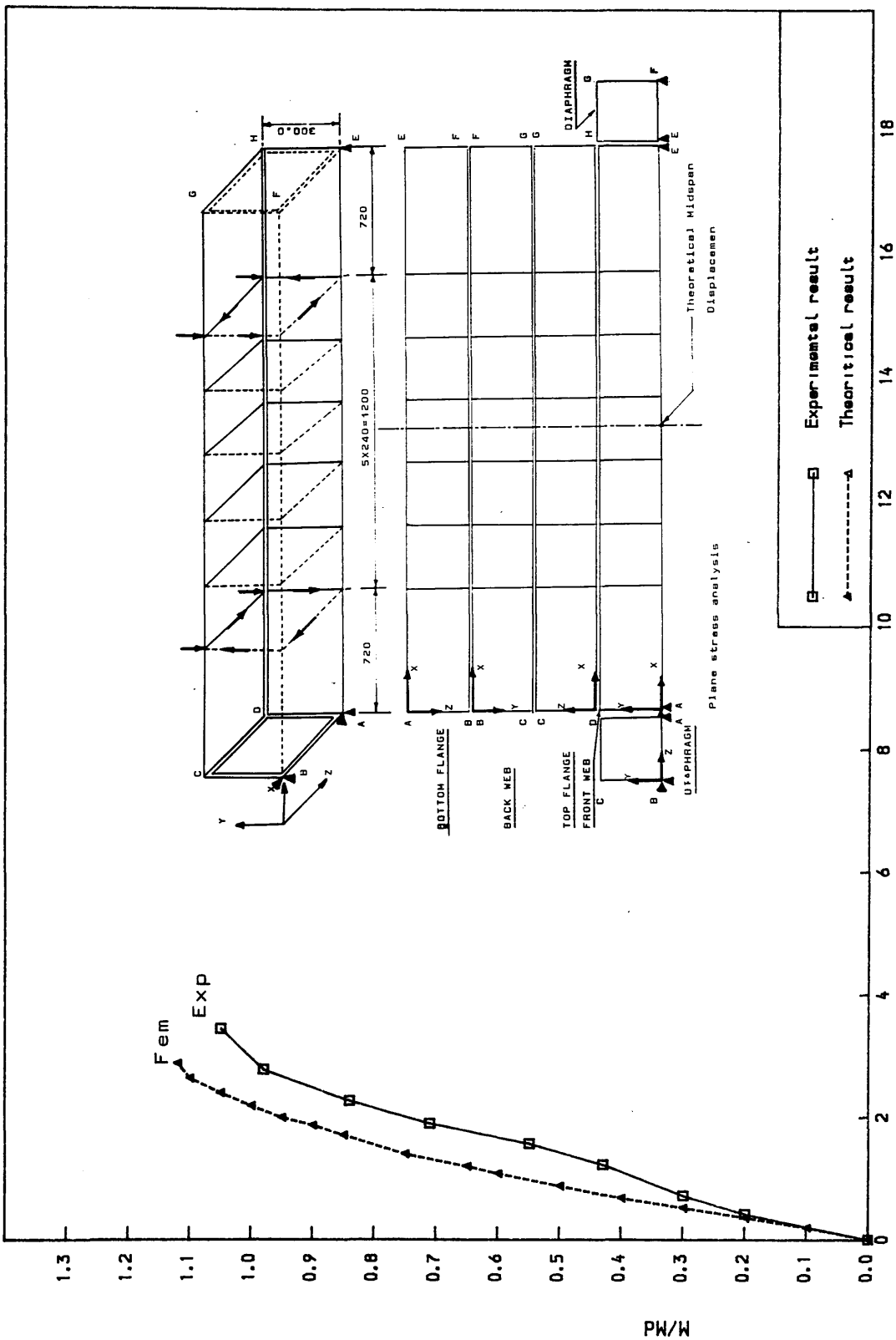

Figure (6.9) Comparison of Theoretical to Experimental results of reinforced concrete beam tested by J.Ebirri (23)

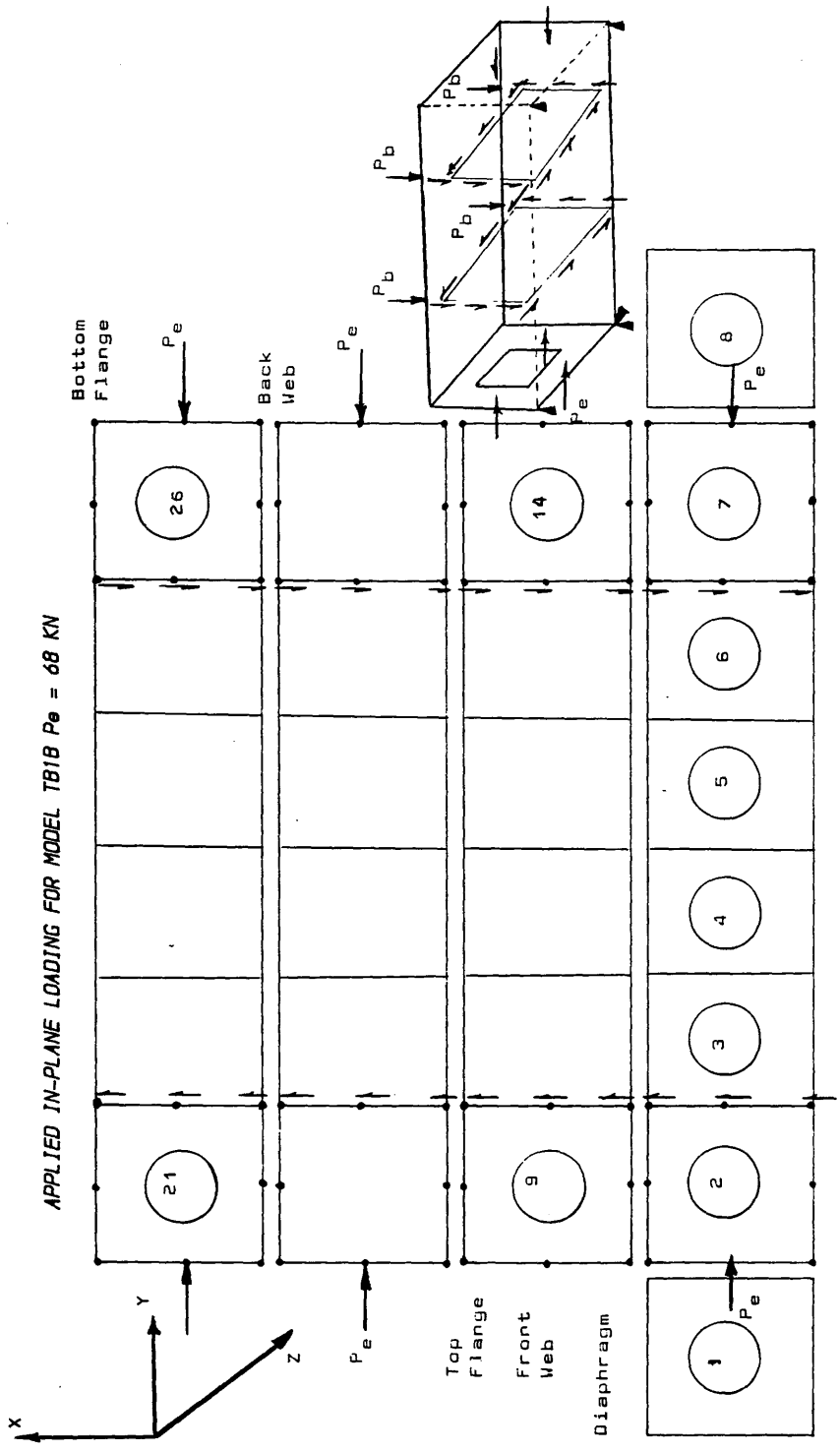

Figure (6.10)Idealisation of the total applied loading for model TB1B.
Note: The total prestress Pe is distributed through all parts of the section

the applied loads. Prestressing force is represented by axial forces. The actual quantity of steel was inserted in two orthogonal directions in the relevant finite element layer. The steel strain predictions are examined for both the longitudinal and transverse reinforcement. Care has been taken to choose the gauss point for strain readings as near as possible to the location of strain gauge in the experiment.

6.8.1.1 Model TB1B

Figure (6.11) shows the comparison between the experimental load deflection curve at midspan and the corresponding theoretical values. The theoretical cracking load was 1.13 of the experimental cracking load. Figure (6.15) shows the theoretical load– longitudinal steel strain curves at different position of the bottom flange where test results are also shown. Similarly Figure (6.16) shows the load– transverse steel strain curves at different locations. The predicted steel strains agree reasonably well with the test results. The theoretical yield load is 1.15 of the experimental load. The ultimate theoretical load is 1.12 of the experimental failure load.

6.8.1.2 Model TB2B

In Figure (6.12) comparisons are presented for the load– deflection curves obtained experimentally and those obtained numerically. The predicted results compare reasonably well with the experimental results at midspan. The predicted cracking load is 1.26 of the experimental cracking load. Figure (6.17) and (6.18) show the longitudinal and transverse steel strain values obtained experimentally and theoretically. The predicted steel strain values agree extremely well with the test results. The theoretical yield load is 1.02 of the experimental load. The ultimate theoretical load is 1.02 of the experimental failure load.

6.8.1.3 Model TB3B

The theoretical load central deflection curve is compared in Figure (6.13) with the experimental curve. Very good correlation is obtained between the

experimental and theoretical results particularly in the final stages of loading. The theoretical cracking load is about 1.41 of the experimental cracking load. In Figure (6.19) and (6.20) the predicted load steel strain curves are compared with the experimental ones. Good agreements between the two is obtained in all parts. The theoretical yield load is 1.12 of the experimental load. The ultimate theoretical load is 1.07 of the experimental load.

6.8.1.4 Model TB4B

Load deflection curves are compared in Figure (6.14). This figure shows that the theoretical results compare favourably well with the experimental ones. However the response seems slightly stiffer, especially at the final stages of loading. The predicted cracking load is 1.43 of the experimental load. Figure (6.21) and (6.22) shows the load steel strain curves. It is noticeable that generally speaking the theoretical analysis faithfully reproduces the true behaviour of the model. The predicted yield load in this case is about 1.21 of the experimental value. The comparisons show that the theoretical analysis provides conservative prediction for the ultimate load which in this case is 1.05 of the experimental load.

6.8.2 General discussions of results

6.8.2.1 Service behaviour

The examination of the Figures (6.11) to (6.14) reveal that the load deflection behaviour is predicted with reasonable accuracy. The pre–cracking stage shows good agreement between theory and experiment. However, as shown in Table (6.2) the theoretical cracking load are higher than the experiments. After cracking of concrete, the post–cracking load deflection region are predicted with reasonable accuracy. In most cases, the theoretical results predict a stiffer response than the experiment. The service behaviour of the beams was well predicted. Yielding of steel was observed beyond the service load region in most cases.

6.8.2.2 Ultimate load

The final failure loads showed good agreement with the experimental values. The average ratio of theoretical to experimental ultimate load for Nielsen approach was 1.06 for series one.

The results as summarised in Table (6.2) suggest that the main features of behaviour were well predicted at all stages. No attempt was made to vary the shear retention parameter to get closer prediction of the ultimate load. The adopted model predicted satisfactory results at ultimate load level.

6.8.3 Conclusion

The ensemble of results obtained through the nonlinear analysis agrees reasonablywell with the measurement and observations that emerged from the experiment. The finite element model predicts the service and ultimate behaviour of the beams designed by the proposed direct design procedure with acceptable accuracy.

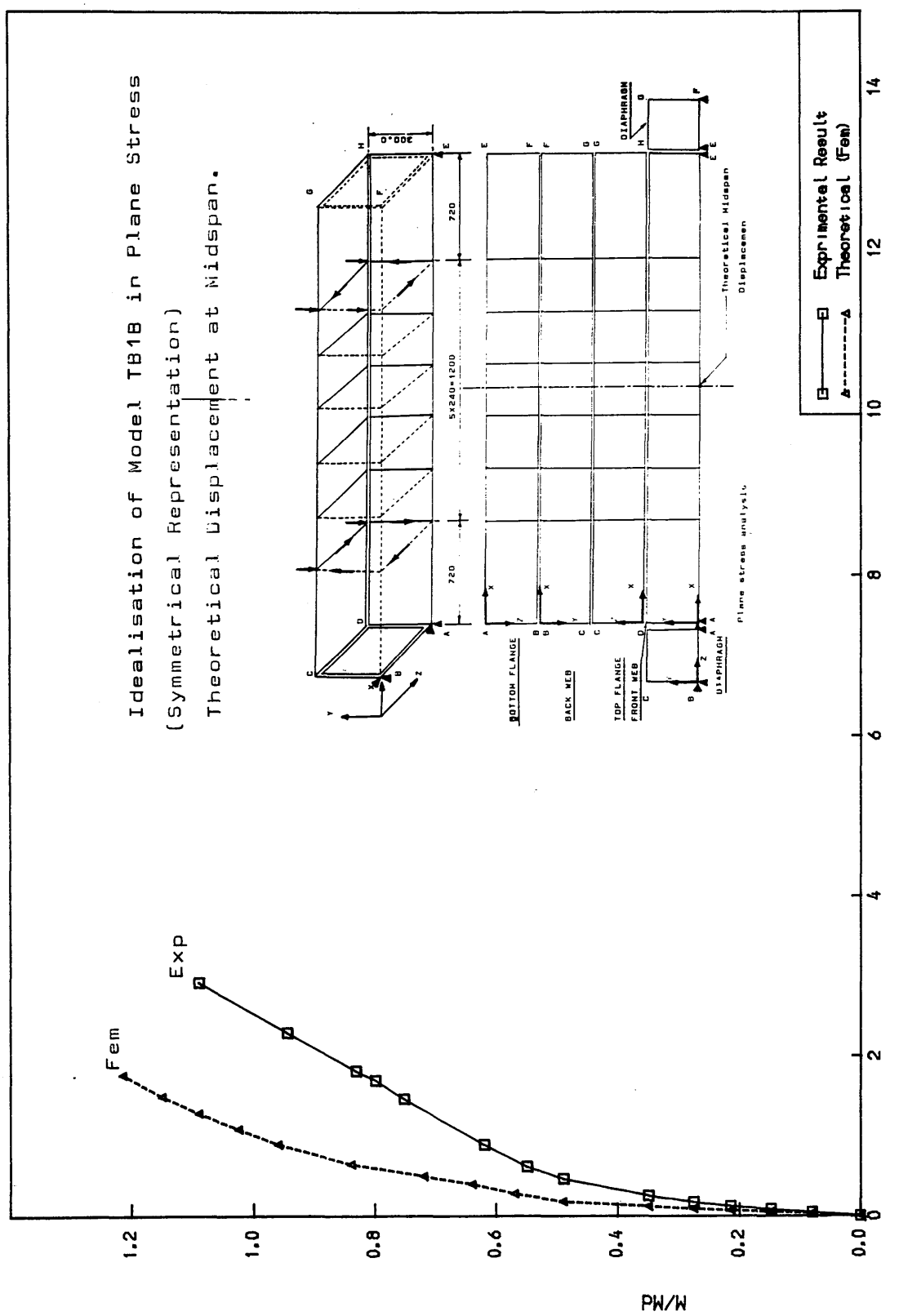

Figure (6.11) Comparison of Theoretical to Experimental Load Deflection Curve of Model TB1B " Pe= 68KN and Ep= -60mm ".

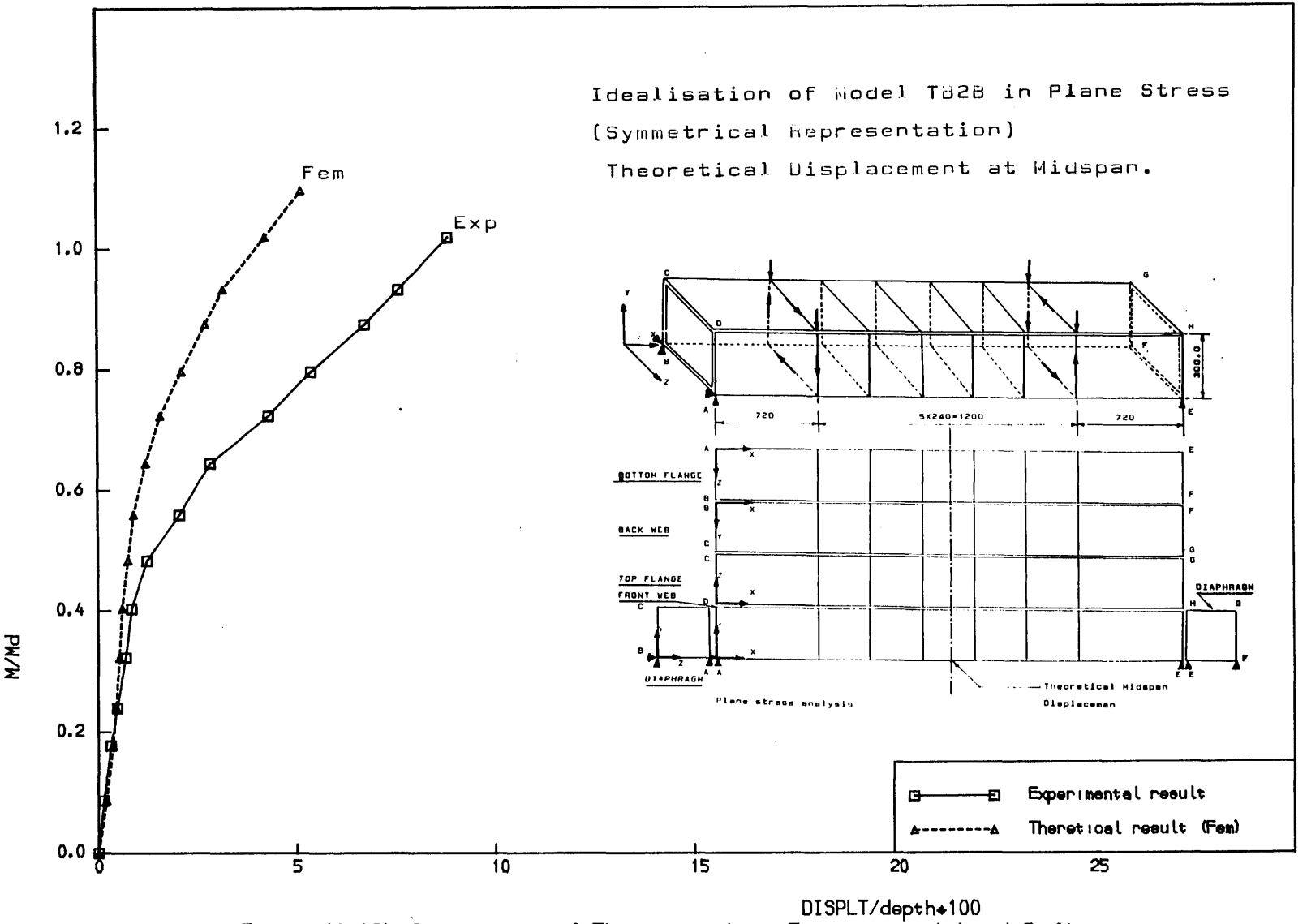

Figure (6.12) Comparison of Theoretical to Experimental Load Deflection Curve of Model TB2B " Pe= 68KN and Ep= -60mm ".

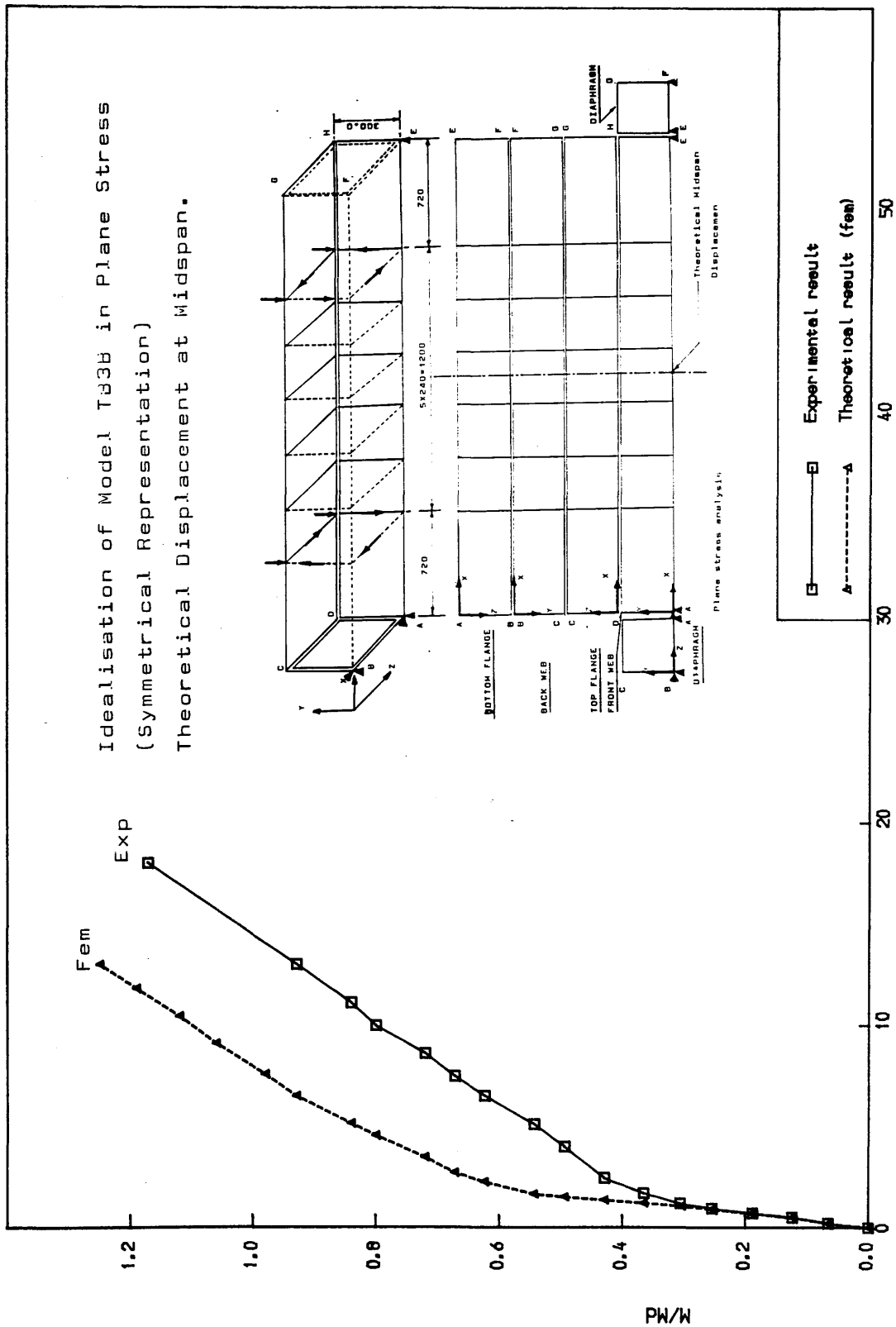

Figure (6.13) Comparison of Theoretical to Experimental Load Deflection Curve of Model TB3B " Pe= 132.8 KN and Ep= -60mm ".

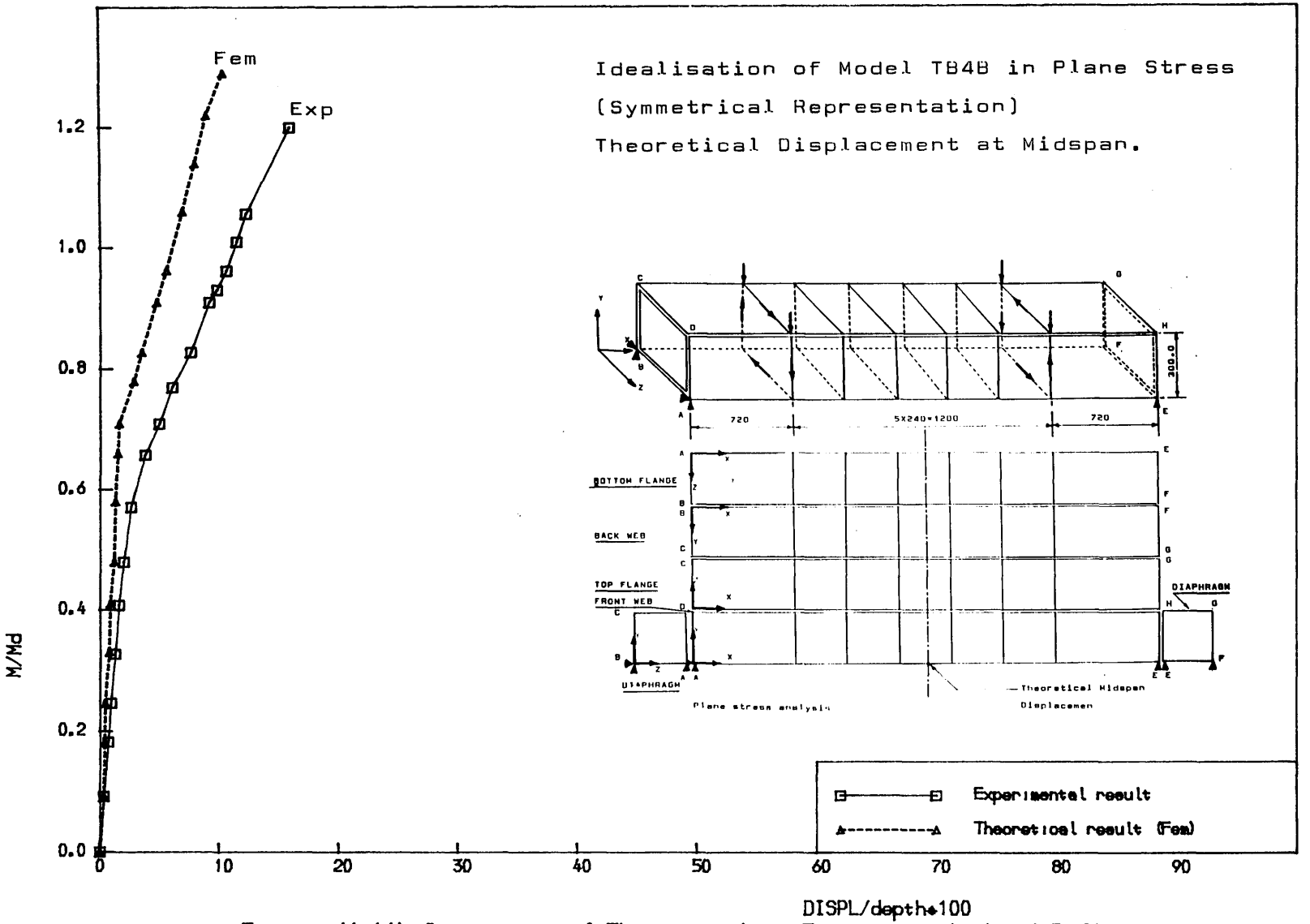

Figure (6.14) Comparison of Theoretical to Experimental Load Deflection Curve of Model TB4B " Pe= 160 KN and Ep= -72mm "

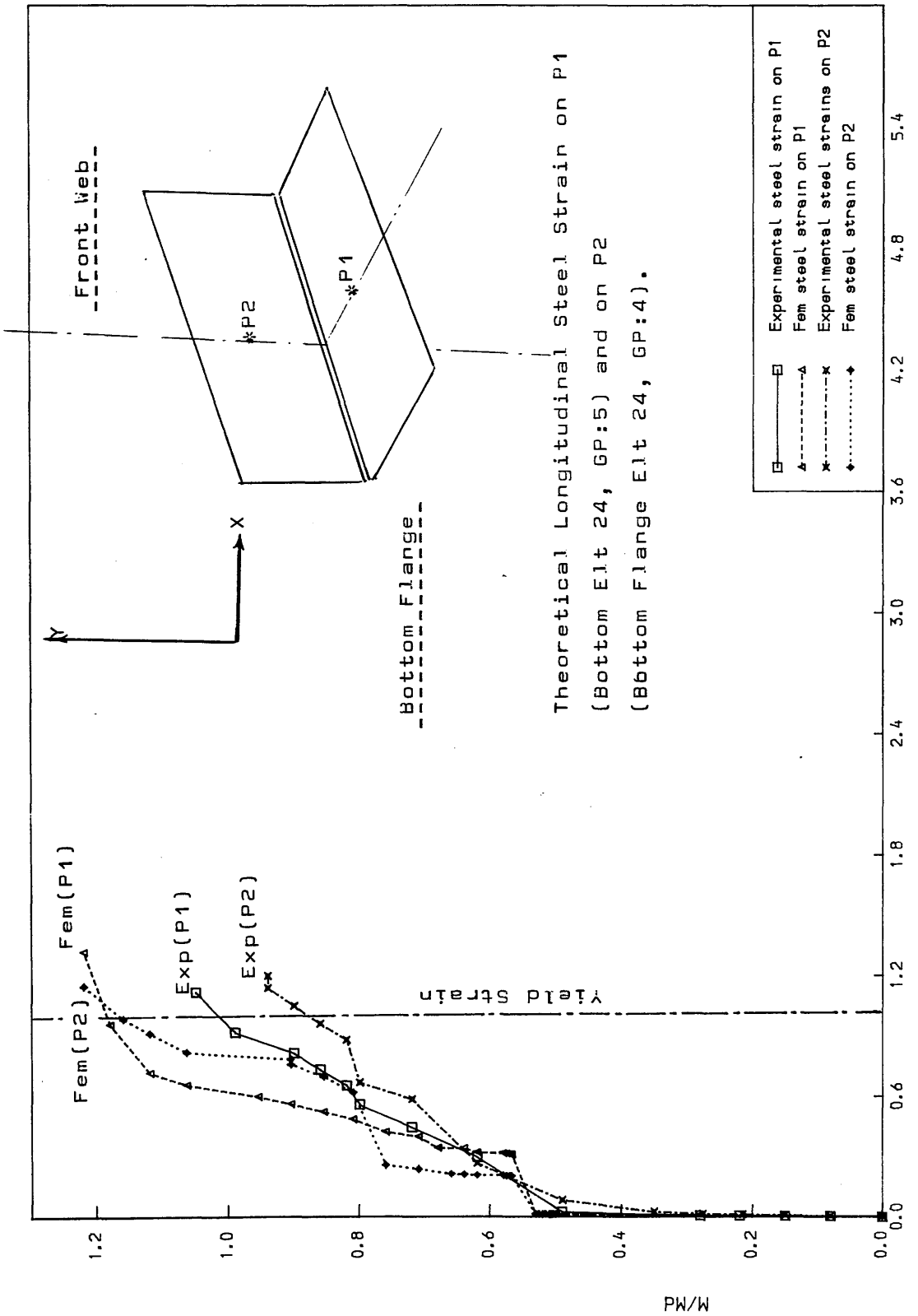

Figure (6.15) Comparison of Theoretical to Experimental Load Longitudinal Strain Curves of Model TB1B

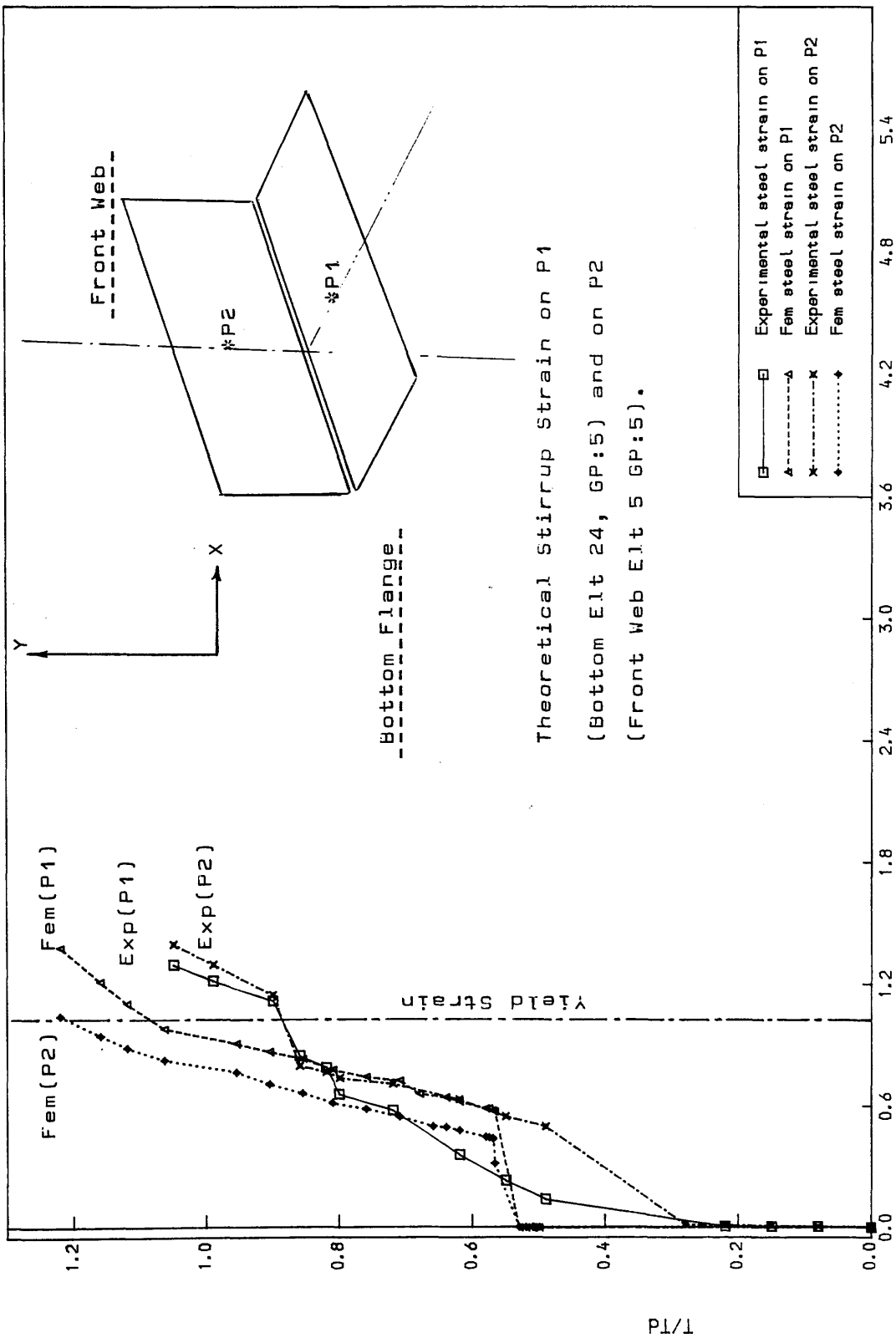

FIGURE (6.16) Comparison of Theoretical to Experimental Load Stirrup Strain Curves of Model TB1B

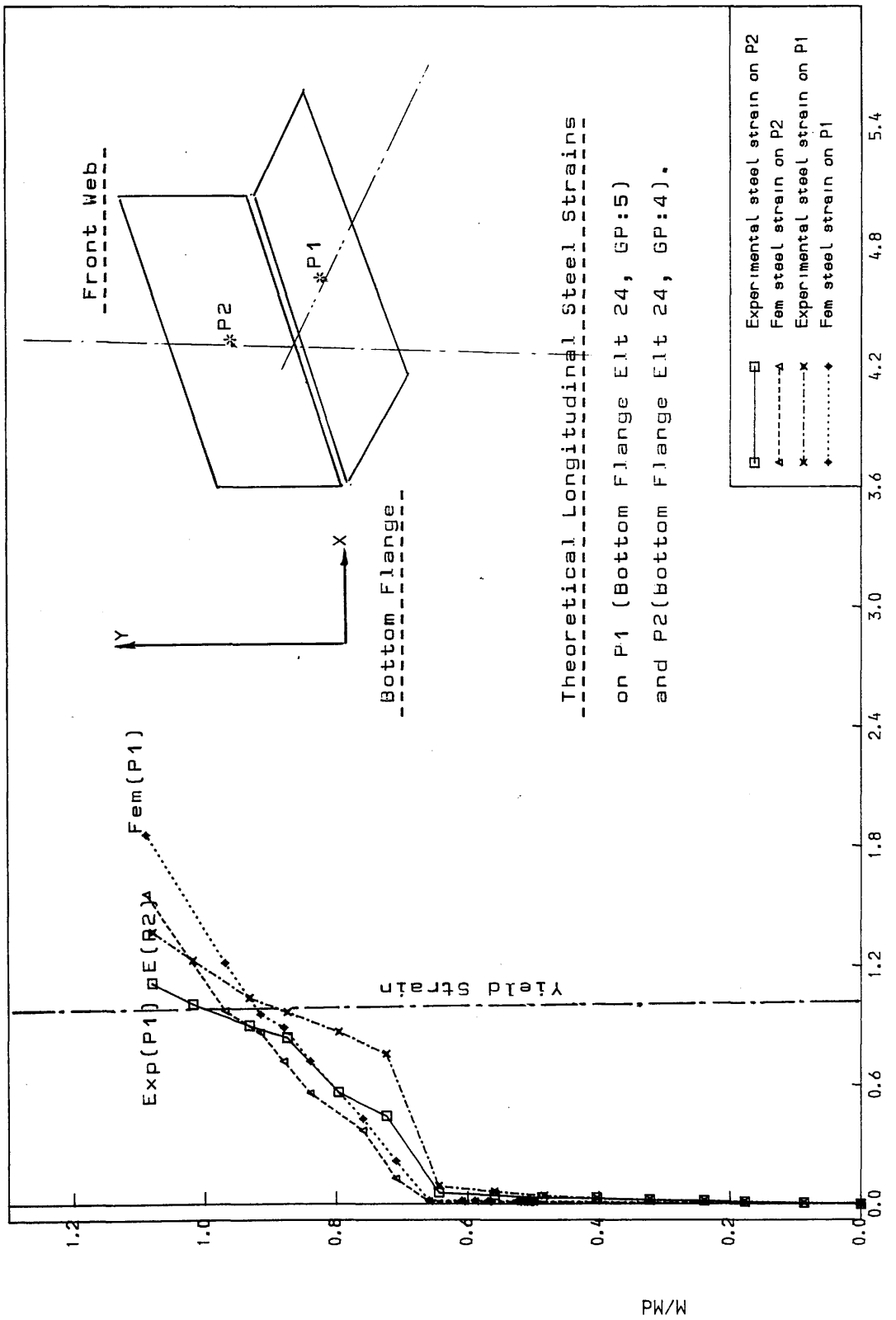

Figure (6.17) Comparison of Theoretical to Experimental Load Longitudinal Steel Strain Curves for Model TB2B

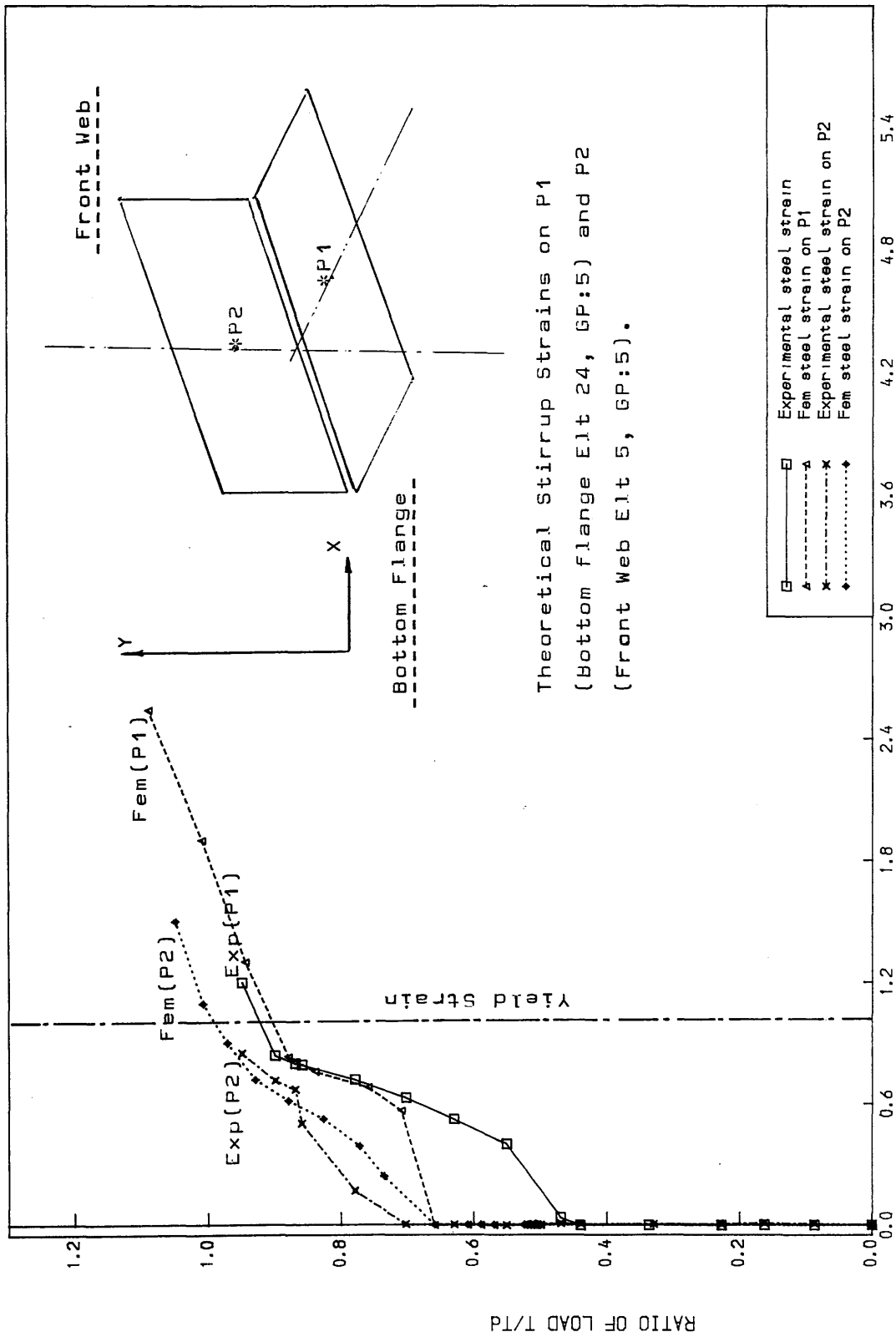

Figure (6.18) Comparison of Theoretical to Experimental Load Stirrup Strain Curves for Model TB2B

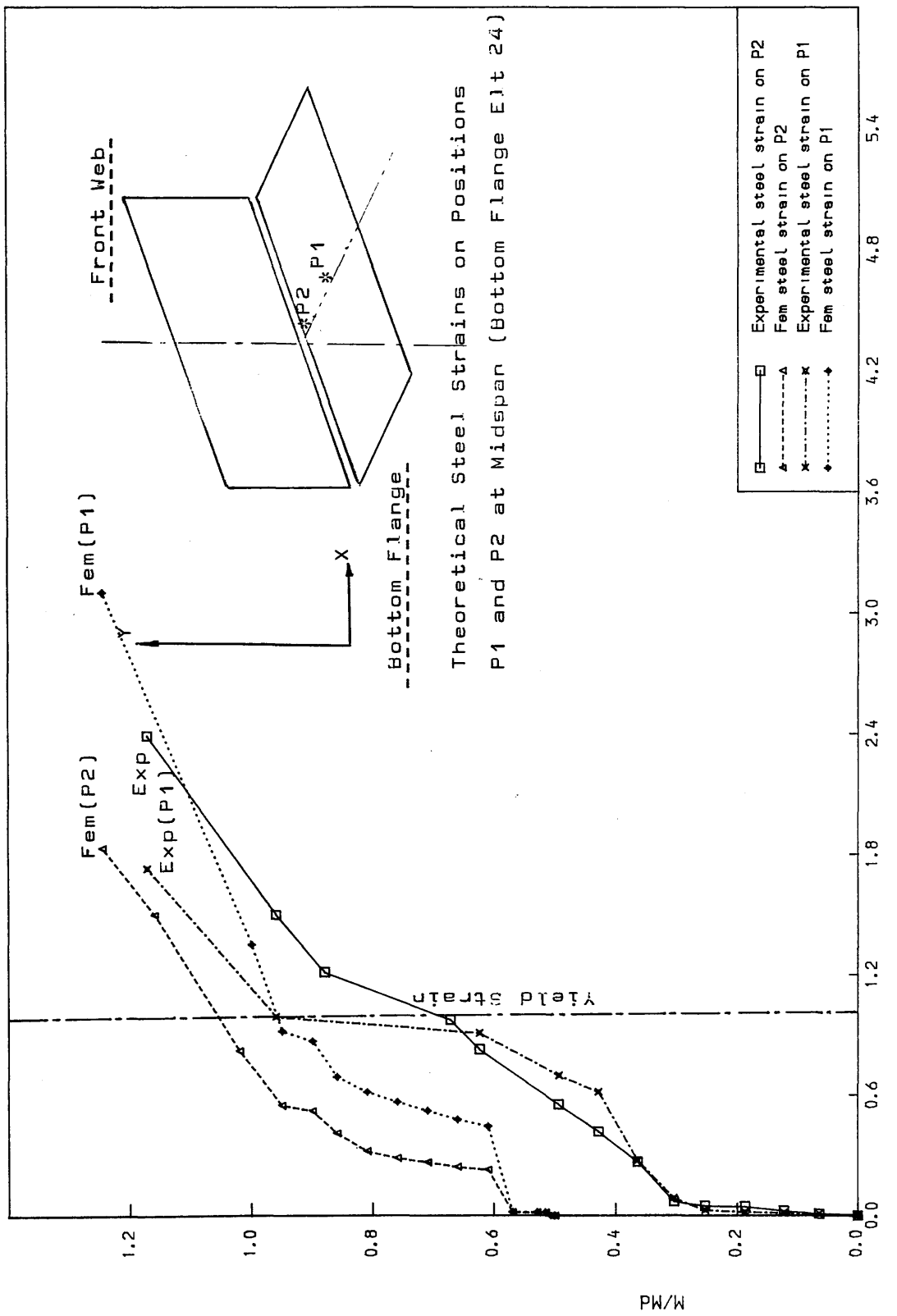

Figure (6.19) Comparison of Theoretical to Experimental Load Longitudinal Steel Strain Curves of Model TB3B

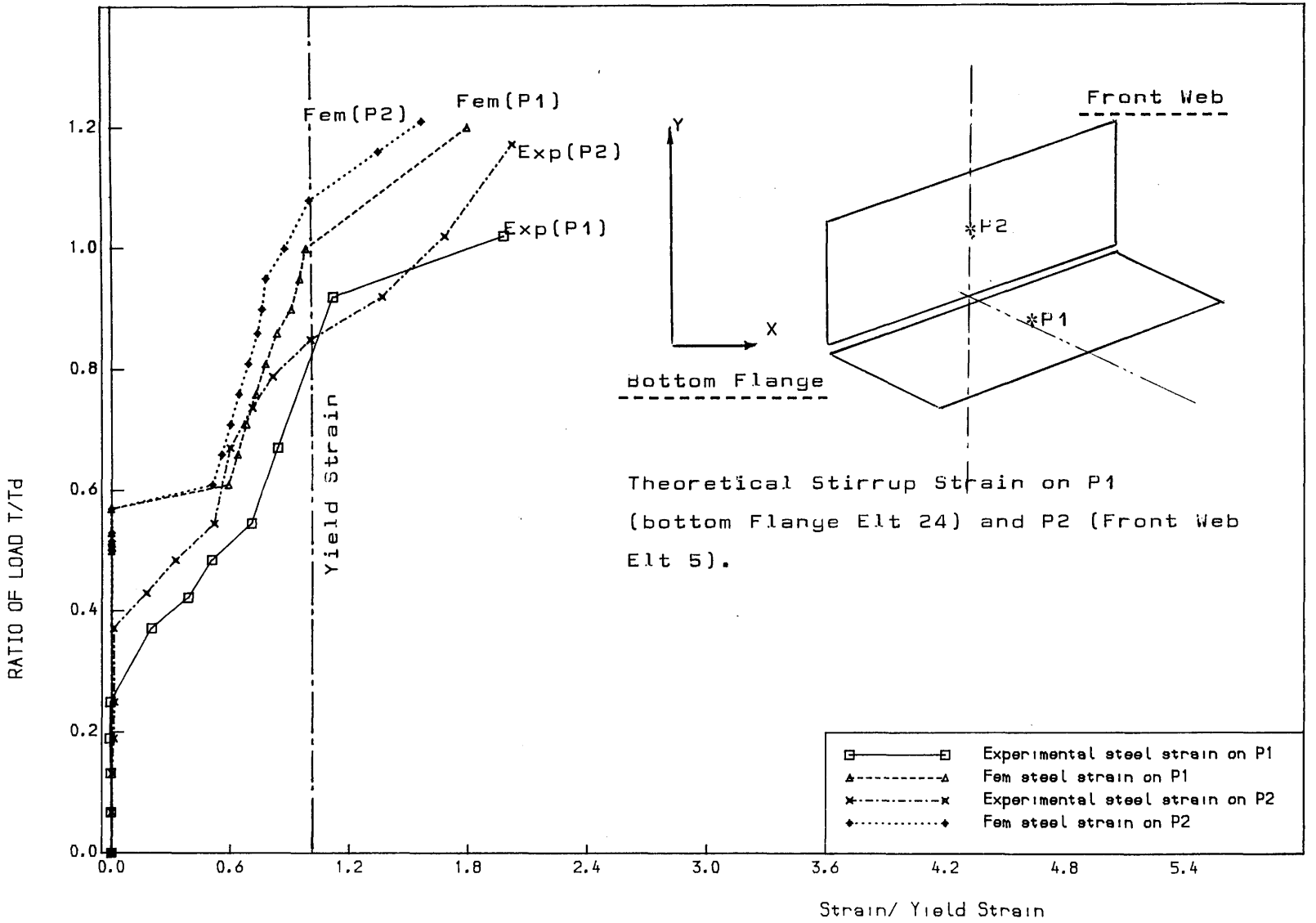

Figure (6.20) Comparison of Theoretical to Experimental Load Stirrup Strain Curves of Model TB3B

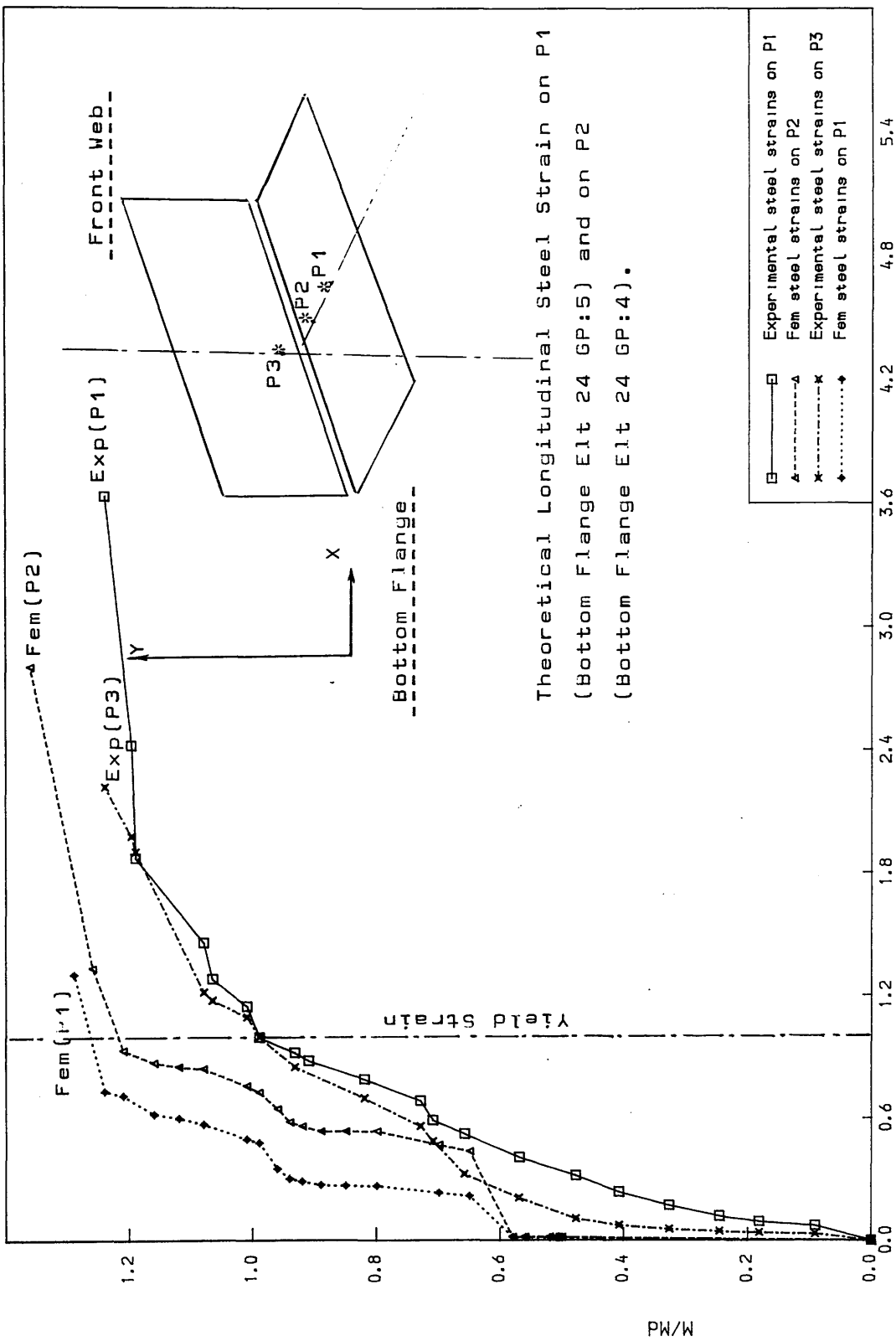

Figure (6.21) Comparison of Theoretical to Experimental Load Longitudinal Steel Strain Curves for Model TB4B

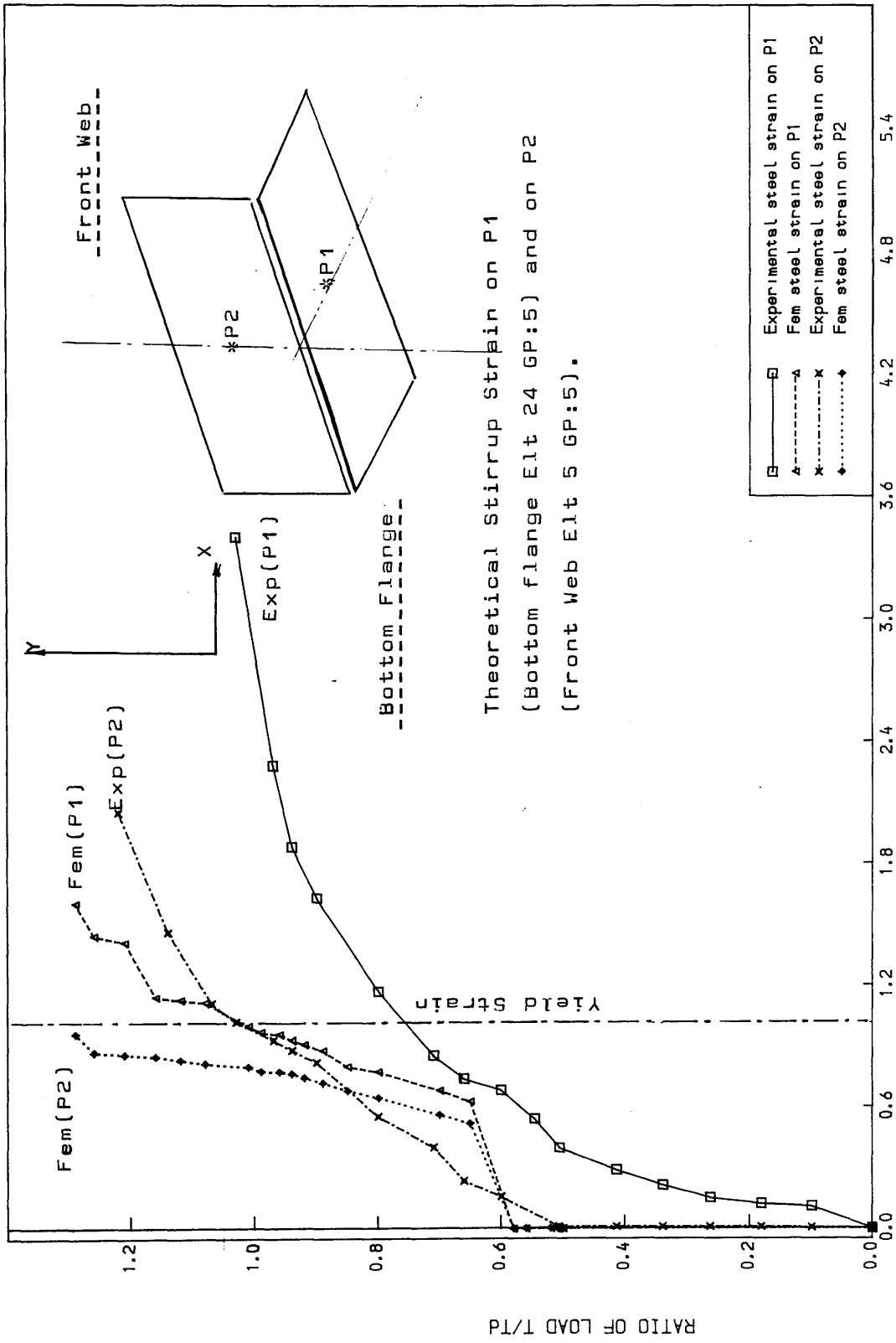

Figure (6.22) Comparison of Theoretical to Experimental Load Stirrup Strain Curves for Model TB4B

Table (6.1) Node Freedom Number at the junction of the plates.

Flange Plate			Web Plate		
Node Number	Unknown node displacement number in		Node Number	Unknown node displacement number in	
	X-dir U	Y-dir V		X-dir U	Y-dir V
1	0	0	2	0	0
3	1	2	4	1	3
5	4	5	6	4	6
7	7	8	8	7	9
9	10	11	10	10	12
11	13	14	12	13	15
13	16	17	14	16	18
15	19	20	16	19	21
17	22	23	18	22	24
19	25	26	20	25	27
21	28	29	22	28	30

Note that the web lies in the X-Y plane and the flange lies in Y-Z plane.

However when modelling both plates are assumed to lie in X-Y plane.

Table(6.2) Comparison of Theoretical Results to the Experimental ones.

Beam Mark	T/B	Ultimate Moments (Exp)		Ratio of Theoret-Crack Load to Exp Cracking Load	Ratio of Theoret-Ultimate Load to Design Load	Ratio of Theoret-Ultimate Load to Exp Ultimate Load
		Torsion T_u (KNm)	Bending M_u (KNm)	P_{crt}/P_{cre}	P_{ut}/P_d	P_{ut}/P_{ue}
TB1B	1.0	34.0	35.0	1.13	1.22	1.12
TB2B	0.8	27.6	34.6	1.26	1.10	1.02
TB3B	1.0	37.0	37.5	1.41	1.25	1.07
TB4B	1.0	39.5	40.0	1.43	1.29	1.05
PT1B	1/0	33.8				
PT2B	1/0	36.9				

Note : P_{crt} and P_{ut} are the Theoretical Cracking and Ultimate Loads.
P_{cre} and P_{ue} are the Experimental Cracking and Ultimate Loads.

CHAPTER SEVEN

CONCLUSIONS, COMMENTS AND SUGGESTIONS FOR FURTHER WORK

7.1 GENERAL CONCLUSIONS

On the basis of the analysis carried out it is concluded that the non– linear finite element model predicts within acceptable accuracy the behaviour of partially prestressed beams under combined bending and torsion.

From the experimental investigation it is concluded that the adopted design approach provided satisfactory designs.

7.2 DETAILED CONCLUSIONS

The main detailled conclusions of this study are summarised as follows:

(A) Experimental study

(1) The adopted approach based on classical ultimate capacity concept showed satisfactory results in terms of prediction of the ultimate strength of prestressed beams under combined bending and torsion.

(2) All the beams designed by the direct design approach recorded failure close to their design loads. The average ultimate failure loads for all the beams tested was 1.15xdesign load for beams tested under combined loading.

(3) Steel remained elastic under the service load limit. The average load at first yield of for series 1 was 0.893xdesign load (for ordinary steel) and 0.985xdesign load for prestressing steel.

(4) The Direct design method ensure practically the simultaneous yielding of both prestressing and ordinary steel with good agreements.

(5) The beams of series one failed by yielding of the bottom steel and formation of hinge at the top flange.

(B) Application of the finite element model

(1) Satisfactory predictions can be obtained by the finite element model provided that attention is paid to the numerical parameters e.g increment size, convergence tolerance, mesh size and boundary conditions.

(2) The results produced by the this finite element model were in reasonable agreement with the experimental results.

(3) The cost of an analysis increases greatly with the increase in the number of the elements.

7.3 SUGGESTIONS FOR FURTHER WORK

Extensions of this study can be conveniently grouped as follows:

(A) Application of the finite element model

(1) Use of the tension stiffening parameter which could be important in the case of combined loading because of presence of flexure.

(2) Incorporation of a suitable material model to study the behaviour under cyclic loading in the provided program.

(B) Experimental studies

(1) More variables to expand the present set of experiments include variation of reinforcement and amount of prestress for rectangular

sections. Aspect ratio of the section and whether the beam is solid or hollow.

(2) For solid beams see if prestressing makes the solid core contribute to the resistance of torsional stresses.

(3) Cyclic loading is undoubtely the first obvious expansion after (1) above

(4) The hollow beams studied herein are assumed to be of rigid cross–section, hence section were designed for in–plane stresses only. However, in practice many hollow section beams are of deformable cross section.

APPENDIX A

Contribution of self weight and sundries to total moments on test beams.

Square sections (300mm x 300mm)

1) Self weight of solid end of beam 580mm.

   0.3 x 0.3 x 24 = 2.16 kN/m

2) Self weight of effective span of beam (hollow section)

   [(0.3 x 0.3) − (0.2 x 0.2)] x 24 = 1.2 kN/m

3) Self weight of torsion arm = 3.0 kN

4) Self weight of secondary beam = 0.65 kN

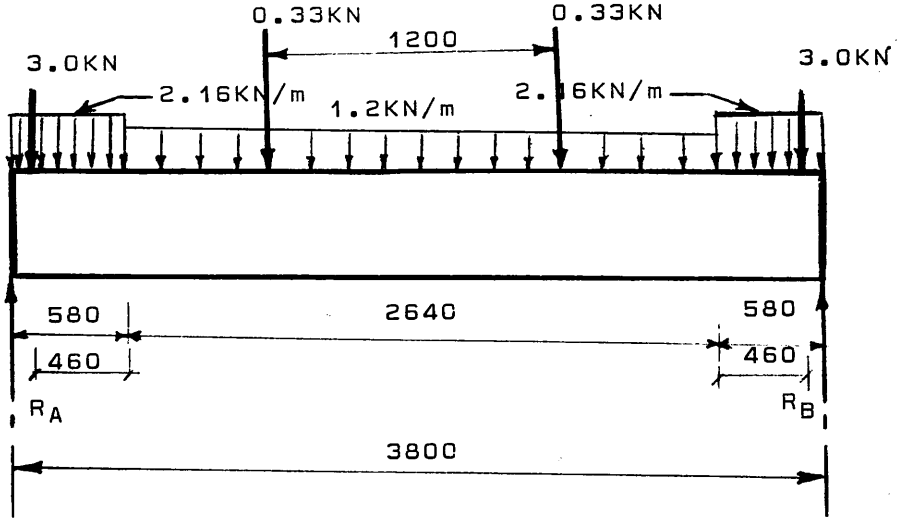

Reaction R_a = (2.16 x 0.58) + 1.27 + 0.33 + (1.2 x 1.32) = 6.17 KN

Moment of midspan is

6.17 x 1.90 − [1.2 x $(1.32)^2/2$] − 0.33 x 0.6 − 3 x 1.78

− 2.16 x 0.58 x 1.61 = 3.12 kNm which represents 9.75% of the design load.

APPENDIX B

As already defined the torsional shear stress in beams is given as:

$$\tau = \frac{T}{2A_0 . t} \qquad B1$$

where τ: shear stress

t: thickness of beam wall

T: applied torque

A_0: $x_1 . y_1$, enclosed area of centre line

The corresponding shear stress from the above equation depends mainly on the enclosed area A_0 adopted, which also affect the required steel area to resist the applied shear. The following alternative in defining A_0 are:

a) centreline of thickness of beam wall

b) centreline of stirrups

c) centreline of longitudial bars

Figure C1 shows details of the adopted section in which A_0 is obtained as:

a) A_0 from centreline of stirrups

$A_0 = (300 - 15 - 5 - 4)^2 = 262$ mm^2

b) A_0 from centreline of beam wall

$A_0 = (300 - 25)^2 = 250$ mm^2

c) A_0 from centreline of longitudinal bars

$A_0 = (300 - 15 - 8 - 5) = 244$ mm^2

Finally the centreline of the beam wall was adopted in calculating the enclosed area, A_0 in this study.

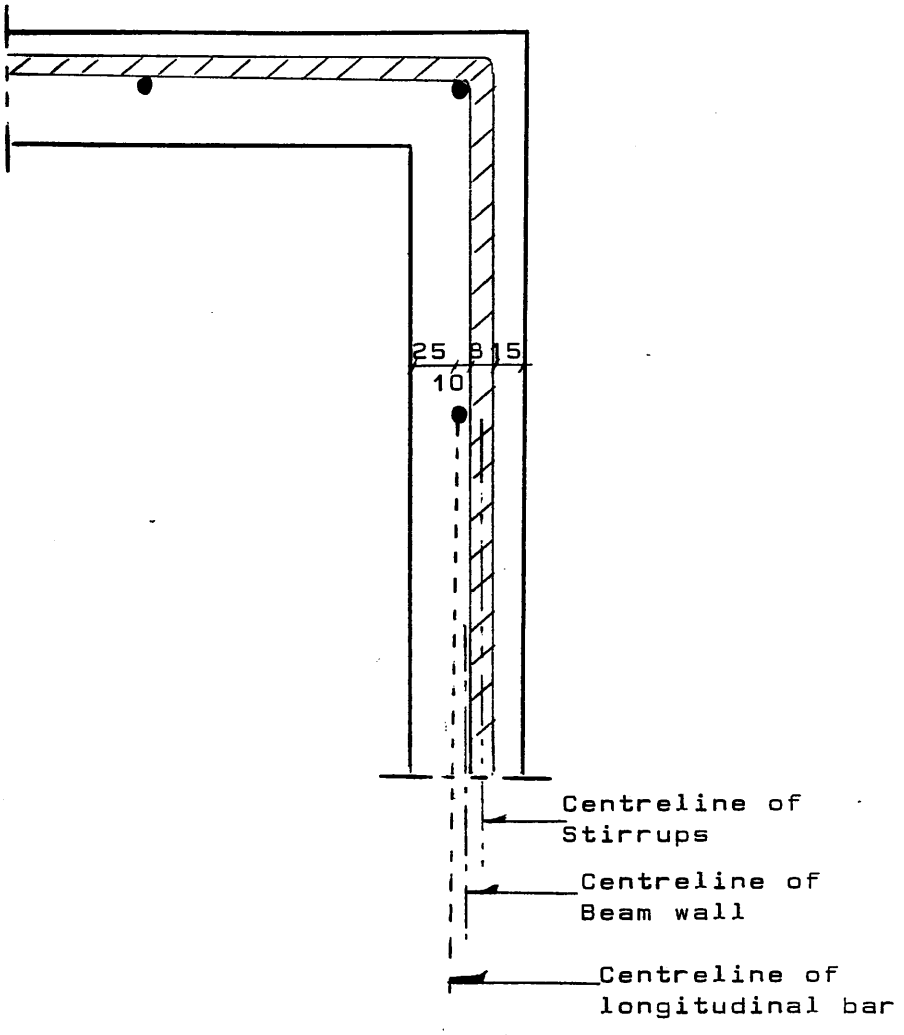

Figure(C.1) Determination of the enclosed area A_0
For beams under pure torsion.

REFERENCES

1. Hsu, T.T.C., " Torsion of reinforced concrete ".
Van. Nostrand Reinhold, 1984

2. Cowan, " Reinforced and Prestressed concrete in torsion ".
Edward Arnold Ltd

3. Nadai, A., " Theory of flow and fracture of solids ",
Volume 1. Mc Graw–Hill, 1950.

4. Hsu, T., " Post–cracking torsional rigidity of reinforced concrete sections ". *Journal of the ACI, Vol 70, N 5, May 1973*

5. Jiang, J and Dong, M., " Calculation of the crack resistance and Strength of prestressed concrete members in torsion ".
Int Symposium on Fundamental Theory of reinforced and Prestressed concrete.

6. Ewida, A. A., and Mc Mullen, A. E., " Concrete members under combined torsion and shear " *Journal of the structural Division, American Society of civil engineers, V.118, April 1982, pp. 911–928.*

7. Victor, D.T., " Ultimate torque of reinforced concrete beams ",
Jounal of structural Div., ASCE, ST.7, July 1976, pp 1337–1352.

8. Lampert, P and Collins, M.P., " Torsion, bending and confusion: an attempt to establish the facts". *Journal of ACI, August 1972, pp 500–505.*

9. Swann, R.A., " Experimental basis for a design method for reinforced rectangular beams in torsion".
Cement and Concrete Association, Tech Report, Dec 1970.

10. Lampert, P., " Torsion and bending in reinforced and prestressed concrete members ".
Proceeding of Inst of Civil Eng, 1972, pp 487–505.

11. Lampert, P and Thurliman, B., " Torsion tests on reinforced concrete beams ". *Bericht Nr 6506–2 June 1968, and Nr 6506–3 Jan 1969, Inst fur Baustatik ETH, Zurich.*

12. Mitchell, D., and Collins, M.P., " Influence of Prestressing on Torsional response of concrete bemas, ". *PCI Journal, V 23, No 3, May–June 1978 pp 54–73.*

13. No reference

14. No reference

15. Hsu, T.T.C., " Discussion of pure torsion in rectangular section and Re examination ", *Journal of the American Concrete Inst., Pro, Vol.76, N°6, June 1979, pp 741–746.*

16. Hsu, T.T.C., " Post– cracking torsional rigidity of reinforced concrete sections ", *Journal of the American Inst., Proc Vol 70, N°5, May 1973.*

17. Timoshenko, S.P and Goodier, J.N, " Theory of Elasticity " *Mc Graw–Hill, Edition, 1970.*

18. BS 8110 : Part 1, 1985
Code of Practice for the structural use of concrete
British Standards Institution, London 1985.

19. ACI comittee 318
Building Code Requirements for Reinforced concrete (ACI 318–77)
ACI, Detroit, Michigan 48219, 1977.

20. Nielson, M.P., " Optimum design of reinforced concrete shell slabs ", *Structural Research laboratory, Technical University of Denmark. Report, NR. R44, 1974, pp 190–200.*

21. Clark, L.A., " The Provision of tension and compression reinforcement to resist in plane forces ", *Magazine of Concrete Research. Vol 28 (N° 94), March 1976, pp3–12.*

22. Lin, C.K., " Ultimate strength design of deep beams ". *University of Glasgow Msc Thesis 1979.*

23. Ebiriri, J., " Direct design of beams for combined bending and torsion ", *PhD Thesis, Civil Eng Dept, Glasgow University 1985.*

24. EL– Nounou, G.F.R., " Design of shear wall floor connections ", *PhD Thesis, Civil Eng Dept, Glasgow University, August 1985.*

25. Abdelhaziz, L., " Direct design of Reinforced concrete skew slabs ". *PhD Thesis, Dept of Civil, University of Glasgow, Oct 1986.*

26. Wood, R.H., " The reinforcement of slabs in accordance with a pre– determined fied of moments ". *Concrete, Feb 1968, pp 69–76.*

27. Armer, G.S.T., Correspondance on " The reinforcement of slabs in accordance with a pre– determined field of moments ", *Concrete, August 1968, pp 319.*

28. Collins, M.P and Mitchell, D., " Shear and torsion design of prestressed and non– prestressed concrete beams ". *Journal of the prestressed Concrete Ins, V 25, N°5, Sept–Oct 1980, pp 32–100.*

29. CEB– FIP Model Code for Concrete Structure, 3rd Edition, Comite Euro– Int du Beton, *Federation Int de la precontrainte, Paris, 1978.*

30. Thurlimann. B., " Shear strength of reinforced and prestressed concrete beams– CEB Approach ", *Journal of the American Inst, Sp 59, 1978, pp 93–115.*

31. Thurlimann, B., " Torsional strength of reinforced and prestressed concrete beams –CEB Approach ", *American Concrete Inst SP 59, 1978, pp 117–143.*

32. Hinton, E and Owen, D.R.J., " Finite Element Programming ". *Academic Press, 1977.*

33. Cheung, Y.K and Yeo, M.F., " A Practical Introduction to Finite Element Analysis ". *Pitman, LOndon, 1979.*

34. Phillips, D.V., " Non Linear Analysis of Structural Concrete by Finite Element Method ". *PhD Thesis, University of wales, 1973.*

35. Zienkiewicz, O.C., " Finite Element Method in Engineering Science ". *Mc Graw Hill, London, 1976.*

36. Owen, D.R.J and Hinton, E.," Finite Element in Plasticity ". *Prineridge press, 1980.*

37. J.Moussa, " Direct design approach of reinforced and partially prestressed beams subjected to multiple load cases". *Msc Thesis, Civil Eng Dept, University of Glasgow, Jan 1988.*

38. American Society of Civil Engineers., " Finite Element analysis of Reinforced Concrete ". *ASCE, N.York, 1982.*

39. BS 5400 (1984) Part 4

Steel Concrete and Composite Bridges.